

AD-A247 216



2

The NOGAPS Forecast Model: A Technical Description

DTIC
ELECTE
MAR 10 1992
S D D

T. F. Hogan
T. E. Rosmond
R. Gelaro
Prediction Systems Division
Atmospheric Directorate
Monterey, California 93943-5006

92-06202



92 3 09 150



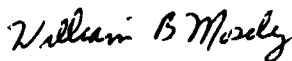
Approved for public release; distribution is unlimited. Naval Oceanographic and Atmospheric Research Laboratory, Stennis Space Center, Mississippi 39529-5004.

Foreword

The Navy Operational Global Atmospheric Prediction System (NOGAPS) provides numerical guidance and products in support of a wide range of Navy oceanographic and atmospheric requirements. The forecast model component of NOGAPS is the heart of the system and represents a multiyear development effort by the scientists of the Naval Oceanographic and Atmospheric Research Laboratory's Atmospheric Directorate.

Because many other Navy oceanographic and atmospheric research efforts depend on NOGAPS for environmental inputs, there is continuing demand for detailed technical descriptions of the forecast model's physical, mathematical, and computational processes. Only with this documentation can other Navy scientists understand research results influenced by NOGAPS output products. Because such numerical weather prediction systems as NOGAPS are constantly evolving, periodic updates to system documentation are also a key to supporting future Navy environmental research.

NOGAPS development directly responds to validated Chief of Naval Operations requirements, but in a larger sense it is fair to say that because so many Navy environmental needs depend on NOGAPS to some degree, nearly every meteorological and oceanographic requirement benefits from NOGAPS and its continuing development.



W. B. Moseley
Technical Director



L. R. Elliott, Commander, USN
Commanding Officer

Executive Summary

The forecast model of the Navy Operational Global Atmospheric Prediction System (NOGAPS) is described in complete physical and mathematical detail. NOGAPS 3.2 is the latest in the NOGAPS forecast models developed by the scientists of the Naval Oceanographic and Atmospheric Research Laboratory. The model is a key part of Fleet Numerical Oceanographic Center's (FNOC) central site environmental support of the fleet.

The spectral spherical harmonic formulation of the NOGAPS model's governing equations are described, particularly the unique hybrid vertical coordinate. The nonlinear normal mode initialization is described. The initialization removes unwanted gravity waves from initial conditions to ensure subsequent forecast fields are free from "noise." The techniques used to increase the length of the maximum allowable NOGAPS timestep are described. This procedure is of great operational importance because the computational requirements of NOGAPS are enormous; anything that reduces this requirement directly benefits FNOC's operational scheduling.

The NOGAPS model's diabatic processes, i.e., moist physics, dissipation, and radiation, are described in detail. Emphasis is given to those aspects of the NOGAPS model that are of particular importance to special Navy requirements: the physics of the marine planetary boundary layer, cumulus convection, and cloud/radiation interactions. The interaction of shortwave solar radiation and longwave terrestrial radiation with the model's predicted cloud field is the single, most important process in determining systematic errors in the model's near-surface conditions. Therefore, the model's cloud and radiation physical parameterizations are given special emphasis.

NOGAPS is the foundation of much of the Navy's operational environmental central site fleet support. Nearly every environmental product produced by FNOC is, to some degree, dependent on NOGAPS input. Some users understanding of the NOGAPS model and its formulation is important to the understanding of these products. Navy scientists who develop environmental models will invariably depend on NOGAPS inputs. The description of NOGAPS formulation will greatly assist them in interpreting their research results. This guidance will become even more important in the future as atmospheric and ocean models become more closely coupled and interdependent.

Acknowledgments

This work was funded by the Office of Naval Technology, Program Element 62435N, J. Cauffman, program manager.

Several NOARL and FNOC scientists were active participants in the development and evaluation of NOGAPS 3.2. NOGAPS is far more than just the forecast model described in this report. Without the complete system, the forecast model would be of little use to the Navy. Nancy Baker, Ed Barker, Robin Brody, and Jim Goerss of NOARL, and Howard Lewit of FNOC developed and refined the other components of NOGAPS that make it the tremendous naval asset it is today.

NOARL visiting scientists also made significant contributions to NOGAPS developments. Ron Errico and Dave Williamson of NCAR and Bryant McAveney of the Australian Bureau of Meteorology provides several valuable suggestions that improved the system. Thanks also must go to Terry Williams of the Naval Postgraduate School for his careful review of the manuscript.

Additional thanks must go to John Hovermale, Director, Atmospheric Directorate, who was supportive throughout the development of NOGAPS; to Capt. Jesus Tupaz, while Commanding Officer at FNOC, who made the Development and operational implementation of NOGAPS 3.2 one of his highest priorities; and to his successor, Capt. Jack Jensen, who has continued this enthusiastic support.

The mention of commercial products or the use of company names does not in any way imply endorsement by the U.S. Navy or NOARL.

Contents

Introduction	1
Appendix. Technical Description	3



Accession For	
NTIS CRA&I	<input checked="checked" type="checkbox"/>
DTIC TAB	<input type="checkbox"/>
Unannounced	<input type="checkbox"/>
Justification	
By	
Distribution/	
Availability Codes	
Dist	Avail and/or Special
A-1	

The NOGAPS Forecast Model: A Technical Description

Introduction

This report describes the initialization and forecast model of the Navy's Operational Global Atmospheric System, NOGAPS 3.2 developed by the Naval Oceanographic and Research Laboratory. The performance of the system, however, is not presented. Seasonal statistics and evaluation of NOGAPS are given in the Fleet Numerical Oceanography Center's (FNOC) Quarterly Performance Summaries. We emphasize that NOGAPS is a forecast system that includes data quality control, optimum interpolation analysis, normal mode initialization, forecast model, post processing, and verification components. A description of the quality control and the optimum interpolation analysis is given by Barker et al. (1989) and Baker (1989).

The Navy began global numerical weather prediction with the introduction of NOGAPS (Rosmond, 1981) in August 1982 after several years of development. It was a 9-layer, finite difference model with a full physics package and a horizontal resolution of $2.4^\circ \times 3.0^\circ$. The major components of the model's dynamics and physics were based on those originally developed for the University of California at Los Angeles' (UCLA) general circulation model (Arakawa and Lamb, 1977). The operational forecasts were run to 5 days with the model showing skill to 96 hours.

A major correction, NOGAPS 2.2, was implemented in July 1986 to correct some apparent deficiencies in the ground temperature and wetness parameterizations. In January 1988, a global spectral model, NOGAPS 3.0, replaced NOGAPS 2.2. The model's resolution was 47 wave triangular truncation (T47) in the horizontal and 18 levels in the vertical. Completely new diabatic parameterizations were introduced with NOGAPS 3.0, and initially not all of the various components were compatible. To meet operational deadlines, it was necessary to apply a major engineering fix to NOGAPS 3.0's radiative forcing.

In March 1989, several major corrections to the parameterizations were implemented, and the new version of the model was called NOGAPS 3.1. The horizontal and vertical resolutions of versions 3.0 and 3.1 were the same. In August 1989, the horizontal resolution of the model was increased to 79 wave triangular truncation (T79), and this version was designated as NOGAPS 3.2. The model parameterizations are the same as NOGAPS 3.1. Aside from the increase in resolution, the only important change in NOGAPS 3.2 is the introduction of a spectral filter that allows longer model time steps in the presence of high winds.

The development of the various forecast components for 3.0/3.1/3.2 drew heavily from many different sources and the references are noted in the text. With the exception of the radiation code, however, all of the forecast and initialization coding was performed. The longwave and shortwave codes, without the cloud parameterizations, were obtained in 1984 from the Laboratory for Atmospheres, NASA Goddards Space Flight Center, and revisions were introduced by the authors to correct the cold bias that developed when the radiation scheme interacted with the other physical parameterizations.

The authors have gone into considerable detail describing the initialization scheme, adiabatic calculations, and physical parameterizations so that the reader will be able to understand the parameterizations and numerical techniques used in NOGAPS. Any suggestions that provide improvements to the Navy's forecast ability will be greatly appreciated.

Appendix

Technical Description

Chapter 1. Introduction	5
Chapter 2. The Equations of Motion with a Hybrid Coordinate System	7
Chapter 3. The Vertical Finite Difference Formulation	15
Chapter 4. The Spectral Expansions	27
Chapter 5. Nonlinear Normal Mode Initialization	35
Chapter 6. The Time Step Integration Strategy	65
Chapter 7. The Adiabatic and Implicit Adjustments	75
Chapter 8. Adiabatic Truncation and Implicit Smoothing Calculations	89
Chapter 9. Gravity Wave Drag	99
Chapter 10. Vertical Flux Parameterization	105
Chapter 11. Shallow Convection	119
Chapter 12. Cumulus Parameterization	123
Chapter 13. Large Scale Precipitation	157
Chapter 14. Longwave Radiation	161
Chapter 15. Shortwave Radiation	185
Chapter 16. Summary	211
Chapter 17. Bibliography	213

Chapter 1

Introduction

We discuss the equations for the model using the hybrid coordinate system in Chapter 2. This chapter is a review of basic transformation theory for the primitive equations, but it is included as an introduction to the technical points presented in the next chapters. The hybrid vertical finite difference formulation of the model is given in Chapter 3. The potential temperature is the thermodynamic forecast variable and the vertical finite difference relations for both the potential temperature equation and the hydrostatic equation are slightly different from most spectral models. The moisture variable used in the forecast model is the reciprocal of the natural log of specific humidity, rather than the specific humidity itself. The vertical differencing of the moisture is also discussed in Chapter 3. We present a discussion of the spectral representations for the forecast fields on hybrid pressure surfaces in Chapter 4, together with a description of the spectral transform procedure. A short discussion on the use of spectral filtering to reduce the Gibb's phenomena and its application to the terrain field is also given in the last section of Chapter 4. The nonlinear normal mode initialization (NNMI) scheme is presented in Chapter 5. The NNMI discussion is placed after the development of the equations since the initialization draws heavily on the adiabatic formulation of the model and the spectral representations of the model variables. This chapter marks the beginning

of the discussion of the workings of the forecast model. Chapter 6 presents the overall time step strategy of the forecast model. This chapter describes the time splitting of the adiabatic and the diabatic processes. Later chapters will refer back to Chapter 6 in their discussions of the provisional forecast fields as input into the different parameterizations. The calculation procedure for the explicit adiabatic tendencies is given in the first section of Chapter 7. The discussion there is brief, since the equations are fully discussed in Chapter 3 and the transformation theory is given in Chapter 4. Section 7.2 explains the details of the semi-implicit treatment of gravity wave propagation, and Section 7.3 presents the implicit advection calculations for vorticity and moisture. Chapter 8 describes the adiabatic tendency truncation procedure, which ensures a sufficiently large time step for the operational runs, the Newtonian cooling filter of potential temperature at the top of the atmosphere, the Robert time filter, and the fourth order implicit horizontal diffusion of the divergence, vorticity, potential temperature and moisture variables. We describe the physical parameterizations of the model in Chapters 9-15. The model contains physical parameterizations as sophisticated as can be found in any numerical weather prediction model. The parameterizations include gravity wave drag due to mountains (Chapter 9), vertical turbulent diffusion (Chapter 10), shallow cumulus mixing (Chapter 11), cumulus convection (Chapter 12), large scale stable precipitation (Chapter 13), and the heating due to longwave radiation (Chapter 14) and solar radiation (Chapter 15).

Chapter 2

The Equations of Motion With a Hybrid Coordinate System

We introduce the partial differential equations of motion for the forecast model in this chapter. A similar discussion can be found in the work of Simmons and Strüfing (1981). The horizontal coordinates are the longitude, λ , and the latitude, φ ; the vertical coordinate is represented by the variable η which ranges from 0 at the model top to 1 at the surface. We shall call the combination of the spherical coordinates (λ, φ) with η the hybrid coordinate system. The pressure p is a function of η and is given by the relation:

$$p = A(\eta) + B(\eta) \pi. \quad (2.1)$$

The functions $A(\eta)$ and $B(\eta)$ are any two functions defined on the interval 0 to 1 and with the boundary conditions:

$$\left. \begin{aligned} A(0) &= p_{top} \\ A(1) &= p_{top} \\ B(0) &= 0 \\ B(1) &= 1 \end{aligned} \right\} \quad (2.2)$$

where p_{top} is the model's top pressure, and π is the difference between the surface pressure, p_S , and p_{top} :

$$\pi = p_S - p_{top}. \quad (2.3)$$

The hybrid vertical coordinate system is a cross between a pressure coordinate system and a sigma coordinate system. The hybrid vertical coordinate is a pressure-like coordinate in regions where $B(\eta)$ is 0; η is a sigma-like coordinate in regions where $A(\eta)$ is a constant and $B(\eta)$ is not equal to 0.

We begin by deriving the mass continuity equation for any finite volume, V , that is moving with the fluid with a mass density ρ . The total change of mass following the flow, without mass sources, is zero, which we write as,

$$\frac{d}{dt} \int \int \int_V \rho dA dz = 0, \quad (2.4)$$

where dA is a differential element. We transform the z coordinate in (2.4) to η using the differential relation:

$$dz = \frac{\partial z}{\partial p} \frac{\partial p}{\partial \eta} d\eta.$$

It is assumed that the vertical variations in pressure are hydrostatic, so that the term, $\partial z / \partial p$, is replaced by $-1/\rho g$. With this transformation, we write the integral mass conservation equation (2.4) as

$$\frac{d}{dt} \int \int \int_V \frac{\partial p}{\partial \eta} dA d\eta = 0.$$

For finite volumes, the above integral relation is equivalent to the differential form of the continuity equation:

$$\frac{\partial}{\partial t} \left(\frac{\partial p}{\partial \eta} \right) + \nabla \cdot \left(\mathbf{u} \frac{\partial p}{\partial \eta} \right) + \frac{\partial}{\partial \eta} \left(\eta \frac{\partial p}{\partial \eta} \right) = 0. \quad (2.5)$$

where \mathbf{u} is the horizontal velocity vector.

We obtain the equation for π by integrating Equation (2.5) from $\eta = 0$ to $\eta = 1$, and employing the upper and lower boundary conditions for $\dot{\eta}$, which are

$$\dot{\eta}(0) = \dot{\eta}(1) = 0; \quad (2.6)$$

and the boundary conditions for B , which are given by Equation (2.1). The final form of the π tendency equation is

$$\frac{\partial \pi}{\partial t} = - \int_0^1 \nabla \cdot \left(\mathbf{u} \frac{\partial p}{\partial \eta} \right) d\eta = - \int_{p_{top}}^{p_s} \nabla \cdot (\mathbf{u} dp), \quad (2.7)$$

where dp is a function of λ , φ , and η .

We obtain the vertical motion equation by integrating (2.5) from 0 to η . Substituting for the $\partial \pi / \partial t$ term with the right hand side of Equation (2.7), we obtain the vertical motion equation:

$$\left[\dot{\eta} \frac{\partial p}{\partial \eta} \right] (\eta) = B(\eta) \int_0^1 \nabla \cdot \left(\mathbf{u} \frac{\partial p}{\partial \eta} \right) d\eta - \int_0^\eta \nabla \cdot \left(\mathbf{u} \frac{\partial p}{\partial \eta} \right) d\eta. \quad (2.8)$$

The time rate of change of any dynamic variable, denoted by X , due to advection is expressed in the hybrid coordinate system by

$$\left(\frac{\partial X}{\partial t} \right)_{adv} = - \frac{u}{a \cos \varphi} \frac{\partial X}{\partial \lambda} - \frac{v}{a} \frac{\partial X}{\partial \varphi} - \dot{\eta} \frac{\partial X}{\partial \eta}, \quad (2.9)$$

where a is the radius of the earth. Since the vertical advection term is evaluated at constant λ and φ , we use the chain rule to transform the η -derivative in (2.9) to a p derivative, which yields

$$\left(\frac{\partial X}{\partial t} \right)_{adv} = - \frac{u}{a \cos \varphi} \frac{\partial X}{\partial \lambda} - \frac{v}{a} \frac{\partial X}{\partial \varphi} - \left[\dot{\eta} \frac{\partial p}{\partial \eta} \right] \frac{\partial X}{\partial p}. \quad (2.10)$$

This is the form for the advection term we use throughout the forecast model.

The thermodynamic variable of the forecast model is the virtual potential temperature θ , which is

$$\theta = T \left(\frac{1 + .608q}{P} \right), \quad (2.11)$$

where q is the specific humidity. The variable P in Equation (2.11) is defined as

$$P = \left(\frac{p}{p_0} \right)^\kappa, \quad (2.12)$$

where p_0 denotes 1000 mb and κ is the gas constant divided by the heat capacity, $\kappa = R/c_p$. Two major advantages of using θ in place of T are (1) an equation for the vertical velocity, $\omega = dp/dt$, is not needed, and (2) the conservation of total energy is easily satisfied for the finite difference formulation. We derive the discrete form of the energy conservation equations in Chapter 3. We obtain the prognostic equation for θ by combining the advection term with the diabatic forcing, which yields

$$\frac{\partial \theta}{\partial t} = -\frac{u}{a \cos \varphi} \frac{\partial \theta}{\partial \lambda} - \frac{v}{a} \frac{\partial \theta}{\partial \varphi} - \left[\dot{\eta} \frac{\partial p}{\partial \eta} \right] \frac{\partial \theta}{\partial p} + Q_\theta. \quad (2.13)$$

The diabatic forcing, Q_θ , is due to radiation, latent heat release processes, horizontal diffusion, and vertical mixing.

We write the hydrostatic equation in the form

$$\frac{\partial \phi}{\partial P} = -c_p \theta, \quad (2.14)$$

where ϕ is the geopotential and P is defined by (2.12). This form is chosen since the finite difference form of (2.14) ensures total energy conservation (see Chapter 3 and Haltiner and Williams [1980], Chapter 7-2).

The moisture equation is usually written for the specific humidity, q . A conservation equation, however, can be written for any continuously differentiable function of q , which we denote by $f[q]$. The form of the moisture equation, which is the same as the θ equation, is:

$$\frac{\partial f[q]}{\partial t} = -\frac{u}{a \cos \varphi} \frac{\partial f[q]}{\partial \lambda} - \frac{v}{a} \frac{\partial f[q]}{\partial \varphi} - \left[\dot{\eta} \frac{\partial p}{\partial \eta} \right] \frac{\partial f[q]}{\partial p} + Q_{f[q]}. \quad (2.15)$$

The forcing term, $Q_{f[q]}$, is due to condensation/evaporation processes and turbulent and cumulus vertical mixing. In NOGAPS 3.2 the moisture function is $1/\ln(q)$.

Our choices for the variables describing the velocity field are the vorticity, ζ , and the divergence, D , since both ζ and D are easily expanded in terms of Legendre polynomials and the semi-implicit scheme adjustments are given in terms of D . The vorticity and the divergence are defined by the relations

$$\zeta = \frac{1}{a \cos \varphi} \left[\frac{\partial v}{\partial \lambda} - \frac{\partial}{\partial \varphi} (u \cos \varphi) \right] \quad (2.16)$$

and

$$D = \frac{1}{a \cos \varphi} \left[\frac{\partial u}{\partial \lambda} + \frac{\partial}{\partial \varphi} (v \cos \varphi) \right]. \quad (2.17)$$

We obtain ζ and D equations by differentiating the horizontal velocity equations, which are given by

$$\begin{aligned} \frac{\partial u}{\partial t} = & -\frac{u}{a \cos \varphi} \frac{\partial u}{\partial \lambda} - \frac{v}{a} \frac{\partial u}{\partial \varphi} - \left[\dot{\eta} \frac{\partial p}{\partial \eta} \right] \frac{\partial u}{\partial p} \\ & + uv \frac{\tan \varphi}{a} + fv - \frac{1}{a \cos \varphi} \frac{\partial \phi}{\partial \lambda} - \frac{1}{a \cos \varphi} \frac{\partial \phi}{\partial \eta} \frac{\partial \eta}{\partial \lambda} + Q_u \end{aligned} \quad (2.18)$$

and

$$\begin{aligned} \frac{\partial v}{\partial t} = & -\frac{u}{a \cos \varphi} \frac{\partial v}{\partial \lambda} - \frac{v}{a} \frac{\partial v}{\partial \varphi} - \left[\dot{\eta} \frac{\partial p}{\partial \eta} \right] \frac{\partial v}{\partial p} \\ & -u^2 \frac{\tan \varphi}{a} - fu - \frac{1}{a} \frac{\partial \phi}{\partial \varphi} - \frac{1}{a} \frac{\partial \phi}{\partial \eta} \frac{\partial \eta}{\partial \varphi} + Q_v. \end{aligned} \quad (2.19)$$

The variable f denotes the Coriolis parameter,

$$f = 2\Omega \sin \varphi,$$

with the angular rotation rate of the earth denoted by Ω . The diabatic forcing terms in (2.18) and (2.19) are due to vertical turbulent fluxes, gravity wave drag, and horizontal diffusion. The second to last term on the right side of (2.18) describes the forcing of the velocity field due to variations in the η -coordinate with respect to the terrain, and is evaluated as

$$\begin{aligned} \left(\frac{\partial \phi}{\partial \eta} \right)_{\lambda, \varphi} \left(\frac{\partial \eta}{\partial \lambda} \right)_p &= \left(\frac{\partial \phi}{\partial P} \right) \left(\frac{\partial P}{\partial \eta} \right)_{\lambda, \varphi} \left(\frac{\partial \eta}{\partial \lambda} \right)_p \\ &= \left(\frac{\partial \phi}{\partial P} \right) \left(\frac{\partial P}{\partial \eta} \right)_{\lambda, \varphi} \left(\frac{\partial \eta}{\partial \pi} \right)_p \left(\frac{\partial \pi}{\partial \lambda} \right), \end{aligned}$$

where the subscripted variables indicate the variables that are held constant during the partial differentiation. It is easily shown that at constant pressure (and therefore constant P) we have

$$\left(\frac{\partial P}{\partial \eta}\right)_{\lambda, \varphi} \left(\frac{\partial \eta}{\partial \pi}\right)_p = - \left(\frac{\partial P}{\partial \pi}\right)_\eta.$$

We use this result together with the hydrostatic equation (2.14) to replace the terrain pressure term in (2.18) by

$$\left(\frac{\partial \phi}{\partial \eta}\right) \left(\frac{\partial \eta}{\partial \lambda}\right) = c_p \theta \left(\frac{\partial P}{\partial \pi}\right) \left(\frac{\partial \pi}{\partial \lambda}\right). \quad (2.20)$$

A similar relation is obtained for the terrain pressure term in (2.19). With these results, we write Equations (2.18) and (2.19) in the forms

$$\begin{aligned} \frac{\partial u}{\partial t} = & -\frac{u}{a \cos \varphi} \frac{\partial u}{\partial \lambda} - \frac{v}{a} \frac{\partial u}{\partial \varphi} - \left[\dot{\eta} \frac{\partial p}{\partial \eta} \right] \frac{\partial u}{\partial p} + uv \frac{\tan \varphi}{a} + fv \\ & - \frac{1}{a \cos \varphi} \frac{\partial \phi}{\partial \lambda} - c_p \frac{\theta}{a \cos \varphi} \left(\frac{\partial P}{\partial \pi}\right) \left(\frac{\partial \pi}{\partial \lambda}\right) + Q_u, \end{aligned} \quad (2.21)$$

and

$$\begin{aligned} \frac{\partial v}{\partial t} = & -\frac{u}{a \cos \varphi} \frac{\partial v}{\partial \lambda} - \frac{v}{a} \frac{\partial v}{\partial \varphi} - \left[\dot{\eta} \frac{\partial p}{\partial \eta} \right] \frac{\partial v}{\partial p} - u^2 \frac{\tan \varphi}{a} - fu \\ & - \frac{1}{a} \frac{\partial \phi}{\partial \varphi} - c_p \frac{\theta}{a} \left(\frac{\partial P}{\partial \pi}\right) \left(\frac{\partial \pi}{\partial \varphi}\right) + Q_v. \end{aligned} \quad (2.22)$$

We can now obtain the equations for vorticity and divergence by differentiating (2.21) and (2.22) and by using the definitions given by (2.16) and (2.17). The derivation is simplified considerably by introducing the following definitions. The cosine weighted velocities, which vanish at the poles, are given by

$$U = u \frac{\cos \varphi}{a}, \quad (2.23)$$

and

$$V = v \frac{\cos \varphi}{a}. \quad (2.24)$$

We define the functions G , H , and I by:

$$G = U(\zeta + f) + \left[\dot{\eta} \frac{\partial p}{\partial \eta} \right] \left(\frac{\partial V}{\partial p} \right) + \frac{c_p}{a^2} \theta \left(\frac{\partial P}{\partial \pi} \right) \left(\frac{\partial \pi}{\partial \mu} \right) \cos^2 \varphi - Q_v \frac{\cos \varphi}{a}, \quad (2.25)$$

$$H = V(\zeta + f) - \left[\dot{\eta} \frac{\partial p}{\partial \eta} \right] \left(\frac{\partial U}{\partial p} \right) - \frac{c_p}{a^2} \theta \left(\frac{\partial P}{\partial \pi} \right) \left(\frac{\partial \pi}{\partial \lambda} \right) + Q_u \frac{\cos \varphi}{a}, \quad (2.26)$$

and

$$I = \left(\frac{U^2 + V^2}{2} \right) \frac{a^2}{\cos^2 \varphi}. \quad (2.27)$$

The variable μ , which replaces φ in the above definitions, is given by

$$\mu = \sin \varphi. \quad (2.28)$$

Finally we define an operator, $\alpha(g, h)$, which operates on any two functions g and h , by

$$\alpha(g, h) = \frac{1}{\cos^2 \varphi} \frac{\partial g}{\partial \lambda} + \frac{\partial h}{\partial \mu} \quad (2.29)$$

With the above definitions, we write definitions of the vorticity and the divergence as

$$\zeta = \alpha(V, -U) \quad (2.30)$$

and

$$D = \alpha(U, V), \quad (2.31)$$

and the vorticity and the divergence equations as

$$\frac{\partial \zeta}{\partial t} = -\alpha(G, H) \quad (2.32)$$

and

$$\frac{\partial D}{\partial t} = \alpha(H, -G) - \nabla^2(\phi + I). \quad (2.33)$$

Equations (2.7), (2.8), (2.13), (2.14), (2.15), (2.30), (2.31), (2.32), and (2.33) are the basic equations for the spectral model with a vertical hybrid coordinate system. In the next chapter, we derive the vertical finite difference versions for these equations and we show that these equations conserve the total energy for adiabatic motions.

Chapter 3

The Vertical Finite Difference Formulation

The vertical staggering of the variables is shown in Figure 3.1. We place subscripts on the variables in order to designate the level of the horizontal grid point fields, the variables's spectral coefficients, or the discrete values of the functions $A(\eta)$ and $B(\eta)$. The total number of levels is identified by L ; at present there are $L=18$ vertical levels. The functions A and B , the pressure p , the function P that is defined by (2.12), and the vertical velocity $[\eta\partial p/\partial\eta]$ are evaluated at the half pressure levels. The half levels begin at the pressure p_{top} , also denoted as $p_{1/2}$, and end at the pressure p_S , which according to the indexing system is $p_{L+1/2}$. We compute from (2.1) the discrete values of the pressures at the half levels as

$$p_{k+1/2} = A_{k+1/2} + B_{k+1/2}\pi. \quad (3.1)$$

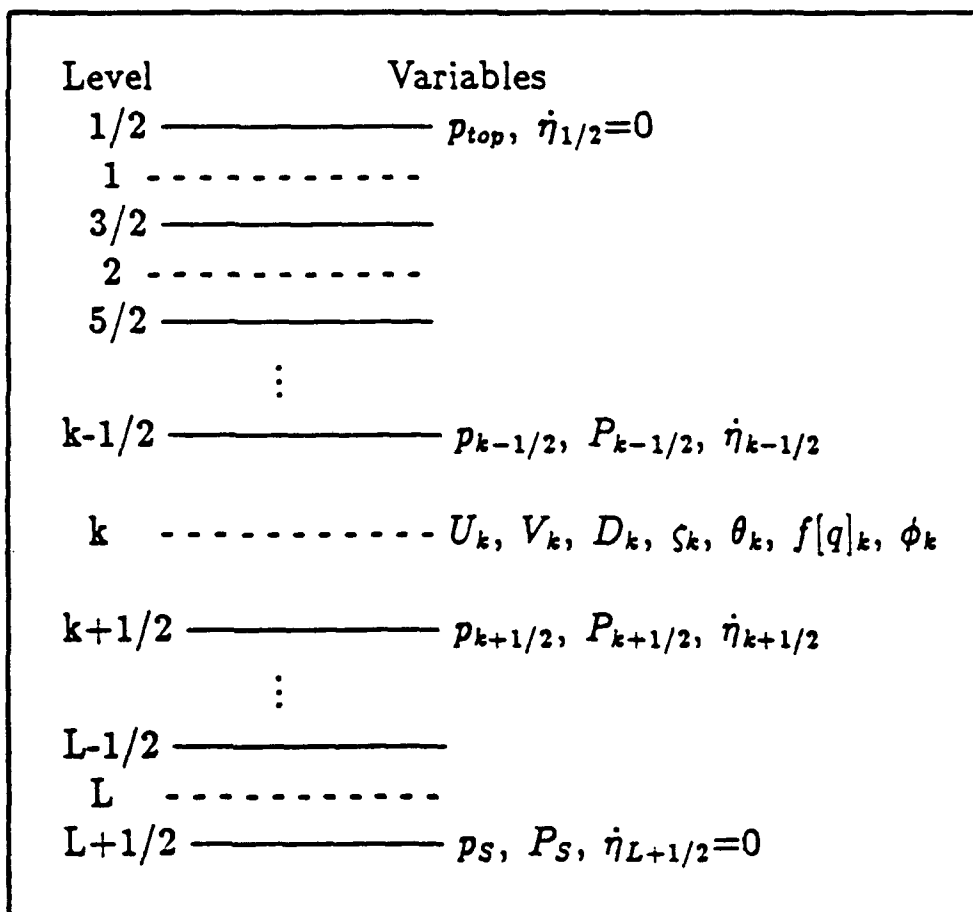


Figure 3.1: The finite difference vertical structure of the forecast model.

The values $A_{k+1/2}$ and $B_{k+1/2}$ are arbitrary except at the top and the bottom where they must satisfy the boundary conditions given by (2.2):

$$\left. \begin{aligned} A_{1/2} &= p_{top} \\ A_{L+1/2} &= p_{top} \\ B_{1/2} &= 0 \\ B_{L+1/2} &= 1 \end{aligned} \right\}. \quad (3.2)$$

In NOGAPS, p_{top} is set to 1 mb. The discrete values for $A(\eta)$ and $B(\eta)$ are given in Table 3.1. At present the hybrid coordinate is a sigma-like coordinate system.

The virtual potential temperature θ , the moisture function $f[q]$, the geopotential ϕ , the cosine weighted velocities U and V , the vorticity ζ , and the divergence D are evaluated at the full levels, and their discrete values are indicated by: θ_k , $f(q_k)$, ϕ_k , U_k , V_k , ζ_k , and D_k respectively (see Figure 3.1). From (2.1), we compute the pressure depth for the k^{th} layer as:

$$\Delta p_k = \Delta A_k + \Delta B_k \pi, \quad (3.3)$$

where

$$\Delta A_k = A_{k+1/2} - A_{k-1/2},$$

$$\Delta B_k = B_{k+1/2} - B_{k-1/2}.$$

At the half pressure level, we compute the function P as:

$$P_{k+1/2} = \left(\frac{p_{k+1/2}}{p_0} \right)^\kappa \quad (3.4)$$

In order to compute the temperature from the virtual potential temperature, P must also be defined at the full levels. The definition of P_k is that given by Phillips (1974), which has the form

$$P_k = \frac{1}{(\kappa + 1)p_0^\kappa} \left(\frac{p_{k+1/2}^{\kappa+1} - p_{k-1/2}^{\kappa+1}}{p_{k+1/2} - p_{k-1/2}} \right). \quad (3.5)$$

Table 3.1. The discrete values of the functions $A(\eta)$ and $B(\eta)$.

Level	A	B
1/2	1.000000	0.000000
3/2	1.000000	0.015947
5/2	1.000000	0.039867
7/2	1.000000	0.071761
9/2	1.000000	0.111628
11/2	1.000000	0.159468
13/2	1.000000	0.215282
15/2	1.000000	0.279070
17/2	1.000000	0.350831
19/2	1.000000	0.435382
21/2	1.000000	0.527741
23/2	1.000000	0.622923
25/2	1.000000	0.715947
27/2	1.000000	0.801827
29/2	1.000000	0.875581
31/2	1.000000	0.932226
33/2	1.000000	0.966777
35/2	1.000000	0.989369
37/2	1.000000	1.000000

This form is exact for an isentropic atmosphere as demonstrated by Tokioka (1978). We calculate the pressure values at the full levels by taking the values of P_k in (3.5) and inverting the definition (2.12), which gives the result

$$p_k = p_0 P_k^{1/\kappa}. \quad (3.6)$$

In order to compute the right hand sides of (2.7) and (2.8) for $\dot{\pi}$ and $[\dot{\eta} \partial p / \partial \eta]$ respectively, we must vertically integrate the velocity and the mass divergence. In performing these integrals, we assume that the velocities are constant in the layer Δp_k . With this assumption, the right hand side of (2.7) is computed as

$$\frac{\partial \pi}{\partial t} = - \sum_{l=1}^L [\Delta A_l D_l + \Delta B_l M_l]. \quad (3.7)$$

The quantities D_l and M_l are the layer l values of the divergence and mass divergence:

$$D_l = \nabla \cdot \mathbf{u}_l, \quad (3.8)$$

$$M_l = \nabla \cdot (\pi \mathbf{u}_l). \quad (3.9)$$

We integrate (2.8) by using the same integration strategy as we used in the derivation of (3.7), so the vertical motion is given at the half levels by

$$\left[\dot{\eta} \frac{\partial p}{\partial \eta} \right]_{k+1/2} = B_{k+1/2} \sum_{l=1}^L (\Delta A_l D_l + \Delta B_l M_l) - \sum_{l=1}^k (\Delta A_l D_l + \Delta B_l M_l). \quad (3.10)$$

Note that (3.10) satisfies the boundary conditions given by (2.6), namely:

$$\left[\dot{\eta} \frac{\partial p}{\partial \eta} \right]_{1/2} = \left[\dot{\eta} \frac{\partial p}{\partial \eta} \right]_{L+1/2} = 0. \quad (3.11)$$

The half pressure level values for U , V , and θ are also needed to evaluate the vertical advection terms for the vorticity, divergence, and temperature equations. The finite difference form of the vertical advection term that is consistent with the

flux conserving form is given by Haltiner and Williams (1980) as

$$\begin{aligned} \left(\left[\dot{\eta} \frac{\partial p}{\partial \eta} \right] \frac{\partial X}{\partial p} \right)_k &= \left[\dot{\eta} \frac{\partial p}{\partial \eta} \right]_{k+1/2} \left(\frac{X_{k+1/2} - X_k}{\Delta p_k} \right) \\ &+ \left[\dot{\eta} \frac{\partial p}{\partial \eta} \right]_{k-1/2} \left(\frac{X_k - X_{k-1/2}}{\Delta p_k} \right), \end{aligned} \quad (3.12)$$

where X represents any dynamic variable. The choice of the interpolated values of X is crucial to the energy conservation of the vertical finite difference scheme. The interpolation that conserves the square of X is given by

$$X_{k+1/2} = \left(\frac{X_k + X_{k+1}}{2} \right). \quad (3.13)$$

We use the interpolation given by (3.13) for the velocities, $U_{k+1/2}$ and $V_{k+1/2}$. With (3.13) we now write the vertical finite difference forms for (2.25)–(2.27) and (2.27)–(2.33) as

$$\begin{aligned} G_k &= U_k(\zeta + f) + \left[\dot{\eta} \frac{\partial p}{\partial \eta} \right]_{k+1/2} \left(\frac{V_{k+1} - V_k}{2\Delta p_k} \right) + \left[\dot{\eta} \frac{\partial p}{\partial \eta} \right]_{k-1/2} \left(\frac{V_k - V_{k-1}}{2\Delta p_k} \right) \\ &+ c_p \theta_k \left(\frac{\partial P}{\partial \pi} \right)_k \frac{\partial \pi \cos^2 \varphi}{\partial \mu a^2} - Q_{V_k} \frac{\cos \varphi}{a}, \end{aligned} \quad (3.14)$$

$$\begin{aligned} H_k &= V_k(\zeta + f) - \left[\dot{\eta} \frac{\partial p}{\partial \eta} \right]_{k+1/2} \left(\frac{U_{k+1} - U_k}{2\Delta p_k} \right) - \left[\dot{\eta} \frac{\partial p}{\partial \eta} \right]_{k-1/2} \left(\frac{U_k - U_{k-1}}{2\Delta p_k} \right) \\ &- \frac{c_p \theta_k}{a^2} \left(\frac{\partial P}{\partial \pi} \right)_k \frac{\partial \pi}{\partial \lambda} + Q_{U_k} \frac{\cos \varphi}{a}, \end{aligned} \quad (3.15)$$

$$I_k = \left(\frac{U_k^2 + V_k^2}{2} \right) \frac{a^2}{\cos^2 \varphi}, \quad (3.16)$$

$$\zeta_k = \alpha(V_k, -U_k), \quad (3.17)$$

$$D_k = \alpha(U_k, V_k), \quad (3.18)$$

$$\frac{\partial \zeta_k}{\partial t} = -\alpha(G_k, H_k), \quad (3.19)$$

and

$$\frac{\partial D_k}{\partial t} = \alpha(H_k, -G_k) - \nabla^2(\phi_k + I_k). \quad (3.20)$$

In order to calculate (3.14) and (3.15), we must evaluate the term $(\partial P / \partial \pi)_k$. This is done by inserting the definition (3.1) of $p_{k+1/2}$ into the definition of P_k given by (3.5) and differentiating with respect to π . The final result is

$$\frac{\partial P_k}{\partial \pi} = \left[\frac{B_{k+1/2} (P_{k+1/2} - P_k) + B_{k-1/2} (P_k - P_{k-1/2})}{\Delta p_k} \right], \quad (3.21)$$

where we have used the definitions of P_k and $P_{k+1/2}$ in order to simplify the final relation.

We vertically integrate the hydrostatic equation (2.14) to obtain the geopotential field ϕ_k . The result above the surface layer (*i.e.* $1 \leq k < L$) is

$$\phi_{k+1} - \phi_k = -c_p \theta_{k+1/2} (P_{k+1} - P_k); \quad (3.22)$$

and in the surface layer the geopotential is computed as

$$\phi_L = \phi_S + c_p \theta_L (P_{L+1/2} - P_L), \quad (3.23)$$

where ϕ_S is the surface geopotential given by gz_S .

The vertical finite difference formulation of the virtual potential temperature equation (2.13) is given by

$$\begin{aligned} \frac{\partial \theta_k}{\partial t} = & -\mathbf{u}_k \cdot \nabla (\theta_k) - \left[\dot{\eta} \frac{\partial p}{\partial \eta} \right]_{k+1/2} \left(\frac{\theta_{k+1/2} - \theta_k}{\Delta p_k} \right) \\ & - \left[\dot{\eta} \frac{\partial p}{\partial \eta} \right]_{k-1/2} \left(\frac{\theta_k - \theta_{k-1/2}}{\Delta p_k} \right) + Q_{\theta_k}. \end{aligned} \quad (3.24)$$

We determine the interpolation formula for θ on the half level pressure surfaces by computing the total energy and requiring that the adiabatic vertical finite difference equations conserve energy. In the following discussion we again draw heavily from the work of Haltiner and Williams (1980). In the layer Δp_k , the kinetic energy is defined as

$$K_{E_k} = \Delta p_k \left(\frac{u_k^2 + v_k^2}{2} \right). \quad (3.25)$$

We compute the kinetic energy equation by first formulating the vertical finite difference equations for u and v , which are given by (2.21) and (2.22), and multiplying the u_k and v_k equations by $\Delta p_k u_k$ and $\Delta p_k v_k$, respectively. The result, with the right and left hand sides of the kinetic energy equation having been switched, is

$$\begin{aligned} \mathcal{G}_{K_{E_k}} = & \Delta p_k \frac{\partial}{\partial t} \left(\frac{u_k^2 + v_k^2}{2} \right) + \Delta p_k \mathbf{V}_k \cdot \nabla \left(\frac{u_k^2 + v_k^2}{2} \right) \\ & + \left[\dot{\eta} \frac{\partial p}{\partial \eta} \right]_{k+1/2} \left(\frac{u_{k+1} u_k + v_{k+1} v_k - u_k^2 - v_k^2}{2 \Delta p_k} \right) \\ & - \left[\dot{\eta} \frac{\partial p}{\partial \eta} \right]_{k-1/2} \left(\frac{u_{k-1} u_k + v_{k-1} v_k + u_k^2 + v_k^2}{2 \Delta p_k} \right). \end{aligned} \quad (3.26)$$

The term $\mathcal{G}_{K_{E_k}}$ is the generation of kinetic energy, which is composed of the terms

$$\mathcal{G}_{K_{E_k}} = -\Delta p_k \mathbf{u}_k \cdot \nabla \phi_k - \Delta p_k c_p \theta_k \left(\frac{\partial P_k}{\partial \pi} \right) \mathbf{u}_k \cdot \nabla \pi + \Delta p_k \mathbf{u}_k \cdot \mathbf{Q}_{\mathbf{u}_k}. \quad (3.27)$$

The vertical finite difference form for the pressure equation (2.5) is

$$\frac{\partial}{\partial t} (\Delta p_k) + \nabla \cdot (\mathbf{u}_k \Delta p_k) + \left[\dot{\eta} \frac{\partial p}{\partial \eta} \right]_{k+1/2} - \left[\dot{\eta} \frac{\partial p}{\partial \eta} \right]_{k-1/2} = 0. \quad (3.28)$$

By multiplying Equation (3.28) by $(u_k^2 + v_k^2)/2$ and adding this result to Equation (3.26) we obtain the final result, which in flux form is

$$\frac{\partial K_{E_k}}{\partial t} + \nabla \cdot (\mathbf{u}_k K_{E_k}) + \mathcal{F}_{K_{E_{k+1/2}}} - \mathcal{F}_{K_{E_{k-1/2}}} = \mathcal{G}_{K_{E_k}}, \quad (3.29)$$

where $\mathcal{F}_{K_{E_{k+1/2}}}$ are the vertical fluxes,

$$\mathcal{F}_{K_{E_{k+1/2}}} = \left[\dot{\eta} \frac{\partial p}{\partial \eta} \right]_{k+1/2} \left(\frac{u_{k+1} u_k + v_{k+1} v_k}{2} \right). \quad (3.30)$$

The sum over all levels, together with the integral over the entire sphere, reduces the left hand side to the time derivative of the total kinetic energy of the atmosphere. We simplify the generation term by first integrating by parts the first term of (3.27), and then using Equation (3.28) to obtain the result that

$$\begin{aligned} \mathcal{G}_{K_{E_k}} = & -\nabla \cdot (\mathbf{u}_k \Delta p_k) - \phi_k \left(\frac{\partial \Delta p_k}{\partial t} + \left[\dot{\eta} \frac{\partial p}{\partial \eta} \right]_{k+1/2} - \left[\dot{\eta} \frac{\partial p}{\partial \eta} \right]_{k-1/2} \right) \\ & - \Delta p_k c_p \theta_k \frac{\partial P_k}{\partial \pi} \mathbf{u}_k \cdot \nabla \pi. \end{aligned} \quad (3.31)$$

Adding and subtracting the term,

$$\left[\dot{\eta} \frac{\partial p}{\partial \eta} \right]_{k+1/2} \phi_{k+1/2} - \left[\dot{\eta} \frac{\partial p}{\partial \eta} \right]_{k-1/2} \phi_{k-1/2}$$

to the right hand side of (3.31) and using the definition of Δp_k given by (3.3), we obtain

$$\begin{aligned} \mathcal{G}_{K_{E_k}} = & -\nabla \cdot (\mathbf{u}_k \Delta p_k) - \phi_k (B_{k+1/2} - B_{k-1/2}) \frac{\partial \pi}{\partial t} \\ & - \left(\left[\dot{\eta} \frac{\partial p}{\partial \eta} \right]_{k+1/2} \phi_{k+1/2} - \left[\dot{\eta} \frac{\partial p}{\partial \eta} \right]_{k-1/2} \phi_{k-1/2} \right) \\ & + \left[\dot{\eta} \frac{\partial p}{\partial \eta} \right]_{k+1/2} (\phi_{k+1/2} - \phi_k) - \left[\dot{\eta} \frac{\partial p}{\partial \eta} \right]_{k-1/2} (\phi_k - \phi_{k-1/2}) \\ & - \Delta p_k c_p \theta_k \frac{\partial P_k}{\partial \pi} \mathbf{u}_k \cdot \nabla \pi. \end{aligned} \quad (3.32)$$

The final form is obtained by adding and subtracting the term,

$$(B_{k+1/2} \phi_{k+1/2} - B_{k-1/2} \phi_{k-1/2}) \frac{\partial \pi}{\partial t},$$

to (3.32), with the result

$$\begin{aligned} \mathcal{G}_{K_{E_k}} = & -\nabla \cdot (\mathbf{u}_k \phi_k \Delta p_k) - \left(\left[\dot{\eta} \frac{\partial p}{\partial \eta} \right]_{k+1/2} \phi_{k+1/2} - \left[\dot{\eta} \frac{\partial p}{\partial \eta} \right]_{k-1/2} \phi_{k-1/2} \right) \\ & - (B_{k+1/2} \phi_{k+1/2} - B_{k-1/2} \phi_{k-1/2}) \frac{\partial \pi}{\partial t} + B_{k+1/2} (\phi_{k+1/2} - \phi_k) \frac{\partial \pi}{\partial t} \\ & - B_{k-1/2} (\phi_k - \phi_{k-1/2}) \frac{\partial \pi}{\partial t} + \left[\dot{\eta} \frac{\partial p}{\partial \eta} \right]_{k+1/2} (\phi_{k+1/2} - \phi_k) \\ & - \left[\dot{\eta} \frac{\partial p}{\partial \eta} \right]_{k-1/2} (\phi_k - \phi_{k-1/2}) - \Delta p_k c_p \theta_k \frac{\partial P_k}{\partial \pi} \mathbf{u}_k \cdot \nabla \pi. \end{aligned} \quad (3.33)$$

Note that the first three terms of (3.33) are in flux form, so they integrate to zero over the entire atmosphere.

The derivation of the total potential energy equation (the sum of the internal energy plus the gravitational potential energy) starts with the writing the temperature equation from the potential temperature equation given by (3.24). The virtual

temperature is related to the virtual potential temperature by

$$\theta_k = \frac{T_k}{P_k}, \quad (3.34)$$

and therefore we write the virtual temperature equation as

$$\begin{aligned} & \frac{\partial T_k}{\partial t} + \mathbf{u}_k \cdot \nabla (T_k) \\ & + \left[\dot{\eta} \frac{\partial p}{\partial \eta} \right]_{k+1/2} \left(\frac{T_{k+1/2} - T_k}{\Delta p_k} \right) + \left[\dot{\eta} \frac{\partial p}{\partial \eta} \right]_{k-1/2} \left(\frac{T_k - T_{k-1/2}}{\Delta p_k} \right) \\ & = \theta_k \frac{\partial P_k}{\partial \pi} \left[\frac{\partial}{\partial t} + \mathbf{u}_k \cdot \nabla \right] (\pi) + \left[\dot{\eta} \frac{\partial p}{\partial \eta} \right]_{k+1/2} \left(\frac{T_{k+1/2} - P_k \theta_{k+1/2}}{\Delta p_k} \right) \\ & + \left[\dot{\eta} \frac{\partial p}{\partial \eta} \right]_{k-1/2} \left(\frac{P_k \theta_{k-1/2} - T_{k-1/2}}{\Delta p_k} \right) + Q_{\Theta_k}, \end{aligned} \quad (3.35)$$

where we have added the term,

$$\left[\dot{\eta} \frac{\partial p}{\partial \eta} \right]_{k+1/2} \left(\frac{T_{k+1/2}}{\Delta p_k} \right) - \left[\dot{\eta} \frac{\partial p}{\partial \eta} \right]_{k-1/2} \left(\frac{T_{k-1/2}}{\Delta p_k} \right)$$

to both sides of Equation (3.35). The total potential energy in the layer Δp_k is defined by

$$P_{E_k} = c_p T_k \Delta p_k. \quad (3.36)$$

We obtain the equation for P_{E_k} by multiplying Equation (3.35) by $c_p \Delta p_k$ and multiplying Equation (3.28) by $c_p T_k$, and then adding the resultant equations. The final result is

$$\frac{\partial P_{E_k}}{\partial t} + \nabla \cdot (\mathbf{u}_k P_{E_k}) + \mathcal{F}_{P_{E_{k+1/2}}} - \mathcal{F}_{P_{E_{k-1/2}}} = \mathcal{G}_{P_{E_k}}. \quad (3.37)$$

The vertical fluxes $\mathcal{F}_{P_{E_{k+1/2}}}$ are defined by

$$\mathcal{F}_{P_{E_{k+1/2}}} = \left[\dot{\eta} \frac{\partial p}{\partial \eta} \right]_{k+1/2} (c_p T_{k+1/2}), \quad (3.38)$$

and the generation of total potential energy is given by

$$\mathcal{G}_{P_{E_k}} = c_p \theta_k \Delta p_k \frac{\partial P_k}{\partial \pi} \left[\frac{\partial}{\partial t} + \mathbf{u}_k \cdot \nabla \right] (\pi)$$

$$\begin{aligned}
& + \left[\dot{\eta} \frac{\partial p}{\partial \eta} \right]_{k+1/2} (T_{k+1/2} - P_k \theta_{k+1/2}) \\
& + \left[\dot{\eta} \frac{\partial p}{\partial \eta} \right]_{k-1/2} (P_k \theta_{k-1/2} - T_{k-1/2}) + c_p \Delta p_k Q_{\theta_k}. \quad (3.39)
\end{aligned}$$

We obtain the equation for total energy by adding (3.29) and (3.37), and then summing over all levels and integrating over λ and φ . By comparing the generation terms given by Equations (3.33) and (3.39), we observe that, in order to conserve total energy, the following three terms must match in the $\mathcal{G}_{K_{E_k}}$ equation and in the $\mathcal{G}_{P_{E_k}}$ equation:

$$\phi_{k+1/2} - \phi_k = c_p (T_{k+1/2} - P_k \theta_{k+1/2}), \quad (3.40)$$

$$\phi_k - \phi_{k-1/2} = c_p (P_k \theta_{k-1/2} - T_{k-1/2}), \quad (3.41)$$

and

$$B_{k+1/2} (\phi_{k+1/2} - \phi_k) - B_{k-1/2} (\phi_k - \phi_{k-1/2}) = c_p \theta_k \Delta p_k \frac{\partial P_k}{\partial \pi}. \quad (3.42)$$

Equations (3.40) and (3.41) are equivalent to the hydrostatic equation (3.22). This can be seen by solving Equation (3.41) for $\phi_{k+1/2}$ (by changing the index k to $k+1$) and substituting the result into Equation (3.40). We rewrite the third condition, (3.42), using the results of (3.21), (3.40), and (3.41) to obtain the result that

$$\begin{aligned}
& B_{k+1/2} (T_{k+1/2} - P_k \theta_{k+1/2}) - B_{k-1/2} (P_k \theta_{k-1/2} - T_{k-1/2}) \\
& = B_{k+1/2} \theta_k (P_{k+1/2} - P_k) + B_{k-1/2} \theta_k (P_k - P_{k-1/2}). \quad (3.43)
\end{aligned}$$

Equation (3.43) will be satisfied if the following two relations hold:

$$T_{k+1/2} - P_k \theta_{k+1/2} = \theta_k (P_{k+1/2} - P_k) \quad (3.44)$$

and

$$P_k \theta_{k-1/2} - T_{k-1/2} = \theta_k (P_k - P_{k-1/2}). \quad (3.45)$$

Solving Equation (3.45) for $T_{k+1/2}$ and substituting into Equation (3.44), we obtain the necessary interpolation form for $\theta_{k+1/2}$:

$$\theta_{k+1/2} = \theta_k \left(\frac{P_{k+1/2} - P_k}{P_{k+1} - P_k} \right) + \theta_{k+1} \left(\frac{P_{k+1} - P_{k+1/2}}{P_{k+1} - P_k} \right). \quad (3.46)$$

Note that $\theta_{k+1/2}$ is a nonlinear interpolation of the function P . This interpolation is a price one must pay to ensure that the vertical finite differencing conserves total energy.

We write the vertical finite difference form for the moisture equation (2.15) as

$$\begin{aligned} \frac{\partial f[q]_k}{\partial t} = & -\mathbf{u}_k \cdot \nabla (f[q]_k) - \left[\dot{\eta} \frac{\partial p}{\partial \eta} \right]_{k+1/2} \left\{ \frac{f[q]_{k+1/2} - f[q]_k}{\Delta p_k} \right\} \\ & - \left[\dot{\eta} \frac{\partial p}{\partial \eta} \right]_{k-1/2} \left\{ \frac{f[q]_k - f[q]_{k-1/2}}{\Delta p_k} \right\} + Q_{f(q_k)}. \end{aligned} \quad (3.47)$$

We chose the interpolation formula of $f[q]$ that is a linear interpolation in P , namely:

$$f[q]_{k+1/2} = f[q]_{k+1} \left(\frac{P_{k+1/2} - P_k}{P_{k+1} - P_k} \right) + f[q]_k \left(\frac{P_{k+1} - P_{k+1/2}}{P_{k+1} - P_k} \right). \quad (3.48)$$

This interpolation does not formally conserve q , so it may not be appropriate for climate simulations.

Equations (3.7), (3.10), (3.14)–(3.20), (3.22)–(3.24), and (3.47) are the equations for the discrete vertical fields of the model. In the next chapter we discuss the spectral representation of the fields, the transformation between the variable's grid point and its spectral representation, and the computation of the horizontal derivatives.

Chapter 4

The Spectral Expansions

In this chapter we first derive the spectral representation of the field variables and discuss the nature of the corresponding Gaussian grid point values. In the following section the spectral filtering of the terrain field is briefly discussed.

4.1 The Spectral Expansion of the Variables

The π , ζ_k , D_k , θ_k , and $f(q_k)$ fields are the dynamic variables of the forecast model. They are expanded in terms of spherical harmonics, which are the associated Legendre polynomials, $P_n^m(\mu)$ multiplied by the complex Fourier series, $e^{im\lambda}$. The subscript n is the total wavenumber. The series are truncated assuming a triangular truncation with M indicating the total number of resolvable waves. At present, NOGAPS 3.2 has a spectral resolution of 79. The spectral expansion of any variable X is written as

$$X(\lambda, \mu, t) = \sum_{m=-M}^M \sum_{n=|m|}^M X_n^m(t) P_n^m(\mu) e^{im\lambda}. \quad (4.1)$$

The spectral coefficients $X_n^m(t)$ are complex and satisfy the condition ensuring that the field X is real:

$$X_n^{-m}(t) = [X_n^m(t)]^*, \quad (4.2)$$

where the asterisk indicates a complex conjugate.

The spectral coefficients are obtained from (4.1) by applying the orthogonality property of the spherical harmonics:

$$X_n^m(t) = \frac{1}{2\pi} \int_{-1}^1 \int_0^{2\pi} X(\lambda, \mu, t) P_n^m(\mu) e^{-im\lambda} d\lambda d\mu. \quad (4.3)$$

The grid point values of the fields are evaluated at points that facilitate the exact evaluation of the sums in Equation (4.1) and the integrals in Equation (4.3). The integral with respect to λ in (4.3) is performed using a fast Fourier transform (FFT). Accordingly, there must be at least $3(M+1)$ evenly spaced, discrete values of λ , which are given by

$$\lambda_l = 2\pi \left[\frac{l}{3(M+1)} \right], \quad l = 1, 3(M+1). \quad (4.4)$$

After the FFT integration, Equation (4.3) can be written in the shorthand form,

$$X_n^m(t) = \int_{-1}^1 \mathcal{F}^m[X](\mu, t) P_n^m(\mu) d\mu, \quad (4.5)$$

where $\mathcal{F}^m[X](\mu, t)$ is the Fourier transform, defined by the integral relation,

$$\mathcal{F}^m[X](\mu, t) = \frac{1}{2\pi} \int_0^{2\pi} X(\lambda, \mu, t) e^{-im\lambda} d\lambda. \quad (4.6)$$

The remaining integration of (4.5) is performed using the method of Gaussian quadrature. This procedure is based on the theorem that, given any polynomial $g(\mu)$, of degree $2n-1$ or less, the integral of g from -1 to 1 is computed exactly as

$$\int_{-1}^1 g(\mu) d\mu = \sum_{j=1}^n w_j g(\mu_j),$$

where μ_j are the roots of the Legendre polynomial $P_n^0(\mu)$ and w_j , are the weights given by

$$w_j = \int_0^\infty e^{-\mu} \prod_{i \neq j}^n \left[\frac{\mu - \mu_i}{\mu_j - \mu_i} \right] d\mu.$$

The roots and the weights are tabulated by Carnahan *et al.* (1969). The integrand in (4.5) can be shown to be a polynomial in μ of degree less than or equal to $3M$, so that the minimum number of latitudinal points needed is $(3M + 1)/2$. These latitudinal points, which are identified by μ_j , are called the Gaussian latitudes. The spectral coefficients are finally evaluated by using the results of the Gaussian quadrature theorem:

$$X_n^m(t) = \sum_{j=1}^{(3M+1)/2} w_j \mathcal{F}^m[X](\mu_j, t) P_n^m(\mu_j). \quad (4.7)$$

The discrete grid point values for the fields, $X_{lj}(t)$, are obtained by evaluating Equation (4.1) at the Gaussian grid points,

$$X_{lj}(t) = \sum_{m=-M}^M \sum_{n=|m|}^M X_n^m(t) P_n^m(\mu_j) e^{im\lambda_l}. \quad (4.8)$$

The summation over m in (4.8) is performed using FFT's. The grid point values of the horizontal derivatives are needed for the calculation of the time tendencies of the dependent variables. The discrete values of the horizontal derivatives are obtained from the expansion (4.1), which we use to obtain

$$\left[\frac{\partial X}{\partial \lambda} \right]_{lj}(t) = \sum_{m=-M}^M \sum_{n=|m|}^M im X_n^m(t) P_n^m(\mu_j) e^{im\lambda_l} \quad (4.9)$$

and

$$\left[\frac{\partial X}{\partial \mu} \right]_{lj}(t) = \sum_{m=-M}^M \sum_{n=|m|}^M X_n^m(t) \left[\frac{\partial P_n^m}{\partial \mu} \right](\mu_j) e^{im\lambda_l}. \quad (4.10)$$

The evaluation of the advection tendency terms requires the computation of the grid point values of the cosine weighted velocities, U_k and V_k . To obtain the

spectral expansions for the velocity components, we first introduce the streamfunction ψ_k and the potential function χ_k . The velocity vector \mathbf{u}_k is expanded in terms of ψ_k and χ_k as

$$\mathbf{u}_k = \nabla \chi_k - \nabla \times (\mathbf{k} \psi_k), \quad (4.11)$$

where \mathbf{k} is the unit vector in the vertical. The vorticity and the divergence are related to the streamfunction and to the velocity potential by the relations

$$\zeta_k = \nabla^2 \psi_k \quad (4.12)$$

and

$$D_k = \nabla^2 \chi_k. \quad (4.13)$$

We obtain the expansions for the cosine weighted velocities, U_k and V_k , from the results of (4.11):

$$U_k = \frac{1}{a^2} \frac{\partial \chi_k}{\partial \lambda} - \frac{\cos^2 \varphi}{a^2} \frac{\partial \psi_k}{\partial \mu}, \quad (4.14)$$

and

$$V_k = \frac{\cos^2 \varphi}{a^2} \frac{\partial \chi_k}{\partial \mu} + \frac{1}{a^2} \frac{\partial \psi_k}{\partial \lambda}. \quad (4.15)$$

The spherical harmonics, $P_n^m(\mu)e^{im\lambda}$, are eigenfunctions of the Laplacian operator, ∇^2 , with the eigenvalues, $-[n(n+1)/a^2]$:

$$\nabla^2 \{P_n^m(\mu)e^{im\lambda}\} = - \left[\frac{n(n+1)}{a^2} \right] P_n^m(\mu)e^{im\lambda}. \quad (4.16)$$

The above eigenvalue equation is used to obtain the relationship of the spectral coefficients of the vorticity and divergence to the coefficients of the streamfunction and the divergence:

$$\zeta_{kn}^m = - \left[\frac{n(n+1)}{a^2} \right] \psi_{kn}^m, \quad (4.17)$$

$$D_{kn}^m = - \left[\frac{n(n+1)}{a^2} \right] \chi_{kn}^m. \quad (4.18)$$

Inserting the spectral expansion of the form given by (4.1) for the streamfunction and the potential function into Equations (4.14) and (4.15) and using the relations (4.17) and (4.18), we obtain the final spectral expansion for the velocity fields as

$$U_k(\lambda, \mu, t) = \sum_{m=-M}^M \sum_{n=|m|}^M \frac{-im}{n(n+1)} D_{kn}^m(t) P_n^m(\mu) e^{im\lambda} + \sum_{m=-M}^M \sum_{n=|m|}^M \frac{\cos^2 \varphi}{n(n+1)} \zeta_{kn}^m(t) \frac{dP_n^m(\mu)}{d\mu} e^{im\lambda}, \quad (4.19)$$

and

$$V_k(\lambda, \mu, t) = \sum_{m=-M}^M \sum_{n=|m|}^M -\frac{-im}{n(n+1)} \zeta_{kn}^m(t) P_n^m(\mu) e^{im\lambda} - \sum_{m=-M}^M \sum_{n=|m|}^M \frac{\cos^2 \varphi}{n(n+1)} D_{kn}^m(t) \frac{dP_n^m(\mu)}{d\mu} e^{im\lambda}. \quad (4.20)$$

The spectral coefficients of the vorticity and the divergence can be obtained from the grid point fields of U_k and V_k by using the spectral representations, which are given by (4.19) and (4.20), the orthogonality of the expansion functions, and the zero boundary conditions of U_k and V_k at the poles. The final form is written

$$\zeta_{kn}^m(t) = \frac{1}{2\pi} \int_0^{2\pi} \int_{-1}^1 \frac{im}{\cos^2 \varphi} V_k(\lambda, \mu, t) P_n^m(\mu) e^{im\lambda} + \frac{1}{2\pi} \int_{-1}^1 \int_{-1}^1 U_k(\lambda, \mu, t) \frac{dP_n^m(\mu)}{d\mu} e^{im\lambda}, \quad (4.21)$$

and

$$D_{kn}^m(t) = \frac{1}{2\pi} \int_0^{2\pi} \int_{-1}^1 \frac{im}{\cos^2 \varphi} U_k(\lambda, \mu, t) P_n^m(\mu) e^{im\lambda} - \frac{1}{2\pi} \int_{-1}^1 \int_{-1}^1 V_k(\lambda, \mu, t) \frac{dP_n^m(\mu)}{d\mu} e^{im\lambda}. \quad (4.22)$$

The above integrals are calculated in the same manner as Equation (4.7).

4.2 Spectral Filters and the Terrain Field

For any field that is expanded in terms of spherical harmonics using Equation (4.1), a spectral average (spectrally smoothed) field, \bar{X} , can be defined as

$$\bar{X}(\lambda, \mu, t) = \sum_{m=-M}^M \sum_{n=|m|}^M \sigma_n X_n^m(t) P_n^m(\mu) e^{im\lambda}. \quad (4.23)$$

The spectral filter coefficients, σ_n , depend only on the total wavenumber n . Different examples of filters are the Sardeshmukh and Hoskins (1984) filter:

$$\sigma_n = \exp - \left[\frac{n(n+1)}{n_0(n_0+1)} \right]^r; \quad (4.24)$$

the Bartlett filter (Jenkins and Watts, 1968, Section 6.3.5):

$$\sigma_n = 1 - \frac{n}{M}; \quad (4.25)$$

the Tukey filter (Jenkins and Watts, 1968):

$$\sigma_n = \frac{1}{2} \left(1 + \cos \frac{\pi n}{M} \right); \quad (4.26)$$

and the Lanczos (1956) filter:

$$\sigma_n = \frac{\sin(n\pi/M)}{n\pi/M}. \quad (4.27)$$

In order to lessen the effect of negative terrain caused by spectral truncation, we apply a spectral filter to the terrain field. Comparisons of the various filters to the unfiltered silhouette terrain are presented in Table 4.1. The results are for a spectral resolution of 47 and the units are in meters. The rms difference is the root mean square difference of the filter to the silhouette terrain. The unfiltered field is the terrain field that has only been spectrally truncated (that is $\sigma_n=1$). It was felt that the Lanczos (1956) filter produced the best results of the filters (4.24)–(4.27); i.e., reducing the negative overshoots of the terrain with the smallest rms difference.

Table 4.1: Comparisons of different filters to the silhouette terrain for a spectral resolution of 47.

Filter Type	Max Height	Min Height	RMS Error
Silhouette	5912.17	0.0	–
Unfiltered	6457.05	-700.80	176.79
Lanczos	5717.10	-93.817	245.89
Sardeshmukh	5241.42	-235.274	333.31
Bartlett	5047.76	3.67	280.80
Tukey	5496.15	-42.2809	275.59

It is of interest to note that the Bartlett filter gives non-negative results but the maximum heights are greatly reduced. The final terrain field used by the model is given by the spectral representation,

$$z_S = \sum_{m=-M}^M \sum_{n=|m|}^M \frac{\sin(n\pi/M)}{n\pi/M} Z_n^m P_n^m(\mu) e^{im\lambda}, \quad (4.28)$$

The unfiltered spectral coefficients, Z_n^m , are obtained from a spectral representation of a silhouette profile of the U.S. Navy's global terrain field, which has a horizontal resolution of 10 minutes.

Chapter 5

Nonlinear Normal Mode

Initialization

The removal of inconsistencies between externally derived initial conditions (as obtained from an objective analysis scheme) and the internal dynamics of the NOGAPS model is achieved through the use of nonlinear normal mode initialization (NNMI), as originally proposed by Machenhauer (1977) and independently by Baer (1977) and Baer and Tribbia (1977). In this section, we derive the normal modes of the NOGAPS model and describe the initialization procedure used to achieve a balanced set of initial data. To accomplish this, we need only consider the adiabatic model equations linearized about some basic state, in a manner analogous to that used in Chapter 7 to derive the semi-implicit time differencing scheme. In general, the basic state that is chosen is a state at rest with a uniform pressure and temperature field given by $p_s = \bar{p}$ and $T = \bar{T}(\eta)$, where p is the pressure at some height, p_s is the surface pressure, $T(\eta)$ is the temperature defined on η -surfaces (η being a hybrid vertical coordinate defined in Chapter 2) and the overbar denotes a suitable horizontal average. Note that the choice $\bar{T} = \bar{T}(\eta)$ differs

from the isothermal basic state used in the semi-implicit scheme. In tests with the NOGAPS model, the former appears to be better suited for use with the NNMI iterative procedure described in Section 5.2. As pointed out by Errico (1987), the mode structures are independent of \bar{p} , but depend significantly on $\bar{T}(\eta)$ in that $\bar{T}(\eta)$ should correspond to a statically stable environment. In the NOGAPS model, $\bar{T}(\eta)$ is taken to be the global mean values of $T(\eta)$ derived from a specified data set. In order to get a limited eigenvalue problem, a separation of the equations into vertical and horizontal structures is sought (Andersen, 1977). The development outlined in this section closely follows that of Errico (1987) and Andersen (1977).

5.1 The Normal Modes of the NOGAPS Model

As in most numerical forecast models, the dependent variables in the NOGAPS model are defined on discrete surfaces as described in Chapter 3. It turns out that it is simpler to describe the derivation of the vertical modes in terms of this discrete structure. Thus, we consider the dependent variables to be column vectors at discrete points whose elements are the dependent variables on the L model η -surfaces ($L=18$); e.g.,

$$\underline{x}(\lambda, \mu) = [x(\mu, \lambda, \eta_1), x(\mu, \lambda, \eta_2), \dots, x(\mu, \lambda, \eta_L)]^T, \quad (5.1)$$

where an underline denotes a column vector with L data elements x . The symbols λ and μ are the longitude and sine of the latitude, respectively, and the superscript T denotes a transpose.

Using the notation in (5.1), we can write the adiabatic, linearized vertically discrete model equations in the form

$$\frac{\partial \underline{\zeta}}{\partial t} = -2\Omega \underline{\mu D} - 2\Omega \underline{V}, \quad (5.2)$$

$$\frac{\partial \underline{D}}{\partial t} = 2\Omega\mu\underline{\zeta} - 2\Omega\underline{U} - \nabla^2 \underline{\Phi}, \quad (5.3)$$

$$\frac{\partial \underline{\theta}}{\partial t} = -\mathbf{A} \underline{D}, \quad (5.4)$$

$$\frac{\partial \pi}{\partial t} = -\mathbf{q}^T \underline{D}, \quad (5.5)$$

where

$\underline{\zeta} = \nabla^2 \underline{\psi}$ is the vertical vorticity,

$\underline{D} = \nabla^2 \underline{\chi}$ is the horizontal divergence,

$\underline{\theta} = T(p_0/\bar{p})^{R/c_p}$ is the potential temperature,

$\pi = \bar{p} - p_{top}$,

$\underline{U} = \underline{u}(\cos \varphi)/a$,

$\underline{V} = \underline{v}(\cos \varphi)/a$,

$p_0 = 1000$ mb,

$\underline{\psi}$ is the streamfunction,

$\underline{\chi}$ is the velocity potential,

$\underline{u}, \underline{v}$ are the horizontal velocity components,

Ω is the angular velocity of the earth,

p_{top} is the pressure at the top of the model,

φ is the latitude,

μ is the $\sin \varphi$,

a is the radius of the earth,

∇^2 is the horizontal Laplacian,

and the operators \mathbf{A} and \mathbf{q} are discussed below.

In the linearized form of the model, the time-tendencies of the velocity fields depend on the thermodynamic fields via the pseudo-geopotential

$$\underline{\Phi} = \underline{\phi}_s + \mathbf{B}\underline{\theta} + \mathbf{c}\pi, \quad (5.6)$$

where $\underline{\phi}_s$ is a vector whose L components are all equal to the terrain geopotential ϕ_s .

Note that in the vertically discrete form, certain operators in (5.4)–(5.6) take the form of matrix or vector operators that closely resemble those derived in Chapter 7 for the semi-implicit time differencing scheme. For the purposes of this discussion, we need only note that

$\mathbf{B} = \mathbf{B}(\bar{T}, \bar{p})$ is an $L \times L$ matrix related to the linearized hydrostatic relation,

$\mathbf{A} = \mathbf{A}(\eta \partial \theta / \partial \eta)$ is an $L \times L$ matrix related to the linearized vertical advection of potential temperature,

$\mathbf{c} = \mathbf{c}(\bar{T}, \bar{p})$ is an L -column vector related to the linearized hydrostatic relation and to the η -coordinate representation of the pressure gradient force,

\mathbf{q} is an L -column vector with elements $\Delta \eta_k$, and is proportional to the discrete form of the integral operator $\int_0^1 d\eta$.

We can differentiate (5.6) with respect to t in order to obtain

$$\frac{\partial \underline{\Phi}}{\partial t} = \mathbf{B} \frac{\partial \underline{\theta}}{\partial t} + \mathbf{c} \frac{\partial \pi}{\partial t}, \quad (5.7)$$

and then use (5.4) and (5.5) to write

$$\frac{\partial \underline{\Phi}}{\partial t} = -\mathbf{S}\underline{D}, \quad (5.8)$$

where

$$\mathbf{S} = (\mathbf{B}\mathbf{A} + \mathbf{c}\mathbf{q}^T) \quad (5.9)$$

is an $L \times L$ matrix. The prognostic equations (5.2), (5.3) and (5.8) form the foundation for the separation of the dependent variables ζ , D and Φ into horizontal and vertical structures.

In the NOGAPS model, the normal mode decomposition of the fields is carried out in terms of the spectral representations of the dependent variables (Chapter 4). Accordingly, we obtain the spectral representations of (5.2), (5.3) and (5.8), by expanding the dependent variables in the form

$$\underline{x}(\lambda, \mu, t) = \sum_{m=-M}^M \sum_{n=|m|}^M \underline{x}_n^m(t) P_n^m(\mu) \exp(im\lambda), \quad (5.10)$$

where \underline{x}_n^m is a column vector of spherical harmonic coefficients, and $P_n^m(\mu)$ is an associated Legendre polynomial of order m and degree n . Because (5.10) is truncated (triangularly) at zonal wave number M ($M=79$), (5.2), (5.3) and (5.8) are transformed into a finite system of ordinary differential equations given by

$$\frac{d}{dt} \underline{\zeta}_n^m = -2\Omega\mu \underline{D}_n^m - 2\Omega \underline{V}_n^m, \quad (5.11)$$

$$\frac{d}{dt} \underline{D}_n^m = 2\Omega\mu \underline{\zeta}_n^m - 2\Omega \underline{U}_n^m + \frac{n(n+1)}{a^2} \underline{\Phi}_n^m, \quad (5.12)$$

$$\frac{d}{dt} \underline{\Phi}_n^m = -\mathbf{S} \underline{D}_n^m. \quad (5.13)$$

The problem obtains a more suitable form after using the definitions

$$\underline{U}_n^m = -\frac{im}{n(n+1)} \underline{D}_n^m - \frac{\epsilon_n^m}{n} \underline{\zeta}_{n-1}^m + \frac{\epsilon_{n+1}^m}{n+1} \underline{\zeta}_{n+1}^m, \quad (5.14)$$

$$\underline{V}_n^m = -\frac{im}{n(n+1)} \underline{\zeta}_n^m + \frac{\epsilon_n^m}{n} \underline{D}_{n-1}^m - \frac{\epsilon_{n+1}^m}{n+1} \underline{D}_{n+1}^m, \quad (5.15)$$

and the recurrence relation

$$\mu x_n^m = \epsilon_n^m x_{n-1}^m + \epsilon_{n+1}^m x_{n+1}^m, \quad (5.16)$$

where

$$\epsilon_n^m = \left[\frac{n^2 - m^2}{4n^2 - 1} \right]^{1/2}, \quad (5.17)$$

to rewrite (5.11)–(5.13) in the form

$$\frac{d}{dt} \underline{\zeta}_n^m = 2\Omega \left[\frac{im}{n(n+1)} \underline{\zeta}_n^m - \epsilon_n^m \left(\frac{n+1}{n} \right) \underline{D}_{n-1}^m - \epsilon_{n+1}^m \left(\frac{n}{n+1} \right) \underline{D}_{n+1}^m \right], \quad (5.18)$$

$$\begin{aligned} \frac{d}{dt} \underline{D}_n^m &= 2\Omega \left[\frac{im}{n(n+1)} \underline{D}_n^m + \epsilon_n^m \left(\frac{n+1}{n} \right) \underline{\zeta}_{n-1}^m + \epsilon_{n+1}^m \left(\frac{n}{n+1} \right) \underline{\zeta}_{n+1}^m \right] \\ &\quad + \frac{n(n+1)}{a^2} \underline{\Phi}_n^m, \end{aligned} \quad (5.19)$$

$$\frac{d}{dt} \underline{\Phi}_n^m = -\mathbf{S} \underline{D}_n^m. \quad (5.20)$$

5.1.1 Vertical structure

The only vertical coupling in (5.18)–(5.20) occurs through the matrix operator \mathbf{S} in (5.20). Thus, the separation of the horizontal and vertical structures is obtained by first computing the eigenvectors of \mathbf{S} . These eigenvectors represent the vertical structures of the normal mode solutions, while the corresponding eigenvalues play the roles of the equivalent depths in a series of shallow water equations. The vertical structures are determined by solving the eigenvalue problem

$$\mathbf{S}\mathbf{Z} = g\mathbf{Z}\mathbf{H}, \quad (5.21)$$

where g is gravity, \mathbf{Z} is a matrix whose columns are the eigenvectors \mathbf{z}_ℓ (i.e., the vertical modes), and \mathbf{H} is a diagonal matrix whose elements are the eigenvalues H_ℓ (i.e., the equivalent depths). In the NOGAPS model, the vertical modes are normalized such that

$$\sum_{k=1}^L z_{k,\ell} z_{k,\ell} \Delta\eta_k = 1, \quad (5.22)$$

for each vertical mode $\ell = 1, \dots, L$, where $z_{k,\ell}$ represents the k th η -level component of the ℓ th vertical mode, and the values $\Delta\eta_k$ are the discrete components of $d\eta$ that

would appear in the vertically continuous form $\int_0^1 \mathbf{z}_\ell \mathbf{z}_\ell d\eta = 1$. It should be noted that, in the NOGAPS model, the vertical modes are not orthogonal in the sense that

$$\sum_{k=1}^L z_{k,j} z_{k,\ell} \Delta\eta_k = 0, \quad \text{for } j \neq \ell, \quad (5.23)$$

is not true in general. Thus, strictly speaking, the vertical modes do not contribute independently to the total variance of the fields. However, the vertical modes do satisfy (5.23) to a very high degree for all but the shallowest equivalent depths, and therefore, are extremely useful in conventional initialization applications; *i.e.*, in controlling spurious high frequency gravity waves that arise due to inconsistencies between analyzed data and the internal dynamics of a numerical model.

A typical set of values of $\bar{T}(\eta)$ for NOGAPS 3.2 is shown in Table 5.1. The corresponding vertical modes \mathbf{z}_ℓ are shown in Figures 5.1–5.6. The values of $\bar{T}(\eta)$ in Table 5.1 are the global mean values at each η -layer obtained from an extended forecast produced by the NOGAPS model. The 18 equivalent depths H_ℓ are also shown in Table 5.1, ordered from largest to smallest. Note that the values range from nearly 10 km for the external ($\ell = 1$) mode to only a few hundredths of a meter for the shallowest internal ($\ell = 18$) mode. Recall that the equivalent depths H_ℓ in Table 5.1, and the vertical modes \mathbf{z}_ℓ in Figures 5.1–5.6, are the eigenvalues and eigenvectors, respectively, of the vertical structure equation (5.21).

The vertical modes of the NOGAPS model shown in Figures 5.1–5.6 are typical of those in other models having similar vertical resolution (*cf.*, Wergen, 1987). In particular, we see that the external mode in Figure 5.1 is equivalent barotropic (*i.e.*, approximately independent of pressure) throughout the depth of the model atmosphere, while vertical modes $\ell = 2$ and $\ell = 3$ exhibit one and two sign changes with height, respectively. It can be seen in Figures 5.2–5.6 that the number of zero crossings for each mode increases by one for successively shallower equivalent

depths. Note that, in general, the shallower modes have their greatest amplitude in the lower troposphere. However, because the modes have been normalized according to (5.22), no meaningful comparison can be made between the amplitudes of different modes at a given vertical level.

Because the vertical eigenvectors form a complete set, a vector of η -surface data values can be expanded in terms of these eigenvectors to obtain a vector of vertical mode coefficients. Thus, the transform, or projection of a dependent variable \underline{x}_n^m onto the vertical modes is given by

$$\hat{x}_n^m = \mathbf{Z}^{-1} \underline{x}_n^m, \quad (5.24)$$

where \hat{x}_n^m represents the transformed vector of vertical mode coefficients and the superscript -1 denotes an inverse. Conversely, the vector of η -surface values can be determined from the vertical mode coefficients via

$$\underline{x}_n^m = \mathbf{Z} \hat{x}_n^m. \quad (5.25)$$

By applying (5.25) to the prognostic equations (5.18)–(5.20), we can transform that set into one describing the tendencies of the vertical mode coefficients. When this is done, (5.18) and (5.19) retain the same form, except that the dependent variables are replaced by the transformed ones. In contrast, the form of (5.20) changes; the new relation is obtained by using (5.25) combined with (5.21) to yield

$$\frac{d}{dt} \hat{\Phi}_n^m = -g \mathbf{H} \hat{D}_n^m. \quad (5.26)$$

Thus, for each vertical mode ℓ , we have

Table 5.1: Values of $\bar{T}(\eta)$ from a 30-day simulation with the NOGAPS model, and the set of equivalent depths H_ℓ , corresponding to the vertical modes in Figures 5.1–5.6. Note that ℓ is a model index for η and \bar{T} , but refers to the ordering of the vertical modes in the case of H .

ℓ	η	p	\bar{T} (K)	H (m)
1	0.008	8.99	229.25	9669.53
2	0.028	28.97	209.14	3224.16
3	0.049	49.95	198.15	801.71
4	0.092	92.91	199.12	308.66
5	0.136	136.86	214.05	130.55
6	0.187	187.81	217.82	63.85
7	0.247	247.75	227.33	40.60
8	0.315	315.69	236.96	21.30
9	0.393	393.61	247.70	11.48
10	0.482	482.52	258.23	6.63
11	0.575	575.43	266.92	3.99
12	0.669	669.33	273.94	2.36
13	0.759	759.24	279.79	1.45
14	0.839	839.16	283.94	0.75
15	0.904	904.10	287.66	0.40
16	0.950	950.05	290.40	0.18
17	0.978	978.02	291.83	0.10
18	0.995	995.01	292.08	0.02

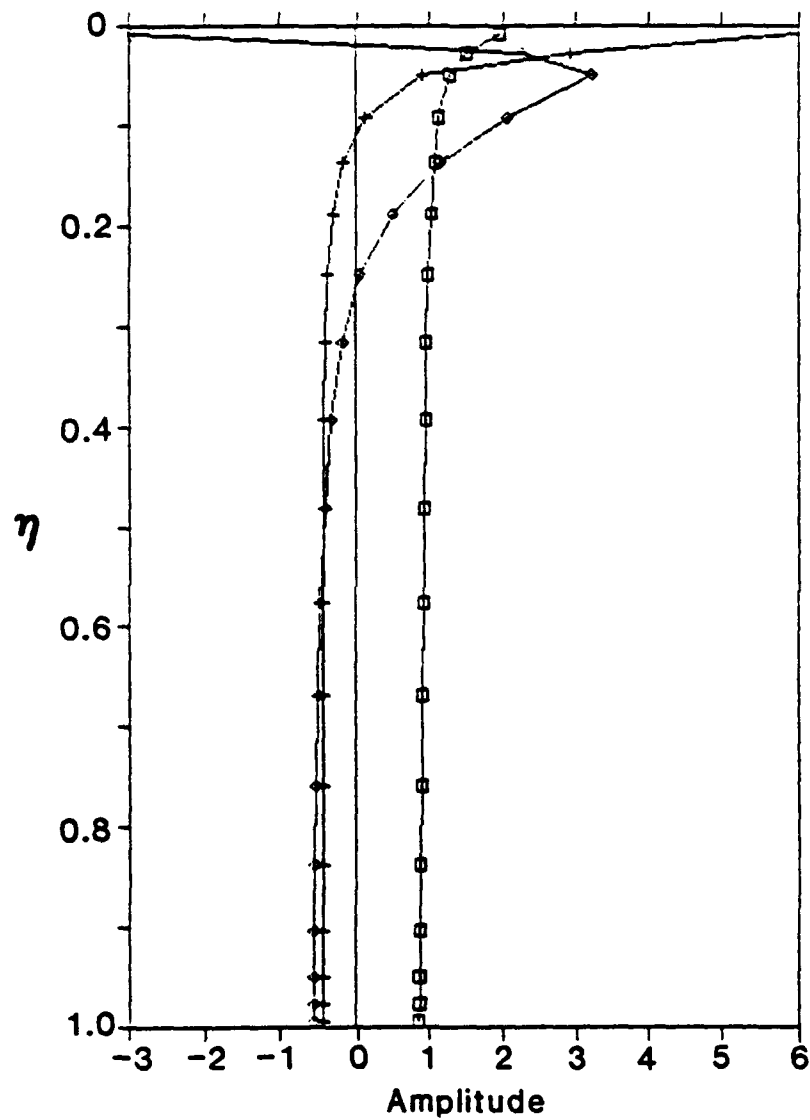


Figure 5.1: The vertical modes of the 18-level NOGAPS model, based on the parameter values in Table 5.1, for vertical modes 1-3.

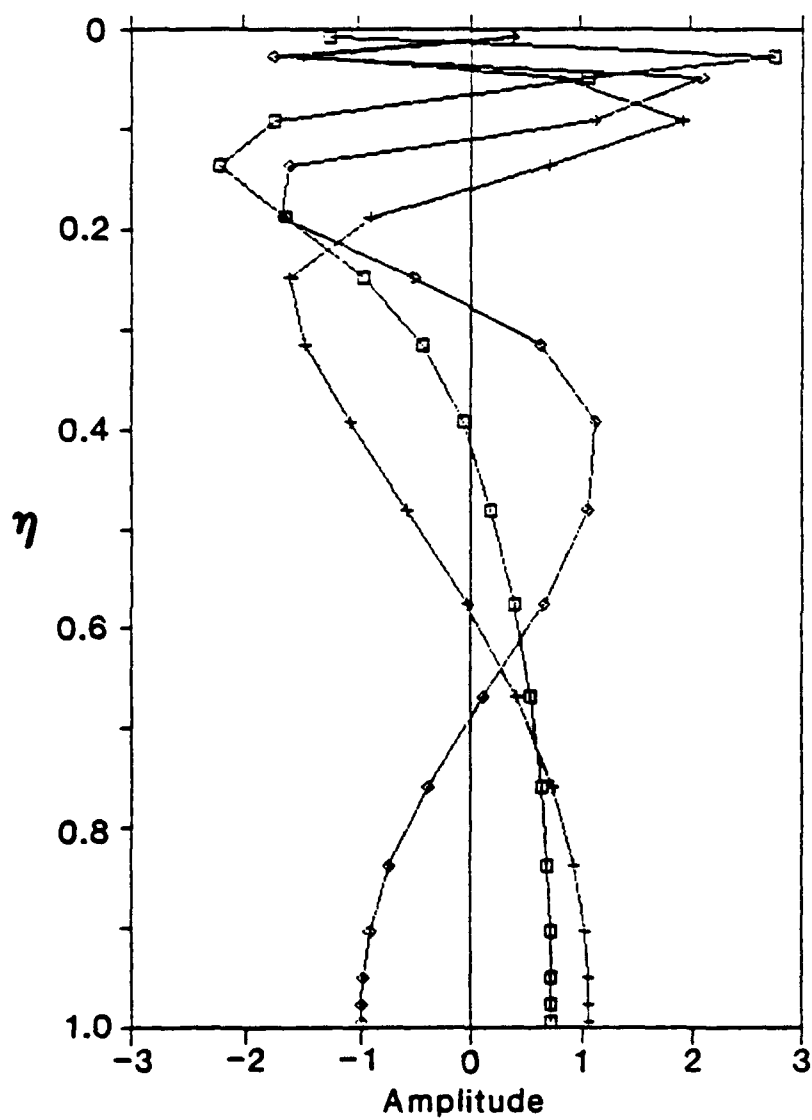


Figure 5.2: The vertical modes of the 18-level NOGAPS model, based on the parameter values in Table 5.1, for vertical modes 4-6.

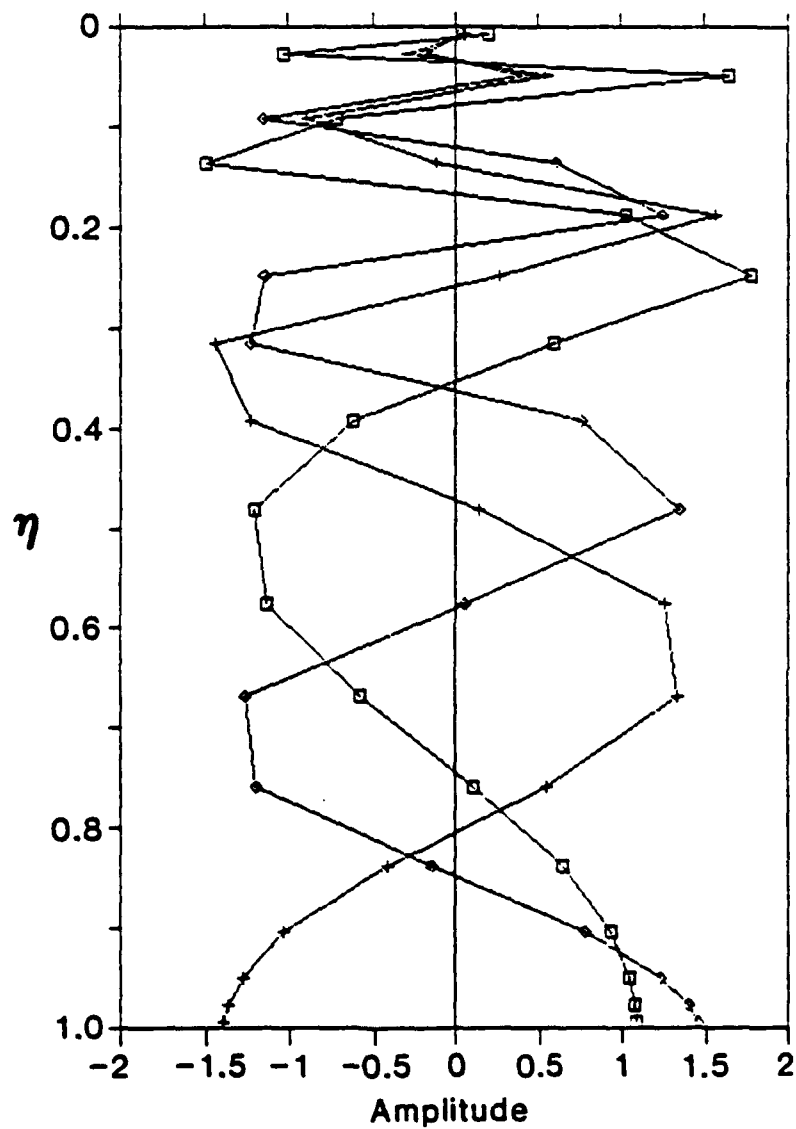


Figure 5.3: The vertical modes of the 18-level NOGAPS model, based on the parameter values in Table 5.1, for vertical modes 7-9.

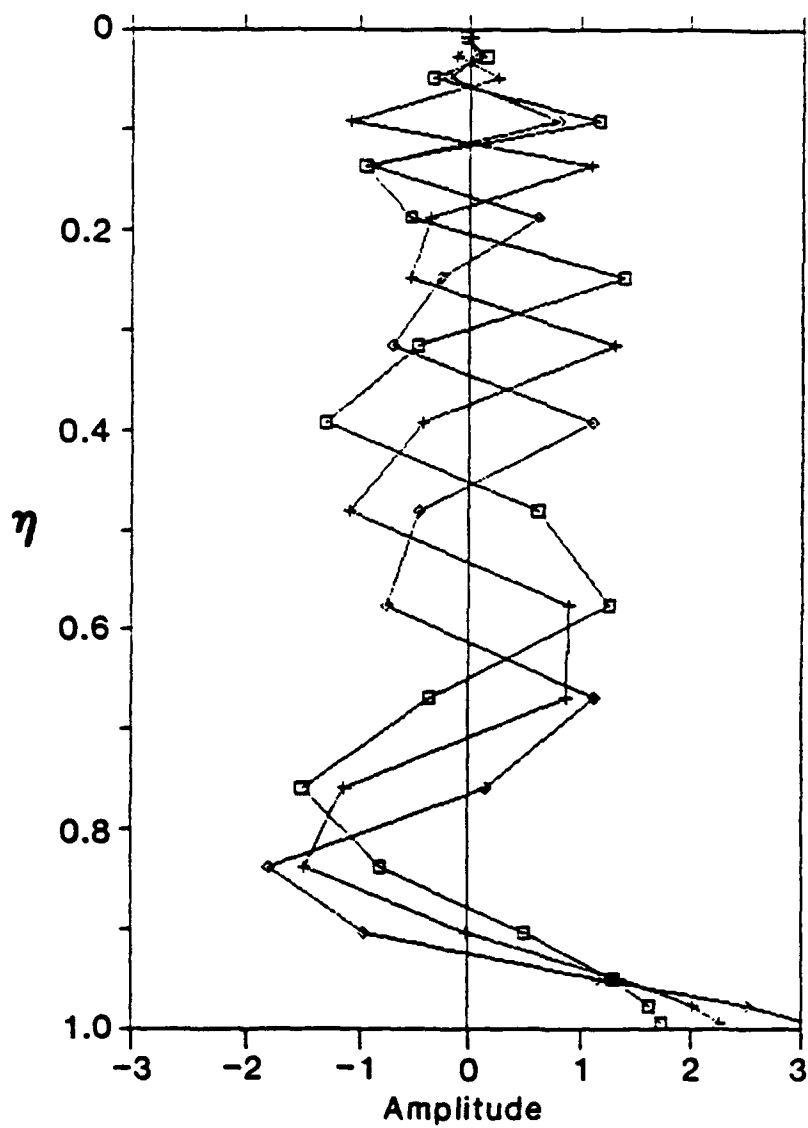


Figure 5.4: The vertical modes of the 18-level NOGAPS model, based on the parameter values in Table 5.1, for vertical modes 10-12.

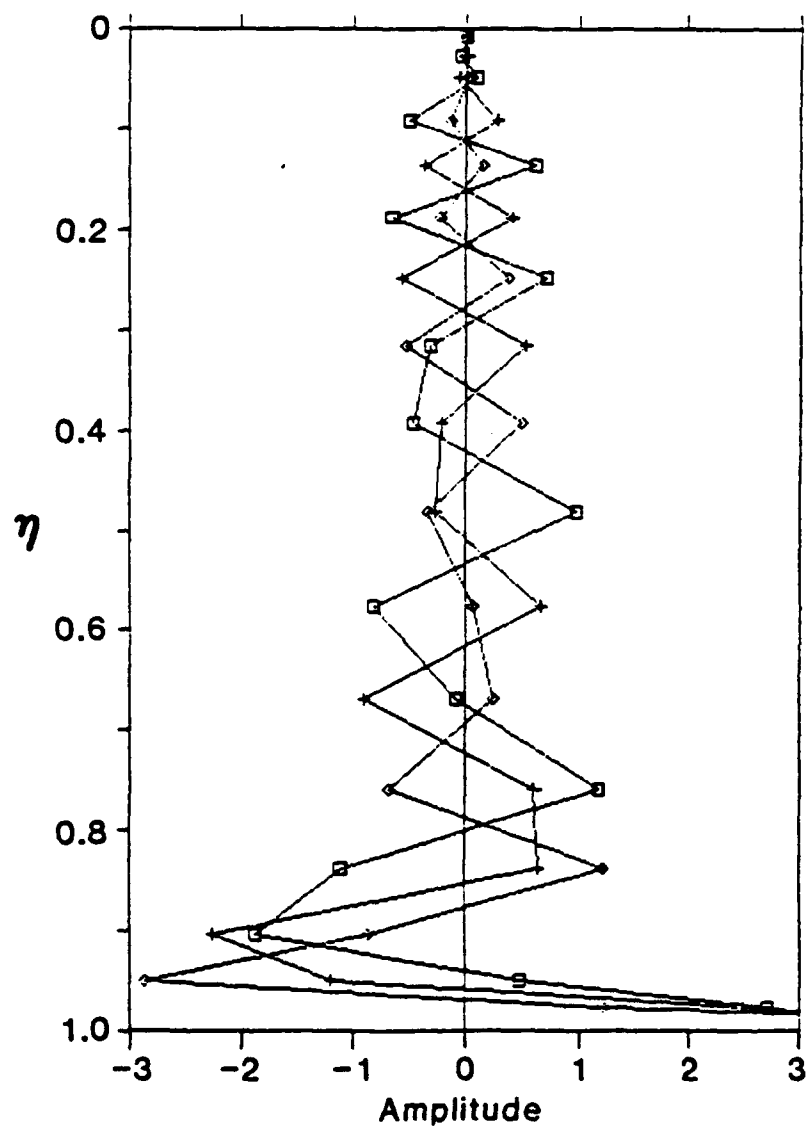


Figure 5.5: The vertical modes of the 18-level NOGAPS model, based on the parameter values in Table 5.1, for vertical modes 13–15.

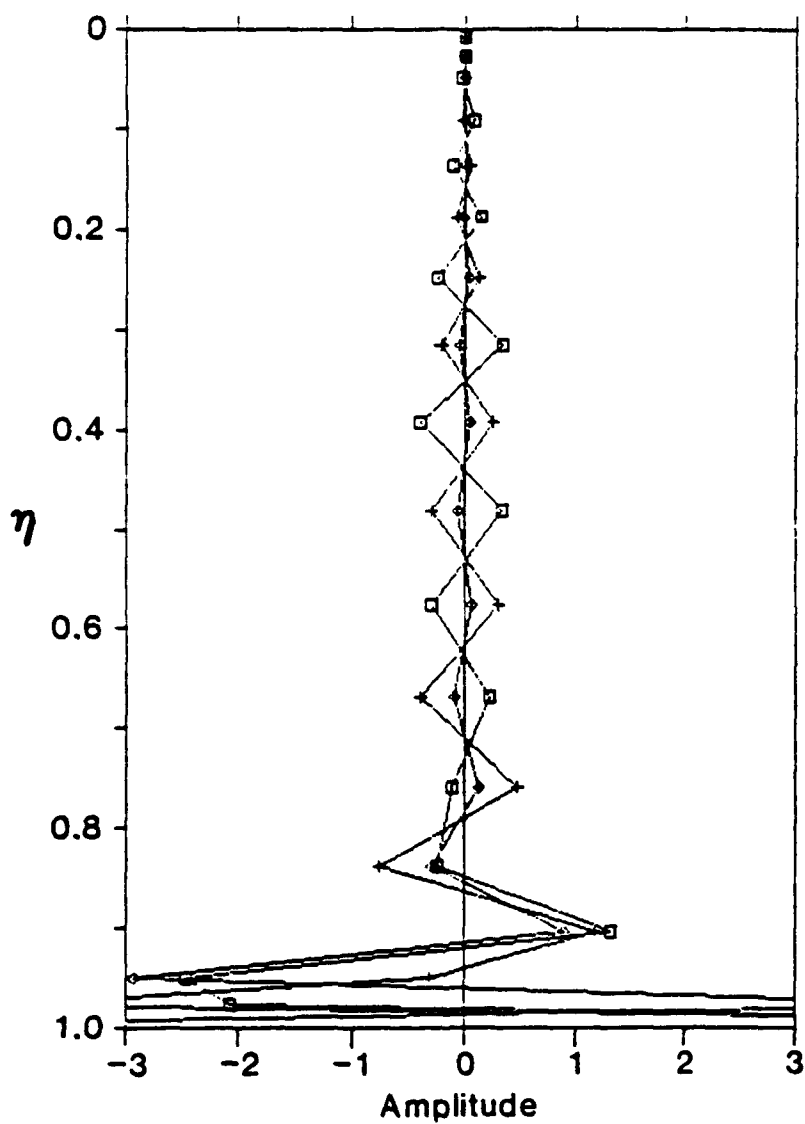


Figure 5.6: The vertical modes of the 18-level NOGAPS model, based on the parameter values in Table 5.1, for vertical modes 16–18.

$$\frac{d}{dt} \hat{\zeta}_{n,\ell}^m = 2\Omega \left[\frac{im}{n(n+1)} \hat{\zeta}_{n,\ell}^m - \epsilon_n^m \left(\frac{n+1}{n} \right) \hat{D}_{n-1,\ell}^m - \epsilon_{n+1}^m \left(\frac{n}{n+1} \right) \hat{D}_{n+1,\ell}^m \right] \quad (5.27)$$

$$\begin{aligned} \frac{d}{dt} \hat{D}_{n,\ell}^m = 2\Omega \left[\frac{im}{n(n+1)} \hat{D}_{n,\ell}^m + \epsilon_n^m \left(\frac{n+1}{n} \right) \hat{\zeta}_{n-1,\ell}^m + \epsilon_{n+1}^m \left(\frac{n}{n+1} \right) \hat{\zeta}_{n+1,\ell}^m \right] \\ + \frac{n(n+1)}{a^2} \hat{\Phi}_{n,\ell}^m, \end{aligned} \quad (5.28)$$

$$\frac{d}{dt} \hat{\Phi}_{n,\ell}^m = -gH_\ell \hat{D}_{n,\ell}^m. \quad (5.29)$$

5.1.2 Horizontal structure

For a given vertical mode ℓ , the system of prognostic equations (5.27)–(5.29) is decoupled from that for any other vertical mode. Each system represents a set of shallow-water equations on a sphere with the corresponding equivalent depth H_ℓ as its scale height. For a given equivalent depth, the horizontal structures of the normal modes are determined from the eigenvectors of this system.

Equations (5.27)–(5.29) obtain a more convenient form if we use the dimensionless forms

$$\begin{aligned} t' &= \Omega t, \\ \hat{\zeta}_n'^m &= \hat{\zeta}_n^m / \Omega, \\ \hat{D}_n'^m &= \hat{D}_n^m / \Omega, \\ \hat{\Phi}_n'^m &= \hat{\Phi}_n^m / \Omega^2 a^2, \end{aligned}$$

and introduce the transformation

$$\tilde{\zeta}_n^m = -h_{n,\ell} \hat{\zeta}_n'^m, \quad (5.30)$$

$$\tilde{D}_n^m = ih_{n,\ell} \hat{D}_n'^m, \quad (5.31)$$

$$\tilde{\Phi}_n^m = \hat{\Phi}_n'^m, \quad (5.32)$$

where

$$h_{n,\ell} = \left(\frac{gH_\ell/\Omega^2 a^2}{n(n+1)} \right)^{1/2}. \quad (5.33)$$

As discussed below, the dependence of the transformation of vorticity and divergence on n in (5.30) and (5.31) enables the prognostic equations to obtain a simple symmetric form well suited for solution as an eigenvalue problem. Note that no such transformation of the pseudo-geopotential is required and that (5.32) is included only for notational consistency. The resulting dimensionless system can thus be written

$$\frac{d}{dt} \tilde{\zeta}_n^m = i[c_n^m \tilde{\zeta}_n^m + a_n^m \tilde{D}_{n-1}^m + a_{n+1}^m \tilde{D}_{n+1}^m], \quad (5.34)$$

$$\frac{d}{dt} \tilde{D}_n^m = i[b_n^m \tilde{\Phi}_n^m + c_n^m \tilde{D}_n^m + a_n^m \tilde{\zeta}_{n-1}^m + a_{n+1}^m \tilde{\zeta}_{n+1}^m], \quad (5.35)$$

$$\frac{d}{dt} \tilde{\Phi}_n^m = i[b_n^m \tilde{D}_n^m], \quad (5.36)$$

where

$$a_0^0 = b_0^0 = c_0^0 = 0, \quad (5.37)$$

and

$$a_n^m = \frac{-2\epsilon_n^m}{n} [(n+1)(n-1)]^{1/2}, \quad (5.38)$$

$$b_n^m = \left[\frac{gH}{\Omega^2 a^2} n(n+1) \right]^{1/2}, \quad (5.39)$$

$$c_n^m = \frac{2m}{n(n+1)}, \quad (5.40)$$

$$\epsilon_n^m = \left[\frac{n^2 - m^2}{4n^2 - 1} \right]^{1/2}, \quad (5.41)$$

for $n > 0$. For convenience, the subscript ℓ is implied, as well as the primes denoting the dimensionless quantities.

Equations (5.34)–(5.36) separate into independent sets for each zonal wave number m . Thus, m may be considered a parameter of the problem, as is H_ℓ , and may be dropped as a superscript unless otherwise necessary. Furthermore, it turns

out that for each m , (5.34)–(5.36) separate into two independent systems: one in which there are only even values of $(n - m)$ for \tilde{D}_n^m and $\tilde{\Phi}_n^m$ and odd values for $\tilde{\zeta}_n^m$, and one in which the even and odd conditions are reversed. These two systems are called the *symmetric* and *antisymmetric* cases, respectively, in reference to the symmetries of the dependent variables about the equator. Note that the reference to the symmetry of the fields about the equator should not be confused with the symmetric form of the equations themselves, which occurs in both cases.

For the symmetric case, (5.34)–(5.36) may be written in the form

$$\frac{d\tilde{\mathbf{x}}_S}{dt} = i\mathbf{M}_S\tilde{\mathbf{x}}_S, \quad (5.42)$$

where the subscript S denotes the symmetric case and $\tilde{\mathbf{x}}_S$ is the vector

$$\tilde{\mathbf{x}}_S = (\tilde{\Phi}_0, \tilde{D}_0, \tilde{\zeta}_1, \tilde{\Phi}_2, \tilde{D}_2, \tilde{\zeta}_3, \dots, \tilde{\Phi}_{N-2}, \tilde{D}_{N-2}, \tilde{\zeta}_{N-1})^T, \quad (5.43)$$

and \mathbf{M}_S is the matrix

$$\mathbf{M}_S = \begin{pmatrix} 0 & b_0 & 0 & 0 & 0 & 0 & \dots & 0 & 0 & 0 \\ b_0 & c_0 & a_1 & 0 & 0 & 0 & \dots & 0 & 0 & 0 \\ 0 & a_1 & c_1 & 0 & a_2 & 0 & \dots & 0 & 0 & 0 \\ 0 & 0 & 0 & 0 & b_2 & 0 & \dots & 0 & 0 & 0 \\ 0 & 0 & a_2 & b_2 & c_2 & a_3 & \dots & 0 & 0 & 0 \\ 0 & 0 & 0 & 0 & a_3 & c_3 & \dots & 0 & 0 & 0 \\ \vdots & \vdots & \vdots & \vdots & \vdots & \vdots & & \vdots & \vdots & \vdots \\ 0 & 0 & 0 & 0 & 0 & 0 & \dots & 0 & b_{N-2} & 0 \\ 0 & 0 & 0 & 0 & 0 & 0 & \dots & b_{N-2} & c_{N-2} & a_{N-1} \\ 0 & 0 & 0 & 0 & 0 & 0 & \dots & 0 & a_{N-1} & c_{N-1} \end{pmatrix}. \quad (5.44)$$

The single subscripts in (5.43) and (5.44) denote values of $(n - m)$ and the superscript m is implied. The value N denotes the truncation size associated with zonal

wave number m , which for a triangular truncation at wave number $m = M$ is given by $N = M - |m| + 1$. Thus, the truncation size N decreases with increasing zonal wave number m , such that $N = M + 1$ for $m = 0$, $N = M$ for $m = 1$, $N = M - 1$ for $m = 2$, and so on, down to $N = 1$ for $m = M$. The relationship between the truncation size N and the order of the matrix \mathbf{M}_S is discussed below. It should be noted that the last element of $\tilde{\mathbf{x}}_S$ in (5.43) has been described for the case when N is even; when N is odd the last element of $\tilde{\mathbf{x}}_S$ is \tilde{D}_{N-1} . Similarly, the matrix \mathbf{M}_S has been described for the case when N is even, otherwise the last row and column will have forms like the next-to-last row and column in (5.44).

For the antisymmetric case, (5.34)–(5.36) may be written in the form

$$\frac{d\tilde{\mathbf{x}}_A}{dt} = i\mathbf{M}_A\tilde{\mathbf{x}}_A, \quad (5.45)$$

where the subscript A denotes the antisymmetric case and $\tilde{\mathbf{x}}_A$ is the vector

$$\tilde{\mathbf{x}}_A = (\tilde{\zeta}_0, \tilde{\Phi}_1, \tilde{D}_1, \tilde{\zeta}_2, \tilde{\Phi}_3, \tilde{D}_3, \dots, \tilde{\zeta}_{N-2}, \tilde{\Phi}_{N-1}, \tilde{D}_{N-1})^T, \quad (5.46)$$

and \mathbf{M}_A is the matrix

$$\mathbf{M}_A = \begin{pmatrix} c_0 & 0 & a_1 & 0 & 0 & 0 & \dots & 0 & 0 & 0 \\ 0 & 0 & b_1 & 0 & 0 & 0 & \dots & 0 & 0 & 0 \\ a_1 & b_1 & c_1 & a_2 & 0 & 0 & \dots & 0 & 0 & 0 \\ 0 & 0 & a_2 & c_2 & 0 & a_3 & \dots & 0 & 0 & 0 \\ 0 & 0 & 0 & 0 & 0 & b_3 & \dots & 0 & 0 & 0 \\ 0 & 0 & 0 & a_3 & b_3 & c_3 & \dots & 0 & 0 & 0 \\ \vdots & \vdots & \vdots & \vdots & \vdots & \vdots & & \vdots & \vdots & \vdots \\ 0 & 0 & 0 & 0 & 0 & 0 & \dots & c_{N-2} & 0 & a_{N-1} \\ 0 & 0 & 0 & 0 & 0 & 0 & \dots & 0 & 0 & b_{N-1} \\ 0 & 0 & 0 & 0 & 0 & 0 & \dots & a_{N-1} & b_{N-1} & c_{N-1} \end{pmatrix}. \quad (5.47)$$

As before, the last element of $\tilde{\mathbf{x}}_A$ in (5.46) has been described for the case when N is even; when N is odd the last element of $\tilde{\mathbf{x}}_A$ is $\tilde{\zeta}_{N-1}$. Similarly, the matrix \mathbf{M}_A has been described for the case when N is even, otherwise the last row and column will have forms like the *second-to-last* row and column in (5.47).

The order of the matrix \mathbf{M} for a given value of m is given by the sum of the gravitational components (equal to the number of geopotential and divergence elements) plus the rotational components (equal to the number of vorticity elements) in the state vector $\tilde{\mathbf{x}}$. Recalling that $N = M - |m| + 1$, and following Andersen (1977), we compute the number of gravity modes N_{grav} for zonal wave number m by the formulae

$$N_{grav} = \begin{cases} 2[(N+1)/2] & \text{symmetric} \\ 2[N/2] & \text{antisymmetric} \end{cases}, \quad (5.48)$$

and the number of rotational modes N_{rot} by the formula

$$N_{rot} = \begin{cases} N/2 & \text{symmetric} \\ (N+1)/2 & \text{antisymmetric} \end{cases}, \quad (5.49)$$

where the symbol “//” denotes integer division. Thus, the order N_{ord} of the matrix \mathbf{M} is

$$N_{ord} = \begin{cases} 2[(N+1)/2] + N/2 & \text{symmetric} \\ 2[N/2] + (N+1)/2 & \text{antisymmetric} \end{cases}. \quad (5.50)$$

It should be noted that for the zonally symmetric ($m = 0$) fields there arises a formal problem in defining the components $\tilde{\zeta}_0^0$, \tilde{D}_0^0 and $\tilde{\Phi}_0^0$. The components $\tilde{\zeta}_0^0$ and \tilde{D}_0^0 correspond to zero-valued velocity fields, and thus, have no physical significance. The component $\tilde{\Phi}_0^0$ corresponds to the horizontal mean geopotential field so that data will, in general, have a non-zero projection onto this mode. However, rather than reduce the order of the matrix \mathbf{M} for $m = 0$, we simply set the corresponding elements to zero (as shown in (5.37)) since the remaining meaningful components

are mapped invariant by the matrix (Andersen, 1977). Thus, we retain the formula in (5.50) for all m and simply note that, for $m = 0$, the number of gravity modes is reduced by two in the symmetric case, while the number of rotational modes is reduced by one in the antisymmetric case. A formal treatment of these special modes is given in Errico (1987).

The horizontal structures of the modes are given by the eigenvectors of \mathbf{M} , which we determine from the eigenvalue problem

$$\mathbf{M}\mathbf{E} = \mathbf{E}\mathbf{W}, \quad (5.51)$$

where \mathbf{E} is a matrix whose columns are the horizontal eigenvectors \mathbf{e}_j (*i.e.*, the horizontal modes), \mathbf{W} is a diagonal matrix whose elements are the eigenvalues ω_j (*i.e.*, the frequencies of the modes), and the subscript j denotes a particular mode. Note that there is a *unique* horizontal eigenvector \mathbf{e}_j for each mode. The normal mode solutions to (5.34)–(5.36) take the form

$$\tilde{\mathbf{x}} = \alpha_j \mathbf{e}_j \exp(i\omega_j t), \quad (5.52)$$

where α_j is the time-dependent amplitude coefficient, or normal mode coefficient. Again, the subscripts ℓ and m are implied; *i.e.*, each mode is uniquely identified by a triplet of indices (ℓ, m, j) .

Because the matrices (5.44) and (5.47) are real and symmetric, all α and \mathbf{e} are real-valued. For a given equivalent depth, all the modes corresponding to $m \neq 0$ are orthonormal in the sense that

$$\langle \mathbf{e}_i, \mathbf{e}_j \rangle = \begin{cases} 1 & \text{for } i = j, \\ 0 & \text{for } i \neq j, \end{cases} \quad (5.53)$$

where the operation on the left side denotes a vector inner-product. For $m = 0$ the rotational modes are stationary and degenerate having $\alpha_j = 0$. The eigenvectors

corresponding to these eigenvalues are not uniquely determined, and thus, are not orthogonal in the sense of (5.53). However, this problem is of little relevance within the context of conventional nonlinear normal mode initialization since we seek to balance only the gravitational components of the flow. Methods for dealing with this ambiguity are discussed by Kasahara (1978) and by Errico (1987).

For $m \neq 0$, the modes can be ordered from smallest to largest according to their frequencies ω_j , and then divided into three separate bands corresponding to the three types of modes. In the NOGAPS model, the smallest third in this sequence are negative-valued, and correspond to eastward propagating inertia-gravity modes (EG modes) in the linearized model. These include the Kelvin modes, which are low frequency eastward propagating gravity modes. The middle third of the frequencies for each zonal wave number are positive valued and correspond to rotational, or Rossby modes (RT modes), while the largest third in this ordering corresponds to the westward propagating inertia-gravity modes (WG modes). For increasing values of m , the number of modes decreases by three from $3(M + 1)$ —or $(M + 1)$ of each type—for $m = 0$, down to 3—or one of each type—for $m = M$, including those for the symmetric and antisymmetric cases together.

Finally, in a manner analogous to (5.24) and (5.25), the projection of the state vector, or vertical mode coefficients, $\tilde{\mathbf{x}}$, onto the normal modes is given by

$$\alpha = \mathbf{E}^T \tilde{\mathbf{x}}, \quad (5.54)$$

where α is a vector containing the N normal mode amplitude coefficients corresponding to vertical mode ℓ and zonal wave number m , and $\mathbf{E}^T = \mathbf{E}^{-1}$ owing to the symmetric form of the matrix \mathbf{M} . Conversely, the vertical mode coefficients can be expanded in terms of the normal modes via

$$\tilde{\mathbf{x}} = \mathbf{E}\alpha. \quad (5.55)$$

5.2 Adiabatic Initialization: Machenhauer's Method

The unforced, nonlinear equations for the NOGAPS model can be written in the general form

$$\frac{d\tilde{\mathbf{x}}}{dt} = i\mathbf{M}\tilde{\mathbf{x}} + \mathcal{N}, \quad (5.56)$$

where \mathcal{N} represents the nonlinear contributions to the tendencies, which were omitted in the determination of the normal modes. We obtain the normal mode form of (5.56) by transforming $\tilde{\mathbf{x}}$ according to (5.54) and then applying (5.51), which yields

$$\frac{d\alpha}{dt} = i\mathbf{W}\alpha + \mathcal{R}, \quad (5.57)$$

where $\mathcal{R} = \mathbf{E}^T \mathcal{N}$. Thus, for mode j we have

$$\frac{d\alpha_j}{dt} = i\omega_j\alpha_j + \mathcal{R}_j, \quad (5.58)$$

where again ω_j is the frequency of the mode in the *linearized* model determined as an eigenvalue of the matrix \mathbf{M} . The nonlinear term \mathcal{R}_j generally depends on modes other than α_j alone, and thereby acts to couple the linear modes in the nonlinear model (Errico, 1987).

The aim of the initialization procedure is to eliminate dynamic imbalances in the initial data that lead to unrealistically large gravity mode oscillations during the early part of a model forecast. Machenhauer (1977) proposed the balance condition

$$\frac{d\alpha_j}{dt} = 0, \quad (5.59)$$

initially for all gravity modes, based on scaling arguments regarding the magnitudes of the terms in (5.58). It is clear from (5.58) that balance is thus obtained when the mode amplitude satisfies

$$\alpha_j = -\mathcal{R}_j/i\omega_j. \quad (5.60)$$

As (5.60) is a nonlinear equation, Machenhauer proposed an iterative solution

$$\alpha_j^{(n+1)} = -\mathcal{R}_j^{(n)} / i\omega_j, \quad (5.61)$$

where the superscript (n) denotes an iteration number and $\mathcal{R}_j^{(n)}$ is computed from data in terms of $\alpha_j^{(n)}$. In its present form, (5.61) is extremely cumbersome owing to the difficulty in deriving the expression $\mathcal{R}_j^{(n)}$ for each new set of coefficients. However, it obtains a far more convenient form if we use (5.58) to substitute for $\mathcal{R}_j^{(n)}$, giving

$$\Delta\alpha_j^{(n)} = \alpha_j^{(n+1)} - \alpha_j^{(n)} = -\frac{1}{i\omega_j} \frac{d\alpha_j^{(n)}}{dt}, \quad (5.62)$$

where $\Delta\alpha_j^{(n)}$ is the nonlinear correction to the mode amplitude. The advantage of this approach is that we may now use the forecast model to compute the nonlinear term $\mathcal{R}_j^{(n)}$ implicitly as the difference between the mode tendency and its linear forcing. The term $d\alpha_j^{(n)}/dt$ may be approximated by first computing $\alpha_j^{(n)}(t_0)$, and then making a short forecast (say, one model time step) to obtain $\alpha_j^{(n)}(t_0 + \Delta t)$ and the tendency

$$\frac{d\alpha_j^{(n)}}{dt} \approx \frac{\alpha_j^{(n)}(t_0 + \Delta t) - \alpha_j^{(n)}(t_0)}{\Delta t}, \quad (5.63)$$

where t_0 refers to the initial conditions and Δt is a small time-step. In practice this procedure is further simplified by taking a model step and then transforming the *tendencies* of the dependent variables directly into normal mode space, rather than transforming data from two time levels. Thus, the term $d\alpha_j^{(n)}/dt$ is analyzed in terms of the actual time-differencing scheme used in the model. In NOGAPS, a forward time step is used for the first iteration and centered time steps are used thereafter.

The convergence of the iterative scheme is monitored by computing the squared sum of the tendencies of the *initialized* coefficients, as introduced by Andersen (1977). This quantity is usually computed for each vertical mode ℓ after each

iteration, and may be written

$$\text{BAL}_\ell = \sum_{j \in G_\ell} \frac{d\alpha_j}{dt} \frac{d\alpha_j}{dt}^* , \quad (5.64)$$

where the asterisk denotes a complex conjugate and G_ℓ is the set of initialized gravity modes pertaining to vertical mode ℓ . The closer BAL is to zero, the closer the initial data are to the desired balance. Experience with NOGAPS shows that, for a conventional adiabatic initialization, two or three iterations of (5.62) are sufficient for obtaining values of BAL that may be considered zero at half precision machine accuracy. Of course, the number of iterations required to obtain $\text{BAL} \approx 0$, or more importantly, the likelihood of (5.62) converging, depends strongly on the number of modes initialized. The number of vertical modes initialized operationally in NOGAPS 3.2 as well as the determination of the subset G_ℓ , is discussed in Section 5.3.

5.2.1 Rasch's scheme

As an alternative to (5.62), Rasch (1985) proposed an iterative scheme that generally converges for a larger subset of modes than does the Machenhauer scheme. Although it is not used operationally at the present time, this scheme is an available option in NOGAPS that may be invoked by simply resetting a parameter value. In the Rasch scheme, the balance condition (5.59) is the same, but (5.62) is replaced by

$$\Delta\alpha_j^{(n)} = -\beta \left(\frac{\alpha_j^{(n)} - \alpha_j^{(n-1)}}{\dot{\alpha}_j^{(n)} - \dot{\alpha}_j^{(n-1)}} \right) \frac{d\alpha_j^{(n)}}{dt} , \quad (5.65)$$

where the overdots in the denominator denote time derivatives and β is a relaxation coefficient that controls the rate of convergence. Typical values of β are in the range $0.5 \leq \beta \leq 1$. Because (5.65) requires coefficients from two time levels, the values for $n = 1$ are obtained by using a drastically under-relaxed Machenhauer step of

the form

$$\alpha_j^{(1)} = \alpha_j^{(0)} - \frac{\varepsilon}{i\omega_j} \frac{d\alpha_j^{(0)}}{dt}, \quad (5.66)$$

where ε is a small number; *e.g.*, $\varepsilon = 0.05$ has been used successfully in the NOGAPS model. By comparison with (5.62), we can view the parenthesized quantity

$$\frac{\dot{\alpha}_j^{(n)} - \dot{\alpha}_j^{(n-1)}}{\alpha_j^{(n)} - \alpha_j^{(n-1)}} = i\omega_e, \quad (5.67)$$

that appears in (5.65) as an empirically derived frequency for a given normal mode (Rasch, 1985). Note that the denominator of this quantity represents a potential singularity and, under certain conditions, might need to be replaced by some nonzero number. This is discussed in more detail by Rasch (1985). Finally, it should be noted that the Rasch scheme may be particularly useful in NNMI applications that require robust convergence properties, such as initializing many vertical modes or including diabatic forcing terms on the right side of (5.58).

5.2.2 Correction of the prognostic variables

After each iteration, the corrections $\Delta\alpha$ to the mode coefficients must be transformed back to "model space" (*e.g.*, spherical harmonic coefficients in the case of NOGAPS) and then added to the fields before computing the next set of tendencies. Accordingly, we perform the inverse horizontal and vertical transforms (see Sections 5.1.1 and 5.1.2) on $\Delta\alpha$ to obtain the corrections $\Delta\zeta_n^m$, ΔD_n^m and $\Delta\Phi_n^m$. At this point, the corrections to the vorticity and divergence fields can be applied in a straightforward manner by simply adding $\Delta\zeta_n^m$ and ΔD_n^m to ζ_n^m and D_n^m , respectively.

The remaining problem is to extract the corrections to the pressure and potential temperature fields from $\Delta\Phi_n^m$. To accomplish this, we make use of (5.13), which states that the divergence may be expressed solely in terms of the time change

of the pseudo-geopotential as

$$\underline{D}_n^m = -\mathbf{S}^{-1} \frac{d}{dt} \underline{\Phi}_n^m . \quad (5.68)$$

The time change of the pressure field can thus be expressed in terms of the time change of the pseudo-geopotential by combining (5.68) with the spectral form of (5.5) to obtain

$$\frac{d}{dt} \pi_n^m = \mathbf{p} \frac{d}{dt} \underline{\Phi}_n^m , \quad (5.69)$$

where $\mathbf{p} = \mathbf{q}^T \mathbf{S}^{-1}$ is an L -vector whose elements depend on linear operators described in Section 5.1. Then from (5.69), it follows that the correction to the surface pressure is given by

$$\Delta \pi_n^m = \mathbf{p} \Delta \underline{\Phi}_n^m . \quad (5.70)$$

In the same manner, the time change of the potential temperature field may be expressed in terms of the time change of the pseudo-geopotential by combining (5.68) with the spectral form of (5.4) to obtain

$$\frac{d}{dt} \theta_n^m = \mathbf{T} \frac{d}{dt} \underline{\Phi}_n^m , \quad (5.71)$$

where $\mathbf{T} = \mathbf{A} \mathbf{S}^{-1}$ is an $L \times L$ matrix. From (5.71), it follows that the correction to the potential temperature is given by

$$\Delta \theta_n^m = \mathbf{T} \Delta \underline{\Phi}_n^m . \quad (5.72)$$

Having obtained $\Delta \zeta_n^m$, $\Delta \underline{D}_n^m$, $\Delta \theta_n^m$ and $\Delta \pi_n^m$, we adjust the values of each prognostic variable accordingly, and then take a model step to obtain a new set of tendencies for the next iteration of (5.62). The process is repeated until $\text{BAL}_t \approx 0$ for all vertical modes initialized (or until some pre-specified number of iterations is performed), indicating that the initial values of ζ_n^m , \underline{D}_n^m , θ_n^m and π_n^m have obtained the desired state of balance.

5.3 Summary of the NOGAPS NNMI

Procedure

NOGAPS 3.2's NNMI is configured to initialize three vertical modes $\ell = 1-3$ (*i.e.*, the external and first two internal modes) using the Machenhauer iterative scheme (5.62). Two iterations of (5.62) are performed, not including the calculations of the initial tendencies at $n = 0$. In addition to a vertical mode cutoff at $\ell = 3$, a frequency cut-off is employed that restricts the subset of initialized modes G_ℓ to those with natural periods less than 24 hours (as determined from their linear frequencies ω). The cutoff values for ℓ and ω were determined empirically and appear to eliminate most of the undesired initial gravity wave noise without severely damaging meteorologically significant divergent circulations. This is especially crucial for preserving the character of certain tropical circulations. Future research with NOGAPS's NNMI will be aimed at improving the initialization of these circulations through, for example, the inclusion of diabatic processes in (5.58) or more specialized choices of G_ℓ .

The sequence of operations performed during NOGAPS's NNMI is summarized below. In the following, we denote the model data corresponding to time t and iteration n by $x^{(n)}(t)$. The sequence of operations is as follows:

0. Set $n = 0$ to begin the procedure with the uninitialized data $x^{(0)}(t_0)$.
1. Perform a nonlinear model step to determine $dx^{(n)}/dt$ from $x^{(n)}(t_0)$.
2. Transform $dx^{(n)}/dt$ into $d\alpha^{(n)}/dt$ using (5.7), (5.24), (5.30)–(5.32) and (5.54).
Check for convergence using (5.64).
3. Compute the corrections to the mode amplitudes $\Delta\alpha^{(n)}$ from $d\alpha^{(n)}/dt$ using (5.62).

4. Transform $\Delta\alpha^{(n)}$ into corrections in “model space” $\Delta x^{(n)}$ using (5.55), (5.30)–(5.32), (5.25), (5.70) and (5.72).
5. Apply the corrections to the model fields, where the corrected values are given by $x_C^{(n)}(t_0) = x^{(n)}(t_0) + \Delta x^{(n)}$.
6. Set $x^{(n)}(t_0) = x_C^{(n)}(t_0)$ and $n = n + 1$. If $n < 2$ (or some other pre-specified number of iterations), then return to step (1). Otherwise, the corrected values $x^{(n)}(t_0)$ represent the initialized data at t_0 and the procedure is complete.

Chapter 6

The Time Step Integration Strategy

In this chapter we present an overall view of the numerical procedures that are used to compute the time tendencies of the dynamical variables. In the subsequent chapters we describe the details of the adiabatic calculations (Chapter 7), the implicit adjustments (Chapter 7), the horizontal smoothing (Chapter 8), and the diabatic calculations (Chapters 9-14).

A schematic diagram of the NOGAPS 3.2 forecast system is presented in Figure 6.1. The forecast model saves 3 time levels of spectral coefficients corresponding to the previous time level ($t-\Delta t$), the current time level (t), and the spectral time tendency for π , ζ_k , D_k , θ_k , and $f[q_k]$. The time tendency is computed using central differencing:

$$\frac{\partial X}{\partial t} = \frac{X(t + \Delta t) - X(t - \Delta t)}{2\Delta t}, \quad (6.1)$$

where X represents any variable. In addition, we store the spectral coefficients of the potential temperature tendency due to radiation, since the radiative parameterizations are not called every time step. As opposed to the spectral coefficients,

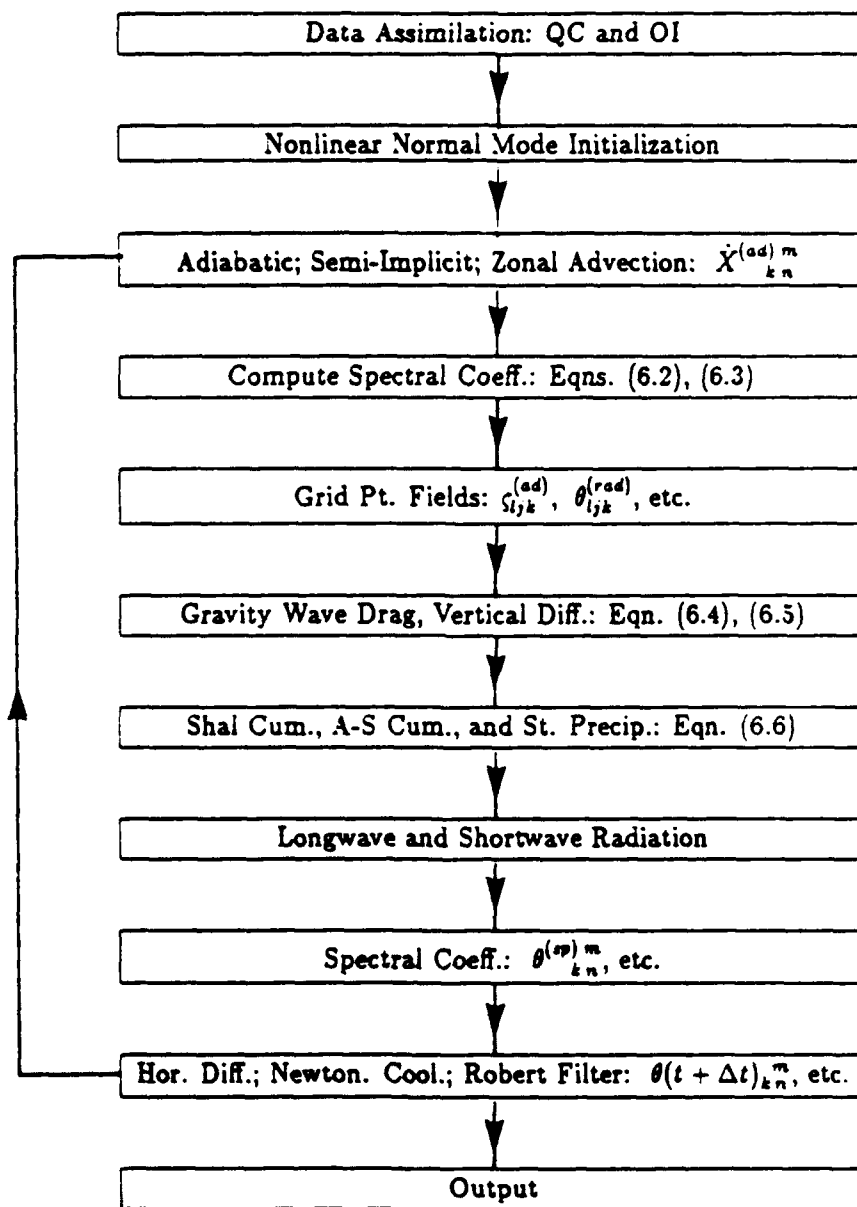


Figure 6.1: A schematic flow chart of NOGAPS 3.2 numerical computations.

however, we store only 1 time level of the Gaussian grid point fields: π , ζ_k , D_k , U_k , V_k , θ_k , $f[q_k]$, P_k , and $P_{k+1/2}$.

The forecast cycle begins with the adiabatic calculations, which use either (at the first time step) the nonlinear normal mode initialization adjustments (described in Chapter 5) to the optimum interpolation analysis fields interpolated to the model coordinates, or (for all subsequent time steps) the results from the previous time step. The fields, π , ζ_k , D_k , θ_k , and $1/\ln[q]_k$ are the dynamical variables of the forecast model and their dynamical equations are given respectively by (3.7), (3.17), (3.18), (3.24), and (3.47). These tendencies are computed explicitly using the fields evaluated at the central time. The details of the adiabatic calculations are given in Chapter 7. We adjust the explicit adiabatic tendencies of π , D_k , and θ_k by treating gravity wave propagation semi-implicitly (Chapter 7), and we modify the explicit adiabatic tendencies of ζ_k and $f[q]_k$ by treating the zonal advection implicitly (Chapter 7). After the above calculations, we compute the adiabatic spectral coefficients at time $t+\Delta t$ for π , $1/\ln[q]_k$, ζ_k and D_k as (X representing π , D_k , ζ_k , or $1/\ln[q]_k$)

$$X^{(ad)}_n(t + \Delta t) = X^n_n(t - \Delta t) + 2\Delta t \dot{X}^{(ad)}_n(t). \quad (6.2)$$

The superscript (*ad*) indicates that the tendency term is from the adiabatic calculations and the $t+\Delta t$ fields are evaluated using only these adiabatic tendencies. The spectral coefficients for the virtual potential temperature are computed from the adiabatic and radiation tendencies as

$$\theta_k^{(rad)}_n(t + \Delta t) = \theta_k^n_n(t - \Delta t) + 2\Delta t \left(\dot{\theta}_k^{(ad)}_n + \dot{\theta}_k^{(rad)}_n \right), \quad (6.3)$$

where the notation, $\theta^{(rad)}$, indicates we use the adiabatic and the radiative tendencies in the calculation. Using the results of (4.8), (4.19), and (4.20), we then compute the grid point fields, corresponding to the spectral coefficients of (6.2)

and (6.3), for the velocities, potential temperature, and the moisture function. We denote these fields, respectively, as $U_{ijk}^{(ad)}$, $V_{ijk}^{(ad)}$, $\theta_{ijk}^{(rad)}$, and $f[q]_{ijk}^{(ad)}$, where the subscripts have the range: $l = 1, 3M + 1$, $j = 1, (3M + 1)/2$, and $k = 1, L$. The grid point specific humidities are then obtained by inverting the moisture function:

$$q_{ijk}^{(ad)} = \exp\{1/f[q]\}_{ijk}^{(ad)}.$$

The details of the diabatic parameterizations are given in Chapters 9–15. All the NOGAPS 3.2 diabatic processes calculate implicit vertical adjustments to the grid point fields based on the current values of these fields. Therefore, the order that we call the diabatic routines has an impact on the final grid point fields. The order that the parameterizations are called is: the gravity wave drag, the turbulent vertical diffusion, the shallow convection, the penetrative cumulus convection, and the large scale precipitation. The output from the large scale precipitation parameterization is the final diabatic grid point prediction. If the time step is a multiple of 2 hours, then the radiation tendency is computed from the final diabatic predictions of temperature and moisture. Gravity wave drag and the vertical diffusion are the only two parameterizations that alter the velocity fields. For the velocities we write the adjustment scheme as

$$\left. \begin{aligned} U_{ijk}^{(gw)}(t + \Delta t) &= U_{ijk}^{(ad)}(t + \Delta t) + \Delta U_{ijk}^{(gw)}, \\ U_{ijk}^{(vf)}(t + \Delta t) &= U_{ijk}^{(gw)}(t + \Delta t) + \Delta U_{ijk}^{(vf)}, \end{aligned} \right\} \quad (6.4)$$

and

$$\left. \begin{aligned} V_{ijk}^{(gw)}(t + \Delta t) &= V_{ijk}^{(ad)}(t + \Delta t) + \Delta V_{ijk}^{(gw)}, \\ V_{ijk}^{(vf)}(t + \Delta t) &= V_{ijk}^{(gw)}(t + \Delta t) + \Delta V_{ijk}^{(vf)}. \end{aligned} \right\} \quad (6.5)$$

The superscripts (gw) and (vf) indicate respectively the gravity wave drag and the vertical flux calculations. The temperature and the moisture are changed by the vertical diffusion, the shallow convection mixing, the penetrative cumulus convection, and the large scale precipitation. The diabatic adjustment scheme for

temperature is

$$\left. \begin{aligned} \theta_{ijk}^{(vf)}(t + \Delta t) &= \theta_{ijk}^{(rad)}(t + \Delta t) + \Delta\theta_{ijk}^{(vf)}, \\ \theta_{ijk}^{(sc)}(t + \Delta t) &= \theta_{ijk}^{(vf)}(t + \Delta t) + \Delta\theta_{ijk}^{(sc)}, \\ \theta_{ijk}^{(cu)}(t + \Delta t) &= \theta_{ijk}^{(sc)}(t + \Delta t) + \Delta\theta_{ijk}^{(cu)}, \\ \theta_{ijk}^{(sp)}(t + \Delta t) &= \theta_{ijk}^{(cu)}(t + \Delta t) + \Delta\theta_{ijk}^{(sp)}, \end{aligned} \right\} \quad (6.6)$$

The superscripts (sc), (cu), and (sp) indicate the shallow convection mixing, the large cumulus convection, and the large scale precipitation calculations. A similar sequence as (6.6) can be written for q . The end results of the physics calculations are the grid point fields of temperature, specific humidity, and velocity, which are valid at $t + \Delta t$.

Following the diabatic parameterizations, we first calculate the grid point specific humidity function, $1/\ln[q]$; we then compute the spectral coefficients for the virtual potential temperature, the moisture function, the vorticity, and the divergence from (4.7), (4.21), and (4.22). We adjust the spectral coefficients of potential temperature at the top model level (*i.e.*, θ_1) using a Newtonian cooling term to reduce the false reflection of vertically propagation gravity waves (Chapter 8), and we apply an implicit fourth order diffusion operator to the spectral coefficients of $\zeta_k(t + \Delta t)$, $D_k(t + \Delta t)$, $\theta_k(t + \Delta t)$, and $1/\ln[q]_k(t + \Delta t)$ to reduce small scale noise. Finally, we apply a Robert time filter to the spectral coefficients evaluated at time t to damp the computational mode. We do not, however, recalculate new grid point fields corresponding the implicit spectral coefficients computed above, since experiments indicated that little is gained by the Gaussian grid point parameterization. Instead, the grid point fields are those obtained after the large scale precipitation computation. The spectral fields obtained after horizontal diffusion and the grid point values obtained after the parameterization of large scale precipitation are then used for the next time step.

To demonstrate the difference between the adjustment procedure and the tendency computed from fields using a previous time step, we present results from the forecasts starting at 12Z February 23, 1989. At that time NOGAPS 3.0 (triangular truncation of 47) was operational, and the gravity wave drag and the vertical flux calculations were done by computing a tendency based on the $t - \Delta t$ grid point fields. Since the grid point fields corresponding to this time step are not saved by the model, NOGAPS 3.0 computed the grid point fields from their spectral coefficients, which greatly added to the computational overhead of the model. The time series of NOGAPS 3.0's lower level variables and PBL stresses were often very noisy, especially under stable conditions. This is demonstrated in Figure 6.2 for the lowest level wind speed. Figure 6.3 is the time series for the same case and truncation (NOGAPS 3.1) starting from exactly the same initial conditions with the gravity wave and vertical flux tendencies computed using the current grid point fields. Using the current fields to compute implicitly the adjustments does not remove all variations associated with changes in stability states, but they are greatly reduced as seen by comparing the sensible heat flux computed in NOGAPS 3.0 in Figure 6.4 with that computed for NOGAPS 3.1 starting from the same initial condition given in Figure 6.5.

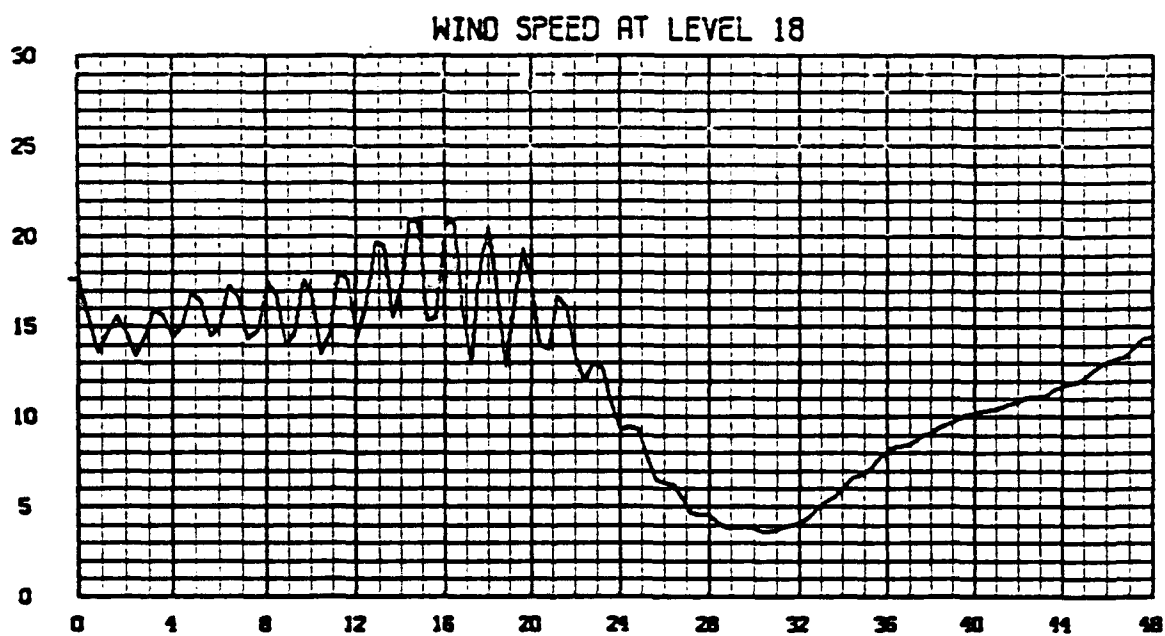


Figure 6.2: The lowest level wind speed for the open sea point $48^{\circ}41\text{N}$, $172^{\circ}5\text{W}$ for 12Z February 23, 1989, from NOGAPS 3.0 calculating the vertical flux tendency from the $t - \Delta t$ fields.

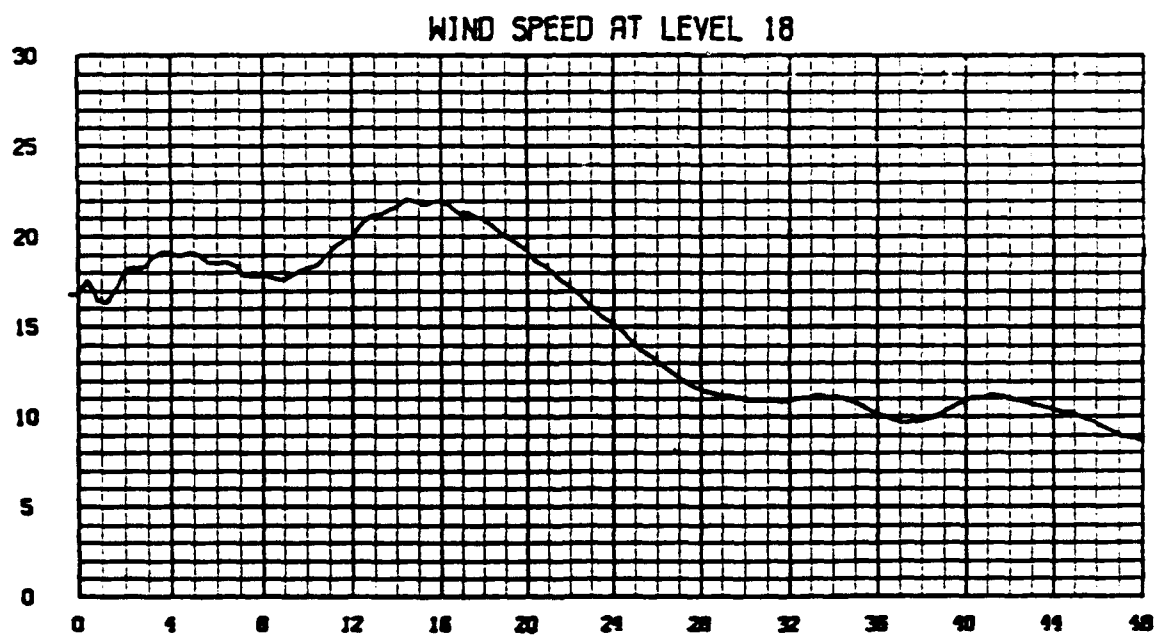


Figure 6.3: The lowest level wind speed for the open sea point 48°41N, 172° 5W for 12Z February 23, 1989, from NOGAPS 3.1 calculating the vertical flux tendency as an adjustment from the current $t + \Delta t$ fields.

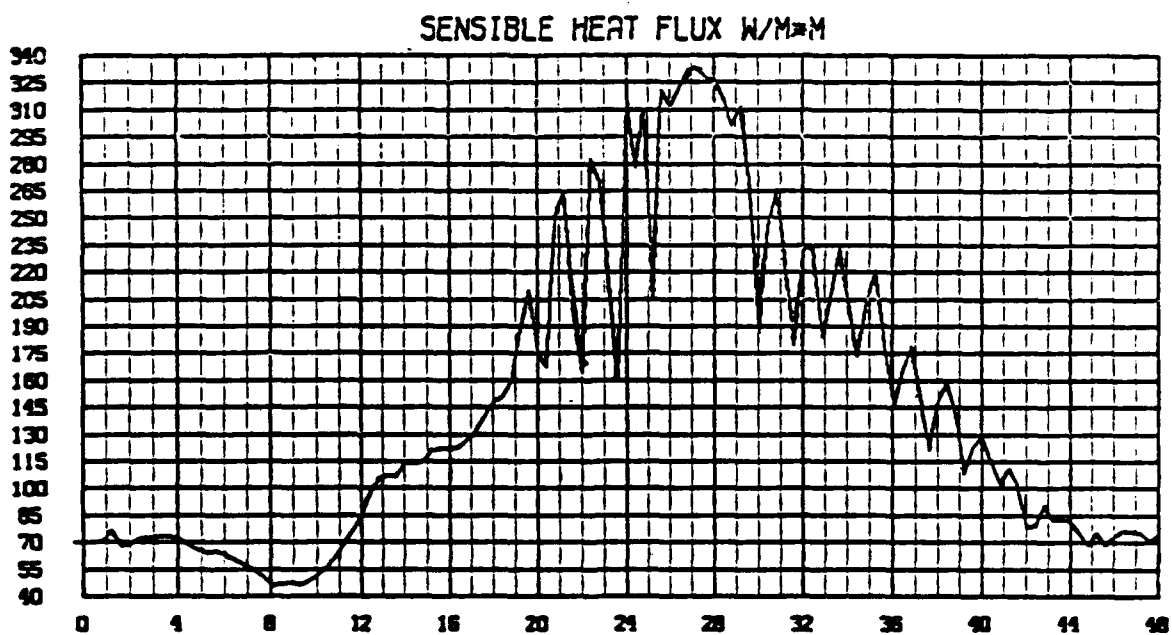


Figure 6.4: The sensible heat flux for the open sea point $58^{\circ}34$ N, $42^{\circ}50$ W for 12Z February 23, 1989, from NOGAPS 3.0 calculating the vertical flux tendency from the $t - \Delta t$ fields.

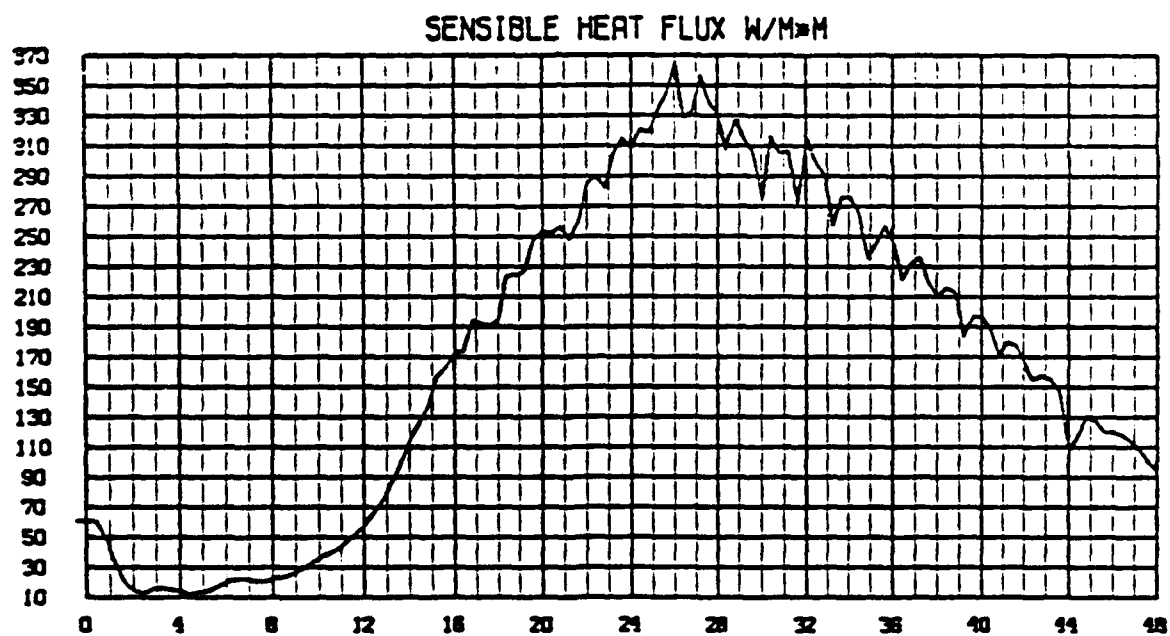


Figure 6.5: The sensible heat flux for the opensea point 58°34 N, 42°50W for 12Z February 23, 1989, from NOGAPS 3.1 calculating the vertical flux tendency as an adjustment from the $t + \Delta t$ fields.

Chapter 7

The Adiabatic and Implicit Adjustments

In this chapter we first present a short description of the procedure to calculate the explicit adiabatic terms. The discussion is brief since all the equations have been presented in previous chapters (Chapters 3 and 4). In the second section of this chapter we give the details of the semi-implicit method and the implicit zonal advection of the moisture function and vorticity.

7.1 The Explicit Adiabatic Calculation

We compute the explicit adiabatic tendencies using central differencing. We start the adiabatic calculations with the calculation of the grid point values of the π time tendency terms given by the right hand side of Equation (3.7). Using the quadrature formula given by (4.7) we compute the corresponding spectral coefficients for the π tendency. The grid point values of the vertical motion, $[\eta \partial p / \partial \eta]_{k+1/2}$, are then computed from Equation (3.10). We calculate the grid point values of G_k and H_k from Equations (3.14) and (3.15) (without the forcing terms); the correspond-

ing spectral coefficients are computed using (4.7), and we compute the derivatives that are needed in Equations (3.19) and (3.20) using the spectral expansions of Equations (4.9) and (4.10). The geopotential term of (2.33) is obtained from Equations (3.22) and (3.23). We calculate the kinetic energy term of (3.16) by squaring the cosine weighted velocities. We add the grid point values of the geopotential and the kinetic energy and then compute the spectral coefficients of the resulting sum. Using the results of the eigenvector/eigenvalue relationship of the spherical harmonics given by Equation (4.16), we multiply the spectral coefficients of the geopotential and kinetic energy by the eigenvalues, $-[n(n+1)/a^2]$, to obtain the spectral contribution of the Laplacian term on the right hand side of Equation (3.20).

The adiabatic calculation of the spectral tendencies for the virtual potential temperature equation (3.24) and the moisture equation (3.47) proceed in the same manner as those of the vorticity and divergence equations. We calculate the necessary terms for the tendency from the grid point values at time t , and then compute the corresponding spectral coefficients. At the end of the explicit adiabatic calculations we have the spectral coefficients for the explicit adiabatic time tendencies of π , ζ_k , D_k , θ_k and $f[q]_k$, which are denoted as $\left(\frac{\partial \pi}{\partial t}\right)_{expl}$, $\left(\frac{\partial \zeta_k}{\partial t}\right)_{expl}$, $\left(\frac{\partial D_k}{\partial t}\right)_{expl}$, $\left(\frac{\partial \theta_k}{\partial t}\right)_{expl}$, and $\left(\frac{\partial f[q]_k}{\partial t}\right)_{expl}$.

7.2 Semi-Implicit Calculation

If we used only the explicit time tendencies for the dynamic variables, a small time step would be needed to prevent computational instability. In general, the time step must satisfy the CFL criterion,

$$\Delta t \leq \frac{a}{u_{max} \sqrt{M(M+1)}},$$

where the velocity u_{max} is the sum of the maximum advective wind speed plus the external gravity wave speed. With an explicit treatment of gravity wave propagation this maximum speed is about 400 m sec^{-1} . In order to achieve a larger time step, we treat gravity wave propagation in a semi-implicit manner using the method developed by Robert *et al.* (1972). The approach that is described below closely follows that given by Hoskins and Simmons (1975). The final results of the procedure are corrections for those terms responsible for the gravity wave propagation, namely the divergence and the geopotential terms in the π , θ_k , and the D_k equations.

First, we define a mean atmospheric reference state that is characterized by a constant π , which we denote by $\bar{\pi}$ and is independent of λ and μ , and a mean virtual potential temperature field denoted by $\bar{\theta}_k$. We use an isothermal mean state of $300K$ to ensure maximum numerical stability as suggested by Simmons *et al.* (1978). We set $\bar{\pi}$ to 600 mbs because our stability analysis also shows a stability advantage for a reference state near minimum expected terrain pressure values. Using these mean states, we write π and θ_k as the sum of the mean and a deviation in the form:

$$\pi = \bar{\pi} + \pi', \quad (7.1)$$

$$\theta_k = \bar{\theta}_k + \theta'_k. \quad (7.2)$$

If we insert (7.1) and (7.2) into the π tendency equation given by (3.7), then the tendency equation takes the form:

$$\frac{\partial \pi}{\partial t} = - \sum_{l=1}^L \bar{\Delta p_l} D_l - \sum_{l=1}^L \nabla \cdot (\pi' \mathbf{V}_l), \quad (7.3)$$

where

$$\bar{\Delta p_l} = \Delta A_l + \Delta B_l \bar{\pi}.$$

We treat implicitly the divergence in the first term on the right hand side of (7.3) by evaluating it as the sum of the forward time divergence $D_l(t + \Delta t)$ and the backward time divergence $D_l(t - \Delta t)$. We compute the remaining terms of (7.3) explicitly; that is, we evaluate them using the central time values. The equation then takes the form:

$$\frac{\partial \pi}{\partial t} = - \sum_{l=1}^L \left[\frac{D_l(t + \Delta t) + D_l(t - \Delta t)}{2} \right] \overline{\Delta p_l} - \sum_{l=1}^L \Delta B_l \nabla \cdot [\pi' \mathbf{V}_l(t)]. \quad (7.4)$$

Adding and subtracting the term $\overline{\Delta p_l} D_l(t)$ to the right hand side of equation (7.4), we obtain the simplified form of the equation:

$$\frac{\partial \pi}{\partial t} = \left(\frac{\partial \pi}{\partial t} \right)_{expl} - \sum_{l=1}^L \overline{\Delta p_l} \widehat{D}_l. \quad (7.5)$$

where from Equation (3.7) the explicit π tendency is given by

$$\left(\frac{\partial \pi}{\partial t} \right)_{expl} = - \sum_{l=1}^L [\Delta A_l D_l(t) + \Delta B_l M_l(t)]. \quad (7.6)$$

In Equation (7.5), we have introduced for any variable X , the quantity \widehat{X} , given by

$$\widehat{X} = \left[\frac{X(t + \Delta t) + X(t - \Delta t)}{2} \right] - X(t). \quad (7.7)$$

Note that \widehat{X} can be viewed as a perturbation due to the implicit scheme and Equation (7.5) expresses the change in the π tendency due to the divergence change.

The divergence term enters the θ_k equation given by (3.24) through the vertical advection terms. Using the same procedure as the π equation, we rewrite the vertical motion, which is given by Equation (3.10), as

$$\begin{aligned} \left[\dot{\eta} \frac{\partial p}{\partial \eta} \right]_{k+1/2} &= B_{k+1/2} \sum_{l=1}^L \overline{\Delta p_l} \widehat{D}_l - \sum_{l=1}^k \overline{\Delta p_l} \widehat{D}_l \\ &+ B_{k+1/2} \sum_{l=1}^L [\Delta A_l D_l(t) + \Delta B_l M_l(t)] \\ &- \sum_{l=1}^k [\Delta A_l D_l(t) + \Delta B_l M_l(t)]. \end{aligned} \quad (7.8)$$

Inserting the vertical motion calculation of Equation (7.8) into the adiabatic form of the θ_k equation given by (3.24), we obtain the final result,

$$\frac{\partial \theta_k}{\partial t} = \left(\frac{\partial \theta_k}{\partial t} \right)_{expl} - \sum_{l=1}^L s_{kl} \widehat{D}_l, \quad (7.9)$$

where s_{kl} denote the components of a matrix S , which are defined by

$$\begin{aligned} s_{kl} = & \left[\frac{\overline{\theta_{k+1/2}} - \overline{\theta_k}}{\overline{\Delta p_k}} \right] B_{k+1/2} \overline{\Delta p_l} + \left[\frac{\overline{\theta_k} - \overline{\theta_{k-1/2}}}{\overline{\Delta p_k}} \right] B_{k-1/2} \overline{\Delta p_l} \\ & - h_{kl} \left[\frac{\overline{\theta_{k+1/2}} - \overline{\theta_k}}{\overline{\Delta p_k}} \right] \overline{\Delta p_l} - h_{kl} \left[\frac{\overline{\theta_k} - \overline{\theta_{k-1/2}}}{\overline{\Delta p_k}} \right] \overline{\Delta p_l}. \end{aligned} \quad (7.10)$$

In the above definition, the components h_{kl} define a matrix H that are given as

$$h_{kl} = \begin{cases} 1 & \text{if } k \geq l \\ 0 & \text{if } k < l \end{cases}.$$

We separate the divergence equation (3.20) in a similar manner as the π and the θ_k equation in order to find the relationship of the divergence tendency to π and θ_k . The dependence of $\partial \overline{D_k} / \partial t$ on π and θ_k comes from the expansion of the pressure gradient forcing terms about the mean state. These terms are treated in the same implicit manner as the divergence term in the π tendency equation given by (7.5). However, before the final implicit expansion of the divergence tendency equation is performed, we need some special handling of the geopotential term to extract the dependence of the geopotential on π and θ_k . If we insert the interpolation formula for $\theta_{k+1/2}$, which is given by (3.46), into the integrated hydrostatic equation (3.22), we obtain the result that

$$\phi_k - \phi_{k+1} = c_p \theta_k (P_{k+1/2} - P_k) + c_p \theta_{k+1} (P_{k+1} - P_{k+1/2}). \quad (7.11)$$

Equation (7.11) demonstrates that the geopotential difference is a function of both θ_k and π . Therefore, we expand this difference in Taylor series about the mean

atmospheric state as

$$\begin{aligned}
\phi_k - \phi_{k+1} = & c_p \overline{\theta_k} (\overline{P_{k+1/2}} - \overline{P_k}) + c_p \overline{\theta_{k+1}} (\overline{P_{k+1}} - \overline{P_{k+1/2}}) \\
& + c_p (\theta_k - \overline{\theta_k}) (\overline{P_{k+1/2}} - \overline{P_k}) + c_p (\theta_{k+1} - \overline{\theta_{k+1}}) (\overline{P_{k+1}} - \overline{P_{k+1/2}}) \\
& + c_p \overline{\theta_k} \left(\frac{\partial \overline{P_{k+1/2}}}{\partial \pi} - \frac{\partial \overline{P_k}}{\partial \pi} \right) (\pi - \overline{\pi}) \\
& + c_p \overline{\theta_{k+1}} \left(\frac{\partial \overline{P_{k+1}}}{\partial \pi} - \frac{\partial \overline{P_{k+1/2}}}{\partial \pi} \right) (\pi - \overline{\pi}) + \phi_k'' - \phi_{k+1}''. \quad (7.12)
\end{aligned}$$

The double prime terms above indicate second order terms in a Taylor series expansion. Equation (7.12) is valid for $k < L$. We obtain the expansion form for the bottom geopotential ($k = L$) from Equation (3.23):

$$\begin{aligned}
\phi_L = & \phi_S + c_p \overline{\theta_L} (\overline{P_{L+1/2}} - \overline{P_L}) \\
& + c_p (\theta_L - \overline{\theta_L}) (\overline{P_{L+1/2}} - \overline{P_L}) \\
& + c_p \overline{\theta_L} \left(\frac{\partial \overline{P_{L+1/2}}}{\partial \pi} - \frac{\partial \overline{P_L}}{\partial \pi} \right) (\pi - \overline{\pi}) + \phi_L''. \quad (7.13)
\end{aligned}$$

We put the results of (7.12) and (7.13) into the shorthand form:

$$\sum_{l=1}^L a_{kl} \phi_l = \sum_{l=1}^L b_{kl} \theta_l + c_k (\pi - \overline{\pi}) + \sum_{l=1}^L a_{kl} \phi_l''. \quad (7.14)$$

The components a_{kl} of the matrix A, the components b_{kl} of the matrix B, and the components c_k of the vector C are given, respectively, by

$$a_{kl} = \begin{cases} 1 & \text{if } k = l \\ -1 & \text{if } k = l + 1 \text{ and } k \neq L \\ 0 & \text{otherwise} \end{cases}, \quad (7.15)$$

$$b_{kl} = \begin{cases} c_p (\overline{P_{k+1/2}} - \overline{P_k}) & \text{if } k = l \\ c_p (\overline{P_{k+1}} - \overline{P_{k+1/2}}) & \text{if } k = l + 1 \text{ and } k \neq L \\ 0 & \text{otherwise} \end{cases}, \quad (7.16)$$

and

$$c_k = c_p \overline{\theta_k} \left(\frac{\partial \overline{P_{k+1/2}}}{\partial \pi} - \frac{\partial \overline{P_k}}{\partial \pi} \right) + c_p \overline{\theta_{k+1}} \left(\frac{\partial \overline{P_{k+1}}}{\partial \pi} - \frac{\partial \overline{P_{k+1/2}}}{\partial \pi} \right), \quad (7.17)$$

$$c_L = c_p \overline{\theta_L} \left(\frac{\partial \overline{P_{L+1/2}}}{\partial \pi} - \frac{\partial \overline{P_L}}{\partial \pi} \right). \quad (7.18)$$

Since \mathbf{A} is a non singular matrix, we denote the inverse matrix by \mathbf{A}^{-1} (with elements \mathbf{a}_{kl}^{-1}) and we finally write the geopotential as

$$\phi_k = \sum_{l=1}^L \sum_{j=1}^L \mathbf{a}_{kl}^{-1} \mathbf{b}_{lj} \theta_j + \sum_{l=1}^L \mathbf{a}_{kl}^{-1} c_l (\pi - \bar{\pi}) + \phi_k''. \quad (7.19)$$

We use the result of (7.19) to write the divergence tendency equation (3.20)

as

$$\begin{aligned} \frac{\partial D_k}{\partial t} &= \alpha(H_k, -G_k) - \nabla^2 I_k \\ &- \sum_{l=1}^L \sum_{j=1}^L \mathbf{a}_{kl}^{-1} \mathbf{b}_{lj} \nabla^2 \theta_j + \sum_{l=1}^L \mathbf{a}_{kl}^{-1} c_l \nabla^2 \pi + \nabla^2 \phi_k''. \end{aligned} \quad (7.20)$$

We shall treat all π and θ dependency in the divergence equation above in a similar manner as the divergence in the π and the θ_k equations. Note that both H_k and G_k defined by (3.14) and (3.15) depend on π , and we must take this dependence into account. Therefore, we write the corrected divergence tendency due to the implicit treatment of π and θ_k as

$$\begin{aligned} \frac{\partial D_k}{\partial t} &= \left(\frac{\partial D_k}{\partial t} \right)_{expl} - c_p \overline{\theta_k} \frac{\partial \overline{P_k}}{\partial \pi} \nabla^2 \hat{\pi} \\ &- \sum_{l=1}^L \sum_{j=1}^L \mathbf{a}_{kl}^{-1} \mathbf{b}_{lj} \hat{\theta}_j + \sum_{l=1}^L \mathbf{a}_{kl}^{-1} c_l \hat{\pi}. \end{aligned} \quad (7.21)$$

We evaluate the $P_{k+1/2}$ derivative from Equation (3.21) to compute the derivatives in (7.17) and the definition of Δp_k , which is given by (3.3):

$$\frac{\partial \overline{P_{k+1/2}}}{\partial \pi} = \kappa B_{k+1/2} \frac{\overline{P_{k+1/2}}}{\overline{p_{k+1/2}}}.$$

Combining (7.21) with (7.19), we write the divergence equation in its final form for the semi-implicit method as

$$\frac{\partial D_k}{\partial t} = \left(\frac{\partial D_k}{\partial t} \right)_{expl} - \sum_{l=1}^L f_{kl} \nabla^2 \hat{\theta}_l - g_k \nabla^2 \hat{\pi}, \quad (7.22)$$

where the components f_{kl} comprise the matrix F , defined by

$$F = A^{-1}B, \quad (7.23)$$

and the elements of the vector g_k are given by

$$g_k = c_p \bar{\theta}_k \frac{\partial \bar{P}_k}{\partial \pi} + \sum_{l=1}^L a_{kl}^{-1} c_l. \quad (7.24)$$

Equations (7.5), (7.9), and (7.22) are the governing equations for the adjustment to the adiabatic tendencies due to the semi-implicit treatment of gravity wave propagation. To calculate the hatted variables, we define a modified geopotential,

$$\Phi_k = \sum_{l=1}^L f_{kl} \theta_l + g_k \pi. \quad (7.25)$$

Note the similarity between (7.25) and the pseudo-geopotential discussed in Chapter 5. We obtain an equation for Φ_k by first applying the matrix F to Equation (7.9), then multiplying Equation (7.5) by g_k , and finally adding the resultant equations. In addition, we use (7.25) to simplify (7.22). We write this system of equations as

$$\frac{\partial \Phi_k}{\partial t} = \left(\frac{\partial \Phi_k}{\partial t} \right)_{expl} - \sum_{l=1}^L m_{kl} \hat{D}_l \quad (7.26)$$

$$\frac{\partial D_k}{\partial t} = \left(\frac{\partial D_k}{\partial t} \right)_{expl} - \nabla^2 \hat{\Phi}_k, \quad (7.27)$$

where the components of the matrix M are defined as,

$$m_{kl} = \sum_{j=1}^L f_{kj} s_{jl} + g_k \overline{\Delta p_l}. \quad (7.28)$$

It is assumed that the matrix M has L distinct eigenvalues (L is the total number of model levels, 18), which are denoted as ξ_k . If we denote E as the matrix whose

columns are the eigenvectors of \mathbf{M} , and we denote Ξ as the diagonal matrix whose diagonal elements are the eigenvalues ξ_k , then the matrix \mathbf{M} is given by the canonical form,

$$\mathbf{M} = \mathbf{E}^{-1} \Xi \mathbf{E} \quad (7.29)$$

We define the notation that a superscript E on a vector indicates that the vector has been multiplied by the matrix \mathbf{E}^{-1} . Therefore, as for example, the variable D_k^E is defined as

$$D_k^E = \sum_{l=1}^L \mathbf{e}_{kl}^{-1} D_l. \quad (7.30)$$

Applying the matrix \mathbf{E}^{-1} to Equations (7.26) and (7.27), we get the following wave equation system:

$$\frac{\partial \Phi_k^E}{\partial t} = \left(\frac{\partial \Phi_k^E}{\partial t} \right)_{expl} - \xi_k \widehat{D}_l^E, \quad (7.31)$$

$$\frac{\partial D_k^E}{\partial t} = \left(\frac{\partial D_k^E}{\partial t} \right)_{expl} - \nabla^2 \widehat{\Phi}_k^E. \quad (7.32)$$

The above equations take the same form as the linearized shallow water equations. The dependent variables above define the vertical modes of the forecast model for the given mean atmospheric state, $\bar{\pi}$ and $\bar{\theta}_k$. From the wave equation nature of the above system an eigenvalues ξ_k is equivalent to the square of the gravity wave phase speed for the k^{th} vertical mode.

Equations (7.31) and (7.32) are most easily solved in spectral harmonic space.

We write the spectral coefficients tendency equations as

$$\frac{\partial \Phi_{nk}^{mE}}{\partial t} = \left(\frac{\partial \Phi_{nk}^{mE}}{\partial t} \right)_{expl} - \xi_k \widehat{D}_{nl}^{mE}. \quad (7.33)$$

$$\frac{\partial D_{nk}^{mE}}{\partial t} = \left(\frac{\partial D_{nk}^{mE}}{\partial t} \right)_{expl} + \left[\frac{n(n+1)}{a^2} \right] \widehat{\Phi}_{nk}^{mE}. \quad (7.34)$$

We rewrite the left hand sides of (7.33) and (7.34) by making use of the central difference definition of the time tendency, which is given by (6.1), and the definitions

of \widehat{D}_{nk}^{mE} and $\widehat{\Phi}_{nk}^{mE}$, which are given by (7.7) in order to obtain the following:

$$\frac{\partial \Phi_{nk}^{mE}}{\partial t} = \frac{\widehat{\Phi}_{nk}^{mE} + \Phi_{nk}^{mE}(t) - \Phi_{nk}^{mE}(t - \Delta t)}{\Delta t}, \quad (7.35)$$

$$\frac{\partial D_{nk}^{mE}}{\partial t} = \frac{\widehat{D}_{nk}^{mE} + D_{nk}^{mE}(t) - D_{nk}^{mE}(t - \Delta t)}{\Delta t}. \quad (7.36)$$

By inserting (7.35) and (7.36) into (7.33) and (7.34), we write a matrix equation for the variables $\widehat{\Phi}_{nk}^{mE}$ and \widehat{D}_{nk}^{mE} as

$$\begin{bmatrix} 1 & \xi_k \Delta t \\ -n(n+1)\Delta t/a^2 & 1 \end{bmatrix} \begin{bmatrix} \widehat{\Phi}_{nk}^{mE} \\ \widehat{D}_{nk}^{mE} \end{bmatrix} = \begin{bmatrix} Y_{nk}^{mE} \\ Z_{nk}^{mE} \end{bmatrix}, \quad (7.37)$$

where

$$Y_{nk}^{mE} = \left(\frac{\partial \Phi_{nk}^{mE}}{\partial t} \right)_{expl} \Delta t + \Phi_{nk}^{mE}(t - \Delta t) - \Phi_{nk}^{mE}(t) \quad (7.38)$$

$$Z_{nk}^{mE} = \left(\frac{\partial D_{nk}^{mE}}{\partial t} \right)_{expl} \Delta t + D_{nk}^{mE}(t - \Delta t) - D_{nk}^{mE}(t). \quad (7.39)$$

The solutions to the system (7.37) is given by

$$\widehat{\Phi}_{nk}^{mE} = \frac{Y_{nk}^{mE} - \xi_k \Delta t Z_{nk}^{mE}/a^2}{1 + \xi_k n(n+1)\Delta t^2/a^2}, \quad (7.40)$$

and

$$\widehat{D}_{nk}^{mE} = \frac{Z_{nk}^{mE} + [n(n+1)\Delta t/a^2]Y_{nk}^{mE}}{1 + \xi_k n(n+1)\Delta t^2/a^2}. \quad (7.41)$$

Finally, we compute \widehat{D}_{nk}^{mE} by applying the matrix E to the results of (7.41), so that we obtain

$$\widehat{D}_{nk}^{mE} = \sum_{l=1}^L \mathbf{e}_{kl} \widehat{D}_{nk}^{mE}. \quad (7.42)$$

Once \widehat{D}_{nk}^{mE} and $\widehat{\Phi}_{nk}^{mE}$ are known, the new spectral tendencies for π , and θ_k are computed from Equations (7.5) and (7.9) respectively and we get the new spectral divergence tendency from Equation (7.27) as

$$\frac{\partial D_{nk}^{mE}}{\partial t} = \left(\frac{\partial D_{nk}^{mE}}{\partial t} \right)_{expl} + \left[\frac{n(n+1)}{a^2} \right] \widehat{\Phi}_{nk}^{mE}. \quad (7.43)$$

(This result can also be obtained from (7.36) which is what is done by the code.)

The final results of these calculations are the spectral adiabatic tendencies for π , divergence and the potential temperature: $\dot{\pi}^{(ad)}_n$, $\dot{D}_k^{(ad)}_n$, and $\dot{\theta}_k^{(ad)}_n$.

7.3 Implicit Advection of Vorticity and Moisture

The semi-implicit method discussed above removes the CFL criterion due to the propagation of gravity waves, but there is still the constraint of the advection due to non-divergent horizontal velocities. The ideal approach to remove this stability limit is to couple the semi-implicit method with a semi-Lagrangian formulation. As an alternative, we treat the longitudinal advection of the vorticity and the moisture function in an implicit manner using a technique developed by Simmons and Jarraud (1983). This enables an approximate 25% additional increase in the time step above the semi-implicit method.

We begin by writing the longitudinal cosine weighted velocity U_k for each level as a sum of a mean zonal velocity plus a difference:

$$U_k(\lambda, \mu, t) = \overline{U}_k(\mu, t) + U'_k(\lambda, \mu, t). \quad (7.44)$$

We define $\overline{U}_k(\mu, t)$ as the average of the maximum and the minimum of the longitudinal velocity at time $t - \Delta t$:

$$\overline{U}_k(\mu, t) = \frac{1}{2} \left[\max_{\lambda} U_k(\lambda, \mu, t - \Delta t) + \min_{\lambda} U_k(\lambda, \mu, t - \Delta t) \right]. \quad (7.45)$$

If we represent the vorticity or the moisture function by X_k , we can put the tendency equations for vorticity (3.19) or moisture (3.47) into the form:

$$\frac{\partial X_k}{\partial t} = \left(\frac{\partial X_k}{\partial t} \right)_{expl} - \frac{\overline{U}_k(\mu, t)}{\cos^2 \varphi} \left[\frac{\partial X_k}{\partial \lambda} - \frac{\partial X_k(t)}{\partial \lambda} \right], \quad (7.46)$$

where the *expl* subscript on the tendency indicates that this quantity is the sum of all terms that comprise the explicit adiabatic tendency, which is computed from the fields valid at the central time t . For convenience of notation, we shall suppress the dependence of X_k on λ and μ , but we will display the time level at which the variable is evaluated. We compute the λ derivative in Equation (7.46) implicitly as

$$\frac{\partial X_k}{\partial \lambda} = \frac{\partial}{\partial \lambda} [X_k(t+\Delta t) + X_k(t-\Delta t) - X_k(t)]. \quad (7.47)$$

Using the relation given by (7.47), we write (7.46) as

$$\begin{aligned} \frac{\partial X_k}{\partial t} &= \left(\frac{\partial X_k}{\partial t} \right)_{expl} \\ &- \frac{\overline{U}_k(\mu, t)}{\cos^2 \varphi} \frac{\partial}{\partial \lambda} [X_k(t+\Delta t) + X_k(t-\Delta t) - 2X_k(t)]. \end{aligned} \quad (7.48)$$

We see from the form of Equation (7.48) that the tendency correction has the same structure as a diffusion term. This time diffusion allows an increase in the time step Δt . Using the definition for the computation of the central difference time tendency given by (6.1), we write (7.48) in terms of the time tendency of the dependent variable as

$$\begin{aligned} \frac{\partial X_k}{\partial t} &= \left(\frac{\partial X_k}{\partial t} \right)_{expl} - \frac{\overline{U}_k(\mu, t) 2\Delta t}{\cos^2 \varphi} \frac{\partial}{\partial \lambda} \left[\frac{\partial X_k}{\partial t} \right] \\ &+ 2 \frac{\overline{U}_k(\mu, t)}{\cos^2 \varphi} \frac{\partial}{\partial \lambda} [X_k(t) - X_k(t-\Delta t)]. \end{aligned} \quad (7.49)$$

By calculating the Fourier transform of (7.49), (see [4.6]), we obtain the result that

$$\begin{aligned} \mathcal{F}^m [\partial X_k / \partial t] &= - \frac{\overline{U}_k(\mu, t) 2\Delta t}{2\pi \cos^2 \varphi} \int_0^{2\pi} \frac{\partial}{\partial \lambda} \left[\frac{\partial X_k}{\partial t} \right] e^{-im\lambda} d\lambda \\ &+ \frac{2\overline{U}_k(\mu, t)}{2\pi \cos^2 \varphi} \int_0^{2\pi} \frac{\partial}{\partial \lambda} [X_k(t) - X_k(t-\Delta t)] e^{-im\lambda} d\lambda \\ &+ \mathcal{F}^m [(\partial X_k / \partial t)_{expl}]. \end{aligned} \quad (7.50)$$

Note that $\mathcal{F}^m [X_k]$ is a function of μ and t . We perform the integrals of Equation (7.50) by parts, and use the fact that the variables are periodic in λ to eliminate

the integral of the total derivative, leaving the result

$$\begin{aligned}\mathcal{F}^m [\partial X_k / \partial t] &= - \frac{im \overline{U}_k(\mu, t) 2\Delta t}{\cos^2 \varphi} \mathcal{F}^m [\partial X_k / \partial t] \\ &+ 2 \frac{im \overline{U}_k(\mu, t)}{\cos^2 \varphi} \{ \mathcal{F}^m [X_k(t)] - \mathcal{F}^m [X_k(t - \Delta t)] \} \\ &+ \mathcal{F}^m [(\partial X_k / \partial t)_{expl}].\end{aligned}\quad (7.51)$$

Solving for the Fourier transform of the tendencies, we obtain

$$\mathcal{F}^m [\partial X_k / \partial t] = \mathcal{G}^m [X_k] / \{ 1 + im \overline{U}_k(\mu, t) 2\Delta t / \cos^2 \varphi \}, \quad (7.52)$$

where

$$\begin{aligned}\mathcal{G}^m [X_k] &= \mathcal{F}^m [(\partial X_k / \partial t)_{expl}] \\ &+ [2im \overline{U}_k(\mu, t) / \cos^2 \varphi] \{ \mathcal{F}^m [X_k(t)] - \mathcal{F}^m [X_k(t - \Delta t)] \}\end{aligned}\quad (7.53)$$

Given the Fourier transform computed above, we compute the new spectral tendencies for the vorticity and the moisture function by using the Gaussian quadrature calculation of Equation (4.7). The final results of these calculations are the spectral adiabatic tendencies for the vorticity and moisture function: $\dot{\zeta}_k^{(ad)m}_n$, and $\dot{f}[q]_k^{(ad)m}_n$.

Chapter 8

Adiabatic Truncation and Implicit Smoothing Calculations

In this chapter we discuss several algorithms that enhance the stability of the numerical solutions. These are the truncation of the top levels' adiabatic tendencies, the Newtonian cooling term for the top level temperature, the fourth order implicit diffusion of the fields, and the Robert time filter.

8.1 Adiabatic Tendency Truncation

The T79 forecast model uses a time step of 1200 seconds. We have truncated the top 2 or 3 level adiabatic tendencies in order to preserve the stability of the model in the presence of intense stratospheric polar night jets. If the maximum wind speed of the model is less than 120 m sec^{-1} then the adiabatic tendencies in the top level are truncated to a total wavenumber of 63, and the second level adiabatic tendencies are truncated to 71. However, if the maximum wind speed exceeds 120 m/sec then the top 3 level adiabatic tendencies are truncated to resolutions of 47, 63, and 71, respectively. Under most circumstances, this algorithm preserves the

1200 second time step. However, if the maximum winds exceed 160 m sec^{-1} the time step of the model is reduced to 900 seconds for the remaining forecast.

8.2 Top Level Newtonian Cooling Term

In order to damp falsely reflecting vertically propagating gravity waves from the model's top, we added a Newtonian damping term to the top level virtual potential temperature tendency equation to relax the top 2 model levels toward an isothermal condition. The relation between the virtual temperature and virtual potential temperature is given by Equation (3.34). If we ignore the small amount of moisture present in the stratosphere, then the condition that the top two levels be isothermal is given by

$$\theta_1 = \theta_2 \frac{P_2}{P_1}. \quad (8.1)$$

If we add a term of the form,

$$K_c \nabla^2 \left(\theta_1 - \theta_2 \frac{P_2}{P_1} \right),$$

to the top virtual potential temperature equation, it has the effect of damping the temperature difference at the higher wavenumbers. In order to reduce the overhead of calculating the Gaussian quadratures associated with the grid point values of P_1 and P_2 , we use the average values of P_1 and P_2 associated with the mean state of the atmosphere, $\bar{\pi}$. We then write the θ_1 equation in the form:

$$\frac{\partial \theta_1}{\partial t} = \dot{\theta}_1^{(sp)} \bar{\pi} + K_c \nabla^2 \left(\theta_1 - \theta_2 \frac{\bar{P}_2}{\bar{P}_1} \right), \quad (8.2)$$

where $\dot{\theta}_1^{(sp)} \bar{\pi}$ contains the explicit adiabatic tendency, the semi-implicit correction, and all diabatic adjustments (see Chapter 6 for the discussion of the integration scheme and the superscript notation). If we use the central difference definition of

the time derivative, and we define (Chapter 6):

$$\theta_1^{(sp)m}(t + \Delta t) = \theta_1^m(t - \Delta t) + 2\Delta t \dot{\theta}_1^{(sp)m}.$$

then we can put (8.2) into the form:

$$\theta_{1n}^m(t + \Delta t) = \theta_1^{(sp)m}(t + \Delta t) - 2\Delta t K_c \left[\frac{n(n+1)}{a^2} \right] \left\{ \theta_{1n}^m(t + \Delta t) - \theta_2^{(sp)m}(t + \Delta t) \frac{\bar{P}_2}{\bar{P}_1} \right\}. \quad (8.3)$$

Solving (8.3) for $\theta_1(t + \Delta t)$, we obtain the new spectral coefficients of the virtual potential temperature as

$$\theta_{1n}^m(t + \Delta t) = \frac{\left\{ \theta_1^{(sp)m}(t + \Delta t) + 2\Delta t K_c \left[\frac{n(n+1)}{a^2} \right] \theta_2^{(sp)m}(t + \Delta t) \frac{\bar{P}_2}{\bar{P}_1} \right\}}{\left\{ 1 + 2\Delta t K_c \left[\frac{n(n+1)}{a^2} \right] \right\}}. \quad (8.4)$$

We choose the damping coefficient K_c so that the highest wavenumber coefficient has a e-folding relaxation time of 4 hours, so that the reciprocal of K_c is given by:

$$K_c^{-1} = 4 \times 3600 \text{ sec} \times \frac{M(M+1)}{a^2} \quad (8.5)$$

The effect of the damping term can be seen by comparing Figure 8.1 with Figure 8.2. Both figures are taken from forecasts starting at 12Z July 30, 1988, at which time a strong stratospheric jet was present around Antarctica. The initial conditions are the same for both runs. Figure 8.1 is taken from NOGAPS 3.0, which did not contain the Newtonian damping term. With a time step of 1440 seconds significant noise developed in the stratospheric heights. From analysis of time series of heights and temperatures it was evident that the temperature profile was buckling at the top of the model, probably due to false reflection of upward propagating gravity waves generated at the larger time step. This noise problem was not evident at smaller time steps. The inclusion of the damping term eliminates

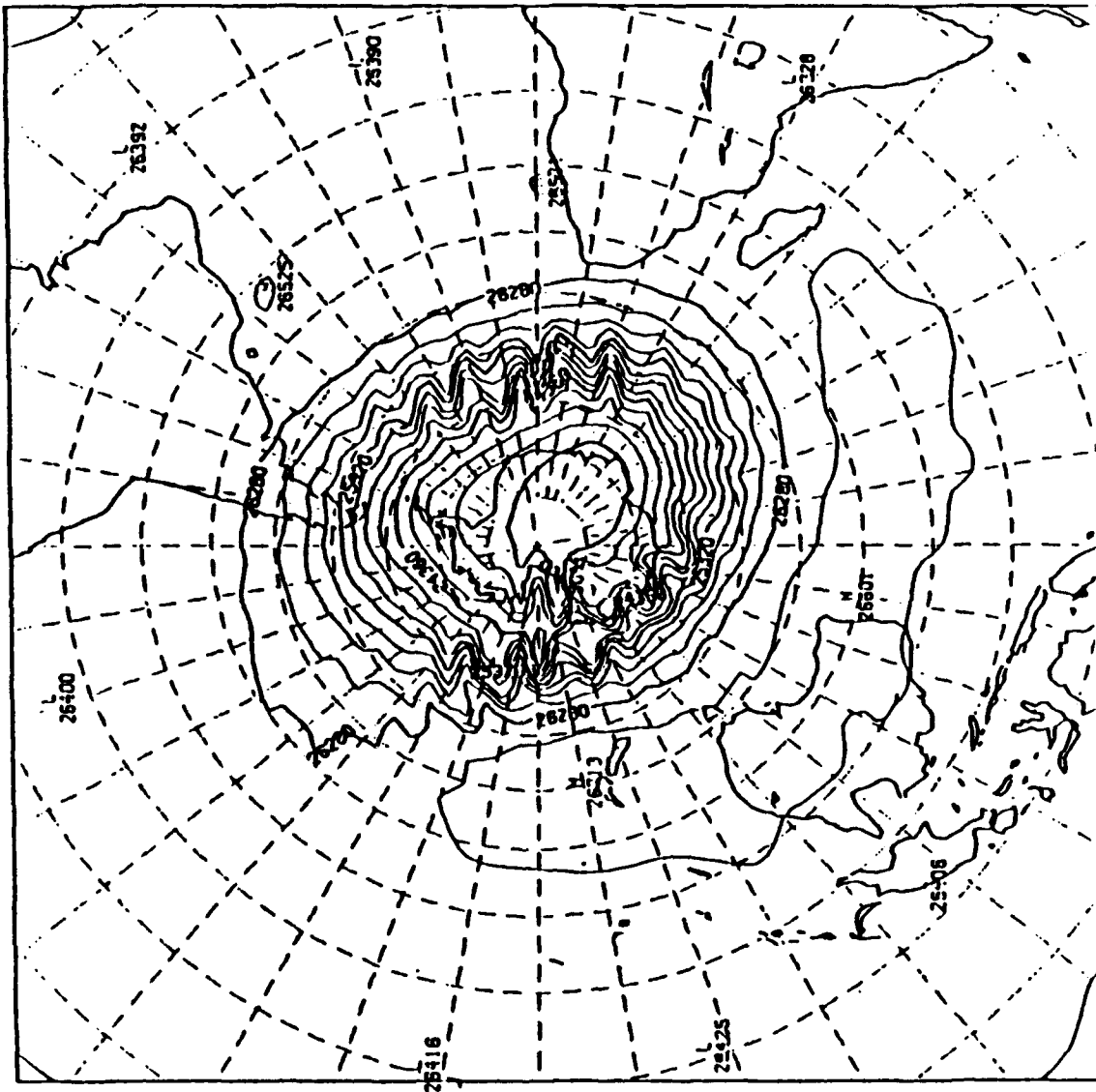


Figure 8.1: The NOGAPS 3.0 20 mb height field forecast for $\tau = 18$ hrs starting from July 30, 1988.

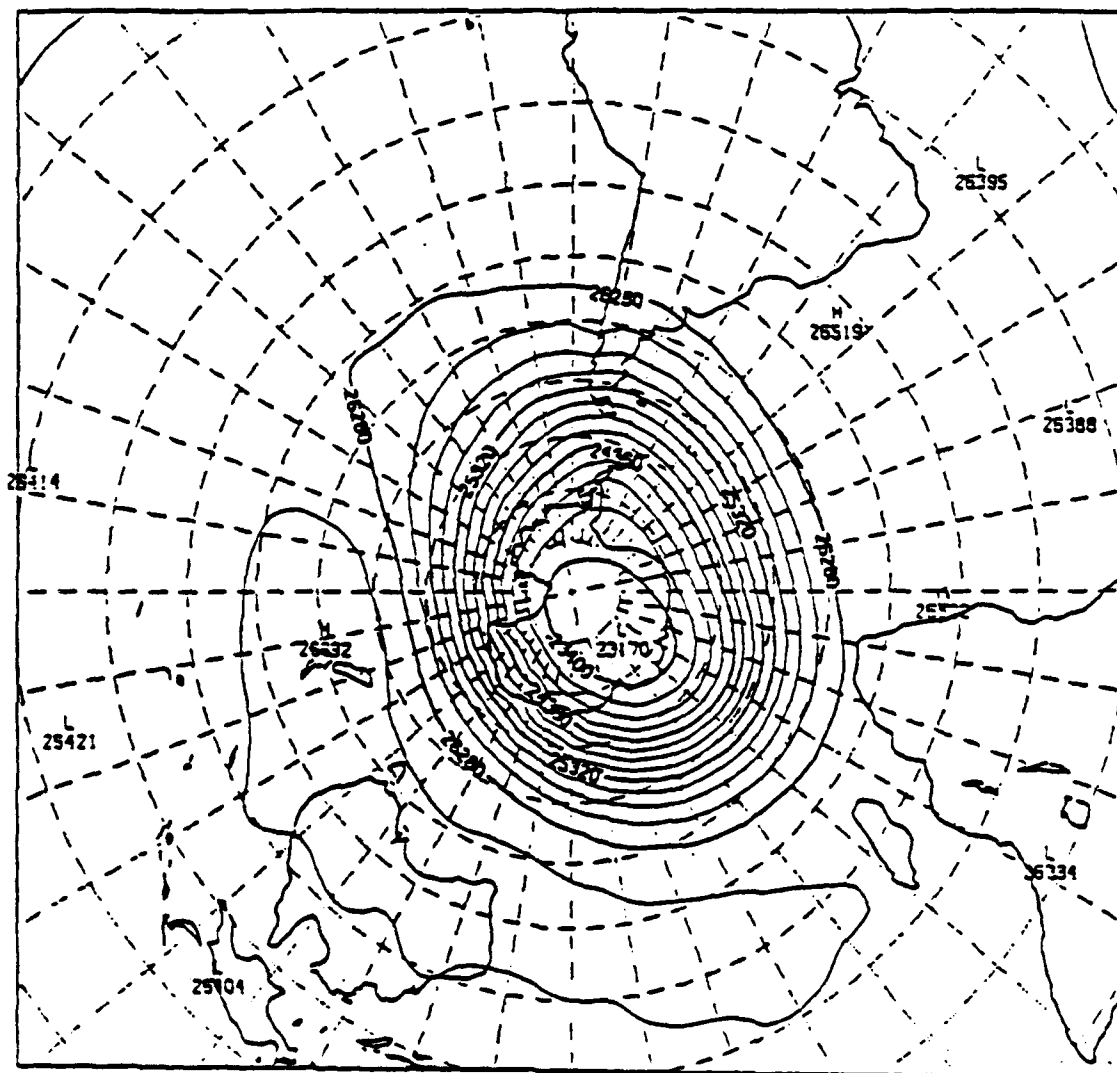


Figure 8.2: The NOGAPS 3.1 20 mb height field forecast for $\tau = 18$ hrs starting from July 30, 1988.

the stratospheric height noise at the larger time step as seen in NOGAPS 3.1 run of Figure 8.2. An examination of time series indicates that the Newtonian cooling term also eliminates the temperature buckling.

8.3 Horizontal Diffusion

We apply an implicit fourth order diffusion operation to spectral coefficients of vorticity, divergence, virtual potential temperature, and the moisture function at the time step $t + \Delta t$. The procedure is similar to that performed with the Newtonian cooling of the top level virtual potential temperature with the exception that a fourth order diffusion operator is used instead of the second order diffusion operator used with the Newtonian cooling. The effect of the terrain following hybrid coordinates must also be taken into account for the moisture and the temperature fields.

If we let X_k represent either the vorticity or divergence at level k , we can write the tendency equation with diffusion as

$$\frac{\partial X_k}{\partial t} = \dot{X}_k^{(sp) m} - K_d \nabla^4 X_k \quad (8.6)$$

The term $\dot{X}_k^{(sp) m}$ is the sum of all the preceding adiabatic, adjustment, and diabatic adjustments terms (see Chapter 6 for the discussion of the integration scheme and the superscript notation). For central time differencing and with the definition of $X_k^{(sp) m}(t + \Delta t)$ from Chapter 6:

$$X_k^{(sp) m}(t + \Delta t) = X_{kn}^m(t - \Delta t) + 2\Delta t \dot{X}_k^{(sp) m},$$

we put (8.6) into the form:

$$\begin{aligned} X_{kn}^m(t + \Delta t) &= X_k^{(sp) m}(t + \Delta t) \\ &- 2\Delta t K_d \left[\frac{n(n+1)}{a^2} \right]^2 X_{kn}^m(t + \Delta t). \end{aligned} \quad (8.7)$$

Solving (8.7) the spectral coefficients for divergence and vorticity, we obtain the spectral coefficients of divergence and vorticity as

$$D_{kn}^m(t+\Delta t) = D_k^{(sp)n}(t+\Delta t) / \left\{ 1 + 2\Delta t K_d \left[\frac{n(n+1)}{a^2} \right]^2 \right\}, \quad (8.8)$$

and

$$\zeta_{kn}^m(t+\Delta t) = \zeta_k^{(sp)n}(t+\Delta t) / \left\{ 1 + 2\Delta t K_d \left[\frac{n(n+1)}{a^2} \right]^2 \right\}. \quad (8.9)$$

We see from (8.8) and (8.9) that the diffusion is highly wavenumber selective, damping the higher wavenumbers greater than the smaller ones. Under most circumstances a value of the diffusion coefficient is chosen to yield an e-folding damping time for the highest wave number of 1 day:

$$K_d^{-1} = 24 \times 3600 \text{ sec} \times \left[\frac{M(M+1)}{a^2} \right]^2. \quad (8.10)$$

At the top level, divergence diffusion is increased by a factor of 5, and moisture and temperature diffusion by a factor of 4. In the second level, divergence diffusion is increased by a factor of 2.5, and moisture and temperature diffusion by a factor of 2. For any level with maximum winds exceeding 80 m/sec, we increase the divergence diffusion by a factor of 10. A similar strategy is described by Simmons *et al.* (1989) for the ECMWF model.

Since the hybrid coordinate varies with the terrain pressure, the virtual potential temperature and the moisture function will contain some high wavenumber features that are due to the terrain variations. Instead of applying the diffusion operator directly to these fields, we write the equivalent of Equation (8.7) in terms of $\theta_k - \theta_k^{ref}$ and $f(q_k) - f[q]_k^{ref}$, where the *ref* superscript denotes a reference state. We calculate the reference state for potential temperature by first defining a surface pressure from the standard atmospheric pressure at the model's terrain height, which we denote as π^{ref} . We then obtain the pressure values, p_k^{ref} , from (3.1), (3.5), and (3.6). We then calculate the standard atmospheric values of potential

temperature, which we denote as θ_k^{ref} . We define the reference moisture function as the value of the moisture function evaluated at the saturation specific humidity value for a virtual potential temperature given by θ_k^{ref} and a pressure of p_k^{ref} . This is computed as

$$f[q]_k^{ref} = f[q_{sat}(\theta_k^{ref}, p_k^{ref})].$$

These reference values are independent of time and are computed at the initial time of the forecast and are saved by the model. The procedure is now the same as that used to obtain (8.7). The results for the virtual potential temperature and the moisture function are

$$\begin{aligned} \theta_{kn}^m(t + \Delta t) &= \left\{ \theta_k^{(sp)m}(t + \Delta t) + 2\Delta t K_d \left[\frac{n(n+1)}{a^2} \right]^2 \theta_k^{refm} \right\} \\ &\times \left\{ 1 + 2\Delta t K_d \left[\frac{n(n+1)}{a^2} \right]^2 \right\}^{-1}, \end{aligned} \quad (8.11)$$

and

$$\begin{aligned} f[q]_{kn}^m(t + \Delta t) &= \left\{ f[q]_k^{(sp)m}(t + \Delta t) + 2\Delta t K_d \left[\frac{n(n+1)}{a^2} \right]^2 f[q]_k^{refm} \right\} \\ &\times \left\{ 1 + 2\Delta t K_d \left[\frac{n(n+1)}{a^2} \right]^2 \right\}^{-1}. \end{aligned} \quad (8.12)$$

As a final point, in place of $\theta_1^{(sp)m}(t + \Delta t)$ in (8.11), we use the results from the Newtonian cooling computation given by (8.4).

8.4 Robert Time Filter

We apply a Robert time filter to the spectral coefficients of the dynamical variables in order to damp the computational mode inherent in using central time differencing. This time filter changes the spectral coefficients at the t time step and is the last modification to the variables. If we let X represent either π , ζ_k , D_k , θ_k , or

$f(q_k)$, we calculate the final values of the spectral coefficients at time t , $X^{(fin)}_n(t)$, by using the Robert filter:

$$X^{(fin)}_n(t) = \widetilde{X}_n^m(t) + K_R [X_n^m(t+\Delta t) - 2X_n^m(t) + X_n^m(t-\Delta t)]. \quad (8.13)$$

The spectral coefficients on the right hand side of (8.13) are the values obtained after the fourth order diffusion operator. The Robert time filter constant, which is given by K_R , is set at 0.05.

Chapter 9

Gravity Wave Drag

The effect of increased vertical shear due to the breaking of subgrid scale vertically propagating gravity waves, which are generated by orography, is modeled by the gravity wave drag parameterization. Palmer *et al.* (1986) show that the introduction of a gravity wave drag parameterization reduces the Northern Hemispheric zonal wind bias. Our parameterization is based on the work of Palmer *et al.* (1986) and the following discussion closely follows their work.

If we represent the vertical flux vector, which describes the upward transport of horizontal momentum by the gravity waves, by $\mathbf{T}_{\mathbf{gw}}$, then we can write the vertical flux equation for the horizontal velocity vector, \mathbf{u} , as

$$\frac{\partial \mathbf{u}}{\partial t} = -g \frac{\partial \mathbf{T}_{\mathbf{gw}}}{\partial p}. \quad (9.1)$$

The vertical structure of the model is shown in Figure 3.1. With the fluxes evaluated at the half pressure levels, we write the vertical finite difference form of (9.1) as,

$$\frac{\partial \mathbf{u}_k}{\partial t} = g \frac{\mathbf{T}_{\mathbf{gw}_{k+1/2}} - \mathbf{T}_{\mathbf{gw}_{k-1/2}}}{\Delta p_k}. \quad (9.2)$$

The computation of the vertical gravity wave flux utilizes the Eliassen-Palm theorem (Eliassen and Palm [1961]), which states that, in the absence of transients

and dissipation, vertically propagating waves preserve their vertical flux. Using this result, we assume that the surface flux, which is due to the generation of gravity waves, will be transported upward until some turbulent layer is reached, where this flux will be reduced and thereby dissipate the mean flow. At each-half level, we define the Brunt-Vaisälä frequency, $N_{k+1/2}$, and the bulk Richardson number, $Ri_{k+1/2}$, which are given as

$$N_{k+1/2} = \sqrt{\frac{g(\theta_k - \theta_{k+1})}{\Delta z_k \theta_{k+1/2}}}, \quad (9.3)$$

$$Ri_{k+1/2} = \frac{g(\theta_k - \theta_{k+1})\Delta z_k}{\theta_{k+1/2}[(u_{k+1} - u_k)^2 + (v_{k+1} - v_k)^2]}, \quad (9.4)$$

where we use the simple interpolation formula:

$$\theta_{k+1/2} = \frac{\theta_{k+1} + \theta_k}{2}. \quad (9.5)$$

We use the adiabatic velocities and temperature to calculate $N_{k+1/2}$ and $Ri_{k+1/2}$. We compute the layer thickness Δz_k from the hydrostatic equation (3.22):

$$\Delta z_k = c_p \theta_{k+1/2} (P_k - P_{k+1}) / g. \quad (9.6)$$

We take the surface stress to be in the direction of the surface layer wind, \mathbf{u}_L , and we denote the component of any level wind vector projected in the surface wind direction by u_k^\dagger :

$$u_k^\dagger = \mathbf{u}_k \cdot \frac{\mathbf{u}_L}{|\mathbf{u}_L|}. \quad (9.7)$$

The projection of the horizontal wind at the half-level hybrid surface is given by

$$u_{k+1/2}^\dagger = \frac{(\mathbf{u}_{k+1} + \mathbf{u}_k)}{2} \cdot \frac{\mathbf{u}_L}{|\mathbf{u}_L|}. \quad (9.8)$$

We assume that the surface stress vector, defined as $\mathbf{T}_{\mathbf{g}\mathbf{w}\mathbf{S}}$, is proportional to the surface density, the surface wind, the surface buoyancy frequency, and the variance

of the terrain field, $(\delta z_S)^2$, which is obtained from the U.S. Navy's 10 minute resolution global terrain field. This relationship is

$$\mathbf{T}_{gw_S} = K_{gw} \rho_S N_{L-1/2} \mathbf{u}_L (\delta z_S)^2. \quad (9.9)$$

A maximum of 400 meters has been set for δz_S and the adjustable constant K_{gw} is set to $2.5 \times 10^{-5} \text{ m}^{-1}$, (Palmer *et al.* [1986]).

Starting at the $L - 3/2$ level and continuing to the top of the model, we compute a wave bulk Richardson number, $Ri_{k+1/2}^*$, which is based on linear wave theory, as

$$Ri_{k+1/2}^* = Ri_{k+1/2} \frac{1 - [N\delta h/u^\dagger]_{k+1/2}}{\{1 + Ri_{k+1/2}^{1/2} [N\delta h/u^\dagger]_{k+1/2}\}^2}, \quad (9.10)$$

where the wave amplitude $\delta h_{k+1/2}$ is obtained by assuming that relation given by Equation (9.9) is valid in the vertical with δz_S replaced by $\delta h_{k+1/2}$, ρ_S by $\rho_{k+1/2}$, and the surface stress by the stress at $k+1/2$:

$$\delta h_{k+1/2} = \sqrt{\frac{\tau_{k+1/2}}{K_{gw} [\rho N u^\dagger]_{k+1/2}}}, \quad (9.11)$$

The scalar, $\tau_{k+1/2}$, is the magnitude of the gravity wave drag:

$$\tau_{k+1/2} = |\mathbf{T}_{gw_{k+1/2}}|.$$

At the lowest level we set $\tau_{L-1/2} = \tau_S$ and $\delta h_{L-1/2} = \delta z_S$.

We use the results of the Eliassen-Palm theorem to assume that $\tau_{k+1/2}$ remains equal to τ_S until a layer of turbulent dissipation is reached. This occurs when the wave bulk Richardson number, given by (9.10), is less than 1/4. When this occurs, $Ri_{k+1/2}^*$ is reset to 1/4 and Equation (9.10) is solved for $\delta h_{k+1/2}$. The solution of the quadratic equation is given by

$$\begin{aligned} \delta h_{k+1/2} = & (u^\dagger/N)_{k+1/2} Ri_{k+1/2}^{-1/2} (1 + 2Ri_{k+1/2}^{1/2}) \\ & \times \{2Ri_{k+1/2}^{1/4} (1 + 2Ri_{k+1/2}^{1/2})^{-1/2} - 1\}. \end{aligned} \quad (9.12)$$

Resetting the wave bulk Richardson number back to the critical value of 1/4 is based on a "saturation hypothesis," which assumes that with the transition to turbulence the wave amplitude has reached its maximum (Lindzen [1981]). Given the new value of the wave amplitude, we calculate the vector gravity wave stress as

$$\tau_{k+1/2} = K_{gw} \rho_{k+1/2} N_{k+1/2} u_{k+1/2}^\dagger \quad (9.13)$$

All of the above calculations assume that $u_{k+1/2}^\dagger$ is greater than zero. If at any half level $u_{k+1/2}^\dagger$ is less than or equal to zero, it is assumed that at this level a critical layer has been reached, the gravity wave breaks totally, and we set $\tau_{k+1/2}$ equal to zero. All the dissipation of the mean flow is assumed to occur at this critical layer.

Only the component of the mean flow projected onto the surface wind vector is dissipated by the breaking of the gravity waves. Therefore, given the values of the gravity wave stresses in the 2 adjacent layers, we calculate the new value of $u_k^{(gw)\dagger}$ from Equation (9.1) as

$$u_k^\dagger = u_k^{(ad)\dagger} - 2\Delta t \frac{g}{\Delta p_k} (\tau_{k+1/2} - \tau_{k-1/2}). \quad (9.14)$$

The discussion of the time integration strategy and the superscript notation is presented in Chapter 6. We obtain the new winds, $u_k^{(gw)}$ and $v_k^{(gw)}$, which are adjusted by gravity wave drag, from (9.14) as

$$u_k^{(gw)} = u_k^{(ad)} - 2\Delta t \frac{g}{\Delta p_k} (\tau_{k+1/2} - \tau_{k-1/2}) \frac{u_L^{(ad)}}{\sqrt{u_L^{(ad)2} + v_L^{(ad)2}}}, \quad (9.15)$$

and

$$v_k^{(gw)} = v_k^{(ad)} - 2\Delta t \frac{g}{\Delta p_k} (\tau_{k+1/2} - \tau_{k-1/2}) \frac{v_L^{(ad)}}{\sqrt{u_L^{(ad)2} + v_L^{(ad)2}}}. \quad (9.16)$$

At the top of the model, we set the gravity wave stress, $\tau_{1/2}$, to zero so that any excess gravity wave drag is deposited in the top layer.

We have incorporated one modification to the Palmer *et al.* (1986) algorithm. With the above formulation, a large percentage of the gravity wave drag is completely deposited in the lowest layers of the model. To enable more of the gravity

wave drag to reach the upper atmosphere, we set the maximum gravity wave stress reduction in layer k to 50% of the stress at level $k + 1/2$ for $p_k > 450$ mb and $u_{k+1/2}^{(ad)\dagger} > 0$. Above 450 mb, we allow the stress to be absorbed completely in a single layer. Also, if at any level, $u^{(ad)\dagger} < 0$, the gravity wave stress is set to zero for all levels above this critical level.

Chapter 10

Vertical Flux Parameterization

The calculation of the subgrid vertical diffusive fluxes is based on the work of Louis (1979) and Louis *et al.* (1982). If we let X represent either the horizontal velocity components u or v , the virtual potential temperature θ , or the specific humidity q , then we can write the vertical diffusion equation for X , in z coordinates as

$$\frac{\partial X}{\partial t} = \frac{1}{\rho} \frac{\partial \mathcal{F}_X}{\partial z}. \quad (10.1)$$

The vertical flux \mathcal{F}_X is defined as

$$\mathcal{F}_X = \overline{-\rho w' X'}, \quad (10.2)$$

where the primed variables indicate the turbulent eddy difference from the mean and the overline indicates an averaging (temporal) process. The full diffusive equation would include horizontal turbulent diffusion in addition to the vertical diffusion, but we neglect the horizontal terms under the assumption that they are small in comparison to the vertical term.

The vertical diffusive fluxes are related to the derivatives of the mean quantities through a first order closure assumption (K theory). Introducing a mass mixing length l_h and a momentum mixing length l_m , we assume that the turbulent fluxes

are assumed are given by the relationships:

$$\mathcal{F}_\theta = \rho l_h^2 \left| \frac{\partial \mathbf{u}}{\partial z} \right| \frac{\partial \theta}{\partial z}, \quad (10.3)$$

$$\mathcal{F}_q = \rho l_h^2 \left| \frac{\partial \mathbf{u}}{\partial z} \right| \frac{\partial q}{\partial z}, \quad (10.4)$$

$$\mathcal{F}_u = \rho l_m^2 \left| \frac{\partial \mathbf{u}}{\partial z} \right| \frac{\partial u}{\partial z}, \quad (10.5)$$

$$\mathcal{F}_v = \rho l_m^2 \left| \frac{\partial \mathbf{u}}{\partial z} \right| \frac{\partial v}{\partial z}. \quad (10.6)$$

The forms for the momentum and mass mixing lengths are based on the Monin-Obukhov (1954) similarity theory and are defined on the half levels (see Figure 3.1). Their functional forms are defined below. The vertical fluxes are computed on the half level surfaces. At each half level a bulk Richardson number $Ri_{k+1/2}$ is defined for the layer centered at $z_{k+1/2}$, with a thickness given by $\Delta z_{k+1/2}$. The heights and thicknesses are computed from the hydrostatic equation (3.22) starting at the surface level $L + 1/2$ as

$$\begin{aligned} z_{L+1/2} &= z_S, \\ z_{k-1/2} &= z_{k+1/2} + \frac{c_p}{g} \theta_k (P_{k+1/2} - P_{k-1/2}), \\ \Delta z_{k+1/2} &= \frac{\phi_k - \phi_{k+1}}{g}. \end{aligned}$$

For the Richardson numbers and the exchange coefficient calculations in this section, we use the winds computed from the gravity wave drag, $u_k^{(gw)}$ and $v_k^{(gw)}$, the temperatures from the adiabatic and radiative tendencies, $T_k^{(rad)}$, and the adiabatic specific humidity, $q_k^{(ad)}$. We present a complete discussion of the time integration scheme in Chapter 6. Also, we omit the horizontal grid point indices, i and j , on all the variables. The functional relations for the bulk Richardson number are given below by (10.30) and (10.32). We assume that a positive bulk Richardson number implies that the layer is stable to thermally forced turbulence, while a negative bulk Richardson numbers indicates this layer is unstable to thermally forced turbulence.

Above the surface, we calculate the fluxes at the half levels as

$$\mathcal{F}_{X_{k+1/2}} = \rho_{k+1/2} l_{X_{k+1/2}}^2 \left| \frac{u_{k+1} - u_k}{z_{k+1} - z_k} \right| \left(\frac{X_k - X_{k+1}}{z_k - z_{k+1}} \right), \quad (10.7)$$

where, if $X = u$ or $X = v$ then $l_X = l_m$, and if $X = \theta$ or $X = q$ then $l_X = l_h$. For the u and v fluxes we set the velocity at the surface to zero so that the surface wind stresses can be expressed as

$$\mathcal{F}_{u_s} = \rho_s u_*^2 \frac{u_L}{|u_L|} \quad (10.8)$$

and

$$\mathcal{F}_{v_s} = \rho_s u_*^2 \frac{v_L}{|u_L|} \quad (10.9)$$

where the frictional velocity given by u_* is defined as

$$u_* = \sqrt{\frac{l_{ms}^2 |u_L|^2}{(z_L - z_s)^2}}. \quad (10.10)$$

The surface sensible heat flux and the surface flux for the virtual potential temperature are defined as

$$\mathcal{F}_{T_s} = \nu \{T_s - \theta_L P_L / (1 + .608 q_l)\} \quad (10.11)$$

and

$$\mathcal{F}_{\theta_s} = \nu (\theta_s - \theta_L), \quad (10.12)$$

where the mass flux coefficient ν (sometimes call the ventilation factor) is given by

$$\nu = \frac{\rho_s l_{hs}^2 |u_L|}{(z_L - z_s)^2}. \quad (10.13)$$

The surface value of the virtual potential temperature θ_s is related to the surface temperature T_s and surface moisture q_s from (3.34) as

$$\theta_s = \frac{T_s(1 + .608 q_s)}{P_{L+1/2}}. \quad (10.14)$$

We define the ground moisture q_S as a combination of the ground saturation specific humidity, $q_{sat}(T_S)$, and the surface air specific humidity by the relation:

$$q_S = W_S q_{sat}(T_S) + (1 - W_S) q_L. \quad (10.15)$$

The factor W_S is the ground wetness. Finally, we calculate the surface evaporative flux by assuming Equation (10.12) is valid for the moisture:

$$\mathcal{F}_{q_S} = \nu W_S (q_S - q_L). \quad (10.16)$$

We specify the following constants for the computation of the momentum exchange coefficient:

$$\left. \begin{aligned} b_m &= 5.0 \\ c_m &= 7.5 \\ d_m &= 5.0 \\ \kappa_m &= 0.4 \\ \lambda_m &= 150.0 \end{aligned} \right\}; \quad (10.17)$$

and we define the neutral stability ($Ri=0$) mixing length for momentum at the surface and at the half levels as

$$l_m^{(n)} = \frac{\kappa_m z}{1 + \kappa_m z / \lambda_m}, \quad (10.18)$$

$$l_{m_S}^{(n)} = \frac{\kappa_m}{\ln [(z + z_0)/z_0]}; \quad (10.19)$$

and we specify the function:

$$f_m = \frac{l_m^2}{\Delta z^{3/2} z^{1/2}} \left[\left(\frac{z + \Delta z}{z} \right)^{1/3} - 1 \right]^{3/2}. \quad (10.20)$$

The variables z and Δz are evaluated at the half levels. The variable z_0 is the roughness length. For water points we update the value of the roughness length, z_0 at each time step using Charnock's relation (Charnock [1955]):

$$z_0 = \frac{0.032}{g} u_*^2. \quad (10.21)$$

For land points the roughness length is fixed throughout the forecast by its climatological value, which is obtained by interpolation to the valid initial time from monthly values. Using these definitions, for positive bulk Richardson numbers, Louis *et al.* (1982) specify l_m by

$$l_m = l_m^{(n)} \left\{ \frac{1}{1 + 2b_m Ri / \sqrt{1 + d_m Ri}} \right\}^{1/2}, \quad (Ri > 0), \quad (10.22)$$

while for negative bulk Richardson numbers, they define l_m as

$$l_m = l_m^{(n)} \left\{ 1 - \frac{2b_m Ri}{1 + 2b_m c_m f_m \sqrt{|Ri|}} \right\}^{1/2}, \quad (Ri \leq 0). \quad (10.23)$$

In the above formulas we have omitted the subscript $k+1/2$ on the Richardson number and the momentum exchange coefficient.

For the mass exchange coefficient computation, we set the following constants:

$$\left. \begin{aligned} b_h &= 5.0 \\ c_h &= 5.0 \\ d_h &= 5.0 \\ \kappa_h &= 0.4 \\ \lambda_h &= 450.0 \end{aligned} \right\} \quad (10.24)$$

and we define the surface and half level neutral mixing lengths as

$$l'_h = \frac{\kappa_h z}{1 + \kappa_h z / \lambda_h}, \quad (10.25)$$

$$l_{hs}^{(n)} = \frac{\kappa_h}{\ln[(z + z_0)/z_0]}, \quad (10.26)$$

together with the function:

$$f_h = \frac{l_h^2}{\Delta z^{3/2} z^{1/2}} \left[\left(\frac{z + \Delta z}{z} \right)^{1/3} - 1 \right]^{3/2}. \quad (10.27)$$

With the above definitions, for positive bulk Richardson numbers, Louis *et al.* (1982) specify l_h as

$$l_h = l_h^{(n)} \left\{ \frac{1}{1 + 3b_h Ri / \sqrt{1 + d_h Ri}} \right\}^{1/2}, \quad (Ri > 0), \quad (10.28)$$

while for negative bulk Richardson numbers, they define l_h by

$$l_h = l_h^{(n)} \left\{ 1 - \frac{3b_h Ri}{1 + 3b_h c_h f_h \sqrt{|Ri|}} \right\}^{1/2}, \quad (Ri \leq 0). \quad (10.29)$$

The bulk Richardson numbers are computed at the half levels. Above the surface, we set $Ri_{k+1/2}$ by the relationship:

$$Ri_{k+1/2} = \frac{g(z_k - z_{k-1})(s_k - s_{k+1})}{c_p |u_k - u_{k+1}|^2 T_{v_{k+1/2}}}. \quad (10.30)$$

The variable s_k is the virtual dry static energy, which is defined by the equation,

$$s_k = c_p T_{v_k} + \phi_k. \quad (10.31)$$

At the surface, we use the formula for the bulk Richardson number that is suggested by Randall (1976):

$$Ri_S = \frac{g(z_L - z_S)[c_p(T_S - T_L) + .608 W_S T_S(q_S - q_L)]}{(c_p T_S + g z_S) |u_L|^2}. \quad (10.32)$$

We form the $u_k^{(vf)}$ equations by inserting (10.3) into (10.1), together with the central time formula for the time derivative and the definition of $u_k^{(gw)}$. This implicit u_k system of equations is given by

$$u_1^{(vf)} = u_1^{(gw)} - \left\{ \frac{g}{\Delta p_1} 2\Delta t \rho_{3/2} l_{m_{3/2}}^2 \left| \frac{u_2^{(gw)} - u_1^{(gw)}}{z_2 - z_1} \right| \right\} \left(\frac{u_1 - u_2}{z_1 - z_2} \right), \quad (10.33)$$

$$u_k^{(vf)} = u_k^{(gw)} - \left\{ \frac{g}{\Delta p_k} 2\Delta t \rho_{k+1/2} l_{m_{k+1/2}}^2 \left| \frac{u_{k+1}^{(gw)} - u_k^{(gw)}}{z_{k+1} - z_k} \right| \right\} \left(\frac{u_k - u_{k+1}}{z_k - z_{k+1}} \right) + \left\{ \frac{g}{\Delta p_k} 2\Delta t \rho_{k-1/2} l_{m_{k-1/2}}^2 \left| \frac{u_k^{(gw)} - u_{k-1}^{(gw)}}{z_k - z_{k-1}} \right| \right\} \left(\frac{u_{k-1} - u_k}{z_{k-1} - z_k} \right), \quad (10.34)$$

$$u_L^{(vf)} = u_L^{(gw)} - \left\{ \frac{g}{\Delta p_L} 2\Delta t \rho_S l_{m_S}^2 \left| \frac{u_L^{(gw)}}{z_L - z_S} \right| \right\} \left(\frac{u_L}{z_L - z_S} \right) + \left\{ \frac{g}{\Delta p_L} 2\Delta t \rho_{L-1/2} l_{m_{L-1/2}}^2 \left| \frac{u_L^{(gw)} - u_{L-1}^{(gw)}}{z_L - z_{L-1}} \right| \right\} \left(\frac{u_{L-1} - u_L}{z_{L-1} - z_L} \right). \quad (10.35)$$

The system given by (10.33)–(10.35) is implicit and linear for $u_k^{(vf)}$. However, it is not fully implicit since the bracket terms are calculated using the gravity wave drag

(input) fields. An iterative procedure could be set up to adjust these coefficients, but we feel that this is too expensive and the final results would not be greatly changed. The system (10.33)–(10.35) is a tridiagonal system of equations, which can be expressed in the form:

$$a_{m_k} u_{k-1}^{(vf)} + b_{m_k} u_k^{(vf)} + c_{m_k} u_{k+1}^{(vf)} = u_k^{(gw)}, \quad (10.36)$$

We obtain the momentum tridiagonal coefficients a_{m_k} , b_{m_k} , and c_{m_k} from Equations (10.33)–(10.35), which for $1 \leq k \leq L$ are

$$a_{m_1} = 0, \quad (10.37)$$

$$a_{m_k} = - \left\{ \frac{g}{\Delta p_k} 2\Delta t \rho_{k-1/2} l_{m_{k-1/2}}^2 \frac{|u_k^{(gw)} - u_{k-1}^{(gw)}|}{(z_{k-1} - z_k)^2} \right\}, \quad (10.38)$$

$$b_{m_k} = 1 - (a_{m_k} + c_{m_k}), \quad (10.39)$$

$$b_{m_L} = 1 + \rho_s u_*^2 \frac{2\Delta t g}{\Delta p_L |u_1|} - a_{m_L}, \quad (10.40)$$

$$c_{m_1} = - \left\{ \frac{g}{\Delta p_1} 2\Delta t \rho_{3/2} l_{m_{3/2}}^2 \frac{|u_2^{(gw)} - u_1^{(gw)}|}{(z_1 - z_2)^2} \right\}, \quad (10.41)$$

$$c_{m_k} = - \left\{ \frac{g}{\Delta p_k} 2\Delta t \rho_{k+1/2} l_{m_{k+1/2}}^2 \frac{|u_{k+1}^{(gw)} - u_k^{(gw)}|}{(z_k - z_{k+1})^2} \right\}, \quad (10.42)$$

$$c_{m_L} = 0. \quad (10.43)$$

The $v_k^{(vf)}$ equations take the same form as above, and we write the equation system:

$$a_{m_k} v_{k-1}^{(vf)} + b_{m_k} v_k^{(vf)} + c_{m_k} v_{k+1}^{(vf)} = v_k^{(gw)}. \quad (10.44)$$

We solve the tridiagonal systems (10.36) and (10.44) for $u_k^{(vf)}$ and $v_k^{(vf)}$ using the double sweep (Gaussian elimination) method (Carnahan *et al.* [1969]).

The vertical diffusion of momentum removes kinetic energy from the mean flow. We account for this lost of energy by assuming that it goes directly into the internal energy and therefore increases the temperature of the air. After the horizontal velocity calculations, we compute a new temperature as

$$T_k^{(vf')} = T_k^{(rad)} + \frac{(u_k^{(gw)2} + v_k^{(gw)2}) - (u_k^{(vf)2} + v_k^{(vf)2})}{2c_p}. \quad (10.45)$$

Above the surface level ($k=L=18$), the potential temperature and the specific humidity equations are similar in form to Equations (10.33) and (10.34), except that the mass exchange coefficient replaces the momentum coefficient. At the ground, we hold the ground wetness to its climatological value throughout the forecast for all points. However, the surface flux for temperature and moisture, which are given by (10.12) and (10.16), depend on the surface temperature and the saturated specific humidity. Over water points, the sea surface temperature is held at the initial analysis value throughout the forecast, but over land or ice points the temperature is predicted. Therefore, the surface land temperature and saturated specific humidity equations are coupled into the predictive equations for $\theta_k^{(vf)}$ and $q_k^{(vf)}$, and we must solve for these two variables along with the temperature and moisture.

The ground temperature equation for non-water points is given by

$$c_s \frac{dT_s}{dt} = \mathcal{F}_{SW} - \mathcal{F}_{LW} - c_p \nu (T_s - \theta_L P_L) - \nu L_w W_s (q_s - q_L) - L_i S_M + k_s c_s (T_{clim} - T_s). \quad (\text{non water points}) \quad (10.46)$$

For water points, the temperature is fixed by its initial analysis value, so that:

$$T_s = T_w, \quad (\text{water points}). \quad (10.47)$$

In Equation (10.46): the variable \mathcal{F}_{SW} is the incoming surface shortwave radiation flux; \mathcal{F}_{LW} is the outgoing surface longwave radiation flux; L_w is the latent heat of condensation; L_i is the latent heat of fusion; c_p is the specific heat of air; c_s is the heat capacity of the ground; ν is the mass exchange coefficient given by (10.13); S is the snow melting rate with units $\text{kg m}^{-2} \text{sec}^{-1}$; T_w is the sea surface temperature; T_{clim} is the climatological relaxation surface temperature; and k_s is

one over a climatological relaxation time. The surface heat capacity is given by

$$c_S = \begin{cases} 4.20 \times 10^4 \text{ J m}^{-2} \text{ K}^{-1} \sqrt{27.5[.387 + .15W_S(1 + W_S)]} & \text{land} \\ 2.14 \times 10^5 \text{ J m}^{-2} \text{ K}^{-1} & \text{ice} \\ 9.66 \times 10^4 \text{ J m}^{-2} \text{ K}^{-1} & \text{snow.} \end{cases} \quad (10.48)$$

For land points, T_{clim} is the climatological ground temperature. For sea ice points, we set $T_{clim} = 271.2$ K. For land points, we set k_S to

$$k_S = 2\pi/100 \text{ hours};$$

while for sea ice points:

$$k_S = \kappa_i/I_i,$$

where κ_i is the thermal conductivity of ice (5×10^{-3} cal (sec cm K) $^{-1}$) and I_i is the sea ice thickness held fixed at 2 meters (Holloway and Manabe [1971]).

Equation (10.46) depends on the snow melting rate S_M . At a land point, the snow, S , is increased by the amount of precipitation that reaches the ground if the surface temperature is less than 273.15 K. If the ground temperature increases above freezing when snow is present, then the difference, ΔT , between the predicted temperature and 273.15 K is used to melt a snow amount of $c_S \Delta T / (L_i \Delta t)$. The surface temperature is decreased either back to 273.15 K if there is still snow remaining, or to $T_S - L_i S$ if all the snow is melted.

We derive an equation for saturation adjustment from the relationship of saturation specific humidity, $q_{sat}(T, p)$, to saturation vapor pressure, $e_{sat}(T)$:

$$q_{sat}(T, p) = \frac{.62197 e_{sat}(T)}{p - e_{sat}(T)} \quad (10.49)$$

A first order Taylor expansion in temperature with fixed pressure of (10.49) yields:

$$q_{sat}(T + \Delta T, p) = q_{sat}(T, p) + \frac{L_w \gamma}{c_p} \Delta T, \quad (10.50)$$

with the variable γ given by

$$\gamma = \frac{c_p}{L_w} \left(\frac{\partial q_{sat}}{\partial T} \right)_p.$$

Using the Clausius-Claperyon Equation, which is

$$\frac{de_{sat}}{dT} = \frac{m_w L_w e_{sat}}{R^* T^2},$$

we evaluate γ in terms of pressure and temperature as

$$\gamma = \left(\frac{c_p}{L_w} \right) \left(\frac{p}{p - e_{sat}(T)} \right) \left(\frac{m_w q_{sat} L_w}{R^* T^2} \right), \quad (10.51)$$

where R^* is the universal gas constant and m_w is the mass per unit mole of water.

We convert (10.50) to a time tendency equation by dividing both sides by Δt , yielding

$$\frac{dq_s}{dt} = \frac{\gamma L_w}{c_p} \frac{dT_s}{dt}. \quad (10.52)$$

We combine the results of Equations (10.1), (10.3), (10.4), (10.7), (10.12), (10.16), (10.46), (10.52), with the central difference time difference formula, (10.45), and the definition of $q_k^{(ad)}$ to obtain the equations for the virtual potential temperature, surface temperature, the specific humidity, and the surface humidity. These are given by

$$\theta_1^{(vf)} = \theta_1^{(vf')} - \left\{ \frac{g}{\Delta p_1} 2\Delta t \rho_{3/2} l_{h_{3/2}}^2 \left| \frac{u_2^{(gw)} - u_1^{(gw)}}{z_2 - z_1} \right| \right\} \left(\frac{\theta_1^{(vf)} - \theta_2^{(vf)}}{z_1 - z_2} \right), \quad (10.53)$$

$$\begin{aligned} \theta_k^{(vf)} = \theta_k^{(vf')} - \left\{ \frac{g}{\Delta p_k} 2\Delta t \rho_{k+1/2} l_{h_{k+1/2}}^2 \left| \frac{u_{k+1}^{(gw)} - u_k^{(gw)}}{z_{k+1} - z_k} \right| \right\} & \left(\frac{\theta_k^{(vf)} - \theta_{k+1}^{(vf)}}{z_k - z_{k+1}} \right) \\ + \left\{ \frac{g}{\Delta p_k} 2\Delta t \rho_{k-1/2} l_{h_{k-1/2}}^2 \left| \frac{u_k^{(gw)} - u_{k-1}^{(gw)}}{z_k - z_{k-1}} \right| \right\} & \left(\frac{\theta_{k-1}^{(vf)} - \theta_k^{(vf)}}{z_{k-1} - z_k} \right), \end{aligned} \quad (10.54)$$

$$\begin{aligned} \theta_L^{(vf)} = \theta_L^{(vf')} - \left\{ \frac{g}{\Delta p_L} 2\Delta t \rho_s l_{h_s}^2 \left| \frac{u_L^{(gw)}}{z_L - z_s} \right| \right\} & \left(\frac{\theta_L^{(vf)} - T_s[1 + .608q_s]/P_s}{z_L - z_s} \right) \\ + \left\{ \frac{g}{\Delta p_L} 2\Delta t \rho_{L-1/2} l_{h_{L-1/2}}^2 \left| \frac{u_L^{(gw)} - u_{L-1}^{(gw)}}{z_L - z_{L-1}} \right| \right\} & \left(\frac{\theta_{L-1}^{(vf)} - \theta_L^{(vf)}}{z_{L-1} - z_L} \right). \end{aligned} \quad (10.55)$$

$$\begin{aligned}
T_S = T_S(t) + \delta_w \frac{\Delta t}{c_S} \{ \mathcal{F}_{SW} - \mathcal{F}_{LW} - c_p \nu [T_S - \theta_L^{(vf)} P_L] \} \\
+ \delta_w \frac{\Delta t}{c_S} \{ \nu L_w W_S [q_S - q_L] + L_i S - k_S c_S [T_{clim} - T_S] \}
\end{aligned} \quad (10.56)$$

and.

$$q_1^{(vf)} = q_1^{(ad)} - \left\{ \frac{g}{\Delta p_1} 2\Delta t \rho_{3/2} l_{h_{3/2}}^2 \left| \frac{u_2^{(gw)} - u_1^{(gw)}}{z_2 - z_1} \right| \right\} \left(\frac{q_1^{(vf)} - q_2^{(vf)}}{z_1 - z_2} \right), \quad (10.57)$$

$$\begin{aligned}
q_k^{(vf)} = q_k^{(ad)} - \left\{ \frac{g}{\Delta p_k} 2\Delta t \rho_{k+1/2} l_{h_{k+1/2}}^2 \left| \frac{u_{k+1}^{(gw)} - u_k^{(gw)}}{z_{k+1} - z_k} \right| \right\} \left(\frac{q_k^{(vf)} - q_{k+1}^{(vf)}}{z_k - z_{k+1}} \right) \\
+ \left\{ \frac{g}{\Delta p_k} 2\Delta t \rho_{k-1/2} l_{h_{k-1/2}}^2 \left| \frac{u_k^{(gw)} - u_{k-1}^{(gw)}}{z_k - z_{k-1}} \right| \right\} \left(\frac{q_{k-1}^{(vf)} - q_k^{(vf)}}{z_{k-1} - z_k} \right), \quad (10.58)
\end{aligned}$$

$$\begin{aligned}
q_L^{(vf)} = q_L^{(ad)} - \left\{ \frac{g}{\Delta p_L} 2\Delta t \rho_S l_{h_S}^2 \left| \frac{u_L^{(gw)}}{z_L - z_S} \right| \right\} \left(\frac{W_S (q_S^{(vf)} - q_L^{(vf)})}{z_L - z_S} \right) \\
+ \left\{ \frac{g}{\Delta p_L} 2\Delta t \rho_{L-1/2} l_{h_{L-1/2}}^2 \left| \frac{u_L^{(gw)} - u_{L-1}^{(gw)}}{z_L - z_{L-1}} \right| \right\} \left(\frac{q_{L-1}^{(vf)} - q_L^{(vf)}}{z_{L-1} - z_L} \right). \quad (10.59)
\end{aligned}$$

$$q_S^{(vf)} = q_S^{(vf)}(t) + \delta_w \gamma \frac{L_w}{c_p} \{ T_S - T_S(t) \}. \quad (10.60)$$

The variables T_S and q_S without the time variable are the forecasted surface temperature and saturated moisture at the time $t + \Delta t$. Also, the variable δ_w is defined as 0 for water points and 1 for non water points to account for the fixed sea surface temperature.

The above systems are coupled and can be written in the tridiagonal form, for $k = 1, \dots, L - 1$, as

$$\left. \begin{aligned} a_{h_k} \theta_{k-1}^{(vf)} + b_{h_k} \theta_k^{(vf)} + c_{h_k} \theta_{k+1}^{(vf)} &= \theta_k^{(vf')} \\ a_{h_k} q_{k-1}^{(vf)} + b_{h_k} q_k^{(vf)} + c_{h_k} q_{k+1}^{(vf)} &= q_k^{(ad)} \end{aligned} \right\} \quad (10.61)$$

where the tridiagonal mass coefficients a_{h_k} , b_{h_k} , and c_{h_k} are identical to the momentum tridiagonal coefficients given by (10.37)–(10.42) except that l_h^2 replaces l_m^2 .

For $k = L$ we have the equations:

$$\left. \begin{aligned} a_{T_L} \theta_{L-1}^{(vf)} + b_{T_L} \theta_L^{(vf)} + c_{T_L} T_S &= \theta_L^{(vf')} \\ a_{q_L} q_{L-1}^{(vf)} + b_{q_L} q_L^{(vf)} + c_{q_L} q_S &= q_L^{(ad)} \end{aligned} \right\} \quad (10.62)$$

where the coefficients are

$$a_{T_L} = - \left\{ \frac{g}{\Delta p_L} 2\Delta t \rho_{L-1/2} l_{h_{L-1/2}}^2 \frac{|u_L^{(gw)} - u_{L-1}^{(gw)}|}{(z_{L-1} - z_L)^2} \right\}, \quad (10.63)$$

$$b_{T_L} = 1 + \nu \frac{2\Delta t g}{\Delta p_L} - a_{T_L}, \quad (10.64)$$

$$c_{T_L} = -\nu \frac{2\Delta t}{g \Delta p_L P_S} \{1 + .608 q_S(t)\}, \quad (10.65)$$

$$a_{q_L^{(vf)}} = a_{T_L}, \quad (10.66)$$

$$b_{q_L^{(vf)}} = 1 - (a_{q_L^{(vf)}} + c_{q_L^{(vf)}}), \quad (10.67)$$

$$c_{q_L^{(vf)}} = -\nu W_S \frac{2\Delta t}{g \Delta p_L}. \quad (10.68)$$

Finally, we cast the T_S equation, given by (10.56), and the q_S equation, given by (10.60), into the matrix form:

$$\begin{bmatrix} a_{11}^T & a_{12}^T \\ 0 & 0 \end{bmatrix} \begin{bmatrix} \theta_L^{(vf)} \\ q_L^{(vf)} \end{bmatrix} + \begin{bmatrix} b_{11}^T & b_{12}^T \\ b_{21}^T & 1 \end{bmatrix} \begin{bmatrix} T_S \\ q_S \end{bmatrix} = \begin{bmatrix} X^T \\ Y^T \end{bmatrix}, \quad (10.69)$$

where the coefficients and right hand side are defined as:

$$a_{11}^T = -\delta_w c_p \Delta t P_S \{\nu / c_S (1 + .608 q_S(t))\}, \quad (10.70)$$

$$a_{12}^T = -\delta_w W_S L_w \Delta t (\nu / c_S), \quad (10.71)$$

$$b_{11}^T = 1 + \delta_w \Delta t \nu (c_p / c_S) + \delta_w k_S, \quad (10.72)$$

$$b_{12}^T = \delta_w L_w W_S \Delta t (\nu / c_S), \quad (10.73)$$

$$b_{21}^T = -\delta_w L_w (\gamma / c_p), \quad (10.74)$$

$$\begin{aligned} X^T &= T_S(t) + \frac{\delta_w \Delta t}{c_S} (\mathcal{F}_{SW} - \mathcal{F}_{LW}) - \delta_w S \Delta t \frac{L_i}{c_S} \\ &\quad + \delta_w T_{clim} k_S c_S, \end{aligned} \quad (10.75)$$

$$Y^T = q_S(t) - \delta_w \gamma T_S(t) \frac{L_w}{c_p}. \quad (10.76)$$

The equations, given by (10.61), (10.62), and (10.69), are a tridiagonal system, and we solve them by extending the double sweep method, which is used for the velocities, to handle the case where the coefficients are matrices.

Our final vertical diffusion results are the grid point horizontal velocities, specific humidity, virtual potential temperature, surface temperature, and the snow amount, which are denoted by $u_{ijk}^{(vf)}$, $v_{ijk}^{(vf)}$, $\theta_{ijk}^{(vf)}$, $q_{ijk}^{(vf)}$, T_{S_i} , and S_{l_j} , respectively. We also compute the surface drag \mathcal{D} , the surface sensible heat flux \mathcal{F}_{sh} , and the surface latent heat flux \mathcal{F}_{lh} from these new fields as

$$\mathcal{D} = \rho_S u_*^2 \frac{|\mathbf{u}_L^{(vf)}|}{|\mathbf{u}_L^{(vf)}|}, \quad (10.77)$$

$$\mathcal{F}_{sh} = c_p \nu \{T_S - \theta_L^{(vf)} P_L / (1 + .608 q_L^{(vf)})\}, \quad (10.78)$$

$$\mathcal{F}_{lh} = L_w \nu W_S \{q_{sat}(T_S) - q_L^{(vf)}\}. \quad (10.79)$$

Chapter 11

Shallow Convection

The shallow convection parameterization scheme is based on the work of Tiedtke (1984). We include a shallow convection mixing parameterization in order to reproduce more accurately the trade wind inversion layer. Without the shallow cumulus mixing mechanism, the subtropical boundary layer in the NOGAPS's model is too shallow and too moist.

The change in any quantity X due to subgrid scale eddy flux caused by shallow cumulus convection is given by

$$\frac{\partial X}{\partial t} = \frac{1}{\rho} \frac{\partial \mathcal{F}_X}{\partial z}. \quad (11.1)$$

We take into account only the vertical mixing. The vertical flux \mathcal{F}_X is defined as a large scale average over the smaller cumulus scales of the turbulent quantities:

$$\mathcal{F}_X = -\overline{\rho w' X'}_{sc}. \quad (11.2)$$

We relate the flux, which is defined by (11.2), to the large scale quantities by using a simple turbulent mixing theory as,

$$-\overline{\rho w' X'} = K_{sc} \frac{\partial X}{\partial z}. \quad (11.3)$$

We specify the mixing coefficient, K_{sc} , as

$$K_{sc} = \begin{cases} 10.0 \text{ m}^2 \text{ sec}^{-1} & \text{shallow cumulus interior} \\ 2.00 \text{ m}^2 \text{ sec}^{-1} & \text{shallow cumulus top} \\ 0.00 & \text{no shallow cumulus} \end{cases} \quad (11.4)$$

In NOGAPS, we assume that shallow cumulus convection occurs when the following four conditions are met:

1. the relative humidity of the lowest layer is at least 70 percent;
2. the surface temperature is greater than the surface air temperature;
3. the lifted condensation level (LCL) for surface air occurs within the lowest 175 mb of the atmosphere;
4. the atmosphere is moist unstable somewhere in the lowest 175 mb of the atmosphere.

We check for the first item by defining the relative humidity of the bottom layer, Rh_L and we require that,

$$Rh_L = q_L/q_{sat}(T_L) \geq 0.70. \quad (11.5)$$

For the second condition, we compute the surface air temperature by assuming an adiabatic lapse rate between the surface and the lowest pressure level. We assume that there is a constant specific humidity between the lowest level and the surface. With T_S denoting the surface skin temperature, we write the second condition as

$$T_S > \theta_i^{(vf)} P_S / (1 + .608 q_L). \quad (11.6)$$

We check for the third condition by computing the LCL temperature from Inman's (1969) formula:

$$T_{LCL} = T_d - (0.212 + 0.00171 T_d - 0.000436 T_S) D_i, \quad (11.7)$$

where T_d is the dew point in degrees C at the surface and D_i is the surface dew point depression. We assume an adiabatic ascent up to the LCL, and therefore the pressure for the LCL is given by:

$$p_{LCL} = \frac{1000 \text{ mb}}{\{\theta_L/[T_{LCL}(1 + .608q_L)]\}^{c_p/R}}. \quad (11.8)$$

For the final condition, we compute the moist static energy for all levels:

$$h_{sat_k} = c_p T_k + \phi_k + L_w q_{sat}(T_k) \quad (11.9)$$

We assume that the atmosphere is moist unstable if there exists a layer k such that,

$$h_{sat_{k+1}} > h_{sat_k}. \quad (11.10)$$

Note that we check all of the above conditions using the grid point fields from the vertical flux calculation.

If all the criterion are met, then we assume that there is mixing of temperature and moisture by shallow cumulus clouds. The shallow convection layer extends from the surface up to the top of the moist instability with a maximum depth of 175 mb above the surface. We solve for $\theta_k^{(sc)}$ and $q_k^{(sc)}$ in a manner similar to that described in Chapter 10. The equations take the form:

$$\begin{aligned} \theta_k^{(sc)} = & \theta_k^{(vf)} + \left[\frac{g2\Delta t K_{sc_{k+1/2}}}{\Delta p_k} \right] \left(\frac{\theta_{k+1}^{(sc)} - \theta_k^{(sc)}}{z_{k+1} - z_k} \right) \\ & - \frac{g2\Delta t K_{sc_{k-1/2}}}{\Delta p_k} \left(\frac{\theta_k^{(sc)} - \theta_{k-1}^{(sc)}}{z_k - z_{k-1}} \right), \end{aligned} \quad (11.11)$$

$$\begin{aligned} q_k^{(sc)} = & q_k^{(vf)} + \left[\frac{g2\Delta t K_{sc_{k+1/2}}}{\Delta p_k} \right] \left(\frac{q_{k+1}^{(sc)} - q_k^{(sc)}}{z_{k+1} - z_k} \right) \\ & - \frac{g2\Delta t K_{sc_{k-1/2}}}{\Delta p_k} \left(\frac{q_k^{(sc)} - q_{k-1}^{(sc)}}{z_k - z_{k-1}} \right). \end{aligned} \quad (11.12)$$

The notation and the time integration scheme are described in Chapter 6. In the surface layer, $k=L=18$, we assume that the vertical gradients of virtual potential temperature and the specific humidity are zero.

The tridiagonal system for $\theta_k^{(sc)}$ (we omit the horizontal indices l and j) is

$$a_k \theta_{k-1}^{(sc)} + b_k \theta_k^{(sc)} + c_k \theta_{k+1}^{(sc)} = \theta_k^{(vf)}, \quad (11.13)$$

where

$$a_k = -\frac{g2\Delta t K_{sc_{k-1/2}}}{\Delta p_k(z_{k-1} - z_k)}, \quad (11.14)$$

$$b_k = 1 - (a_k + c_k), \quad (11.15)$$

$$c_k = -\frac{g2\Delta t K_{sc_{k+1/2}}}{\Delta p_k(z_k - z_{k+1})}, \quad (11.16)$$

$$c_L = 0. \quad (11.17)$$

An analogous system obtains for $q_k^{(sc)}$. We solve (11.13) using the same Gaussian elimination procedure employed in Chapter 10 (Carnahan *et al.* [1969]).

Chapter 12

Cumulus Parameterization

The cumulus parameterization used in the NOGAPS forecast model is based on the Arakawa-Schubert (A-S) scheme. Arakawa and Schubert (1974) describes the theoretical basis for the approach, Lord and Arakawa (1980) and Lord *et al.* (1982) develop the discrete form of the parameterization to be used in a numerical model, and Lord (1972) presents verification results from semi-prognostic experiments with GARP Atlantic Tropical Experiment GATE data.

The A-S scheme shares similarities with other cumulus parameterization schemes in use today. Like other schemes, the A-S scheme adjusts a model predicted thermodynamic state toward some reference atmosphere. This adjustment process must reduce conditional instability in the model atmosphere. The reference state is defined in terms of a *cloud work function* which is a generalized form of conditional instability. Arakawa and Schubert (1974) show that the cloud work function can be interpreted as the work done by the buoyancy force that is converted into the kinetic energy of the cumulus updrafts. A fundamental assumption of A-S is that there is a *quasi-equilibrium* between the generation of the cloud work function by large scale processes and its conversion to cloud scale motion. Therefore, the cloud work function vertical profile in a convectively active atmosphere always remains

near some reference or climatological state. This reference state has been observationally verified (Lord and Arakawa, [1980]) to be nearly constant over a wide range of convective regimes.

An important property of the cloud work function is that it is dependent on the vertical profile of a composite of temperature and moisture, but is not a function of each variable profile individually. For this reason the cloud work function quasi-equilibrium is a less restrictive constraint than, for example, the moist adiabatic lapse rate, which is a function of temperature only. This gives the A-S scheme more degrees of freedom to reach a convective equilibrium state. Theoretically, this is an attractive property of the scheme, but in practice it can allow undesirable biases to develop in vertical heating profiles. Considerable research on this problem remains before the full advantage of the A-S scheme will be realized.

A second similarity of the A-S scheme with other cumulus parameterization schemes is the use of a cloud model to interact with the large scale environment. A-S differs from most other schemes in allowing an *ensemble* of cloud types with different cloud top pressures to exist at each model grid point. Cloud and environmental thermodynamic budgets are derived for each cloud type. The early A-S formulations use a simple entraining plume model for each cloud in the ensemble, with constant entrainment rate for each cloud defined. All downdrafts take place in the dry environment. Payne (1981) has shown the benefits of including moist downdrafts in the A-S cloud model. In the NOGAPS formulation, the cloud model is generalized to include the effects of a simple cloud scale moist downdraft. This has a beneficial impact on the vertical heating/moistening profiles produced by the NOGAPS A-S scheme.

In all cumulus parameterization schemes, a closure assumption must be made to determine the strength or intensity of the convection. In the A-S scheme, this

closure is defined in terms of the *cloud base mass flux* generated by each cloud in the ensemble. Once found, the cloud base mass fluxes are combined with the environmental budgets to yield the changes to thermodynamic variables. The problem of the parameterization therefore reduces to solving for these mass fluxes.

The cloud ensemble concept is the distinguishing characteristic of the A-S parameterization from nearly all other schemes used in NWP models. Not only do the clouds interact with the large scale environment to stabilize it, but the clouds in an ensemble interact with one another as they modify the environment. This interaction is represented in the A-S scheme through a cloud interaction *kernel* that is a unique feature of the scheme. Much of the following discussion on the cloud and environmental budget equations is from Lord(1978). Readers interested in more details and theoretical discussion are referred there.

12.1 Thermodynamic Profiles and Vertical Structure

The model atmosphere is defined by the thermodynamic state variables potential temperature θ , or temperature T , and specific humidity q . The geopotential ϕ is computed from θ via the hydrostatic equation. The dry static energy and moist static energy are defined as

$$s = c_p T + \phi, \quad (12.1)$$

and

$$h = c_p T + \phi + L_w q. \quad (12.2)$$

For cloud buoyancy effects we use the virtual dry static energy

$$s_v = s + c_p T(\delta q - \ell), \quad (12.3)$$

where $\delta = 0.608$ and ℓ is the cloud liquid water content.

The thermodynamic variables predicted by the model represent the large scale environment. All cloud thermodynamic properties must be expressed in terms of these variables. We assume that cloud air is saturated. From the Clausius-Clapeyron equation

$$q^c = \bar{q}^* + \frac{1}{c_p} \left(\frac{\partial \bar{q}^*}{\partial T} \right)_p (s^c - \bar{s}), \quad (12.4)$$

where the superscript c denotes a cloud variable, the asterisk a saturation value, and the overbar a large scale environment value. Also

$$s^c - \bar{s} = \frac{1}{1 + \gamma} (h^c - \bar{h}^*) \quad (12.5)$$

and

$$q^c - \bar{q}^* = \frac{\gamma}{1 + \gamma} \frac{1}{L_w} (h^c - \bar{h}^*) \quad (12.6)$$

where

$$\gamma = \frac{L_w}{c_p} \left(\frac{\partial \bar{q}^*}{\partial T} \right)_p. \quad (12.7)$$

A convective cloud becomes non-buoyant with respect to the large scale environment when

$$s^c - \bar{s} + c_p \bar{T} [\delta (q^c - \bar{q}) - \ell^c] = 0. \quad (12.8)$$

Neglecting overshooting, the level of vanishing buoyancy is the cloud top. From (12.4 - 12.8) the cloud top moist static energy is

$$\hat{h}^* = \bar{h}^* - \frac{(1 + \gamma)L_w \epsilon}{1 + \gamma \epsilon \delta} [\delta (\bar{q}^* - \bar{q}) - \hat{\ell}], \quad (12.9)$$

where

$$\epsilon = \frac{c_p \bar{T}}{L_w}, \quad (12.10)$$

and the $(\hat{\cdot})$ denotes a cloud top value. In a conditionally unstable environment the condition

$$\bar{h} < \hat{h}^* < \bar{h}^* \quad (12.11)$$

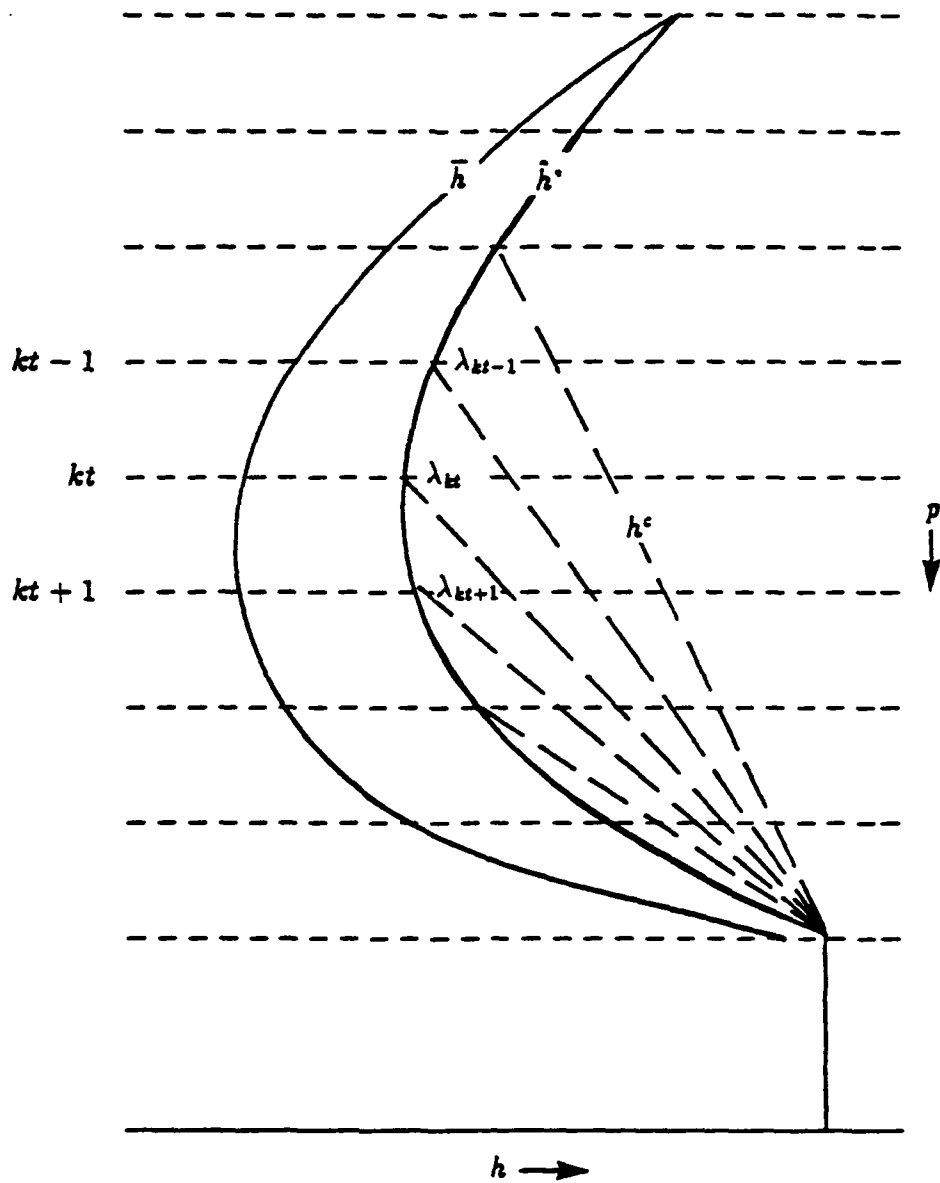


Figure 12.1: Schematic profiles of \bar{h} and \hat{h}^* . Dashed lines are profiles of cloud air h^c produced by entrainment mixing.

must exist. Figure 12.1 shows a typical vertical profile of \bar{h} and \hat{h}^* . The dashed lines are profiles of h^c that result from the entrainment (mixing) of high \bar{h} air from below the lifting condensation level (LCL) with lower \bar{h} air as the cloud rises. Where a dashed line crosses \hat{h}^* defines a cloud top. The smaller the entrainment rate, the less rapidly the cloud loses its buoyancy with respect to the environment and the higher it will penetrate. A non-entraining hot tower cloud can penetrate until \hat{h}^* equals the moist static energy of the sub cloud layer.

12.2 Parameterization of Ice Physics

The release of latent heat of fusion when cloud liquid water freezes is a significant factor in buoyant energy production in deep cumulus convection. The microphysics of precipitation is far too complex and computationally expensive for any attempt to model it as part of a large scale cumulus parameterization. The most we can hope for is to crudely model the bulk effects of ice formation on cloud buoyancy.

Ice formation increases cloud buoyancy over liquid water formation through two mechanisms. First, the equilibrium saturation vapor pressure e^* over ice is less than that over water, so more precipitate will be formed and more latent heat released when we include this dependence. Second, the extra change of phase step from liquid to ice releases the latent heat of fusion, in addition to the latent heat of condensation already released when water vapor condenses. We model the first effect by linearly combining the over water and over ice values of saturation vapor pressure such that:

$$e^* = \begin{cases} e_{\text{vapor}}^* & \text{for } T \geq 0^\circ \text{ C,} \\ e_{\text{vapor}}^* - T/40(e_{\text{ice}}^* - e_{\text{vapor}}^*) & \text{for } -40^\circ \text{ C} \leq T < 0^\circ \text{ C,} \\ e_{\text{ice}}^* & \text{for } T < -40^\circ \text{ C.} \end{cases} \quad (12.12)$$

We model the second effect by linearly combining the latent heat of condensation L_w and latent heat of fusion L_i such that:

$$L_{wi} = \begin{cases} L_w & \text{for } T \geq 0^\circ \text{ C,} \\ L_w - T/40 L_i & \text{for } -40^\circ \text{ C} \leq T < 0^\circ \text{ C,} \\ L_w + L_i & \text{for } T < -40^\circ \text{ C.} \end{cases} \quad (12.13)$$

We replace L_w with L_{wi} in all terms representing vapor/liquid/ice change of phase processes.

12.3 The Discrete Model

We now introduce the vertical structure of the discrete model used in the NOGAPS A-S cumulus scheme. Figure 12.2 shows an example ensemble of 3 clouds with tops at model full levels $K_{top}, K_{top} + 3, K_{top} + 9$, where $K_{top} = 5$. For purposes of demonstration we assume that candidate clouds at the other levels have been eliminated by the variety of mechanisms that will be described later. We introduce a local vertical coordinate k with its origin ($k = 1$) at the top of the deepest cloud (K_{top}). The bottom full level is $k = N_p = L - K_{top} + 1 = 14$. The first full level above the LCL is $k = k_c = 12$. For convenience we also define a cloud type index k_t with its origin at the top of the highest cloud. In the present example the cloud tops are at $k_t = 1, 4$, and 10 respectively. In all subsequent descriptions, vertical indexing will be in terms of k or k_t unless otherwise indicated. K_{top} may have values corresponding to the full range of meteorologically realistic cloud top pressures. In the $L = 18$ level NOGAPS we allow

$$3 \leq K_{top} \leq L - 1,$$

which allows clouds to penetrate to about 70 mbs.

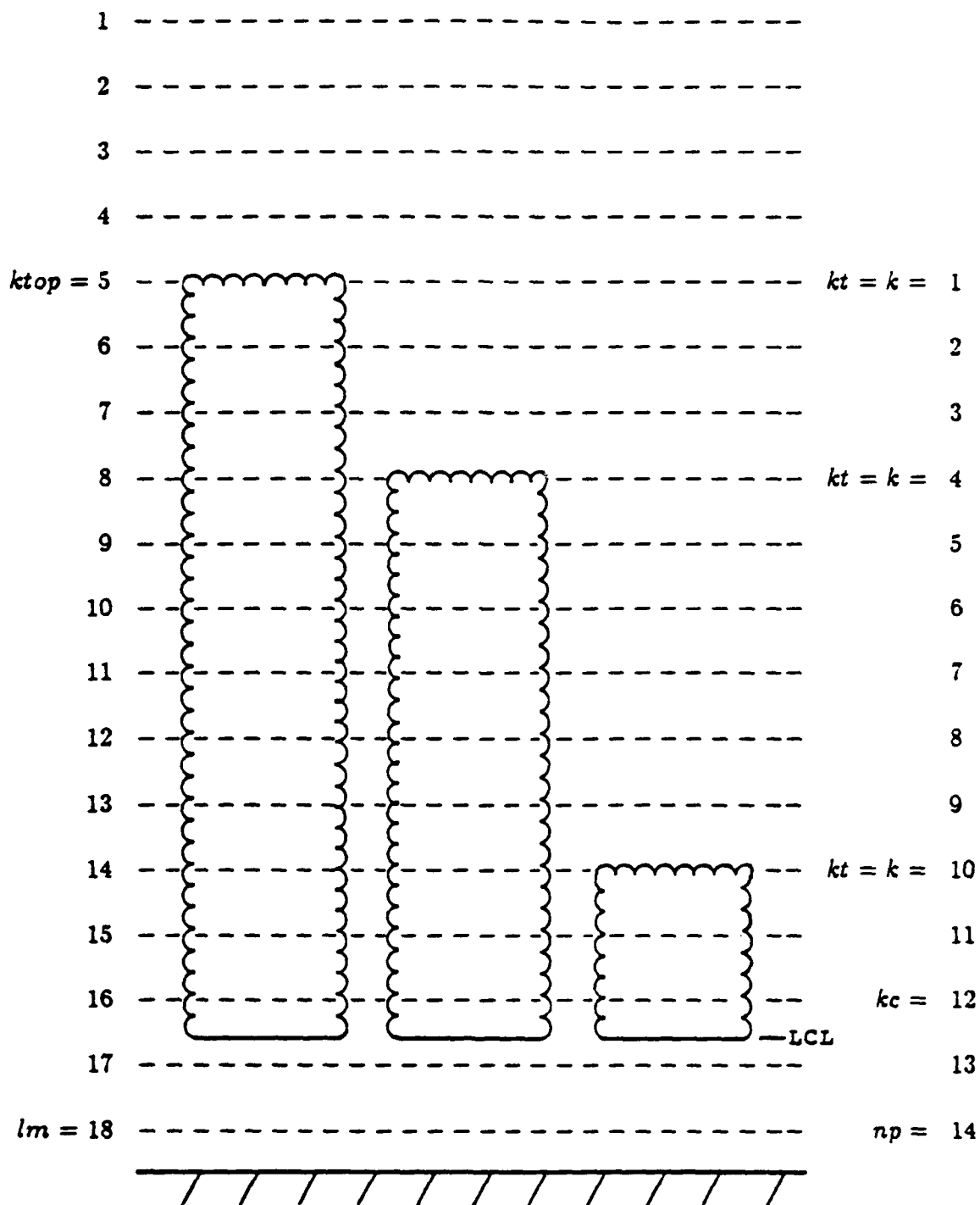


Figure 12.2: Three cloud ensemble showing vertical coordinate and cloud top index coordinate for the A-S scheme.

12.4 Cloud Budget Equations

The cloud model is an entraining plume with constant entrainment rate λ . In continuous form the cloud model is

$$\eta = \exp[\lambda(z - z_o)], \quad z \geq z_o, \quad (12.14)$$

where η is the normalized cloud base mass flux. Above the cloud base, the discrete form of 12.14 is

$$\eta_{k-1/2, k_t} = \eta_{k+1/2, k_t} (1 + \lambda_{k_t} \Delta z_k), \quad k_t < k \leq k_c, \quad (12.15)$$

where at cloud base

$$\eta_{k_c+1/2, k_t} = 1. \quad (12.16)$$

Below the cloud base, the mass flux varies linearly to zero at the surface. The cloud base (LCL) is defined simply as the half level $k_c + 1/2$ below the lowest full level k_c where $q_{N_p} > q_{k_c}^*$. Figure 12.3 schematically shows the discrete cloud mass budget. e_{k, k_t} and d_{k, k_t} are entrainment and detrainment terms which are related to the net entrainment rate and the normalized mass flux by

$$e_{k, k_t} = \lambda_{k_t} (1 + c_d) \Delta z_k \eta_{k+1/2, k_t}, \quad (12.17)$$

$$d_{k, k_t} = \lambda_{k_t} c_d \Delta z_k \eta_{k+1/2, k_t}, \quad (12.18)$$

where c_d is a fractional detrainment parameter (currently we use $c_d = 0$). An alternate form of (12.15) is

$$\eta_{k-1/2, k_t} = \eta_{k+1/2, k_t} + e_{k, k_t} - d_{k, k_t}. \quad (12.19)$$

At the cloud top, all mass must be detrained into the large scale environment; therefore

$$\hat{d}_{k_t} = \eta_{k_t+1/2, k_t} (1 + \lambda_{k_t} \widehat{\Delta z_{k_t}}). \quad (12.20)$$

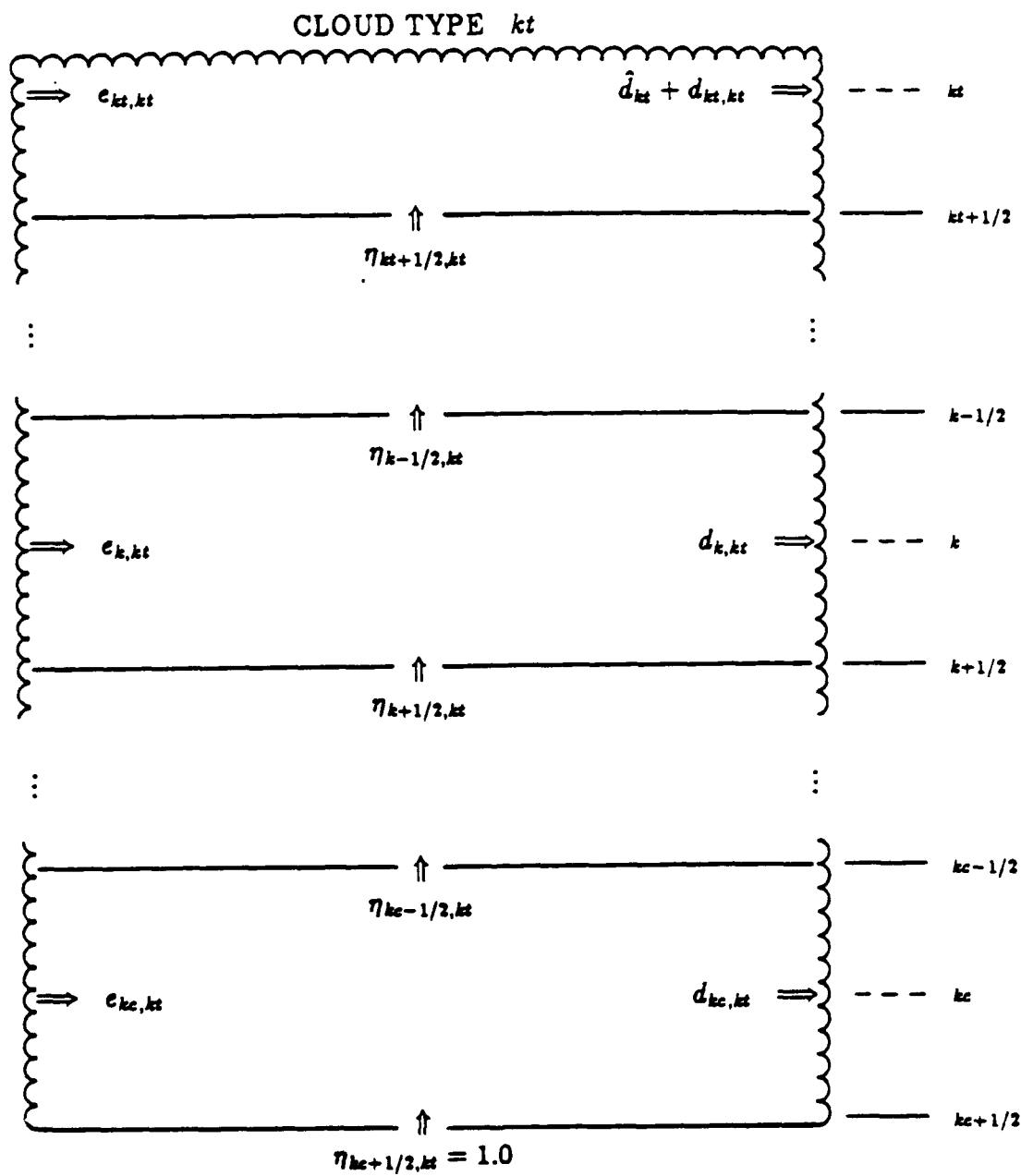


Figure 12.3: Schematic depiction of cloud mass budget for A-S cloud model showing exchange of mass between cloud and large scale environment.

The cloud ensemble moist static energy budget is

$$\begin{aligned} & \eta_{k-1/2,k_t} h_{k-1/2,k_t}^c - \eta_{k+1/2,k_t} h_{k+1/2,k_t}^c \\ &= e_{k,k_t} \bar{h}_k - d_{k,k_t} \frac{h_{k+1/2,k_t}^c + h_{k-1/2,k_t}^c}{2}. \end{aligned} \quad (12.21)$$

Figure 12.4 gives a schematic view of the budget. Using (12.15), (12.16), and (12.18) we can rewrite (12.21) as

$$h_{k-1/2,k_t}^c = \bar{h}_k + I_{k,k_t} (h_{k+1/2,k_t}^c - \bar{h}_k), \quad (12.22)$$

where

$$I_{k,k_t} = \frac{1 - \frac{c_d}{2} \lambda_{k_t} \Delta z_k}{1 + (1 + \frac{c_d}{2}) \lambda_{k_t} \Delta z_k}. \quad (12.23)$$

At cloud top, the moist static energy budget is

$$\begin{aligned} \hat{d}_{k_t} \hat{h}_{k_t} &= \eta_{k_t+1/2,k_t} h_{k_t+1/2,k_t}^c \\ &+ e_{k_t,k_t} \bar{h}_{k_t} - d_{k_t,k_t} \frac{\hat{h}_{k_t} + h_{k_t+1/2,k_t}^c}{2}, \end{aligned} \quad (12.24)$$

which becomes

$$\hat{h}_{k_t} = \bar{h}_{k_t} + \hat{I}_{k_t} (h_{k_t+1/2,k_t}^c - \bar{h}_{k_t}), \quad (12.25)$$

where

$$\hat{I}_{k_t} = \frac{1 - \frac{c_d}{2} \lambda_{k_t} \widehat{\Delta z}_{k_t}}{1 + (1 + \frac{c_d}{2}) \lambda_{k_t} \widehat{\Delta z}_{k_t}}. \quad (12.26)$$

Equations (12.22) and (12.25) require values of $h_{N_p+1/2}^c$ (i.e., surface values) to begin the recursive solution for the cloud budgets of moist static energy. Because we start the budget calculations below the actual cloud bases, however, we can only define virtual values for cloud variables in sub-cloud layers. We have chosen to define $h_{N_p+1/2}^c$ as the pressure weighted mean moist static energy in the subcloud layer. We write

$$h_{N_p+1/2}^c = \frac{\sum_{k=N_p}^{k_c+1} \bar{h}_k \Delta p_k}{\sum_{k=N_p}^{k_c+1} \Delta p_k}, \quad (12.27)$$

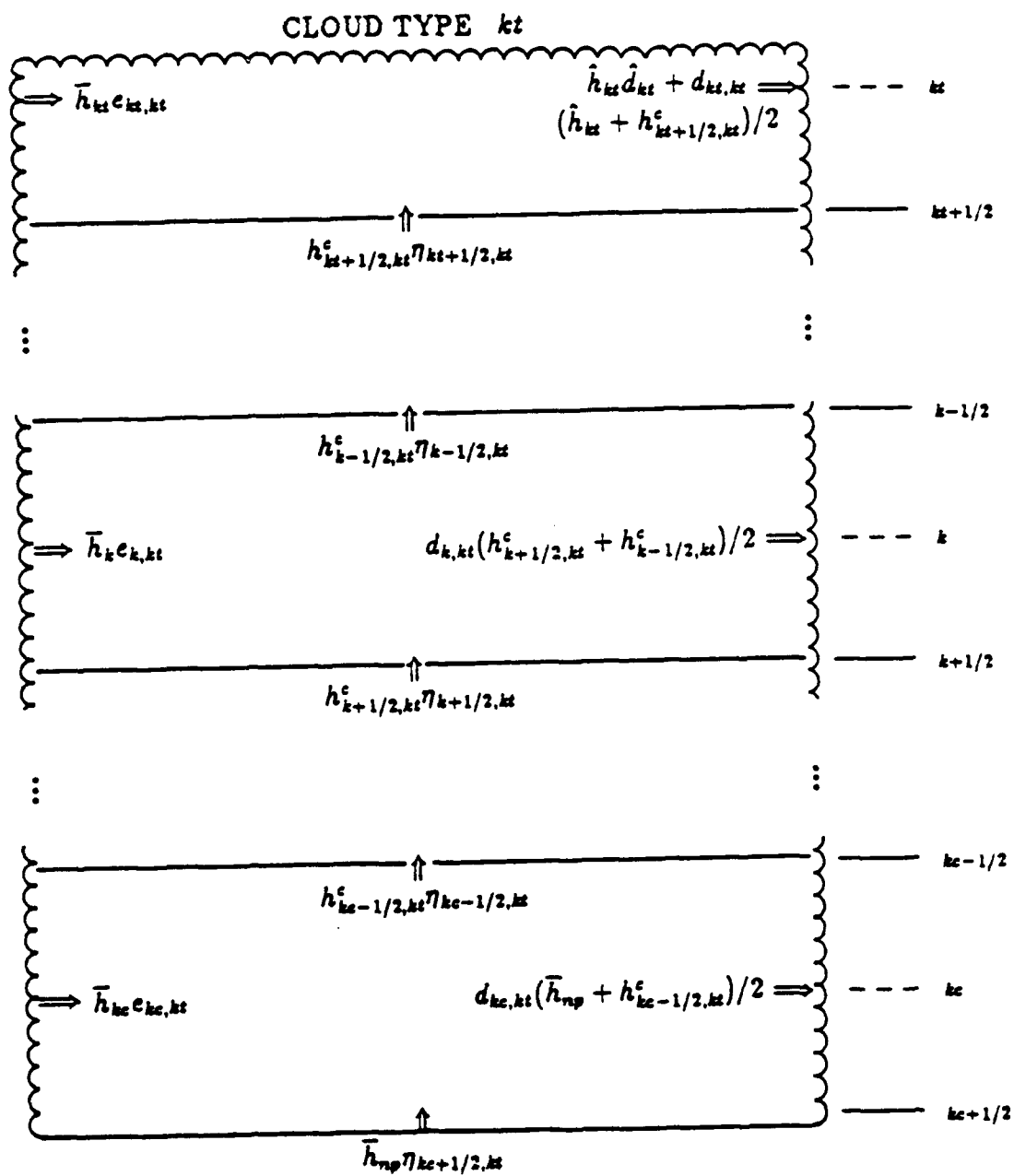


Figure 12.4: Schematic of cloud moist static energy budget showing exchanges between cloud and large scale environment.

where $k_c + 1$ is the first full layer below the LCL.

The cloud ensemble total water budget equation is analogous to the moist static energy budget, with the complication that we must partition the total cloud water among cloud water vapor, non-precipitating liquid water, and precipitating liquid water via a crude microphysics model. The cloud water budget equation is

$$\begin{aligned} \eta_{k-1/2,k_t} q_{k-1/2,k_t}^c - \eta_{k+1/2,k_t} q_{k+1/2,k_t}^c = \\ e_{k,k_t} \bar{q}_k - d_{k,k_t} \frac{q_{k+1/2,k_t}^c + q_{k-1/2,k_t}^c}{2} - \eta_{k,k_t} r_{k,k_t} \Delta z_k. \end{aligned} \quad (12.28)$$

The last term in (12.28) is the moisture sink due to precipitation. Figure 12.5 is a schematic representation of the total cloud water budget process. Notice that η_{k,k_t} is a full level normalized mass flux. For computational convenience we choose

$$\begin{aligned} \eta_{k,k_t} &= \eta_{k+1/2,k_t} + e_{k,k_t} - \frac{d_{k,k_t}}{2} \\ &= \eta_{k+1/2,k_t} [1 + \lambda_{k_t} (1 + \frac{c_d}{2}) \Delta z_k]. \end{aligned} \quad (12.29)$$

The cloud liquid water computations are done at the full levels. The full level water budget equation is

$$\eta_{k,k_t} q_{k,k_t}^c = \eta_{k+1/2,k_t} q_{k+1/2,k_t}^c + e_{k,k_t} \bar{q}_k - \frac{d_{k,k_t}}{2} q_{k+1/2,k_t}^c, \quad (12.30)$$

or

$$q_{k,k_t}^c = \bar{q}_k + I_{k,k_t} (q_{k+1/2,k_t}^c - \bar{q}_k), \quad (12.31)$$

Notice that (12.31) is exactly analogous to (12.22) for the moist static energy budget. This is a consequence of our choice of (12.29) for defining η_{k,k_t} . The cloud saturation water vapor is found using (12.6):

$$q_{k,k_t}^{*c} = \bar{q}_k^* + \frac{\gamma_k}{1 + \gamma_k} \frac{1}{L_w} (h_{k+1/2,k_t}^c - \bar{h}_k^*). \quad (12.32)$$

The total cloud liquid water content is

$$\ell_{k,k_t} = q_{k,k_t}^c - q_{k,k_t}^{*c}. \quad (12.33)$$

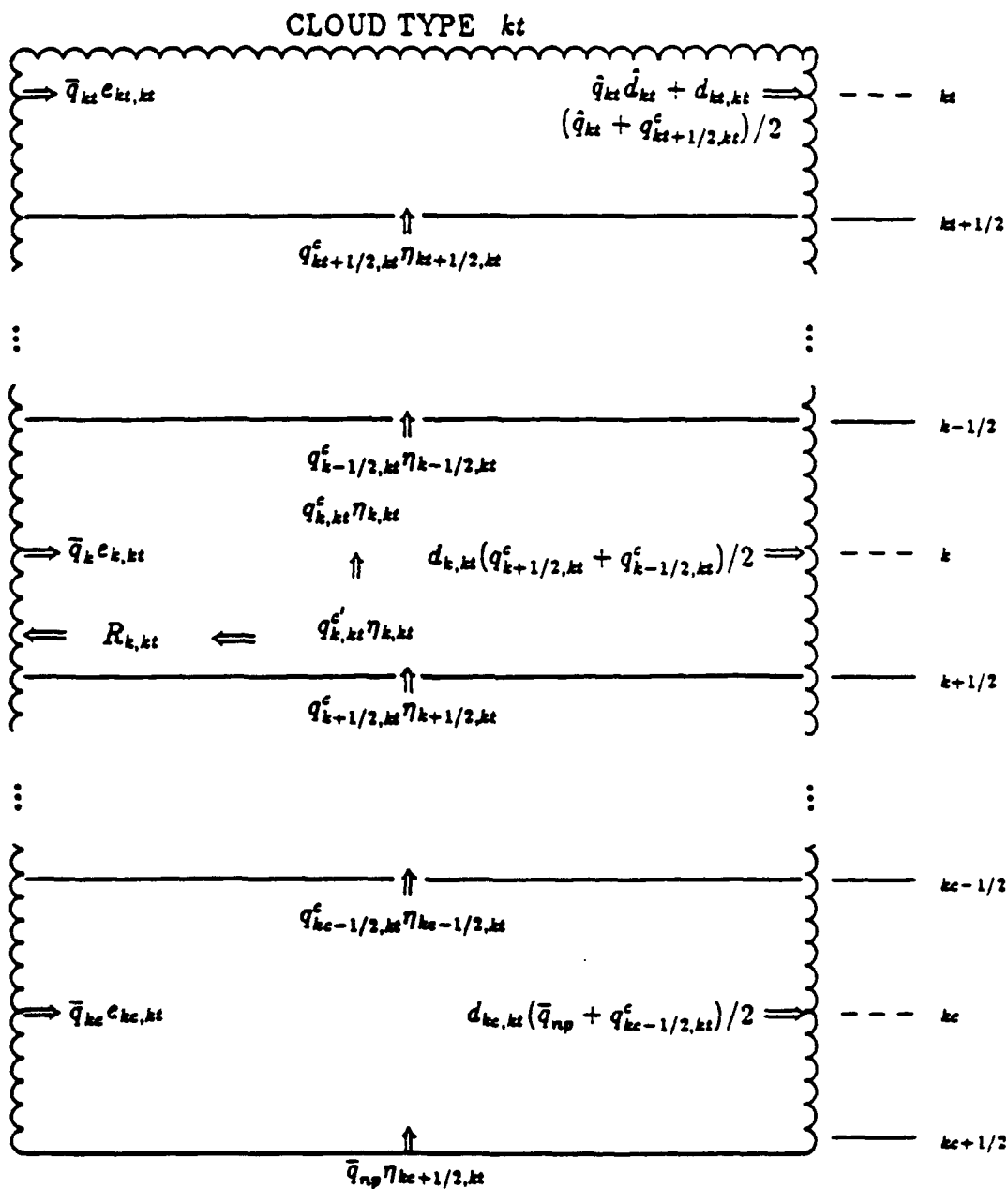


Figure 12.5: Schematic of total cloud water budget showing exchanges between cloud and large scale environment.

The cloud liquid water content after precipitation is removed is

$$\ell'_{k,k_t} = \ell_{k,k_t} - r_{k,k_t} \Delta z_k, \quad (12.34)$$

where

$$r_{k,k_t} = c_{o_{k_t}} [\ell'_{k,k_t} - \ell_c]. \quad (12.35)$$

ℓ_c is the minimum cloud liquid water content at which precipitation can be produced and $c_{o_{k_t}}$ is a cloud microphysics parameter which determines precipitation generation efficiency. Currently ℓ_c is set to 0.0 and $c_{o_{k_t}}$ to 0.002 m^{-1} for all levels within a cloud except at cloud top, where it is 0.004 m^{-1} . Combining (12.34) and (12.35) and solving for ℓ'_{k,k_t} yields

$$\ell'_{k,k_t} = \frac{\ell_{k,k_t} + c_{o_{k_t}} \ell_c \Delta z_k}{1 + c_{o_{k_t}} \Delta z_k}, \quad (12.36)$$

and the amount of precipitation per unit cloud base mass flux produced in layer k from cloud type k_t is

$$R_{k,k_t} = \eta_{k,k_t} r_{k,k_t} \Delta z_k, \quad (12.37)$$

which is also the last term in (12.28). However, if we subtract (12.30) from (12.28) we get

$$q_{k-1/2,k_t}^c \left(\eta_{k-1/2,k_t} + \frac{d_{k_t}}{2} \right) = \eta_{k,k_t} (q_{k,k_t}^c - r_{k,k_t} \Delta z_k). \quad (12.38)$$

The term in parentheses in the last term of (12.38) is total cloud water after precipitation is removed. If we substitute (12.29) and (12.18) into (12.38) the result is

$$q_{k-1/2,k_t}^c = q_{k,k_t}^c - r_{k,k_t} \Delta z_k. \quad (12.39)$$

At cloud top the total water budget equation is exactly analogous to the budget equations at lower levels, so

$$q_{k_t,k_t}^c = \bar{q}_{k_t} + \widehat{I}_{k_t} (q_{k_t+1/2,k_t}^c - \bar{q}_{k_t}). \quad (12.40)$$

A requirement for cloud existence is that at cloud top a cloud be saturated, i.e., that $q_{k_i, k_i}^c > \tilde{q}_{k_i}^*$. At lower levels within each cloud this is not required.

12.5 Special Treatment at Top of Deepest Clouds

In section 12.1 the cloud top moist static energy is defined (Equation 12.9). In the discrete model, each full model level k_i may become a cloud top, and there is a unique value of \hat{h}^* at each of these levels. The deepest possible cloud is one with entrainment rate λ_{k_i} equal to zero, which corresponds to $\hat{h}_{k_i-1/2}^*$ equal to \bar{h}_{N_p} . Because in practice there is seldom an exact match between $\hat{h}_{k_i-1/2}^*$ and \bar{h}_{N_p} at any level, the deepest cloud ($k_i = 1$) actually occurs for the case where $\hat{h}_{k_i-1/2}^* > \bar{h}_{N_p}$ and $\hat{h}_{k_i+1/2}^* < \bar{h}_{N_p}$. During a forecast model integration, however, it is not unusual for \bar{h}_{N_p} to increase enough so that $\hat{h}_{k_i-1/2}^* < \bar{h}_{N_p}$, where earlier in the forecast $\hat{h}_{k_i-1/2}^* > \bar{h}_{N_p}$, meaning that $k_i = 1$ must be defined one model level higher. When this is allowed to occur at a grid point, a cloud type which has previously been excluded from the cloud ensemble spectrum may suddenly appear, or if the process is reversed, suddenly disappear. Such behavior is physically unrealistic as well as a source of computational noise as deep clouds are sporadically turned on and off.

The solution is to redefine the position of the $k_i = 1$ level and the variables values there so that the $k_i = 1$ clouds can smoothly vary in height as \bar{h}_{N_p} varies relative to $\hat{h}_{k_i}^*$. At $k_i = 1$ we have

$$\hat{h}_{1/2}^* \leq \bar{h}_{N_p} < \hat{h}_{3/2}^*. \quad (12.41)$$

Let

$$\hat{h}_1^* = \frac{\bar{h}_{N_p} + \hat{h}_{3/2}^*}{2}, \quad (12.42)$$

and the adjusted height at $k_i = 1$ be

$$\hat{z}_1 = z_{3/2} + \hat{K}(\bar{h}_{N_p})[z_1 - z_{3/2}], \quad (12.43)$$

where $\widehat{K}(\bar{h}_{N_p})$ is the linear interpolation coefficient

$$\widehat{K}(\bar{h}_{N_p}) = \frac{\bar{h}_{N_p} - \hat{h}_{3/2}^*}{\hat{h}_{1/2}^* - \hat{h}_{3/2}^*}. \quad (12.44)$$

Note that $\widehat{K}(\bar{h}_{N_p})$ varies from 0.0 to 1.0 as \bar{h}_{N_p} varies from $\hat{h}_{1/2}^*$ to $\hat{h}_{3/2}^*$, so we have the smoothly varying behavior we want. The thermodynamic variables for layer $k_t = 1$ are redefined as

$$\bar{\Psi}_1 = \bar{\Psi}_{3/2} + \frac{\widehat{K}(\bar{h}_{N_p})}{2} [\bar{\Psi}_{1/2} - \bar{\Psi}_{3/2}], \quad (12.45)$$

where

$$\bar{\Psi} = \{\bar{T}, \bar{q}, \bar{\phi}, \bar{p}\}.$$

We use (12.45) for only these variables, all derived quantities are computed in appropriate ways to preserve non-linearities, e.g., using (12.45) to get $\bar{T}_{k_t=1}$ and $\bar{p}_{k_t=1}$ and then finding $\bar{q}_{k_t=1}^*$ as a function of these interpolated quantities.

The cloud budget equations described in section 12.4 are in no way affected by this redefinition of layer $k_t = 1$. The changes do influence the large scale environmental changes, however, and will be discussed in section 12.13.

12.6 Solution for Entrainment Rate

Equations (12.22) and (12.25) form a recursive system of equations for the budget of cloud moist static energy. Since at its top a cloud must be neutrally buoyant with respect to the large scale environment, we can use (12.9) to close the system. The system is highly non-linear in λ_{k_t} and so must be solved numerically for the root that represents a physical solution. We use the pseudo-secant method, which is a finite difference analog to Newton's method. The buoyancy equation is

$$B(\lambda_{k_t}) = h_{k_t, k_t}^c - \hat{h}_{k_t}^* - \ell_{k_t, k_t}^c \left[\frac{(1 + \gamma_{k_t}) c_p \bar{T}_{k_t}}{1 + \gamma_{k_t} \delta c_p \bar{T}_{k_t} / L_w} \right]. \quad (12.46)$$

The pseudo-secant algorithm is

$$\Delta\lambda^{\nu+1} = -\Delta\lambda^{\nu} \frac{B(\lambda^{\nu})}{B(\lambda^{\nu}) - B(\lambda^{\nu-1})}, \quad (12.47)$$

where

$$\lambda^{\nu+1} = \lambda^{\nu} + \Delta\lambda^{\nu+1}, \quad \nu = \text{iteration counter.}$$

Notice that we must have two estimates of λ_{k_i} to begin the iteration.

We start the iteration with an assumed small value of λ_{k_i} , say 10^{-5} , and recursively solve the moist static energy equations (12.22, 12.25) and the total water budget equations (12.31, 12.39, 12.40) from the bottom up using the sub-cloud base layer values \bar{h}_{N_p} and \bar{q}_{N_p} as $h_{N_p+1/2, k_i}^c$ and $q_{N_p+1/2, k_i}^c$. If the cloud top buoyancy $B(\lambda_{k_i}^{\nu=1})$ is greater than zero, $\lambda_{k_i}^{\nu=1}$ is too small and $\lambda_{k_i}^{\nu=2}$ must be greater than $\lambda_{k_i}^{\nu=1}$. If $B(\lambda_{k_i}^{\nu=1})$ is less than zero, $\lambda_{k_i}^{\nu=1}$ is too big and $\lambda_{k_i}^{\nu=2}$ must be less than $\lambda_{k_i}^{\nu=1}$. We use a $\pm 10\%$ λ increment for these differences. The iteration is terminated when $|B(\lambda_{k_i})|$ is less than $4.0 \text{ Joules kg}^{-1}$, which corresponds to $\pm 0.004^\circ \text{ C}$ or $\pm 0.0016 \text{ g kg}^{-1}$ specific humidity. Six to seven iterations is usually sufficient. Experience has shown that the method converges best when an iteration starts with $\lambda_{k_i}^{\nu=1}$ too small (clouds too buoyant). We therefore begin with the deepest cloud in an ensemble ($k_i = 1$) and use $\lambda_{k_i=1}$ as the initial estimate for $\lambda_{k_i=2}^{\nu=1}$, etc.

A byproduct of the pseudo-secant iteration is a very good estimate of the derivative of the buoyancy function $B(\lambda_{k_i})$ as a function of λ_{k_i} . At convergence we save

$$\frac{d}{d\lambda_{k_i}} [B(\lambda_{k_i})] = \frac{B(\lambda_{k_i}^{\nu}) - B(\lambda_{k_i}^{\nu-1})}{\lambda_{k_i}^{\nu} - \lambda_{k_i}^{\nu-1}}, \quad (12.48)$$

for later use in a true Newton's method iteration when we find the elements of the cloud interaction kernel matrix.

There are several potential physical and computational problems that can occur during a λ_{k_i} iteration. They are

1. $B(\lambda_{k_i}^\nu) - B(\lambda_{k_i}^{\nu-1}) = 0.0$,
2. $\lambda_{k_i}^\nu < 0.0$,
3. $\lambda_{k_i}^\nu$ too large (> 0.01),
4. No convergence (ν greater than 10),
5. Cloud not saturated at top: $q_{k_i, k_i}^c < q_{k_i, k_i}^{*c}$.

In the first four cases the condition is pathological and this cloud must be removed from the ensemble. The last condition normally occurs when the large scale environment is so dry that the entrainment processes never let the cloud air reach saturation. This is a real physical mechanism for rejecting potential clouds from an ensemble. Another situation that requires rejection of clouds from an ensemble occurs when a cloud loses its buoyancy at a level with an unstable layer above that level. Figure 12.6 shows a profile of \hat{h}^* with typical λ solutions for a situation which might occur above a trade wind inversion. The distinguishing characteristic of the λ solutions in this case is for λ to increase for increasing cloud top height, a physically implausible result. To detect these physically unrealistic values of λ , we look for the condition

$$\lambda_{k_i-1} > \lambda_{k_i} > \lambda_{k_i+1}. \quad (12.49)$$

Wherever 12.49 is satisfied, λ_{k_i} is rejected from the cloud ensemble.

After the λ_{k_i} are found, we use (12.15) to get $\eta_{k-1/2, k_i}$, the normalized mass flux profiles. Solution of the total cloud water budget equations (12.31, 12.37, 12.40) also yields the normalized convective precipitation. However, since the precipitation must be equal to the vertically integrated net environmental drying in a column, we use the environmental water budget equations of Section 12.8 to ensure an exact balance between these two terms in global water budget accounting.

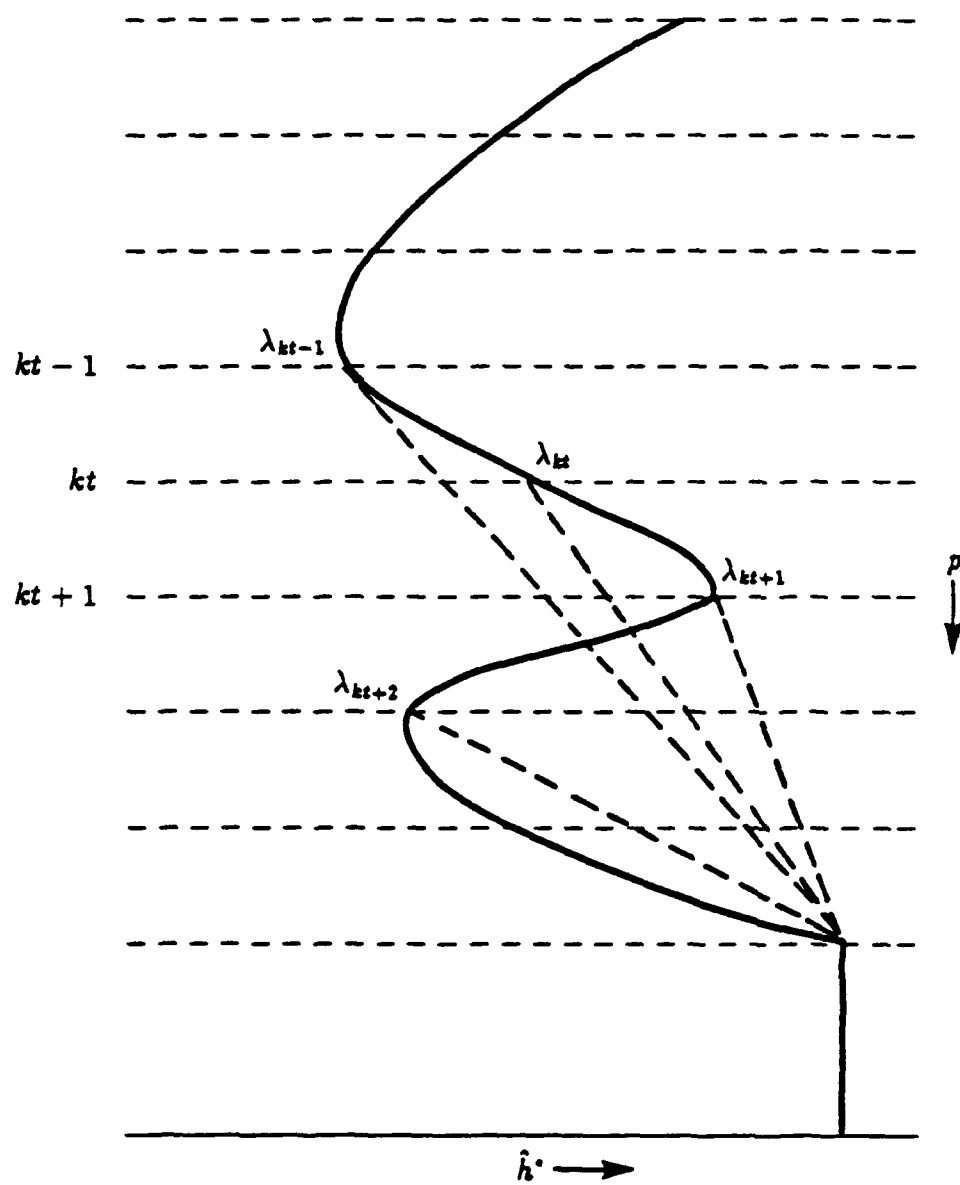


Figure 12.6: Example of λ solution for cloud detraining below unstable layer. Cloud for λ_{k_t} must be rejected.

12.7 The Cloud Work Function

Arakawa and Schubert (1974) show that the generation of kinetic energy by cloud buoyant force is given by

$$A(\lambda) = \int_{z_B}^{\hat{z}(\lambda)} \frac{g}{c_p \bar{T}_{z'}} \eta_{z',\lambda} (s_{v,z',\lambda}^c - \bar{s}_{v,z'}) dz'. \quad (12.50)$$

The cloud work function per unit cloud base mass flux is therefore proportional to the buoyancy of the cloud air relative to its large scale environment and the normalized mass flux within the cloud, integrated from cloud base to cloud top. In discrete form (12.50) can be written as

$$A_{k_t} = g \sum_{k=k_t}^{N_p} \eta_{k+1/2,k_t} \Delta z_{k+1/2} [f_{k+1/2} (h_{k+1/2,k_t}^c - \hat{h}_{k+1/2}^*) - \ell_{k,k_t}^c], \quad (12.51)$$

where

$$f_{k+1/2} = \frac{1 + \gamma_{k+1/2} \delta c_p \bar{T}_{k+1/2} / L_w}{(1 + \gamma_{k+1/2}) c_p \bar{T}_{k+1/2}}.$$

In a convectively active atmosphere the cloud work function A_{k_t} has been shown to be approximately constant, i.e. the quasi-equilibrium condition (Lord, [1978]). In the NOGAPS model we use (12.51) to compute the A_{k_t} and compare them to predefined climatological values $A_{k_t}^{clim}$ (Table 12.7). If

$$A_{k_t} - A_{k_t}^{clim} > 0,$$

then the k_t cloud can exist. If this difference is less than zero, then the k_t cloud is not unstable enough to exist and is removed from the ensemble.

12.8 Large Scale Environmental Budget

Equations

Table 12.1: Climatological cloud work function at a function of cloud top pressure. Values are normalized by pressure depth of cloud.

P_{top}	$\frac{A_{clim}}{P_{bot} - P_{top}}$
10.0	2.0000
100.0	1.8983
200.0	1.2425
300.0	0.5162
400.0	0.3252
500.0	0.1915
600.0	0.0924
700.0	0.0577
800.0	0.0350
900.0	0.0220
1000.0	0.0150

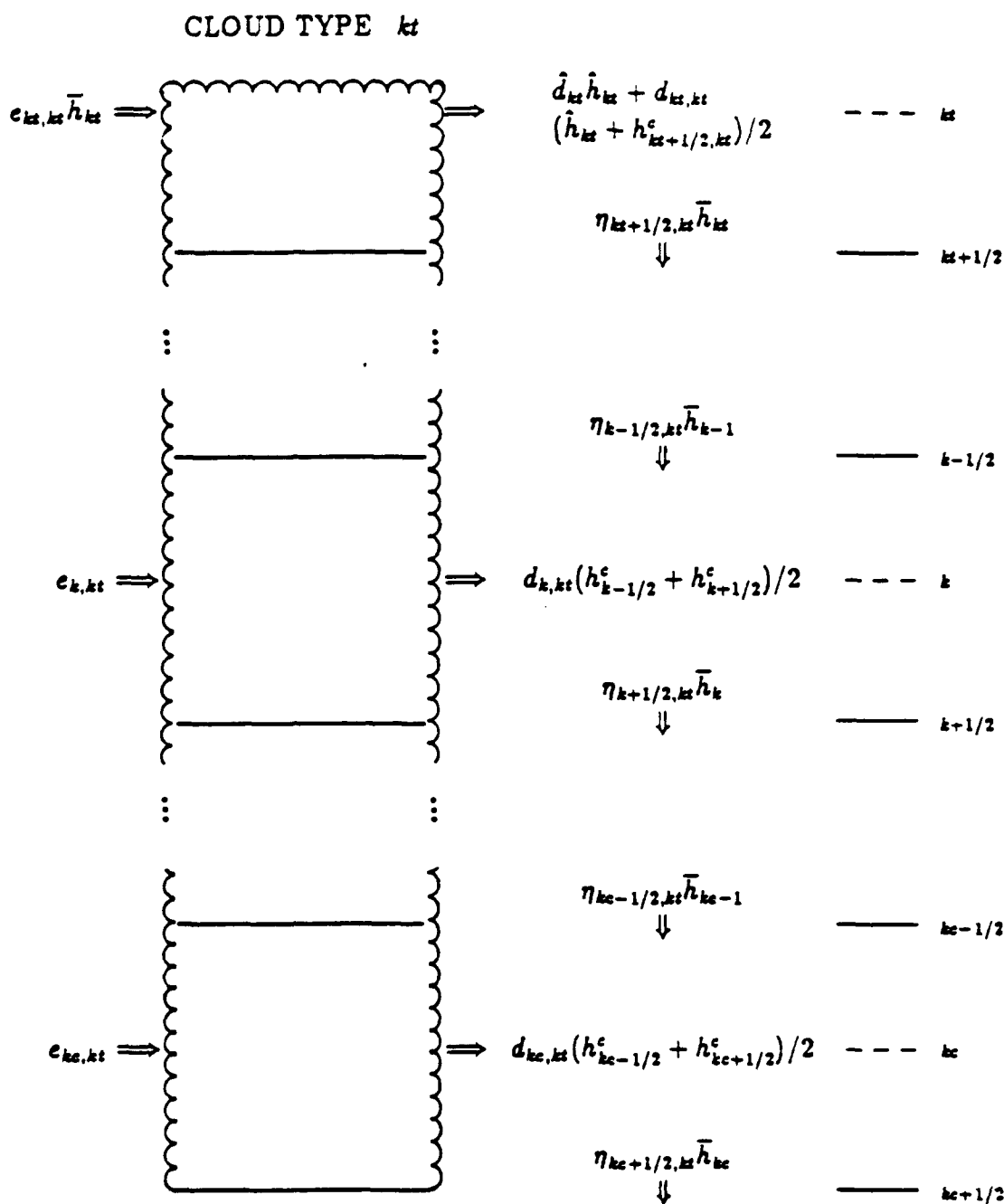


Figure 12.7: Schematic representation of fluxes between clouds and large-scale environment. Each flux in the environmental budgets has a corresponding flux in the cloud budgets.

Figure 12.7 gives a schematic picture of the distribution of fluxes between cloud and large scale environment from the perspective of the budgets of a thermodynamic variable $\bar{\Psi}_k$ in the large scale environment, where $\bar{\Psi}$ is either \bar{h} or \bar{q} . Comparison with Figures 12.4 or 12.5 shows an exact counterpart for every flux in the cloud budget equations. The budget equations for the changes to environmental moist static energy $D\bar{h}$ and total water $D\bar{q}$ per unit cloud base mass flux are

$$D\bar{h}_{k,k_t} = \frac{g}{\Delta p_k} [\eta_{k-1/2,k_t} (\bar{h}_{k-1} - \bar{h}_k) + d_{k,k_t} (\frac{h_{k+1/2,k_t}^c + h_{k-1/2,k_t}^c}{2} - \bar{h}_k)], \quad (12.52)$$

$$D\bar{q}_{k,k_t} = \frac{g}{\Delta p_k} [\eta_{k-1/2,k_t} (\bar{q}_{k-1} - \bar{q}_k) + d_{k,k_t} (\frac{q_{k+1/2,k_t}^c + q_{k-1/2,k_t}^c}{2} - \bar{q}_k)], \quad (12.53)$$

and at cloud top

$$Dh_{k_t,k_t} = \frac{g}{\Delta p_{k_t}} \eta_{k_t+1/2,k_t} [(1 + \lambda_{k_t} \widehat{\Delta z}_{k_t}) (\hat{h}_{k_t} - \bar{h}_{k_t}) + c_d \lambda_{k_t} \widehat{\Delta z}_{k_t} (\frac{\hat{h}_{k_t} + h_{k_t+1/2,k_t}^c}{2} - \bar{h}_{k_t})], \quad (12.54)$$

$$Dq_{k_t,k_t} = \frac{g}{\Delta p_{k_t}} \eta_{k_t+1/2,k_t} [(1 + \lambda_{k_t} \widehat{\Delta z}_{k_t}) (\hat{q}_{k_t} - \bar{q}_{k_t}) + c_d \lambda_{k_t} \widehat{\Delta z}_{k_t} (\frac{\hat{q}_{k_t} + q_{k_t+1/2,k_t}^c}{2} - \bar{q}_{k_t})]. \quad (12.55)$$

The environmental budgets are similar in appearance to the cloud budget equations, although the choice for the subsidence terms is a departure from the form originally proposed by Lord (1978). Notice that the $\bar{\Psi}$ subsidence terms defined on the half levels in Figure 12.7 are the product of the half level normalized mass flux and the $\bar{\Psi}$ gradient between the two full levels above and below that half level. This is a donor cell form of vertical advection and is a flux form of upstream differencing. It has

the property of systematically reducing the drying bias characteristic of the simple entraining plume cloud model. Also, because upstream differencing is diffusive, it eliminates much of the two grid interval noise in the heating profiles that plague centered space differencing forms of the budget equations.

12.9 Evaporation of Convective Precipitation

In section 12.4 convective precipitation per unit cloud base mass flux was generated as an integral part of the total cloud water budget computation. Observational studies have shown that a significant portion of convective precipitate evaporates before it reaches the Earth's surface (Leary and Houze, 1980). This process tends to cool and moisten the lower atmosphere where the evaporation occurs, so including it in the NOGAPS A-S scheme corrects some of the excessive low level drying A-S otherwise produces.

The mass of water evaporated into each layer as it falls is assumed proportional to the mass M of the layer and inversely proportional to the layer relative humidity R_h . For any cloud type k_t there are $k = k_t, \dots, N_p - 1$ layers that may produce precipitate, and the precipitate from each of these layers falls through $N_p - k$ layers. Therefore

$$\Delta q_{k,l}^p = A_l \frac{M_k}{R_{h_k}}, \quad \begin{cases} l = k_t, \dots, N_p - 1 \\ k = l, N_p. \end{cases} \quad (12.56)$$

We assume that the evaporation is a constant fraction of the total precipitate R_l generated by each cloud layer l . Therefore

$$\sum_{k=l}^{N_p} \Delta q_{k,l}^p = A_l \sum_{k=l}^{N_p} \frac{M_k}{R_{h_k}} = b_e R_l, \quad (12.57)$$

so

$$A_l = \frac{b_e R_l}{\sum_{k=l}^{N_p} \frac{M_k}{R_{h_k}}}. \quad (12.58)$$

The final step is to modify the environmental water budget equations by summing over all cloud types l .

$$D\bar{q}_{k,k_t} = D\bar{q}_{k,k_t} + \sum_{l=k_t}^{N_p-1} \Delta q_{k,l}^p, \quad k = l, N_p. \quad (12.59)$$

A value of $b_e = 0.2$ is used. Note that because moist static energy is conserved during moist processes, the $D\bar{h}_{k,k_t}$ are unaffected.

12.10 Saturated Downdraft Model

The total cloud water budget equations partitioned the moisture into three parts: cloud water vapor, non-precipitating liquid water, and precipitating liquid water. In section 12.9 we further divided the precipitating fraction into an evaporating and non-evaporating fraction. The downdraft model exploits the non-precipitating fraction based on empirical evidence that evaporation of suspended cloud water generates negatively buoyant cloud scale air parcels. These downdrafts carry suspended cloud liquid water downward, depositing it at lower levels where it is evaporated. This is in contrast to the A-S cloud model, which evaporates cloud liquid water at the level where it detrains into the environment.

Payne (1981) incorporates a downdraft model directly into the budget equations of the A-S scheme. His approach is quite sophisticated and certainly attractive as a long-term alternative to the current A-S cloud model. However, we have chosen to model the downdrafts in a much simpler manner by taking advantage of the observed biases in the vertical moistening/drying (Q2) profiles of the A-S scheme. Figure 12.8 is from Lord (1978) and shows observed and predicted Q2 from a GATE semi-prognostic study. The difference between the profiles is also shown. This difference is quite typical of Q2 bias from A-S. We can fit it reasonably well with a

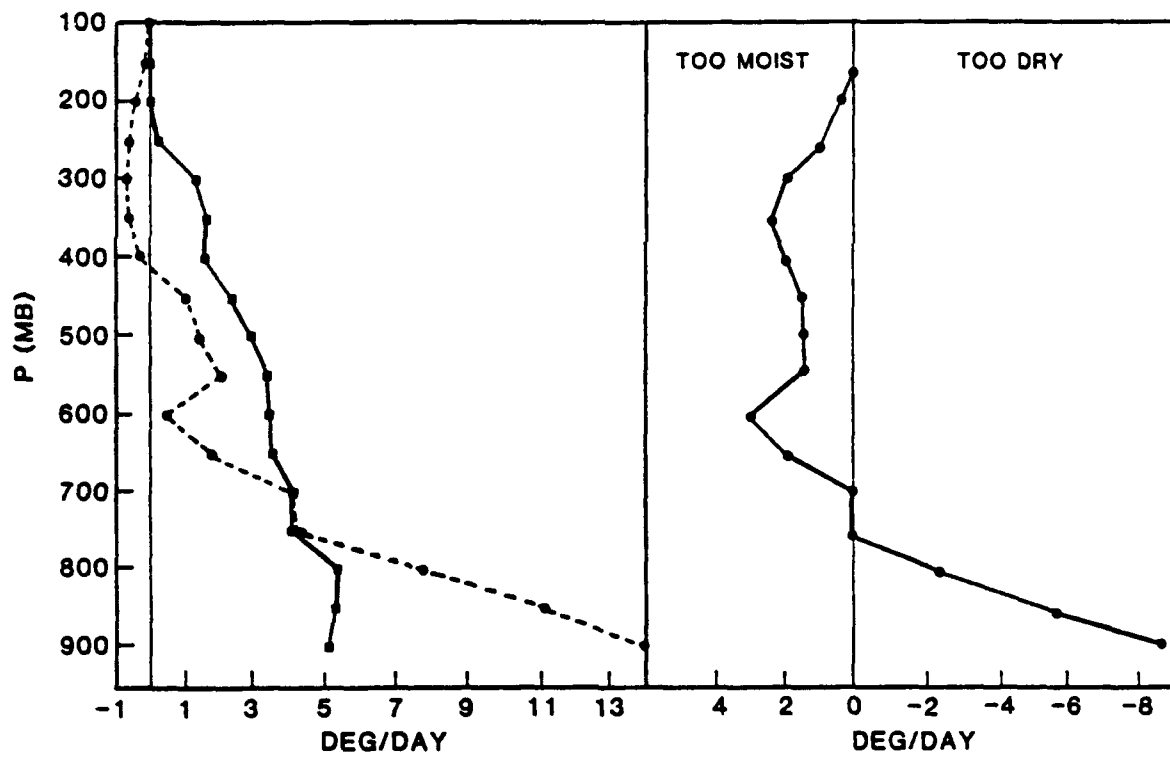


Figure 12.8: Observed Q2 profiles from GATE and Lord (1978) A-S semi-prognostic study, plus difference between two showing typical vertical biases.

12.11 The Perturbed Cloud Budget Equations

We now have a complete set of budget equations describing the interaction of a cumulus cloud ensemble with the large scale environment. For each cloud in an ensemble the cloud work function for a unit cloud base mass flux gives us a measure of the instability in the large scale environment that must be reduced to an equilibrium state. For each cloud in the ensemble we must find the actual cloud base mass flux which reduces the cloud work function to this equilibrium. We can formally write the cloud base mass flux kernel system of equations as

$$\sum_{k'_t=1}^{N_p-1} \mathcal{K}_{k_t, k'_t} m_{B_{k'_t}} + y_{k_t} = 0, \quad k_t = 1, N_p - 1, \quad (12.66)$$

where

$$\mathcal{K}_{k_t, k'_t} = \frac{\partial y_{k_t}}{\partial m_{B_{k'_t}}}, \quad (12.67)$$

$$y_{k_t} = A_{k_t} - A_{k_t}^{clim}. \quad (12.68)$$

The complexity of the cloud and environmental budget equations precludes any hope of an analytic solution to (12.66). A finite difference approach is required. To find the matrix elements \mathcal{K}_{k_t, k'_t} we assume a cloud base test mass flux $m_{B_{k'_t}}^t$ for a cloud type k'_t in an ensemble. We run this test value through the environmental budget equations (12.52), (12.53), (12.54), and (12.55) to get changes to the large scale environment due to this cloud. The perturbed values are

$$\bar{h}'_k = \bar{h}_k + m_{B_{k'_t}}^t D\bar{h}_{k, k'_t}, \quad (12.69)$$

and

$$\bar{q}'_k = \bar{q}_k + m_{B_{k'_t}}^t D\bar{q}_{k, k'_t}. \quad (12.70)$$

Using these adjusted thermodynamic profiles, we resolve the cloud budget equations (12.22), (12.25), (12.31), (12.39), and (12.40) for all values of k_t , with the attendant

simple quadratic profile. Let

$$\Delta q_{k,k_t}^d = \alpha M_k (ax_k^2 - x_k), \quad (12.60)$$

where

$$x_k = (p_k - \hat{p}_{k_t}) / (p_{N_p} - \hat{p}_{k_t}),$$

$$M_k = k \text{ layer mass,}$$

$$\alpha, a = \text{proportionality constants t.b.d.}$$

The parameter x_k is a locally defined pressure coordinate normalized to 0.0 at cloud top and 1.0 at the surface. We assume the downdrafts are non-precipitating, so there is no net change of moisture in the column. Therefore

$$\sum_{k=k_t}^{N_p} \Delta q_{k,k_t}^d = 0, \quad (12.61)$$

so

$$a = \sum_{k=k_t}^{N_p} M_k x_k / \sum_{k=k_t}^{N_p} M_k x_k^2. \quad (12.62)$$

From (12.61) we know that the normalized downdraft moisture flux from the moist bias area to the dry bias area in Figure 12.8 must be equal to the negative (lower) area of the difference profile of Figure 12.61. The flux is therefore

$$\mathcal{F}_{k_t} = \sum_{k=N_p}^J \Delta q_{k,k_t}^d, \quad J = \text{highest layer where } \Delta q_{J,k_t}^d > 0. \quad (12.63)$$

The actual strength of the downdraft moisture flux is assumed to be proportional to the total drying in the column (i.e., precipitation), so

$$\alpha = \frac{b_d R_{k_t}}{\mathcal{F}_{k_t}} \quad (12.64)$$

Based on model sensitivity experiments we use $b_d = 0.1$. The final step is to modify the environmental water budget equations,

$$Dq_{k,k_t} = Dq_{k,k_t} + \Delta q_{k,k_t}^d. \quad (12.65)$$

As was the case for evaporation of convective precipitation, there are no changes to the moist static energy budget.

values of entrainment rate λ'_{k_i} and normalized mass flux η'_{k,k_i} . The cloud work function A'_{k_i} is recomputed for the perturbed environment, where

$$A'_{k_i} = g \sum_{k=k_i}^{N_p} \eta'_{k+1/2,k_i} \Delta z_{k+1/2} [f'_{k+1/2} (h'_{k+1/2,k_i} - \hat{h}^*_{k+1/2}) - \ell^c_{k,k_i}]. \quad (12.71)$$

This entire process is repeated for all allowable values of k'_i . The matrix elements of (12.66) are given by

$$\lambda_{k_i,k'_i} = \frac{A'_{k'_i} - A_{k_i}}{m^i_{B_{k'_i}}}. \quad (12.72)$$

A constant value of $m^i_{B_{k'_i}} = 2.0 \text{ kg m}^{-2} \text{ sec}^{-1}$ is used for all values of k'_i .

The computational effort to find the \mathcal{K}_{k_i,k'_i} is quite large compared to the original cloud budget calculations. In the original cloud budget calculations for a given K_{top} we have $k_i = L - K_{top}$ possible clouds. Finding the elements of (12.68) requires all possible combinations of $k'_i = L - K_{top}$ and $k_i = L - K_{top}$, so the problem is of order k_i^2 , rather than k_i . However, because the test mass flux changes in the cloud budget calculations are small, we can take advantage of the results of (12.48) from the original cloud budget solutions in a Newton's method solution to (12.46), rather than the original pseudo-secant method. So

$$\lambda^{\nu+1}_{k_i} = \lambda^{\nu}_{k_i} - B(\lambda'_{k_i}) / \frac{d}{d\lambda_{k_i}} [B(\lambda_{k_i})]. \quad (12.73)$$

Beginning with $\lambda^{\nu+1}_{k_i} = \lambda_{k_i}$, two iterations give solutions to (12.73) which are within $\pm 4.0 \text{ Joules kg}^{-1}$.

12.12 Solution of the Cloud Kernel Equation

Equation (12.66) is a deceptively simple linear system of equations. However, the physical constraints we impose on the solutions to this system have historically presented a non-trivial problem to implementations of the discrete A-S scheme.

We must minimize

$$\mathcal{G}_i = \sum_{j=1}^{N_p-1} \mathcal{K}_{i,j} m_j + y_i, \quad i = 1, N_p - 1, \quad (12.74)$$

with the constraints

$$m_j \geq 0, \quad (12.75)$$

and

$$\mathcal{G}_i \geq 0. \quad (12.76)$$

Equations (12.74), (12.75), and (12.76) form a constrained linear system of order $N = L - K_{top}$. Schubert (1973) proposed an iterative solution method which was used in early versions of the UCLA general circulation model. The method worked, but was subject to occasional numerical problems. Silva-Dias and Schubert (1977) solved (12.74 - 12.76) as a linear programming problem using the simplex algorithm (Dantzig, 1963). Simplex finds the optimum solution and is numerically robust, but is computationally expensive for the large number of low order linear systems generated by the A-S scheme. More details of these methods are in Lord (1978).

The nature of (12.74 - 12.76) suggests a calculus of variations approach. We want to minimize the functional

$$\mathcal{J}_N = \sum_{i=1}^N [\epsilon_i (m_i - m_{o_i})^2 + \alpha_i (\sum_{j=1}^N \mathcal{K}_{i,j} m_j + y_i)^2], \quad (12.77)$$

where m_{o_i} are the unconstrained solutions to (12.74) which generally will not satisfy (12.75) for all values of i . The factors ϵ_i and α_i are the so-called weak constraint variational weights to be determined. Taking the first variation of (12.77) with respect to m_i and collecting terms yields

$$\sum_{j=1}^N (\sum_{l=1}^N (\alpha_l \mathcal{K}_{i,l} \mathcal{K}_{j,l}) + \epsilon_j) m_j = \sum_{l=1}^N \alpha_l \mathcal{K}_{i,l} y_l + \epsilon_i m_{o_i}, \quad (12.78)$$

which is of the form

$$\sum_{j=1}^N \mathcal{L}_{i,j} m_j = h_i. \quad (12.79)$$

The iterative solution of (12.78) proceeds as follows:

1. Solve (12.74) with $\mathcal{G}_i = 0.0$ to get $m_{o,i}$.
2. If $m_{o,i}$ satisfies (12.75), then set α_i to 0.0 and ϵ_i to 1.0, which causes (12.78) to reduce to $m_i = m_{o,i}$, so (12.75) is satisfied.
3. If $m_{o,i}$ is less than 0.0, then set $m_{o,i}$ to 0.0, ϵ_i to 0.0, and α_i to 1.0 in (12.78). This causes \mathcal{G}_i to be greater than 0.0, so (12.76) is satisfied.
4. With the adjusted values of $m_{o,i}$ and the assigned values of ϵ_i and α_i , solve (12.78) for m_j .
5. Check to see if (12.75) and (12.76) are satisfied for all values of i . If not, then replace $m_{o,i}$ with any positive m_i and return to step 2 above and repeat the iteration.

The method usually converges within 2-3 iterations, even for cloud ensembles with 8-10 positive values of m_i . Non-pivoting Gaussian elimination is used to solve (12.79) because experience has shown that $\mathcal{L}_{i,j}$ is almost always well-conditioned. In rare cases with pathological temperature and moisture structure this method fails. In these cases full-pivoting Gaussian elimination is tried, and if this also fails the mass fluxes for this cloud ensemble are set to zero. Computationally the method is an order of magnitude faster than the simplex algorithm and yields exactly the same solutions in nearly all cases. No meteorologically significant differences between the two methods' solutions is ever observed.

12.13 Update of Large Scale Environment

Solution of (12.74-12.76) closes the A-S parameterization. Since the environmental budget equations are for a unit cloud base mass flux, the changes at each level k in

the environment are

$$\Delta \bar{h}_k = \sum_{k_t=1}^{N_p-1} m_{B_{k_t}} \sum_{k=k_t}^{N_p} D \bar{h}_{k,k_t}, \quad (12.80)$$

$$\Delta \bar{q}_k = \sum_{k_t=1}^{N_p-1} m_{B_{k_t}} \sum_{k=k_t}^{N_p} D \bar{q}_{k,k_t}. \quad (12.81)$$

So

$$\Delta \bar{T}_k = \frac{\Delta \bar{h}_k - L_w \Delta \bar{q}_k}{c_p}. \quad (12.82)$$

The total precipitation is

$$P_{cu} = - \sum_{k=1}^{N_p} \Delta \bar{q}_k. \quad (12.83)$$

The total cloud base mass flux is

$$M_B = \sum_{k_t=1}^{N_p-1} m_{B_{k_t}}. \quad (12.84)$$

In Section 12.5 the need to redefine the definition of the layer containing the tops of the deepest penetrating clouds was described. These redefined layers are always thinner than the full model layer that is otherwise defined at these levels. Therefore the deepest cloud heating and moistening changes computed from the environmental budgets must be adjusted for the difference in thickness between the temporary thin layers and the full model layers. Using 12.44, we obtain the adjusted heating and moistening changes

$$\Delta \bar{h}_{k_t=1} = \widehat{K}(\bar{h}_{N_p}) \Delta \bar{h}_{k_t=1}, \quad (12.85)$$

$$\Delta \bar{q}_{k_t=1} = \widehat{K}(\bar{h}_{N_p}) \Delta \bar{q}_{k_t=1}. \quad (12.86)$$

Chapter 13

Large Scale Precipitation

The large scale precipitation parameterization removes all supersaturation remaining in the model after all previous temperature and moisture adjustments. We perform the computations with the current grid point fields, which in this case, are the temperature and moisture from the Arakawa-Schubert cumulus parameterization: $T_k^{(cu)}$ and $q_k^{(cu)}$ (see Chapter 6 for the discussion of the time integration procedures). The large scale precipitation processes begin at the highest supersaturated model layer and continue downward to the surface.

For level k with temperature T_k and pressure p_k the saturation specific humidity is given by

$$q_{sat}(T_k, p_k) = \frac{.62197 e^*(T_k)}{p_k - e^*(T_k)}, \quad (13.1)$$

where $e^*(T_k)$ is the saturation vapor pressure. We obtain the saturation vapor pressure by solving the Clausius-Claperyon equation:

$$\frac{de^*}{dT} = \frac{.62197 L_w e^*}{RT^2}, \quad (13.2)$$

where .62197 is m_v/m_d , that is the ratio of the mass per unit mole of water vapor, m_v (18.016 g mole⁻¹) to the mass per unit mole of dry air, m_d (28.966 g mole⁻¹); R is the dry air gas constant (287 J K⁻¹ kg⁻¹); and L_w is the temperature dependent

latent heat of condensation L_{wi} given by Equation (12.13). Equation (12.12) is also used to include saturation vapor pressure dependence with respect to ice.

We define R_k as the accumulated liquid water falling into layer k with pressure thickness Δp_k ($R_k = 0$ for the top saturated layer), and define E_k , the amount of evaporation in the layer, as

$$E_k = \max \left\{ \begin{array}{l} \min \left\{ \begin{array}{l} (Rh_c q_{sat_k} - q_k) \frac{\Delta p_k}{g} \\ R_k \end{array} \right. \\ 0, \end{array} \right. \quad (13.3)$$

where Rh_c is the maximum relative humidity to which E_k can raise layer relative humidity. Currently Rh_c is 100%. We assume that the evaporation moistens the layer uniformly and that the heat used to evaporate E_k is removed from the layer, giving new layer specific humidity and temperature

$$q_k^{(sp')} = q_k^{(cu)} + E_k \frac{g}{\Delta p_k}, \quad (13.4)$$

$$T_k^{(sp')} = T_k^{(cu)} - \frac{L_w}{c_p} \frac{g}{\Delta p_k} E_k. \quad (13.5)$$

Using Equations (13.1) and (13.2), we calculate the relative humidity for the layer for the moisture and temperature given by (13.4) and (13.5): $q_k^{(sp')}$ and $T_k^{(sp')}$. If the relative humidity is greater than 100%, we find the saturation temperature and specific humidity, add the excess moisture to the accumulated precipitation, and add the latent heat to the layer's temperature. This procedure is done iteratively and is described below.

We define the n^{th} iterate for moisture and temperature by,

$$q_k^n = q_{sat}(T_k^n, p_k) = q_k^{n-1} - C_k^n, \quad (13.6)$$

and

$$T_k^n = T_k^{n-1} + \frac{L_w}{c_p} C_k^n, \quad (13.7)$$

with C_k^n denoting the amount of moisture removed by the iteration to obtain saturation. The input moisture and temperature are $q_k^{(sp')}$ and $T_k^{(sp')}$. Expanding q_{sat} of Equation (13.6) in a first order Taylor series in temperature about the previous iterate, we get the result:

$$C_k^n = q_k^{n-1} - q_{sat}(T_k^{n-1}, p_k) - \left(\frac{\partial q_{sat}}{\partial T} \right)_p \frac{L_w}{c_p} C_k^n.$$

Solving for C_k^n , we obtain:

$$C_k^n = \frac{q_k^{n-1} - q_{sat}(T_k^{n-1}, p_k)}{1 + \gamma} \quad (13.8)$$

with

$$\gamma = \frac{L_w}{c_p} \left(\frac{\partial q_{sat}}{\partial T} \right)_p. \quad (13.9)$$

Using the Clausius-Claperyon equation (13.2), we write the partial derivative of q_{sat} with respect to temperature as

$$\left(\frac{\partial q_{sat}}{\partial T} \right)_p = .62197 \left(\frac{L_w q_{sat}}{RT^2} \right) \left[\frac{1}{1 - e^*/p} \right]. \quad (13.10)$$

The procedure given by Equations (13.6)–(13.10) is continued until the change C_k^n is sufficiently small (typically 1 or 2 iterations). If N is the total number of iterations, then the rain falling into the next layer, $k + 1$, is given by the excess moisture from level k and by the difference between the accumulated and the evaporated moisture in that layer:

$$R_{k+1} = R_k - E_k + \frac{\Delta p_k}{g} \sum_{n=1}^N C_k^n. \quad (13.11)$$

R_{k+1} falls into the next layer below and the process is repeated, continuing down to the surface layer L , where no evaporation of precipitation is allowed. The accumulated liquid water R_L is the predicted large scale precipitation at the ground. If the ground temperature is below freezing the precipitation is assumed to accumulate as snow.

The temperature and moisture fields are given by (13.6) and (13.7) summed over all iterations and are denoted by $T_k^{(sp)}$ and $q_k^{(sp)}$. These are the $t + \Delta t$ forecast grid point fields used for the next time step plus the radiation calculations if the forecast time is a multiple of 2 hours.

Chapter 14

Longwave Radiation

The time tendency equation for temperature due only to the absorption of longwave radiation is

$$c_p \rho \frac{\partial T}{\partial t} = -\frac{\partial}{\partial z} (\mathcal{F}_{LW}^{\uparrow} - \mathcal{F}_{LW}^{\downarrow}). \quad (14.1)$$

The upward longwave radiative flux, $\mathcal{F}_{LW}^{\uparrow}$, and the downward longwave radiative flux, $\mathcal{F}_{LW}^{\downarrow}$, are the radiative energy per unit time and per unit area (Watts m^{-2}). The variable ρ is the density of air and c_p is the specific heat of air at constant pressure (1005.45 J $\text{K}^{-1} \text{kg}^{-1}$). Equation (14.1) is valid for both a cloud free and a cloudy atmosphere. The longwave calculation proceeds by first calculating the longwave fluxes in the absence of clouds, and then obtaining the longwave fluxes in the presence of clouds by reducing the clear sky fluxes by a probability of the clear line of sight between pressure levels.

14.1 Fundamentals of Longwave Radiation

The following discussion is taken from Liou (1980). We start by considering a pencil of light impinging on a surface area at an angle θ (see Figure 14.1) and by defining dE_{ν} as the differential radiant energy that crosses the area dA , in the direction θ

measured normal to dA , in the time interval t to $t+dt$, in the frequency range ν to $\nu+d\nu$, and in the solid angle span $d\Omega$. The radiance, (monochromatic intensity, brightness) I_ν , is defined as

$$I_\nu = \frac{dE_\nu}{d\nu dt \cos \theta dA d\Omega}. \quad (14.2)$$

The monochromatic flux density \mathcal{F}_ν is the total energy emitted through dA in time dt with the frequency range $d\nu$:

$$\mathcal{F}_\nu = \int_0^{2\pi} \int_0^{\pi/2} I_\nu(\theta, \varphi) \cos \theta \sin \theta d\theta d\varphi. \quad (14.3)$$

If the radiance is isotropic, then the monochromatic flux density is given by

$$\mathcal{F}_\nu = \pi I_\nu \quad (\text{isotropic radiation}).$$

The flux density \mathcal{F} that appears in Equation (14.1) is the integral of the monochromatic flux density over all frequencies:

$$\mathcal{F} = \int_0^\infty \mathcal{F}_\nu d\nu. \quad (14.4)$$

We assume that the atmosphere is locally in a state of thermodynamic equilibrium, so that at each point in the atmosphere we can define a temperature and assume the atmosphere's emissivity is equal to its absorptivity (Kirchhoff's law). Further, we assume that the absorption and emission of longwave radiation dominate any multiple scattering-absorption processes. We will consider only longwave radiation with an upward or downward component, and we will define θ as the angle of the radiation normal to the vertical z coordinate (the plane parallel approximation). Under these conditions, the fundamental equation for radiative transfer is the Schwarzschild's equation for the radiance:

$$\frac{dI_\nu}{dz} = -\rho k_\nu I_\nu \sec \theta + \rho k_\nu B_\nu \sec \theta, \quad (14.5)$$

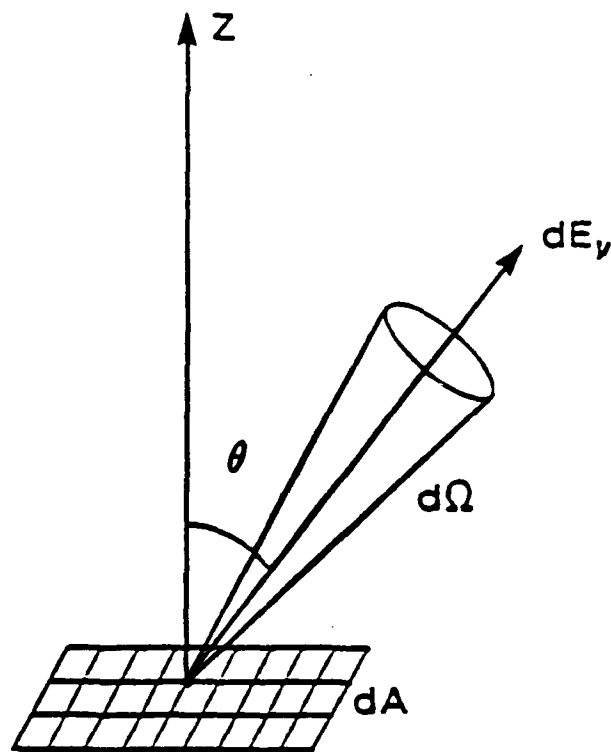


Figure 14.1: A pencil of radiation through area dA in the direction θ and confined to the solid angle $d\Omega$.

where k_ν is the mass extinction cross section and B_ν is the monochromatic intensity for a blackbody:

$$B_\nu[T] = \frac{2h\nu^3}{c^2(e^{h\nu/kT} - 1)}. \quad (14.6)$$

The constants of the blackbody monochromatic intensity are Planck's constant h (6.6262×10^{-27} erg sec), Boltzmann's constant k (1.3806×10^{-16} erg K $^{-1}$), and the speed of light c (2.998×10^{10} cm sec $^{-1}$). The temperature T is a function of the height z or the pressure p . We shall express the dependence of B_ν on T , z , or p interchangeability.

We obtain an equation for the upward longwave radiance, I_ν^\uparrow , from the Schwarzschild equation (14.5) by considering only $\theta > 0$, and we obtain the downward longwave radiance I_ν^\downarrow 's equation by setting $\theta < 0$. The results are

$$\frac{dI_\nu^\uparrow}{dz} = -\rho k_\nu I_\nu^\uparrow \sec \theta + \rho k_\nu B_\nu \sec \theta \quad (14.7)$$

and

$$\frac{dI_\nu^\downarrow}{dz} = \rho k_\nu I_\nu^\downarrow \sec \theta - \rho k_\nu B_\nu \sec \theta. \quad (14.8)$$

The boundary conditions for (14.7) and (14.8) are the surface emits longwave radiation as a blackbody at the surface temperature T_S and there is no downward longwave radiance at the top of the atmosphere. We write these boundary conditions as

$$\left. \begin{aligned} I_\nu^\uparrow(0) &= B_\nu[T_S] \\ I_\nu^\downarrow(z_{top}) &= 0 \end{aligned} \right\}. \quad (14.9)$$

The solutions of (14.7) and (14.8) with boundary conditions (14.9) for the upward and downward intensities are

$$\begin{aligned} I_\nu^\uparrow(z) &= B_\nu[T_S] e^{-\int_0^z \rho k_\nu \sec \theta dz'} \\ &+ \int_0^z B_\nu[z'] \rho k_\nu \sec \theta e^{-\int_z^{z'} \rho k_\nu \sec \theta dz''} dz', \end{aligned} \quad (14.10)$$

and

$$I_{\nu}^{\downarrow}(z) = \int_z^{z_{top}} B_{\nu}[z'] \rho k_{\nu} \sec \theta e^{-\int_z^{z'} \rho k_{\nu} \sec \theta dz''} dz'. \quad (14.11)$$

We compute the upward and downward monochromatic flux density by integrating (14.10) and (14.11):

$$\mathcal{F}_{\nu}^{\uparrow}(z) = \pi B_{\nu}[T_S] \tau_{\nu}^f(z, z'=0) + \int_0^z \pi B_{\nu} \frac{\partial \tau_{\nu}^f}{\partial z'}(z, z') dz', \quad (14.12)$$

$$\mathcal{F}_{\nu}^{\downarrow}(z) = - \int_z^{z_{top}} \pi B_{\nu} \frac{\partial \tau_{\nu}^f}{\partial z'}(z', z) dz'. \quad (14.13)$$

We have simplified the form of the fluxes by introducing the diffuse transmission function, τ_{ν}^f , which is given by the integral:

$$\tau_{\nu}^f(z, z') = 2 \int_0^{\pi/2} \sin \theta \cos \theta e^{-\int_{z'}^z k_{\nu} \rho \sec \theta dz''} d\theta. \quad (14.14)$$

We perform the integrals in (14.12) and (14.13) by parts, which yields the results that

$$\begin{aligned} \mathcal{F}_{\nu}^{\uparrow}(z) &= \pi B_{\nu}[T(z)] + \pi B_{\nu}[T_S] \tau_{\nu}^f(z, 0) - \pi B_{\nu}[T(z=0)] \tau_{\nu}^f(z, 0) \\ &\quad - \int_0^z \tau_{\nu}^f(z, z') \frac{\partial}{\partial z} (\pi B_{\nu}[T(z')]) dz' \end{aligned} \quad (14.15)$$

and

$$\begin{aligned} \mathcal{F}_{\nu}^{\downarrow}(z) &= \pi B_{\nu}[T(z)] - \pi B_{\nu}[T_{z_{top}}] \tau_{\nu}^f(z_{top}, z) \\ &\quad + \int_z^{z_{top}} \tau_{\nu}^f(z', z) \frac{\partial}{\partial z} (\pi B_{\nu}[T(z')]) dz'. \end{aligned} \quad (14.16)$$

In (14.15) and (14.16), we use the fact that

$$\tau_{\nu}^f(z, z) = 1.$$

Note that in (14.15) we have distinguished between the surface ground temperature, T_S , and the temperature of the surface air denoted by $T(z=0)$.

For the numerical computations we evaluate the fluxes at the half level surfaces (see Figure 14.2), and we must replace the integrals of (14.15) and (14.16) by

finite sums over the levels. We add two extra levels to the existing model, where N indicates the total number of levels for the longwave calculation, *i.e.* $N=L+2$, with $L=18$. (see Figure 14.2). We take the top model temperature as the temperatures of the two added levels, and we set the specific humidity of the top level to zero and the next level humidity to 3.0×10^{-6} . With these conventions, we write the finite difference form of (14.15) and (14.16) as

$$\begin{aligned}\mathcal{F}_\nu^l(z_{k+1/2}) &= \pi B_\nu[T(z_{k+1/2})] \\ &+ \pi B[T_S]\tau_\nu^f(z_{k+1/2}, 0) - \pi B_\nu[T_{N+1/2}]\tau_\nu^f(z_{k+1/2}, 0) \\ &- \sum_{j=1}^{N-k} \left\{ \pi B_\nu[T(z_{k+j-1/2})]\tau_\nu^f(z_{k+1/2}, z_{k+j}) \right. \\ &\left. - \pi B_\nu[T(z_{k+j+1/2})]\tau_\nu^f(z_{k+1/2}, z_{k+j}) \right\},\end{aligned}\quad (14.17)$$

and

$$\begin{aligned}\mathcal{F}_\nu^l(z_{k+1/2}) &= \pi B_\nu[T(z_{k+1/2})] \\ &- \pi B[T_{z_{top}}]\tau_\nu^f(z_{top}, z_{k+1/2}) \\ &- \sum_{j=1}^{N+1-k} \left\{ \pi B_\nu[T(z_{k+1-j-1/2})]\tau_\nu^f(z_{k+1-j}, z_{k+1/2}) \right. \\ &\left. - \pi B_\nu[T(z_{k+1-j+1/2})]\tau_\nu^f(z_{k+1-j}, z_{k+1/2}) \right\}.\end{aligned}\quad (14.18)$$

14.2 The Band Model

The following development is based on the work of Harshvardhan *et al.* (1987). To obtain the total clear air longwave fluxes, we must first calculate the diffuse transmission function for all atmospheric longwave absorbers, and second we must integrate (14.17) and (14.18) over all frequencies. The major difficulty is that τ_ν^f is a very complicated and often rapidly varying function of ν , which has a very different transmission property for the different molecular components of the atmosphere. To obtain a solution, we first limit the longwave absorbers to the three major

Model Level	Longwave Radiation Level
-------------	--------------------------

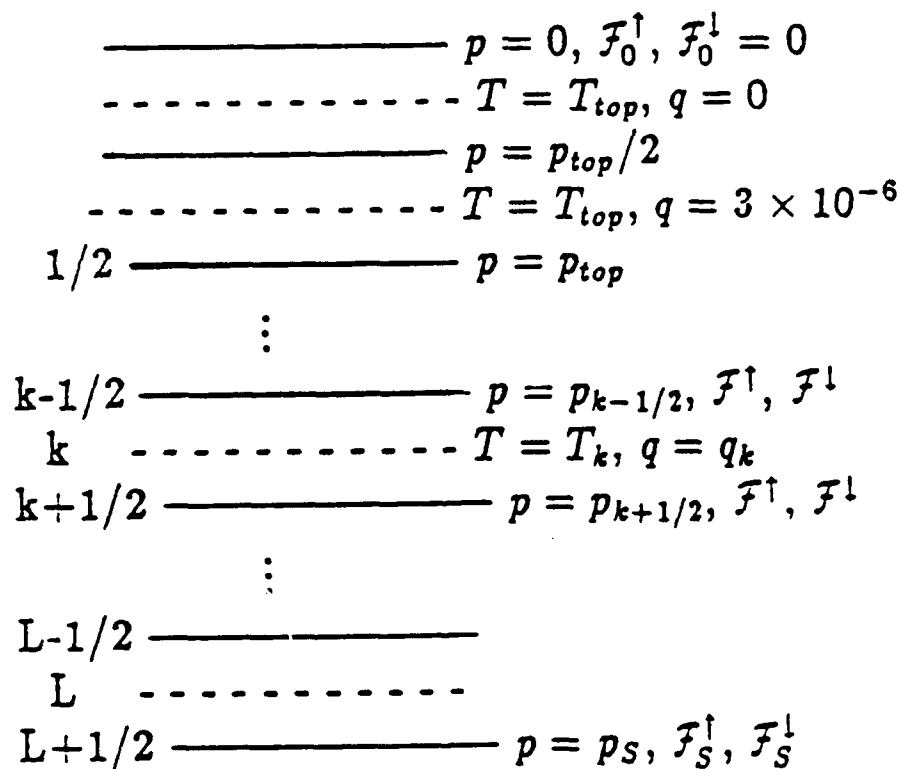


Figure 14.2: The vertical structure for the longwave calculation.

Table 14.1: The spectral longwave band regions in μm .

$\Delta\nu_1$	$\Delta\nu_2$	$\Delta\nu_3$	$\Delta\nu_4$
5.26–7.25	3.330–5.260	12.5–18.5	9.09–10.2
29.41– ∞	7.250–9.090		
	10.20–12.50		
	18.52–29.41		

ones: water vapor, carbon dioxide, and ozone. Second, in order to approximate the fluxes, we break up the frequency domain into four distinct regions, where broadband parameterizations are applied. This technique is called the band model parameterization.

We write the total flux as a finite sum over four frequency bands,

$$\mathcal{F} = \int_0^\infty \mathcal{F}_\nu d\nu = \sum_{i=1}^4 \int_{\Delta\nu_i} \mathcal{F}_\nu d\nu. \quad (14.19)$$

We designate the four bands considered as

1. the water vapor band center ($\Delta\nu_1$),
2. the water vapor band wing ($\Delta\nu_2$),
3. the $15\mu\text{m}$ carbon dioxide band ($\Delta\nu_3$), and
4. the $9\mu\text{m}$ ozone band ($\Delta\nu_4$).

The values of the bands are given in Table 14.1. Three of the four band regions contain more than one type of absorption. We summarize the different absorption properties of the regions as:

- Band region 1 contains solely absorption and emission due to the center band of water vapor alone.

- Band region 2 contains just water vapor absorption and emission with 2 different types of absorption:
 1. the continuous absorption of water vapor, which is dependent on the water vapor's partial pressure, e_v (the e-type absorption); and
 2. the absorption in the wings due to the water vapor amount.
- Band region 3 includes water vapor and carbon dioxide absorption of the following types:
 1. the e-type water vapor absorption,
 2. the wing water vapor absorption,
 3. the carbon dioxide center band absorption, and
 4. the carbon dioxide wing band absorption.
- Band region 4 includes water vapor and ozone absorption:
 1. the e-type water vapor absorption and
 2. all types of ozone absorption in the infrared.

For each region, we define the spectrally integrated Planck flux, $B_i[T]$, by

$$B_i[T] = \int_{\Delta\nu_i} \pi B_\nu[T] d\nu, \quad (14.20)$$

and we define the Planck weighted transmission function, $\tau_i(p, p')$, of the diffuse transmission function (14.14) by the integral,

$$\tau_i(p', p) = \frac{1}{B_i[T(p)]} \int_{\Delta\nu_i} \tau_\nu^f(p, p') \pi B_\nu[T(p)] d\nu. \quad (14.21)$$

In (14.21) we have made the simple change of variables from z to pressure p . Note that the convention is that when we write $\tau(p_1, p_2)$, p_1 is greater than p_2 .

From (14.20) and (14.21), we obtain the total upward and downward fluxes by replacing the integral in (14.17) by the sum over the 4 bands:

$$\begin{aligned}
 \mathcal{F}_{k+1/2}^{\uparrow} = & \sum_{i=1}^4 \left\{ B_i[T_{k+1/2}] + B_i[T_S]\tau_i(p_S, p_{k+1/2}) \right. \\
 & - \left. B_i[T(p_S)]\tau_i(p_S, p_{k+1/2}) \right\} \\
 & - \sum_{i=1}^4 \sum_{j=1}^{N-k} \left\{ B_i[T_{k+j-1/2}]\tau_i(p_{k+j}, p_{k+1/2}) \right. \\
 & - \left. B_i[T_{k+j+1/2}]\tau_i(p_{k+j}, p_{k+1/2}) \right\}
 \end{aligned} \tag{14.22}$$

and

$$\begin{aligned}
 \mathcal{F}_{k+1/2}^{\downarrow} = & \sum_{i=1}^4 \left\{ B_i[T_{k+1/2}] \right. \\
 & - \left. B_i[T(p_{top})]\tau_i(p_{k+1/2}, p_{top}) \right\} \\
 & + \sum_{i=1}^4 \sum_{j=1}^{N+1-k} \left\{ B_i[T_{k+1-j-1/2}]\tau_i(p_{k+1/2}, p_{k+1-j}) \right. \\
 & - \left. B_i[T_{k+1-j+1/2}]\tau_i(p_{k+1/2}, p_{k+1-j}) \right\}.
 \end{aligned} \tag{14.23}$$

In the above equations, p_S is the surface pressure, p_{top} is the model's top pressure, T_S is the surface temperature, and $T(p_S)$ is the surface air temperature.

In order to determine the Planck weighted transmission function (14.21), we integrate the diffuse transmission function (14.14) over the different frequency bands. This requires a parameterization of the functional form of the highly complicated molecular mass extinction cross section $k_{\nu}(p, T)$. We assume that the functional form of the cross section can be written as

$$k_{\nu}(p, T) = k_{\nu}(p_r, T_r)f(p, T), \tag{14.24}$$

where p_r and T_r are representative values of pressure and temperature, and the shape function f is given by the form

$$f(p, T) = \left(\frac{p}{p_r} \right)^m \exp[r(T - T_r)].$$

The units of p and p_r are mb, the temperature units are degrees K, and the coefficient r has units K^{-1} . We define the scaled optical path $u(p, p')$ by

$$u(p, p') = \int_{p'}^p f(p'', T) dp'' / g, \quad (14.25)$$

and with this definition we write the diffuse transmission function as

$$\tau_\nu^f = 2 \int_0^1 \cos \theta e^{-k_\nu(p_r, T_r) u(p, p') \sec \theta} d \cos \theta. \quad (14.26)$$

The water vapor scaled optical path for the e-type absorption in the atmospheric window, u , is given by Chou (1984) as

$$u(p_1, p_2) = \int_{p_1}^{p_2} q e_v \exp \left[1800 \left(\frac{1}{T} - \frac{1}{296} \right) \right] \frac{dp}{g}. \quad (14.27)$$

The partial pressure e_v is in the units of atmospheres and q is the specific humidity.

Using the equation of state for e_v , which is

$$e_v = \frac{pq}{q + .62197},$$

we write u (gm/cm²) as

$$u(p_1, p_2) = 1.02 \int_{p_1}^{p_2} \frac{pq^2}{630.211} \exp \left[\frac{1800}{T} - 6.0811 \right] dp. \quad (14.28)$$

The leading coefficient (1.02) is the conversion factor of mb to g/cm⁻². The water vapor scaled optical path in the water center band, which is denoted by v , is given by Chou (1984) (g/cm²) by

$$v(p_1, p_2) = 1.02 \int_{p_1}^{p_2} q \frac{p}{275} \exp[0.005(T - 225)] dp. \quad (14.29)$$

The water vapor scaled optical path in the water wing band, w , is given by Chou (1984) (g/cm⁻²) as

$$w(p_1, p_2) = 1.02 \int_{p_1}^{p_2} \left(\frac{p}{550} \right) \exp[0.016(T - 256)] dp \quad (14.30)$$

We take the functional form of the carbon dioxide scaled optical path in the CO₂ center band, denoted by x , from Chou and Peng (1983) and is given (g/cm²) by

$$x(p_1, p_2) = 1.02(0.26) \int_{p_1}^{p_2} \left(\frac{p}{30}\right)^{0.85} \exp[0.0089(T - 240)] dp. \quad (14.31)$$

Chou and Peng (1984) give the carbon dioxide scaled optical path in the CO₂ band wing, y (g/cm⁻²) by

$$y(p_1, p_2) = 1.02(0.26) \int_{p_1}^{p_2} \left(\frac{p}{300}\right)^{1/2} \exp[0.025(T - 240)] dp. \quad (14.32)$$

The factor 0.26 corresponds to 330 ppm by volume for the CO₂ concentration. Finally, we write the scaled optical path for ozone, z_{oz} (g/cm²) by

$$z_{oz}(p_1, p_2) = 1.02 \int_{p_1}^{p_2} q_{oz} dp, \quad (14.33)$$

where the ozone mixing ratio, q_{oz} is obtained from the climatological values tabulated by Dopplack (1974).

The Planck weighted transmission functions for the four regions, τ_i , are functions of the different scaled optical paths defined above. We write this formally as

$$\tau_i(p_1, p_2) = \tau_i[u_1(p_1, p_2), u_2(p_1, p_2), \dots].$$

In the water vapor center band region (Band Region 1), the Planck weighted transmission function τ_1 is a function of the scaled optical path v , given by (14.29). Chou (1984) expresses this as the series,

$$\tau_1(v, T) = \tau_1(v, 250) \left[1 + \alpha_1(v)(T - 250) + \beta_1(v)(T - 250)^2 \right]. \quad (14.34)$$

In Harshvardhan *et al.* (1987), equations for $\tau_1(v, 250)$, $\alpha_1(v)$, and $\beta_1(v)$ are derived based on the tabulated values of Chou (1984). These equations, which were obtained from the computer code, are

$$\tau_1(v, 250) = \frac{1}{1 + 9.2\sqrt{v} - .187v^{3/2} + 0.323v},$$

$$\alpha_1(v) = .08\sqrt{v} - .187v^{3/2} + .0323v,$$

$$\beta_1(v) = .001\{.239v - .09v^{3/2} - .016v^2\}.$$

In the water vapor wing band (Band Region 2), the Planck weighted transmission function τ_2 depends on the scaled optical path for the e-type absorption u , which is defined by (14.28), and the water vapor wing absorption path w , which is given by (14.30). A functional form of τ_2 , which is given by Chou (1984), is

$$\begin{aligned} \tau_2(u, w, T) = & \tau_2(u, w, 250) [1 + \alpha_2(u, w)(T - 250) \\ & + \beta_2(u, w)(T - 250)^2], \end{aligned} \quad (14.35)$$

with $\tau_2(u, w, 250)$, $\alpha_2(u, w)$, and $\beta_2(u, w)$ parameterized by Harshvardhan *et al.* (1987) as

$$\begin{aligned} \tau_2(u, w) = & \left[\left(\frac{1 + 32.2u}{1 + 52.85u} \right) + \sqrt{w} \left(\frac{.53 + 199u - 1990.6u^2}{1 + 333.2u} \right) \right] \\ & \div \left[(\sqrt{w} + 1) \left(\frac{1 + 74.1u}{.433 + 24.1u} \right) \right], \\ \alpha_2(u, w) = & .1 \left[\left(\frac{.005 + 1.05u - 39u^2}{1 + 202u} \right) + \left(\frac{.07 + 4.4u + 3.15u\sqrt{w}}{1 + 40.2u} \right) \right. \\ & \left. + \left(\frac{-.038 - 3.6u + 7.9uw^2}{1 + 62u} \right) + w^{3/2} \left(\frac{.006 + .71u - 2.8u^2}{1 + 70u} \right) \right], \\ \beta_2(u, w) = & .001 \left[\left(\frac{-.003 + 2.38u + 5.19u^2}{1 + 10.7u} \right) + \left(\frac{-.029 - 2.3u + 10.9u^2\sqrt{w}}{1 + 63.5u} \right) \right. \\ & \left. + w \left(\frac{.014 + 1.8u - 10.1u^2}{1 + 98.4u} \right) + w^{3/2} \left(\frac{-.002 - .371u + 2.35u^2}{1 + 12u} \right) \right]. \end{aligned}$$

The Planck weighted transmission function in the $15\mu\text{m}$ band (Band Region 3) is a function of the scaled optical paths u , w , x , and y , which are given by (14.28) and (14.30)–(14.32), and weakly depends on the temperature T . The functional form for τ_3 is given by Harshvardhan *et al.* (1987) as

$$\tau_3 = .384\alpha_3(y)\gamma_3(u)\delta_3(w) + .616\beta_3(x)\gamma_3(u)\delta_3(w), \quad (14.36)$$

where $\alpha_3(y)$ is the transmission function for carbon dioxide in the $15\mu\text{m}$ wing band:

$$\alpha_3(y) = \exp\{-0.04y/(1 + 9y^{.57})\}; \quad (14.37)$$

$\beta_3(x)$ is the transmission function in the $15\mu\text{m}$ center band:

$$\beta_3(x) = \exp\{-3.1x/(1 + 15.1x)^{.56}\}; \quad (14.38)$$

$\gamma_3(u)$ is the water vapor e-type transmission function in the $15\mu\text{m}$ band:

$$\gamma_3(u) = \exp\{-27u^{0.83}\}; \quad (14.39)$$

and $\delta_3(w)$ is the water vapor wing band transmission function in the $15\mu\text{m}$ band:

$$\delta_3(w) = \exp\{-6.7w/(1 + 16w^{0.6})\}. \quad (14.40)$$

The Planck weighted transmission function in the $9\mu\text{m}$ region (Band Region 4), τ_4 , is a function of the optical paths u , given by (14.28), and z_{oz} , specified by (14.33). We assume that it is independent of the temperature. The functional form is given by

$$\tau_4(u, z_{oz}) = \alpha_4(u)\beta_4(z_{oz}), \quad (14.41)$$

where $\alpha_4(u)$ is the transmission function for the e-type water vapor absorption, and $\beta_4(z)$ is the transmission function for ozone. These are approximated by

$$\alpha_4(u) = \exp\{-27.0u^{0.08}\},$$

and

$$\beta_4(z_{oz}) = 1 - .677 \left[1 - \exp\{-4.4\gamma_4(\sqrt{\delta_4} - 1)\} \right],$$

where

$$\gamma_4 = z_{oz}/1013 \int_0^{p_s} pq_{oz} dp$$

and

$$\delta_4 = -4.4\gamma_4 \sqrt{1 + \frac{1381.12}{88\gamma_4} \int_0^{p_s} pq_{oz} dp}.$$

The spectrally integrated Planck fluxes, $B_i[T]$, which are defined by (14.20), are given in tables in the code provided by Harshvardhan *et al.* (1987). With these values and with the transmission functions defined above, we compute the cloud-free upward and downward fluxes from (14.22) and (14.23).

14.3 The Cloud Parameterization

A cloud parameterization is a crucial part of any radiation scheme. We diagnose two types of clouds in the forecast model: stratiform and cumulus. For each grid point we define C_{st} as the stratiform cloud fraction and C_{cu} as the cumulus cloud fraction occupying the grid box at the point.

To define the stable cloud fraction function, we use the formulation that was developed for the ECMWF's forecast model (Slingo and Ritter [1985]). At each pressure level p_k , we compute the relative humidity Rh_k , and we define an average relative humidity \overline{Rh}_k by

$$\overline{Rh}_k = 0.5Rh_k + 0.25(Rh_{k-1} + Rh_{k+1}), \quad (14.42)$$

with $\overline{Rh}_1 = Rh_1$ and $\overline{Rh}_L = Rh_L$. We calculate the stratiform cloud fraction at level k from the equation,

$$C_{st_k} = \left(\frac{\overline{Rh}_k - Rh_k^*}{1 - Rh_k^*} \right)^2. \quad (14.43)$$

The variable Rh_k^* , which is a function of the pressure level and the surface pressure p_S , is the cloud critical relative humidity and is specified by the relation:

$$Rh_k^* = 1 + 2 \left[\left(\frac{p_k}{p_S} \right)^2 - \left(\frac{p_k}{p_S} \right) \right] + \sqrt{3} \left(\frac{p_k}{p_S} \right) \left[1 - 3 \left(\frac{p_k}{p_S} \right) + 2 \left(\frac{p_k}{p_S} \right)^2 \right]. \quad (14.44)$$

The values of Rh^* for a surface pressure of 1000 mb as a function of pressure are shown in Table (13.2). As we see from Equation (14.43), the vertically averaged

Table 14.2: The critical relative humidity for stratiform clouds versus pressure (mb) with a surface pressure of 1000 mb.

Pressure	Rh^*
100	0.94
200	0.85
300	0.73
400	0.60
500	0.50
600	0.44
700	0.43
800	0.51
900	0.70
1000	1.00

relative humidity must be greater than the critical relative humidity for the stratiform cloud fraction to be greater than zero. The smaller values of Rh^* in the middle atmosphere favor middle clouds compared to lower and higher level clouds.

We assume that the cumulus cloud fraction starts at the lifting condensation level given by Equation (11.8) and extends to the highest entraining cloud level computed by the Arakawa-Schubert scheme (Chapter 12). We set a constant cumulus cloud fraction up to the level where cumulus anvils are diagnosed ($T \leq 233.16$); above this level we increase the fraction in order to account for the ice anvil. The cumulus cloud fraction is based on the amount of cumulus rainfall. We use the function developed for cumulus clouds by Slingo (1987). For a cumulus precipitation rate P_{cu} given in units of cm/hr the cumulus cloud fraction is

$$C_{cu_k} = 0.93 + 0.124 \ln(P_{cu}) \quad T_k > 233.16, \quad (14.45)$$

Table 14.3: The cumulus cloud fraction versus cumulus precipitation rate in cm/hr .

P_{cu}	C_{cu}
0.0012	0.10
0.0028	0.20
0.0062	0.30
0.0139	0.40
0.0312	0.50
0.0699	0.60
0.1565	0.70
0.3595	0.80

with a maximum cumulus cloud fraction without anvils set at 0.80. The values of cumulus cloud fraction versus cumulus precipitation rate are given in Table 14.3. We enhance the cumulus cloud fraction to take into account the presence of ice anvils. When the temperature is sufficiently cold we increase the value of C_{cu} by 0.20. Therefore, if the temperature is below 233.16 K then the cumulus cloud fraction is

$$C_{cu_k} = 1.13 + 0.124 \ln(P_{cu}) \quad T_k \leq 233.16. \quad (14.46)$$

The probability of clear line of sight through a layer with cloud fraction C_k is simply

$$P_k = 1 - C_k.$$

We compute the total cloud fraction, denoted by \hat{C}_{T_k} , by combining the stable and convective cloud fractions as if their associated clear line-of-sight probabilities were independent:

$$\hat{C}_{T_k} = C_{st_k} + C_{cu_k} - C_{st_k} C_{cu_k}. \quad (14.47)$$

14.4 Longwave Radiation in a Cloudy Atmosphere

We use the total cloud fraction, specified by (14.47), to compute a probability of a clear line of sight between any 2 pressure levels. In order to account for the different emissivities of ice versus liquid water, we reduce the total cloud fraction for the longwave calculations if the temperature is less than freezing. We assume that the emissivity for water clouds (temperatures greater than 273 K) is 1 and that for ice clouds (temperature less than 233 K) the emissivity is 1/2. For temperatures between 273 K and 233 K we compute an emissivity of the cloud by taking a linear interpolation in temperature between the two values. We define the total effective cloud fraction in the longwave as the emissivity times the cloud fraction, which is given by

$$C_{T_k} = \begin{cases} \hat{C}_{T_k} & T \geq 273 \text{ K} \\ [0.5(273 - T) + (T - 233)] \hat{C}_{T_k} / 40 & 233 \text{ K} < T < 273 \text{ K} \\ 0.5 \hat{C}_{T_k} & T \leq 233 \text{ K} \end{cases} \quad (14.48)$$

Two types of cloud overlap strategies are used in the model: maximum and random. For the maximum overlap case, given the total cloud fractions at each layer k (14.48), we define the probability of a clear line of sight between 2 pressure levels, p_i and p_j , as

$$P_{M,i,j} = \begin{cases} \min[(1 - C_{T_i}), (1 - C_{T_{i+1}}), \dots, (1 - C_{T_{j-1}})] & \text{if } i > j \\ \min[(1 - C_{T_{j-1}}), (1 - C_{T_{j-2}}), \dots, (1 - C_{T_i})] & \text{if } i < j \end{cases} \quad (14.49)$$

The form of $P_{M,i,j}$ given by (14.49) assumes that the clouds are stacked one on top of another and that the largest cloud fraction between p_i and p_j determines the probability of a clear line of sight between the two levels. For the random cloud overlap case we assume that the cloud fraction in a layer is independent of the cloud

fraction in any other layer. Therefore we define the probability of the clear line of sight between pressure levels, p_i and p_j , as

$$P_{R,i,j} = \begin{cases} [(1 - C_{T_i})(1 - C_{T_{i+1}}) \cdots (1 - C_{T_{j-1}})] & \text{if } i > j \\ [(1 - C_{T_{j-1}})(1 - C_{T_{j-2}}) \cdots (1 - C_{T_i})] & \text{if } i < j \end{cases} \quad (14.50)$$

The total probability of a clear line of sight $P_{T,i}$ is given as the product of (14.49) and (14.50):

$$P_{T,i} = P_{M,i} P_{R,i}. \quad (14.51)$$

We assume that the clouds can be treated as blackbodies so that the longwave radiation fluxes between 2 pressure levels are given by the clear air fluxes between the two points times the probability of the clear line of sight between the points. Therefore, we write the final form for the upward and downward fluxes for the cloudy atmosphere as

$$\begin{aligned} \mathcal{F}_{k+1/2}^\uparrow &= \sum_{i=1}^4 B_i[T_{k+1/2}] \\ &+ P_{T_{Lk}} \sum_{i=1}^4 \{ B_i[T_S] \tau_i(p_S, p_{k+1/2}) - B_i[T(p_S)] \tau_i(p_S, p_{k+1/2}) \} \\ &- \sum_{i=1}^4 \sum_{j=1}^{N-k} P_{T_{k+j,k}} \{ B_i[T_{k+j-1/2}] \tau_i(p_{k+j}, p_{k+1/2}) \\ &- B_i[T_{k+j+1/2}] \tau_i(p_{k+j}, p_{k+1/2}) \}, \end{aligned} \quad (14.52)$$

and

$$\begin{aligned} \mathcal{F}_{k+1/2}^\downarrow &= \sum_{i=1}^4 \{ B_i[T_{k+1/2}] \\ &- P_{T_{k1}} B_i(T[p_{top}]) \tau_i(p_{k+1/2}, p_{top}) \} \\ &+ \sum_{i=1}^4 \sum_{j=1}^{N+1-k} P_{T_{k+1-j,k}} \{ B_i(T_{k+1-j-1/2}) \tau_i(p_{k+1/2}, p_{k+1-j}) \\ &- B_i(T_{k+1-j+1/2}) \tau_i(p_{k+1/2}, p_{k+1-j}) \}, \end{aligned} \quad (14.53)$$

and the longwave radiation temperature tendency is

$$\left(\frac{dT}{dt} \right)_{LW} = \left(\frac{1}{g c_p \Delta p_k} \right) (\mathcal{F}_{k+1/2}^\uparrow + \mathcal{F}_{k-1/2}^\downarrow - \mathcal{F}_{k-1/2}^\uparrow - \mathcal{F}_{k+1/2}^\downarrow). \quad (14.54)$$

In order to demonstrate the influence of clouds on the longwave radiation, we present some results of a 30 day integration of the 47 wave models starting from 1 December 1989. For every call to the longwave radiation parameterization, we computed the temperature tendency with and without clouds. We present the zonal mean cross section of the 30 day cloud fraction in Figure 14.3; Figure 14.4 is the cross section of the zonal mean longwave cooling without clouds; Figure 14.5 is the cross section of the zonal mean cloudy longwave cooling; and Figure 14.6 is the zonal mean cross section of the difference between the cloudy and cloud-free tendencies. Figure 14.3 demonstrates that the stable cloud parameterization favors the prediction of middle clouds (380–800 mb). The larger cloud fractions in the tropics are due to the cumulus activity. The distribution of longwave cooling without clouds (Figure 14.4) is relatively simple, reflecting the absorption and emission of the atmospheric components. There are two maximums, one at the tropopause and one at the top of the model. The tropospheric maximum corresponds to the position of the maximum cooling due to water vapor; the stratospheric maximum is caused primarily by CO₂. The cloudy longwave distribution (Figure 14.5), however, is more complicated, especially in the troposphere. Large maximums occur near the surface, reflecting strong longwave cooling off stratus and small cumulus tops. As we see from Figure 14.6, the difference is more than 2°C in the tropics. The tropical cumulus cloud fractions, which are constant in the vertical, create relatively constant strong cooling, up to the ice anvil positions. Overall, the clouds have a strong cooling influence in the troposphere, with the maximum difference occurring near the surface. A large amount of longwave radiation emitted by the troposphere is absorbed in the upper atmosphere; and therefore, clouds effectively create a warmer stratosphere.

NOGAPS T47/L18
30 DAY AVERAGE ZAV CLD FRACTION

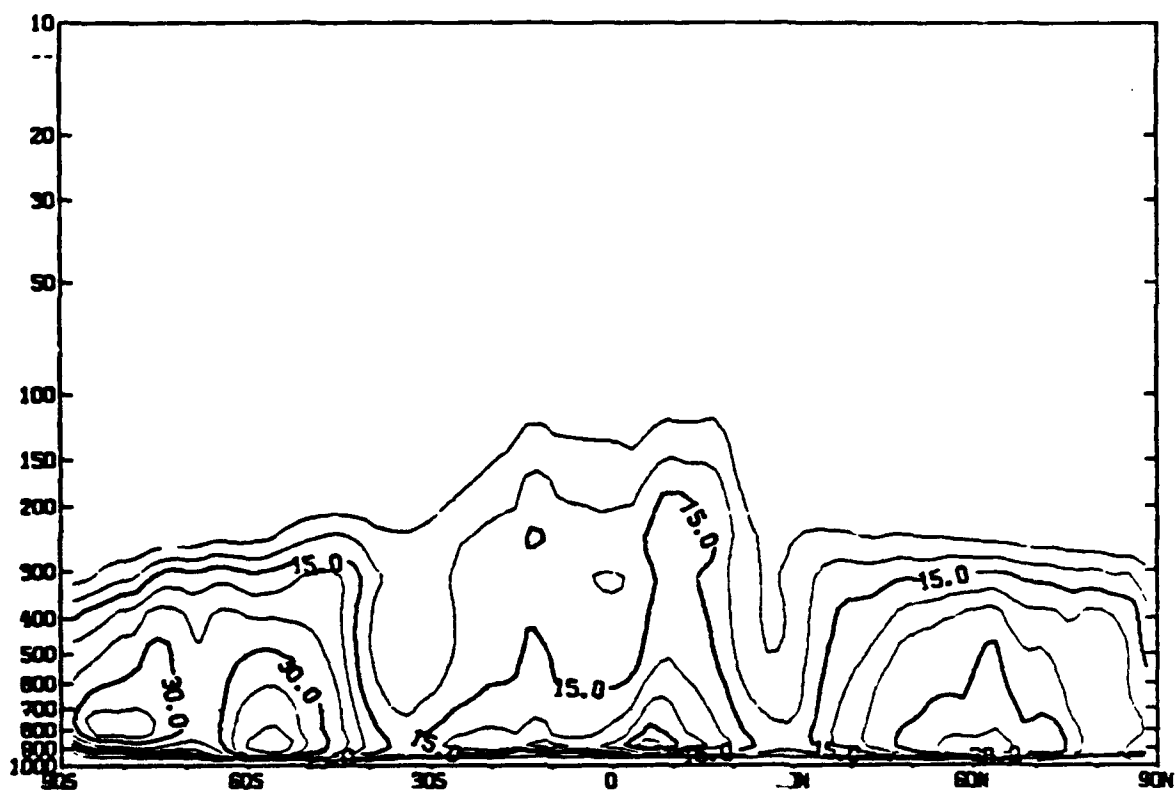


Figure 14.3: The cross section of the 30 day average of the zonal mean cloud fraction for a T47 NOGAPS integration starting at 1 December 1989.

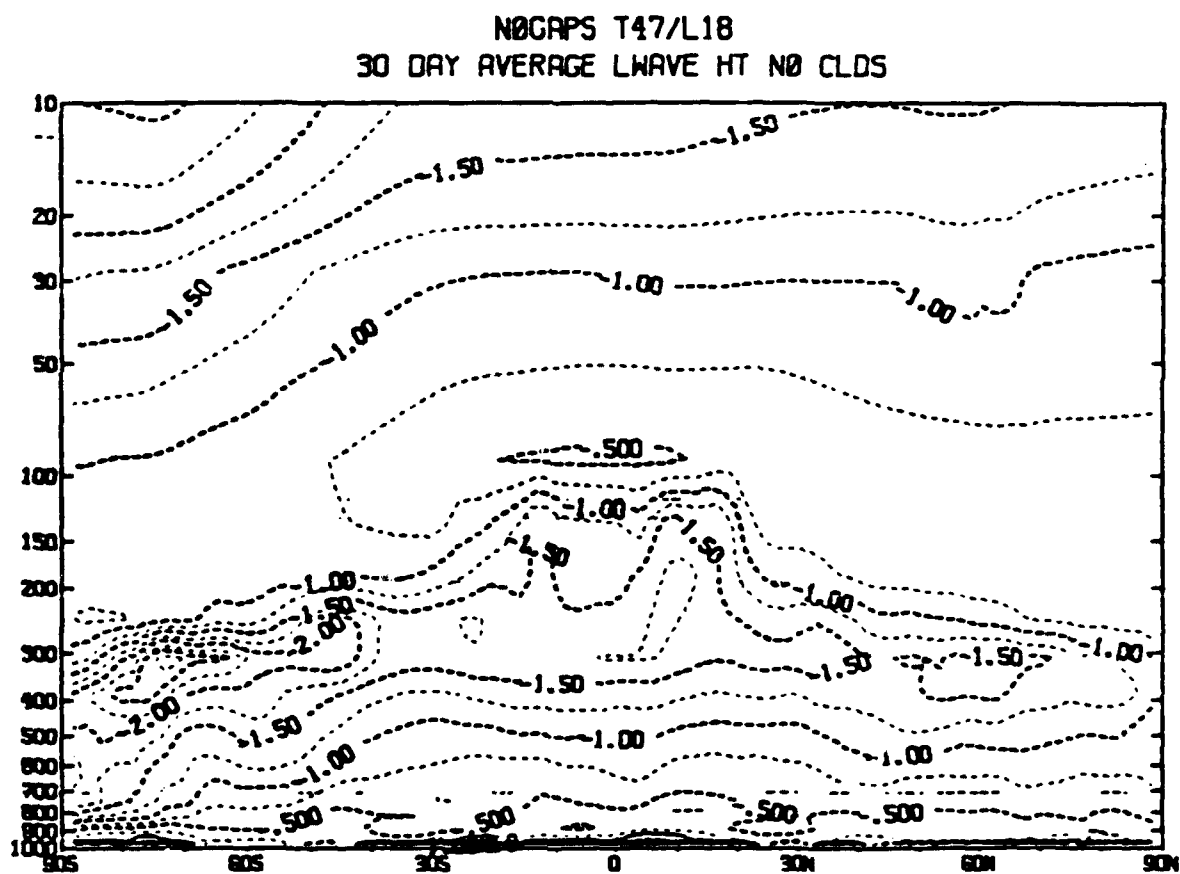


Figure 14.4: The cross section of the 30 day average of the zonal mean cloud-free longwave cooling (deg/day) for a T47 NOGAPS integration starting at 1 December 1989.

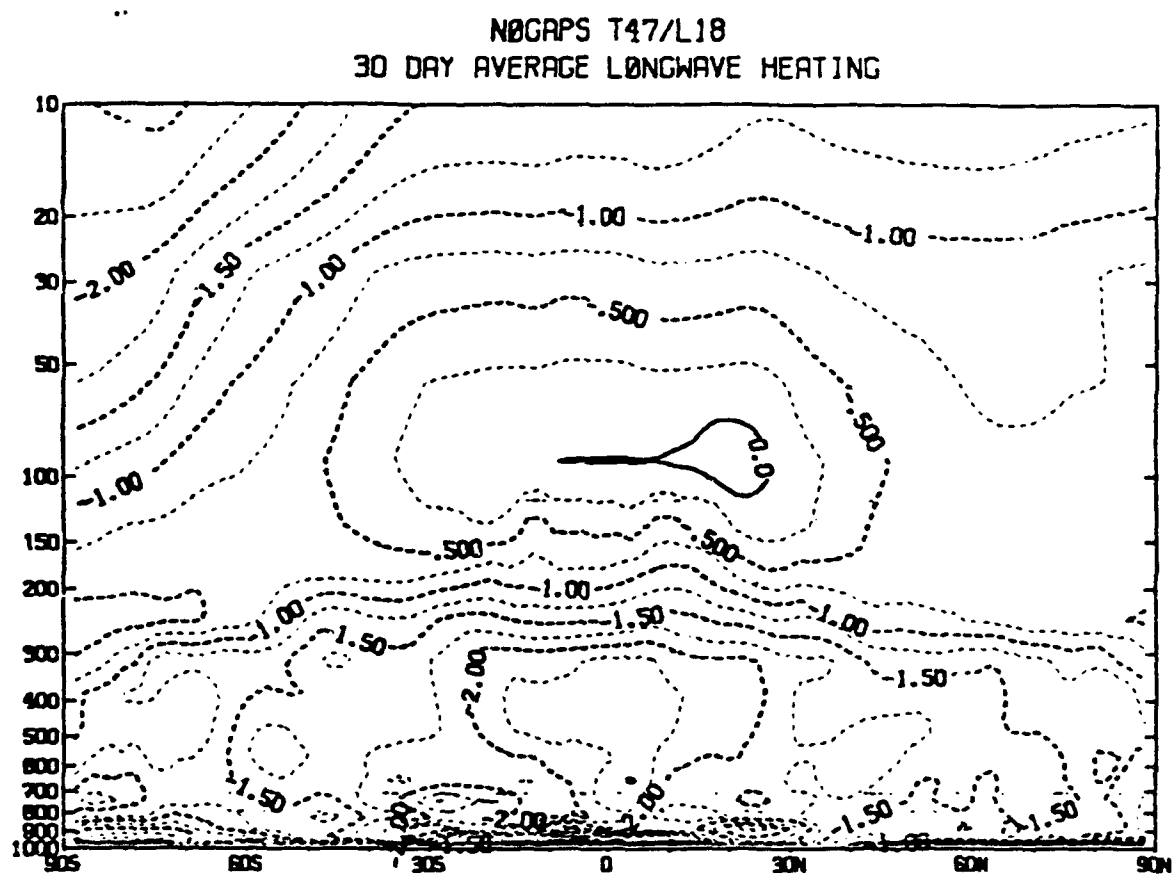


Figure 14.5: The cross section of the 30 day average of the zonal mean cloudy longwave cooling (deg/day) for a T47 NOGAPS integration starting at 1 December 1989.

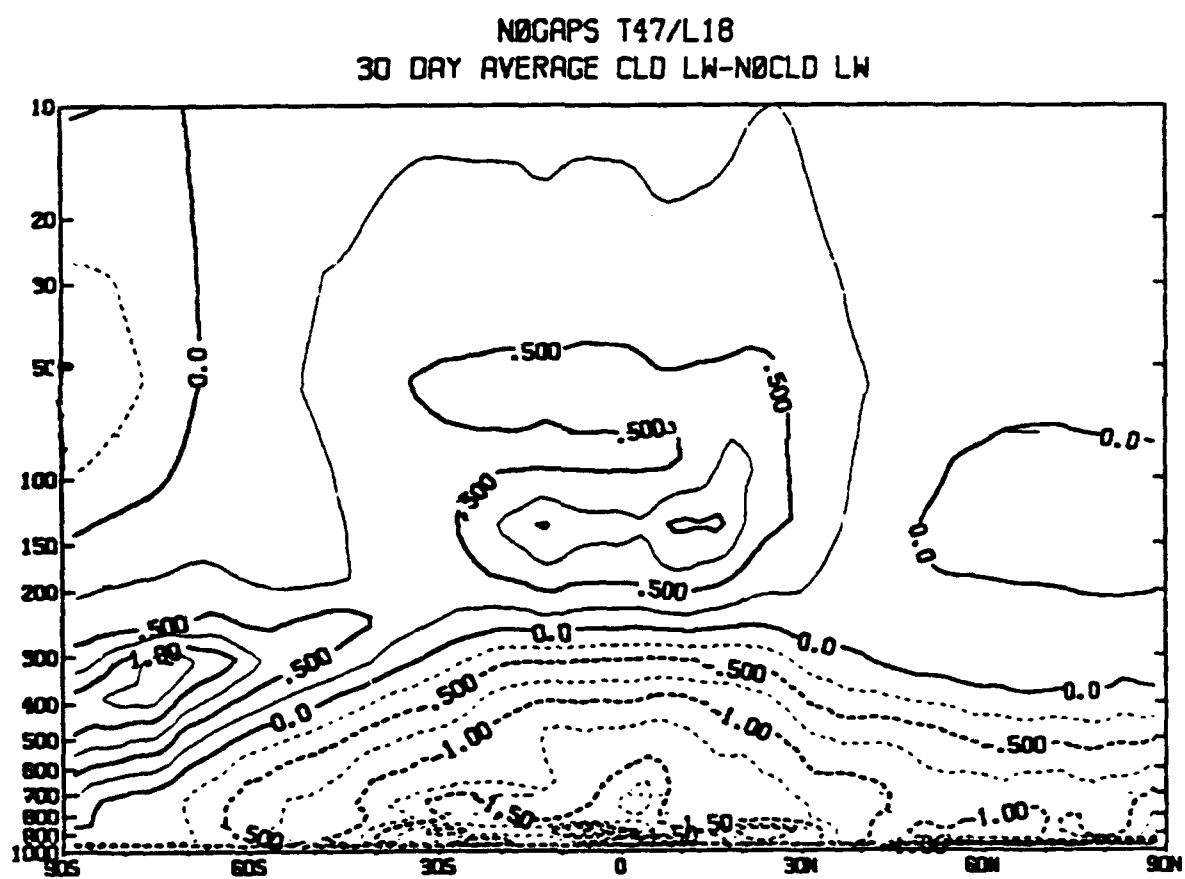


Figure 14.6: The zonal mean cross section of the 30 day difference of the cloud-free and the cloudy longwave cooling (deg/day) for a T47 NOGAPS integration starting at 1 December 1989.

Chapter 15

Shortwave Radiation

The time tendency equation for temperature due to the absorption of solar radiation is

$$c_p \rho \frac{\partial T}{\partial t} = - \frac{\partial \mathcal{A}_{SW}}{\partial z}, \quad (15.1)$$

where \mathcal{A}_{SW} is the absorbed solar flux (Watts/m²), ρ is the density of air, and c_p is the specific heat of air at constant pressure (1005.45 J K⁻¹ kg⁻¹). At the top of the atmosphere the incoming solar radiation is given by

$$S = S_0 \cos \theta_0. \quad (15.2)$$

S_0 is the solar constant, which is taken to be 1368.3 Watts/m². The variable θ_0 is the solar zenith angle, which we define by the relation,

$$\cos \theta_0 = \sin \lambda \sin \delta + \cos \lambda \cos \delta \cos h, \quad (15.3)$$

where λ is the latitude, δ is the inclination of the sun ($\leq |23.5|$ degrees), and h is the hour angle (the degrees that the earth must turn so that the point is at local noon). The shortwave radiation heating is computed every two hours of forecast time, using the current moisture and temperature fields. However, the solar zenith angle is computed for the mid point of the two hour radiation time step.

The shortwave calculations are based on the work of Davies (1982), which in turn drew heavily from the work of Lacis and Hansen (1974). In the present treatment, we assume that water vapor and ozone are the only gases that absorb solar radiation. We ignore the effects of aerosols and cloud droplets and the spectral nature of the surface albedo.

15.1 Absorption by Ozone

We assume that the absorption of ozone takes place above any level of scattering of radiation by clouds (*i.e.*, above the cloud top for a given point) and at wavelengths less than $0.9\mu\text{m}$ ($\lambda < 0.9\mu\text{m}$). The effective path traveled by the direct solar beam to reach the half level $k+1/2$ is given by

$$x_{k+1/2} = M u_{k+1/2} \quad (15.4)$$

where M is the magnification factor, which accounts for the inclined path and refraction of the direct solar radiation (Rogers [1967]):

$$M = \frac{35}{\sqrt{1224 \cos^2 \theta_0 + 1}} \quad (15.5)$$

and $u_{k+1/2}$ is the normal optical path of ozone, defined at the half pressure levels (see Figure 3.1):

$$u_{k+1/2} = \int_{p_{\text{top}}}^{p_{k+1/2}} q_{\text{oz}} dp/g. \quad (15.6)$$

The mixing ratios of ozone are taken from the climatological results tabulated by Dopplack (1974). The reflected radiation effective path is given by

$$x_{k+1/2}^{\text{r}} = M u_{L+1/2} + 1.9(u_{L+1/2} - u_{k+1/2}). \quad (15.7)$$

The empirical factor 1.9 accounts for the diffuse upward radiation and L is the total number of atmospheric layers.

The absorption by ozone in the visible frequencies (the Chappius band) is parameterized by Lacis and Hansen (1974) by the function:

$$A_{oz}^{vis}(x) = \frac{0.02118x}{1 + 0.042x + 0.000323x^2}; \quad (15.8)$$

and the absorption of ozone in the ultraviolet frequencies (the Hartley and Huggins band) is given by Lacis and Hansen (1974) as

$$A_{oz}^{uv}(x) = \frac{1.082x}{(1 + 138.6x)^{0.805}} + \frac{0.0658x}{1 + (103.6x)^3}. \quad (15.9)$$

The total absorption of ozone is the sum of (15.8) and (15.9):

$$A_{oz}(x) = A_{oz}^{vis}(x) + A_{oz}^{uv}(x). \quad (15.10)$$

The total absorption by ozone in the k^{th} layer, which is denoted by \mathcal{A}_{ozk} , is the difference between the absorbed radiation at $k+1/2$ and the absorbed radiation at $k-1/2$, which we compute as

$$\begin{aligned} \frac{\partial \mathcal{A}_{ozk}}{\partial z} \Delta z_k &= S_0 \cos \theta_0 [A_{oz}(x_{k+1/2}) - A_{oz}(x_{k-1/2})] \\ &+ R_{oz} S_0 \cos \theta_0 [A_{oz}(x_{k-1/2}^*) - A_{oz}(x_{k-1/2})]. \end{aligned} \quad (15.11)$$

The factor R_{oz} is the total albedo of the underlying (and probably cloudy) atmosphere to visible and ultraviolet light. We obtain R_{oz} from a solution to the diffuse radiative transfer equation.

15.2 Diffuse Radiation and the Two Stream Solution

In order to calculate the albedo of the lower atmosphere, we must consider the scattered part as well as the direct solar radiation. The radiative transfer equation

for the diffuse radiance, I_ν , for a plane-parallel atmosphere illuminated by a solar flux, $\pi\mathcal{F}_0$, at an angle, θ_0 , (see Liou [1980]) is

$$\begin{aligned}\frac{\partial I_\nu}{\partial z} = & -\rho k_{e\nu} I_\nu \sec \theta_0 \\ & + \rho k_{s\nu} \sec \theta_0 \int_{-1}^1 \int_0^{2\pi} P(\mu, \varphi; \mu', \varphi') I_\nu(z, \mu', \varphi') d\mu' d\varphi' \\ & + \rho k_{s\nu} \sec \theta_0 \pi \mathcal{F}_0 P(\mu, \varphi; -\mu_0, -\varphi_0) e^{-\tau/\mu_0},\end{aligned}\quad (15.12)$$

where ν denotes the frequency and $\mu = \cos \theta$. The first term on the right hand side of (15.12) is the loss of radiance due to absorption and single scattering, with the mass extinction cross section given by $k_{e\nu}$. The second term is the increase of radiance due to multiple scattering, with $k_{s\nu}$ denoting the mass scattering cross section. P is the scattering phase function, which is the probability that a photon will be scattered from the direction given by the angles, (μ', φ') , into the direction (μ, φ) . The phase function P is defined such that

$$\int_{-1}^1 \int_0^{2\pi} P(\mu, \varphi; \mu', \varphi') d\varphi' d\mu' = 4\pi$$

The third term of (15.12) is the increase of radiance due to the single scattering of the direct solar beam whose direction is given by $(-\mu_0, -\varphi_0)$.

We define the upward and downward diffusive fluxes by the integrals:

$$\mathcal{F}_{dif}^\uparrow = \int_0^{2\pi} \int_0^1 I_\nu(z, \mu, \varphi) \mu d\mu d\varphi \quad (15.13)$$

and

$$\mathcal{F}_{dif}^\downarrow = \int_0^{2\pi} \int_0^{-1} I_\nu(z, \mu, \varphi) \mu d\mu d\varphi. \quad (15.14)$$

The total downward flux is the sum of the direct and the diffuse radiation, which is

$$\mathcal{F}_{tot}^\downarrow = \pi \mathcal{F}_0 \mu_0 e^{-\tau/\mu_0} + \int_0^{2\pi} \int_0^{-1} I_\nu(z, \mu, \varphi) \mu d\mu d\varphi. \quad (15.15)$$

We assume that all reflected solar radiation is diffuse, so that the total upward flux is given by (15.13).

The optical thickness, τ , of the air column above a height z is defined as

$$\tau = \int_z^\infty \rho k_{e\nu} dz. \quad (15.16)$$

Replacing the vertical coordinate z with τ in the radiative transfer equation (15.12), we obtain the result that

$$\begin{aligned} \mu \frac{\partial I_\nu}{\partial \tau} = I_\nu & - (\omega_0/4\pi) \int_0^{2\pi} \int_{-1}^1 I_\nu(\tau, \mu', \varphi') P(\mu, \varphi; \mu', \varphi') d\mu' d\varphi' \\ & - (\omega_0/4\pi) \pi \mathcal{F}_0 e^{-\tau/\mu_0} P(\mu, \varphi; -\mu_0, -\varphi_0), \end{aligned} \quad (15.17)$$

where P is phase function ω_0 is the single scattering albedo, which is defined by the relation:

$$\omega_0 = \frac{k_{s\nu}}{k_{e\nu}}.$$

The phase function P is typically taken to be a function of the scattering angle, Θ , only, which is given by the relation

$$\cos \Theta = \mu\mu' + \sqrt{1-\mu^2}\sqrt{1-\mu'^2}\cos(\varphi' - \varphi).$$

The expansion of the phase function in terms of Legendre polynomials, P_l , results in the expansion sum with coefficients, $\tilde{\omega}_l$, of the form:

$$P(\cos \Theta) = \sum_{l=0}^{\infty} \tilde{\omega}_l P_l(\cos \Theta) \quad (15.18)$$

with $\tilde{\omega}_0 = 1$. The first moment of the phase function is called the asymmetry factor, which is denoted by g , and is obtained from the relation:

$$g = \frac{\tilde{\omega}_1}{3} = \frac{1}{2} \int_{-1}^1 P(\cos \Theta) \cos \Theta d \cos \Theta. \quad (15.19)$$

The general form of $P(\cos \Theta)$ is given in terms of Legendre and associated Legendre polynomials (see Liou [1980]) as

$$\begin{aligned} P(\cos \Theta) &= \sum_{l=0}^{\infty} \tilde{\omega}_l P_l(\mu) P_l(\mu') \\ &+ \sum_{l=0}^{\infty} \sum_{m=1}^l 2\tilde{\omega}_l \frac{(l-m)!}{(l+m)!} P_l^m(\mu) P_l^m(\mu') \cos[m(\varphi - \varphi')]. \end{aligned} \quad (15.20)$$

For the remaining discussion, however, we shall restrict ourselves to cases where the radiances are independent of the azimuthal angle φ . From the integral of (15.20) with respect to φ , we define the integrated phase function $P(\mu, \mu')$ as

$$P(\mu, \mu') = \sum_{l=0}^{\infty} \tilde{\omega}_l P_l(\mu) P_l(\mu'). \quad (15.21)$$

We assume that I_ν is independent of φ , so that when we integrate (15.17) with respect to φ , we obtain the azimuthal independent transfer equation for the diffuse radiance:

$$\begin{aligned} \mu \frac{\partial I_\nu}{\partial \tau} = I_\nu(\tau, \mu) & - \left(\frac{\omega_0}{2} \right) \int_{-1}^1 I_\nu(\tau, \mu') P(\mu, \mu') d\mu' \\ & - \left(\frac{\omega_0}{4\pi} \right) \pi \mathcal{F}_0 e^{-\tau/\mu_0} P(\mu, -\mu_0). \end{aligned} \quad (15.22)$$

By performing the integrals of (15.22) with respect to μ from 0 to 1, and from -1 to 0, we obtain the following upward and downward radiance equations:

$$\begin{aligned} \frac{dI_\nu^+}{d\tau} = \int_0^1 I_\nu(\tau, \mu) d\mu & - \left(\frac{\omega_0}{2} \right) \int_0^1 \int_{-1}^1 P(\mu, \mu') I_\nu(\tau, \mu') d\mu' d\mu \\ & - \left(\frac{\omega_0}{4\pi} \right) \pi \mathcal{F}_0 e^{-\tau/\mu_0} \int_0^1 P(\mu, -\mu_0) d\mu \end{aligned} \quad (15.23)$$

and

$$\begin{aligned} \frac{dI_\nu^-}{d\tau} = \int_{-1}^0 I_\nu(\tau, \mu) d\mu & - \left(\frac{\omega_0}{2} \right) \int_{-1}^0 \int_{-1}^1 P(\mu, \mu') I_\nu(\tau, \mu') d\mu' d\mu \\ & - \left(\frac{\omega_0}{4\pi} \right) \pi \mathcal{F}_0 e^{-\tau/\mu_0} \int_{-1}^0 P(\mu, -\mu_0) d\mu, \end{aligned} \quad (15.24)$$

where the functions $I_\nu^+(\tau)$ and $I_\nu^-(\tau)$ are defined by

$$I_\nu^+(\tau) = \int_0^1 \mu I_\nu(\tau, \mu) d\mu \quad (15.25)$$

and

$$I_\nu^-(\tau) = \int_{-1}^0 \mu I_\nu(\tau, \mu) d\mu. \quad (15.26)$$

In order to obtain approximate solutions to the differential/integral equations (15.23) and (15.24), we use certain assumptions to evaluate the integrals. One of

these assumption is that the radiance is approximately constant over μ . With this approximation, we evaluate the first term on the right hand side of (15.23) as

$$\int_0^1 I_\nu(\tau, \mu) d\mu = 2I_\nu^+(\tau). \quad (15.27)$$

This type of approximation will be used throughout the analysis. Defining the function $\beta_0(\mu_0)$ by

$$\beta_0(\mu_0) = \frac{1}{2} \int_0^1 P(\mu, -\mu_0) d\mu, \quad (15.28)$$

which implies (from the normalization of the phase function) that

$$1 - \beta_0(\mu_0) = \frac{1}{2} \int_{-1}^0 P(\mu, -\mu_0) d\mu, \quad (15.29)$$

and defining the number β' as

$$\beta' = \frac{1}{2} \int_{-1}^0 \int_0^1 P(\mu, \mu') d\mu d\mu', \quad (15.30)$$

which implies (from the normalization of the phase function) that

$$1 - \beta' = \frac{1}{2} \int_0^1 \int_0^1 P(\mu, \mu') d\mu d\mu', \quad (15.31)$$

and using the integral approximations demonstrated by (15.27), we convert Equations (15.23) and (15.24) into the Coakley and Chýlek's (1975) two-stream approximation transfer equations:

$$\begin{aligned} \frac{dI_\nu^+}{d\tau} = 2I_\nu^+ & - 2\omega_0(1 - \beta')I_\nu^+ - 2\omega_0\beta'I_\nu^- \\ & - \omega_0\mathcal{F}_0e^{-\tau/\mu_0}\beta_0(\mu_0) \end{aligned} \quad (15.32)$$

and

$$\begin{aligned} \frac{dI_\nu^-}{d\tau} = 2I_\nu^- & - 2\omega_0(1 - \beta')I_\nu^- - 2\omega_0\beta'I_\nu^+ \\ & - \omega_0\mathcal{F}_0e^{-\tau/\mu_0}[1 - \beta_0(\mu_0)]. \end{aligned} \quad (15.33)$$

The Coakley and Chýlek two-stream method is one of many different two-stream approximations to the transfer equations. In general, the two-stream approximation method is any method where the transfer equations can be put into the form (Meador and Weaver [1980]):

$$\frac{dI_{\nu}^{+}}{d\tau} = \gamma_1 I_{\nu}^{+} - \gamma_2 I_{\nu}^{-} - \pi \mathcal{F}_0 e^{-\tau/\mu_0} \omega_0 \gamma_3 \quad (15.34)$$

and

$$\frac{dI_{\nu}^{-}}{d\tau} = \gamma_2 I_{\nu}^{+} - \gamma_1 I_{\nu}^{-} + \pi \mathcal{F}_0 e^{-\tau/\mu_0} \omega_0 \gamma_4. \quad (15.35)$$

The solution to the transfer equations (15.32) and (15.33) for an atmospheric layer of total optical thickness, τ^* , with boundary conditions:

$$\left. \begin{aligned} \pi I_{\nu}^{+}(\tau^*) &= 0 \\ \pi I_{\nu}^{-}(0) &= 0 \end{aligned} \right\}, \quad (15.36)$$

is given by Coakley and Chýlek (1975). We obtain the reflection coefficient $R(\mu_0)$ and the transmission coefficient, $T(\mu_0)$, which are defined by

$$R(\mu_0) = \frac{\pi I_{\nu}^{+}(0)}{\pi \mathcal{F}_0 \mu_0} \quad (15.37)$$

and

$$T(\mu_0) = \frac{\pi I_{\nu}^{-}(\tau^*)}{\pi \mathcal{F}_0 \mu_0} \quad (15.38)$$

from the Coakley and Chýlek (1975) solution as

$$R(\mu_0) = \frac{1}{1 + 2\beta'\tau^*} \{2\beta'\tau^* + (1 - e^{-\tau^*/\mu_0})[\beta_0 - 2\beta'\mu_0]\} \quad (15.39)$$

and

$$T(\mu_0) = \frac{1}{1 + 2\beta'\tau^*} \{(1 - \beta_0 + 2\beta'\mu_0)[1 - e^{-\tau^*/\mu_0}] - 2\beta'\tau^* e^{-\tau^*/\mu_0}\}. \quad (15.40)$$

15.3 The Atmospheric Reflection for $\lambda < 0.9\mu\text{m}$

In order to calculate the total reflection, R_{oz} in Equation (15.11), of an atmospheric layer with a surface albedo for diffuse radiation, α_S , and an albedo for direct radiation, $R_S(\mu_0)$, we use the results of the previous section and the results of Chandrasekhar (1960), who gives the total reflection $R_T(\mu_0)$ by

$$R_T(\mu_0) = R(\mu_0) + \bar{T} \left(\frac{R_S(\mu_0)e^{-\tau^*/\mu_0} + \alpha_S T(\mu_0)}{1 - \alpha_S \bar{R}} \right). \quad (15.41)$$

$R(\mu_0)$ and $T(\mu_0)$ are given by (15.39) and (15.40) and \bar{R} and \bar{T} denote the average reflection and transmission coefficients, which are defined by

$$\bar{R} = 1 - \bar{T} = 2 \int_0^1 \mu_0 R(\mu_0) d\mu_0. \quad (15.42)$$

The albedo for the direct solar radiation is given by Paltridge and Platt (1976) as

$$R_S(\mu_0) = \left(\frac{\alpha_S - 0.05}{0.95} \right) + \left\{ 1 - \left(\frac{\alpha_S - 0.05}{0.95} \right) \right\} \exp \left\{ -\frac{18}{\pi} \left(\frac{\pi}{2} - \theta_0 \right) \right\} \quad (15.43)$$

Over land, α_S are obtained from monthly climatological tables, which are then interpolated to the day at the beginning of each forecast. Over sea ice, the albedo is given a value of 0.60, and over open sea α_S is set to 0.09.

In order to take into account the frequency dependence of the total reflection coefficient for the underlying atmosphere for wavelengths less than $0.9\mu\text{m}$, we perform two separate two-stream calculations for different total optical depths, τ_1^* and τ_2^* , which are the sums of the Rayleigh optical depth, τ_R , and the cloud optical depth, τ_C . The total optical depth of the clouds is defined by

$$\tau_C = \sum_{l=1}^L f(T_l) \hat{C}_{T_l} \Delta p_l \quad (15.44)$$

where L is the total number of model layers ($L=18$), and \hat{C}_{T_l} is the total cloud fraction, which is given by (14.47). The empirical factor $f(T_l)$, which parametrizes

the effect of clouds' liquid water drops, is

$$f(T_l) = \begin{cases} 0.08 & T_l \geq 273 \text{ K} \\ [0.02(273 - T_l + 0.08(T_l - 233))]/40 & 233 \text{ K} < T_l < 273 \text{ K} \\ 0.02 & T_l \leq 233 \text{ K} \end{cases} \quad (15.45)$$

For the first calculation, we set the Rayleigh optical depth to zero, *i.e.* $\tau_R = 0$, so that the optical depth is given by only the cloud optical depth:

$$\tau_1^* = \tau_C$$

The function $\beta_0(\mu_0)$, defined by (15.28), is given by Davies (1982) as

$$\beta_0(\mu_0) = \frac{1}{2} \left\{ 1 - \frac{[1 + a(\mu_0)]g}{1 + a(\mu_0)g} \right\} \quad (15.46)$$

with $a(\mu_0)$ given by

$$a(\mu_0) = -1.01373 + 1.14397\mu_0 + 0.68246\mu_0^2. \quad (15.47)$$

Davies (1982) took the above form of $\beta_0(\mu_0)$ from Figure 3 of Wiscombe and Grams (1976). We assume that the scattering is conservative:

$$\omega_0 = 1, \quad (15.48)$$

and that the asymmetry factor g , defined by (15.19), is constant:

$$g \approx 0.85. \quad (15.49)$$

To improve the accuracy of the solutions, we use empirical adjustments or scalings for g , τ^* , and ω_0 , which we denote by g' , τ' , and ω'_0 . The idea of scaling was originally introduced by Joseph *et al.* (1976) in order to improve on the Eddington solution to the transfer equations. These scalings are given by

$$\left. \begin{aligned} g' &= g/(1 + g), \\ \tau' &= (1 - \omega_0 g^2)\tau_1^*, \\ \omega'_0 &= (1 - g^2)\omega_0/(1 - g^2\omega_0) \end{aligned} \right\}. \quad (15.50)$$

The constant β' defined by (15.30) is given by

$$\beta' = \frac{1}{2} \left(1 - \frac{7}{8} g' \right). \quad (15.51)$$

With the scaling given by (15.50), we compute the reflection and transmission coefficients from (15.39) and (15.40). From (15.42) we calculate the average transmission, \bar{T} as

$$\bar{T} = \frac{1}{1 + .1299 \tau'}, \quad (15.52)$$

and we obtain the total reflection (for the $\tau_R = 0$ case) from (15.41), which we denote by R_{T_1} .

In the second calculation for the total reflection coefficient, we set the Rayleigh optical depth to 0.85, $\tau_R = 0.85$, so that the total optical depth is

$$\tau_2^* = 0.85 + \tau_C. \quad (15.53)$$

Again, we assume that the scattering is conservative:

$$\omega_0 = 1,$$

but we use a asymmetry factor, which is given by the formula,

$$g = 0.85 \frac{\tau_C}{\tau_R + \tau_C}. \quad (15.54)$$

The scaling for this case is given by

$$\left. \begin{aligned} g' &= (g - g^2)/(1 - g^2), \\ \tau' &= (1 - \omega_0 g^2) \tau_2^*, \\ \omega'_0 &= (1 - g^2) \omega_0 / (1 - g^2 \omega_0) \end{aligned} \right\}; \quad (15.55)$$

the function $\beta_0(\mu_0)$ is given by (15.46), with g replaced by g' ; and β' is defined by

$$\beta' = 2(1 - .4375 g'). \quad (15.56)$$

The solutions for the reflection and transmission coefficients are given by (15.39) and (15.40); \bar{T} , which is defined by (15.42), is given by

$$\bar{T} = \frac{1}{1 + 0.866(1 - g)}; \quad (15.57)$$

and we denote R_{T_2} as the total reflection coefficient, (for the $\tau_R = 0.85$ case), which is given by (15.41). Finally, we calculate the total reflection coefficient for wavelengths less than $0.9\mu\text{m}$, which is specified by R_{oz} in (15.11), as the weighted sum of R_{T_1} and R_{T_2} :

$$R_{oz} = \frac{R_{T_1}}{3} + \frac{2R_{T_2}}{3}. \quad (15.58)$$

With this result, we compute the atmospheric absorption due to ozone from (15.11). The absorption of solar radiation by the surface for wavelengths less than $0.9\mu\text{m}$ is

$$A_{S_1} = S_0\mu_0[0.647 - A_{oz}(Mu_\infty)](1 - R_{S_1}). \quad (15.59)$$

In order to calculate the reflection coefficient at the surface, R_{S_1} , we repeat the calculation that resulted in the reflection coefficient, R_{T_2} , which is given by Equation (15.58), using the same scaling, β_0 , and β' but for a Rayleigh optical depth of 0.118, $\tau_R = 0.118$.

15.4 Clear Sky Water Vapor Absorption

We assume that all water vapor absorption occurs at wavelengths greater than $0.9\mu\text{m}$ ($\lambda > 0.9\mu\text{m}$). The effective water vapor path at half level $k+1/2$ is defined as

$$x_{k+1/2} = My_{k+1/2}, \quad (15.60)$$

where the effective water vapor amount, $y_{k+1/2}$, is given by

$$y_{k+1/2} = \frac{1}{g} \int_0^{p_{k+1/2}} q \left(\frac{p}{1013.25\text{mb}} \right) \sqrt{\frac{273}{T}} dp. \quad (15.61)$$

The return path for the reflected solar radiation is given by

$$x_{k+1/2}^* = My_{L+1/2} + \frac{5}{3} (y_{L+1/2} - y_{k+1/2}). \quad (15.62)$$

The 5/3 is an empirical factor that accounts for the diffuse transmission. The cloud free water vapor absorption for the k^{th} layer is

$$\begin{aligned} \frac{\partial A_{wv_k}}{\partial z} \Delta z_k &= S_0 \mu_0 [A_{wv}(x_{k+1/2}) - A_{wv}(x_{k-1/2}) \\ &+ S_0 \mu_0 R_S [A_{wv}(x_{k-1/2}^*) - A_{wv}(x_{k+1/2}^*)], \end{aligned} \quad (15.63)$$

where the water vapor absorption function is given by Lacis and Hansen (1975) as

$$A_{wv}(x) = \frac{2.9x}{(1 + 141.5x)^{0.635} + 5.915x}. \quad (15.64)$$

The total absorption for the cloud free sky case is the sum of (15.11) and (15.63).

The surface absorption for the clear sky case for $\lambda > 0.9 \mu m$ is given by

$$A_{S_2} = S_0 \mu_0 (1 - R_S) [0.353 - A_{wv}(My_{L+1/2})], \quad (15.65)$$

and the total surface absorption is the sum of (15.59) and (15.65).

15.5 Cloudy Sky Water Vapor Absorption

For cloudy conditions there is usually significant scattering of the solar radiation for wavelengths greater than $0.9 \mu m$. In place of one equation of the form of (15.63), we calculate the absorption for different bands of the absorption coefficient. We assume that the transmission can be broken up into discrete values of the absorption coefficient as

$$T(x) = \sum_{i=1}^5 p(k_i) e^{-k_i x}, \quad (15.66)$$

where $p(k_i)$ is the fraction of incident flux that is transmitted with an absorption coefficient k_i with an absorption range δk_i . The absorption coefficient replaces

Table 15.1: The discrete values for the absorption and probability distribution.

i	k_i	$p(k_i)$
1	0.005	0.107
2	0.041	0.104
3	0.416	0.073
4	4.752	0.044
5	72.459	0.025

frequency as the dependent variable because frequency dependent transmissions are not multiplicative (see Stephens [1984]). The values for k_i and $p(k_i)$ are given in Table 15.1.

We write the incoming direct solar radiation for $\lambda > 0.9\mu\text{m}$ at the top of the cloud layer as the sum

$$S = \sum_{i=1}^5 S_0 \mu_0 p(k_i) e^{-k_i y_{ctop}}, \quad (15.67)$$

where y_{ctop} is the effective water vapor amount at the cloud top level, which is defined by (15.61). The numerical procedure is: First, we solve for the total upward and downward fluxes, which are specified by $U_{l+1/2}$ and $D_{l+1/2}$, using the adding method (described below), together with the two-stream solution for the diffuse radiation in each layer. Second, once $U_{l+1/2}$ and $D_{l+1/2}$ are known for all levels, we compute the total absorption for $\lambda > 0.9\mu\text{m}$ for layer l by

$$\frac{\partial \mathcal{A}_{wvl}}{\partial z} \Delta z_l = (D_{l-1/2} - U_{l-1/2}) - (D_{l+1/2} - U_{l+1/2}). \quad (15.68)$$

In order to obtain the total upward and downward fluxes, we must calculate the following quantities:

$S_{l+1/2}$ = the direct solar flux at level $l+1/2$,

$\tilde{U}_{l+1/2}$ = the reflected diffuse flux at level $l+1/2$ due to the direct flux,

$\widetilde{D}_{l+3/2}$ = the transmitted diffuse flux at level $l+3/2$ due to the direct flux,

$r_{l+1/2}$ = reflection coefficient due to diffuse radiation as the source,

$t_{l+3/2}$ = transmission coefficient due to diffuse radiation as the source.

We compute the above quantities by summing the two stream solutions for each of the five absorption coefficients given in Table 15.1. The details are given after the discussion of the adding method. Once the quantities $\widetilde{U}_{l+1/2}$, $\widetilde{D}_{l+3/2}$, $r_{l+1/2}$, and $t_{l+3/2}$ are calculated, we define the following intermediate quantities as part of the adding method:

$\widehat{D}_{l+3/2}$ = the downward diffuse flux at level $l+3/2$ due to all diffuse radiation, which has not previously crossed level $l+3/2$,

$\widehat{U}_{l+1/2}$ = the upward diffuse flux at level $l+1/2$ due to all diffuse radiation, which has not previously crossed level $l+3/2$,

$\widehat{M}_{l+1/2}$ = the magnification factor for multiple reflections at level $l+1/2$ for all levels above $l+1/2$

$$= 1/(1 - \widehat{R}_{l+1/2}r_{l+1/2}),$$

$\widehat{R}_{l+1/2}$ = the composite reflection coefficient of the entire atmosphere above level $l+1/2$

$$= r_{l-1/2} + t_{l-1/2}\widehat{R}_{l-1/2}t_{l-1/2}\widehat{M}_{l-1/2}.$$

The boundary conditions for the various quantities are

$$\left. \begin{aligned} \widetilde{D}_{1/2} &= 0 \\ \widehat{D}_{1/2} &= 0 \\ \widehat{U}_{1/2} &= \widetilde{U}_{1/2} \\ \widehat{R}_{1/2} &= 0 \\ \widehat{M}_{1/2} &= 1 \\ r_{L+1/2} &= \alpha_S \end{aligned} \right\}. \quad (15.69)$$

We obtain the relations for $\hat{U}_{l+1/2}$ and $\hat{D}_{l+1/2}$ by starting at the top of the atmosphere, with the boundary conditions (15.69), and we assume that the two adjacent layers are separated by a small vertical displacement (see Figure 14.1). At level 3/2, the downward intermediate flux is given by the two stream downward flux from the top layer:

$$\hat{D}_{3/2} = \bar{D}_{3/2}.$$

This downward flux, $\hat{D}_{3/2}$, is reflected off the next layer diffusely with the reflection coefficient, $r_{3/2}$, and contributes to the upward flux, so that, in the absence of reflections from the top layer, the upward intermediate flux would be $\tilde{U}_{3/2} + r_{3/2}\hat{D}_{3/2}$. However, this upward flux is repeatedly bounced between the first two layers with a total magnification factor of $\hat{M}_{3/2}$, so that the total intermediate flux is given by

$$\hat{U}_{3/2} = (r_{3/2}\hat{D}_{3/2} + \tilde{U}_{3/2})\hat{M}_{3/2}.$$

The returning downward flux between the first two layers is not counted in $\hat{D}_{3/2}$, since the radiation has already crossed the 3/2 level. This returning flux will be counted as part of the next downward flux. For the 5/2 level, the downward diffuse flux, due to all sources above 5/2, is the sum of the two stream downward flux, $\bar{D}_{5/2}$, plus the contribution from the layers above, which are from two sources. First, the upward flux, $\tilde{U}_{3/2}$, is reflected off all layers above it with a total reflection coefficient of $\hat{R}_{3/2}$, which then undergoes multiple reflections and finally transmitted downward with a coefficient, $t_{5/2}$, to reach level 5/2. The second contribution from above is the downward flux, $\hat{D}_{3/2}$, which undergoes multiple reflections and is transmitted downward to 5/2. The total result is

$$\hat{D}_{5/2} = \bar{D}_{5/2} + t_{5/2}\hat{M}_{3/2}(R_{3/2}\tilde{U}_{3/2} + \hat{D}_{3/2}).$$

The upward diffuse flux due to all sources above level 5/2 is the multiple reflections of the upward flux originating in the layer, $\tilde{U}_{5/2}$, and the reflected downward flux,

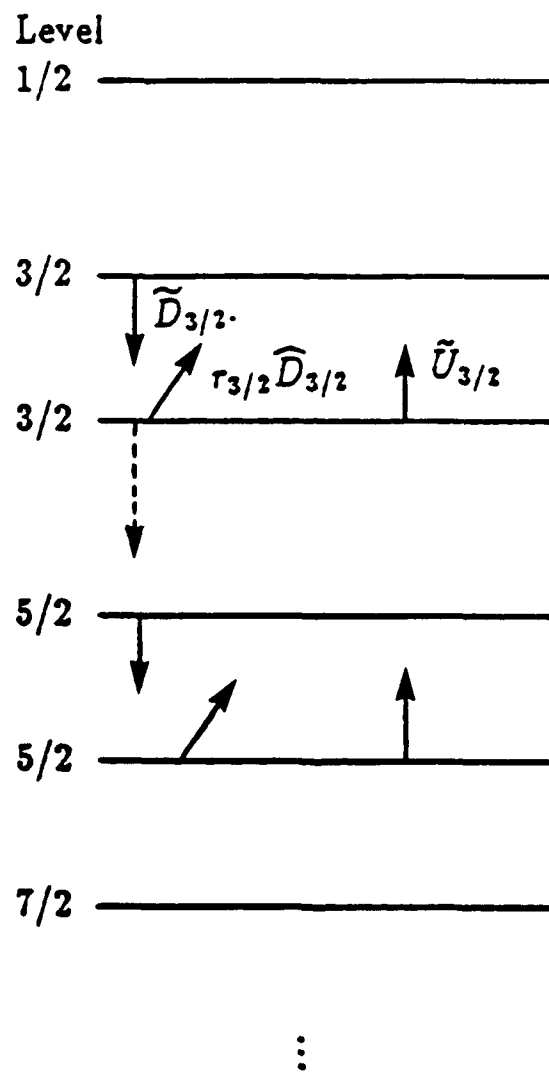


Figure 15.1: The adding method for the intermediate upward and downward fluxes.

$r_{5/2}\widehat{D}_{5/2}$. The total is

$$\widehat{U}_{5/2} = \widehat{M}_{5/2}(\widetilde{U}_{5/2} + r_{5/2}\widehat{D}_{5/2}).$$

The above computational procedure continues down to the surface. For an arbitrary number of levels, the results are summarized by Davies (1982) as

$$\widehat{D}_{l+1/2} = \widetilde{D}_{l+1/2} + t_{l+3/2}\widehat{M}_{l+1/2}(\widehat{D}_{l-1/2} + \widehat{R}_{l-1/2}\widetilde{U}_{l-1/2}), \quad (15.70)$$

and

$$\widehat{U}_{l+1/2} = \widehat{M}_{l+1/2}(r_{l+1/2}\widehat{D}_{l+1/2} + \widetilde{U}_{l+1/2}). \quad (15.71)$$

Once we compute (15.70) and (15.71), we calculate the total fluxes by starting at the bottom of the atmosphere and proceeding upwards. At the surface, the total upward flux is given by the definition of the intermediate flux as

$$U_{L+1/2} = \widehat{U}_{L+1/2}.$$

The total downward flux at the surface is given by the sum of all diffuse downward fluxes due to sources above the surface, $\widehat{D}_{L+1/2}$, plus the amount of the diffuse upward flux reflected off the entire atmosphere, $\widehat{R}_{L+1/2}U_{L+1/2}$, plus the direct solar radiation, $S_{L+1/2}$:

$$D_{L+1/2} = \widehat{D}_{L+1/2} + \widehat{R}_{L+1/2}U_{L+1/2} + S_{L+1/2}.$$

The total upward flux at the first layer above the surface has two sources of diffuse radiation. The first is the upward flux due to all sources above level $L-1/2$, which is given by $\widehat{U}_{L-1/2}$. The second source is the upward flux from the layers below, which in this case is the surface. Only part of this flux is transmitted through the bottom layer, $t_{L-1/2}U_{L+1/2}$, which then undergoes multiple reflections with the atmosphere. Therefore, the total upward radiation at level $L-1/2$ is given by

$$U_{L-1/2} = \widehat{U}_{L-1/2} + \widehat{M}_{L-1/2}t_{L-1/2}U_{L+1/2}.$$

The total downward flux at this level is the sum of all diffuse downward fluxes due to sources above $L-1/2$, $\widehat{D}_{L-1/2}$, plus the amount of the diffuse upward flux reflected off the atmosphere above, $\widehat{R}_{L-1/2}U_{L-1/2}$, plus the direct solar radiation, $S_{L-1/2}$. The result is

$$D_{L-1/2} = \widehat{D}_{L-1/2} + \widehat{R}_{L-1/2}U_{L-1/2} + S_{L-1/2}.$$

The above procedure continues for the all levels. The final results of the adding method for arbitrary levels are given by (Davies [1982]) as

$$U_{l+1/2} = \widehat{U}_{l+1/2} + \widehat{M}_{l+1/2}t_{l+1/2}U_{l+3/2}, \quad (15.72)$$

and

$$D_{l+1/2} = \widehat{D}_{l+1/2} + \widehat{R}_{l+1/2}U_{l+1/2} + S_{l+1/2}, \quad (15.73)$$

with the surface boundary condition:

$$U_{L+1/2} = \widehat{U}_{L+1/2}. \quad (15.74)$$

The solution for the fluxes $S_{l+1/2}$, $\widehat{U}_{l+1/2}$, and $\widehat{D}_{l+3/2}$, and the coefficients $r_{l+1/2}$ and $t_{l+1/2}$ are the summation of two-stream solutions for each of the five absorption coefficients of Table 15.5:

$$\left. \begin{aligned} S_{l+1/2} &= \sum_{i=1}^5 S_{l+1/2}^i \\ \widehat{U}_{l+1/2} &= \sum_{i=1}^5 \widehat{U}_{l+1/2}^i \\ \widehat{D}_{l+3/2} &= \sum_{i=1}^5 \widehat{D}_{l+3/2}^i \\ r_{l+1/2} &= \sum_{i=1}^5 r_{l+1/2}^i \\ t_{l+3/2} &= \sum_{i=1}^5 t_{l+3/2}^i \end{aligned} \right\}. \quad (15.75)$$

The boundary conditions are given by (15.36). The direct flux for each absorption coefficient at the top of any layer l is given by

$$S_{l+1/2}^i = S_0 p(k_i) e^{-k_i y_{\text{top}}} e^{\{-M(k_i y_{l+1/2} + \tau_{C_{l+1/2}})\}}, \quad (15.76)$$

where y_{ctop} is the effective water vapor amount defined by (15.61) at the cloud top level, M is the magnification factor defined by (15.5), and $\tau_{C_{l+1/2}}$ is the optical thickness from the cloud top to level $l + 1/2$ computed as

$$\tau_{C_{l+1/2}} = \sum_{j=l+1}^{N_{ctop}} f(T_j) \hat{C}_T \Delta p_j, \quad (15.77)$$

with the factor $f(T_j)$ given by (15.45).

We obtain the diffuse reflection and transmission coefficients, $r_{l+1/2}^i$ and $t_{l+1/2}^i$, from the Sagan and Pollack (1967) quadrature two-stream solution for diffuse radiation only, i.e. $\mathcal{F}_0 = 0$ in the two-stream transfer equations (15.32) and (15.33). We introduce scaling in order to improve the solution. Defining the quantities:

$$g = 0.85, \quad (15.78)$$

$$f = g^2, \quad (15.79)$$

$$g' = (g - f)/(1 - f), \quad (15.80)$$

$$\tau_{l+1/2}^* = k_i y_{l+1/2} + \tau_{C_{l+1/2}}, \quad (15.81)$$

$$\omega_{0_{l+1/2}} = 0.80 k_i y_{l+1/2} / \tau_{l+1/2}^*, \quad (15.82)$$

$$\omega'_{l+1/2} = (1 - f) \omega_{0_{l+1/2}} / (1 - f \omega_{0_{l+1/2}}), \quad (15.83)$$

$$\tau'_{l+1/2} = \tau_{l+1/2}^* (1 - f \omega_{0_{l+1/2}}), \quad (15.84)$$

$$u_{l+1/2} = \{(1 - g' \omega'_{l+1/2}) / (1 - \omega'_{l+1/2})\}^2, \quad (15.85)$$

$$z_{l+1/2} = \tau'_{l+1/2} \{3(1 - \omega'_{l+1/2})(1 - g' \omega'_{l+1/2})\}^{1/2}; \quad (15.86)$$

we write the Sagan and Pollack (1967) two-stream solution for the diffuse reflection and diffuse transmission functions as

$$r_{l+1/2}^i = \frac{(u_{l+1/2}^2 - 1)(e^{z_{l+1/2}} - e^{-z_{l+1/2}})}{(u_{l+1/2}^2 + 1)^2 e^{z_{l+1/2}} - (u_{l+1/2} - 1)^2 e^{-z_{l+1/2}}} \quad (15.87)$$

and

$$t_{l+3/2}^i = \frac{4u_{l+1/2}}{(u_{l+1/2} + 1)^2 e^{z_{l+1/2}} - (u_{l+1/2} - 1)^2 e^{-z_{l+1/2}}}. \quad (15.88)$$

We place the empirical factor 0.80 on the single scattering albedo formula (15.82) to ensure that an average of 82 Watts/m² are absorbed globally in the shortwave spectrum by the atmosphere.

We get the upward and downward fluxes, $\tilde{U}_{l+1/2}$ and $\tilde{D}_{l+3/2}$, using the Coakley and Chýlek (1975) two-stream solution. These are given by (15.39) and (15.40), and we use the scaling of (15.78)–(15.86). The results are

$$\tilde{U}_{l+1/2}^i = \frac{S_{l+1/2}^i}{1 + 2\beta'\tau'_{l+1/2}} \left\{ 2\beta'\tau'_{l+1/2} + (1 - e^{-\tau'_{l+1/2}/\mu_0})[\beta_0 - 2\beta'\mu_0] \right\} \quad (15.89)$$

and

$$\tilde{D}_{l+3/2}^i = \frac{S_{l+1/2}^i}{1 + 2\beta'\tau'_{l+1/2}} \left\{ (1 - \beta_0 + 2\beta'\mu_0)[1 - e^{-\tau'_{l+1/2}/\mu_0}] - 2\beta'\tau'_{l+1/2}e^{-\tau'_{l+1/2}/\mu_0} \right\}, \quad (15.90)$$

with $\beta_0(\mu_0)$ given by (15.46) with g' replacing g and β' given by

$$\beta' = 0.5 - 0.4375g'. \quad (15.91)$$

For the cloudy part of the atmosphere, the total atmospheric absorption is the sum of (15.11) and (15.68).

For levels $l > N_{ctop}$, the absorption for $\lambda > 0.9\mu\text{m}$ is given by

$$\frac{\partial \mathcal{A}_{wv_l}}{\partial z} \Delta z_l = S_0 \mu_0 [A_{wv}(x_{l+1/2}) - A_{wv}(x_{l-1/2})] \sum_{i=1}^5 \tilde{U}_{ctop}^i (1 - e^{-1.66k_i y_{l+1/2}}). \quad (15.92)$$

The clear sky adsorptions, $A_{wv}(x_{l+1/2})$, are given by (15.64). The incoming solar flux at the surface for $\lambda > 0.9\mu\text{m}$ is $\hat{U}_{L+1/2}$, which we obtain from the adding method.

The 30 day average shortwave heating cross sections, corresponding to Figures 14.4–14.6 are given in Figures 15.2–15.4. Figure 15.2 is the cloud free solar heating. The large water vapor content in the lower tropical atmosphere is reflected

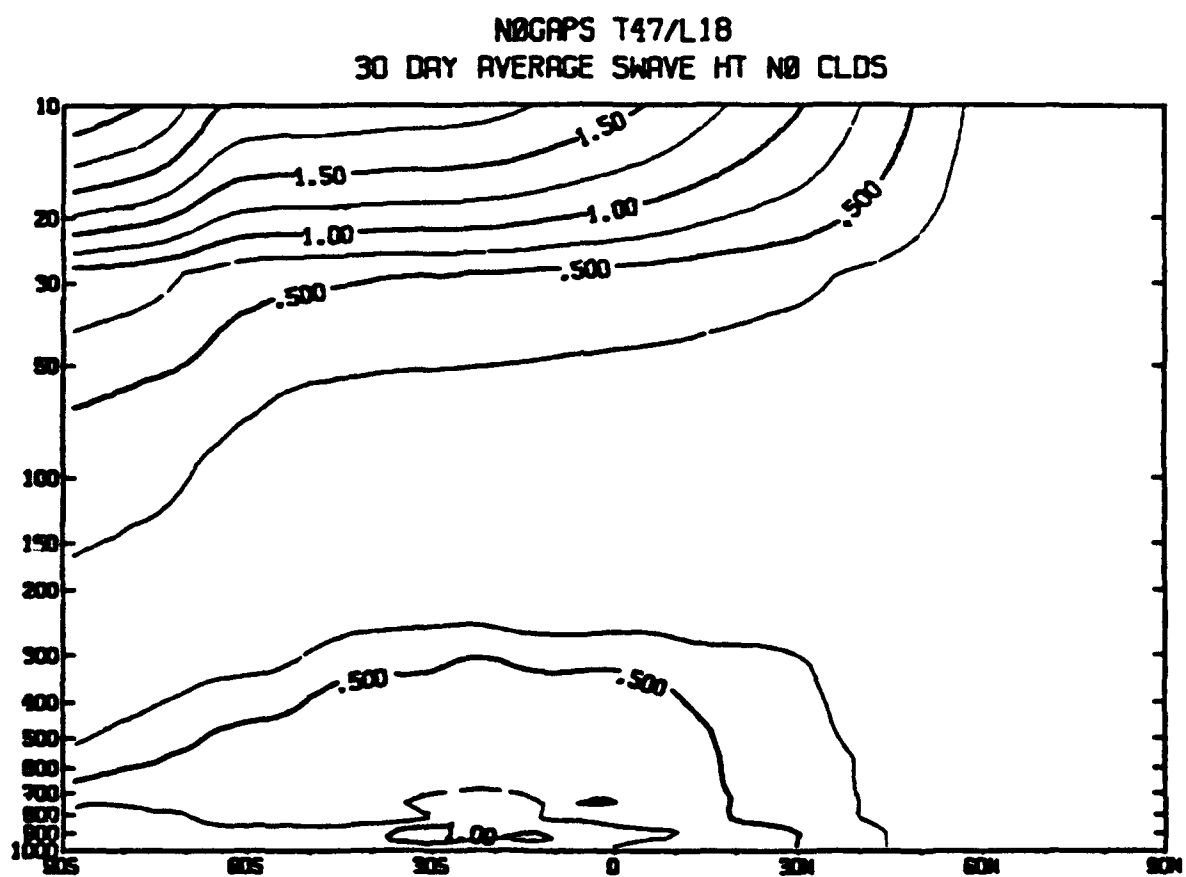


Figure 15.2: The zonal mean cross section of the 30 day cloud-free shortwave heating (deg/day) for a T47 NOGAPS integration starting at 1 December 1989.

in the maximum heating; the stratospheric maximum at the southern pole is caused by ozone absorption. With clouds (Figure 15.3) the distinct tropospheric heating profile is spread out, with large solar absorption occurring near the cloud tops. The difference of the heating profiles (Figure 15.4) demonstrates that clouds warm the entire troposphere; their influence on the stratosphere, however, is small.

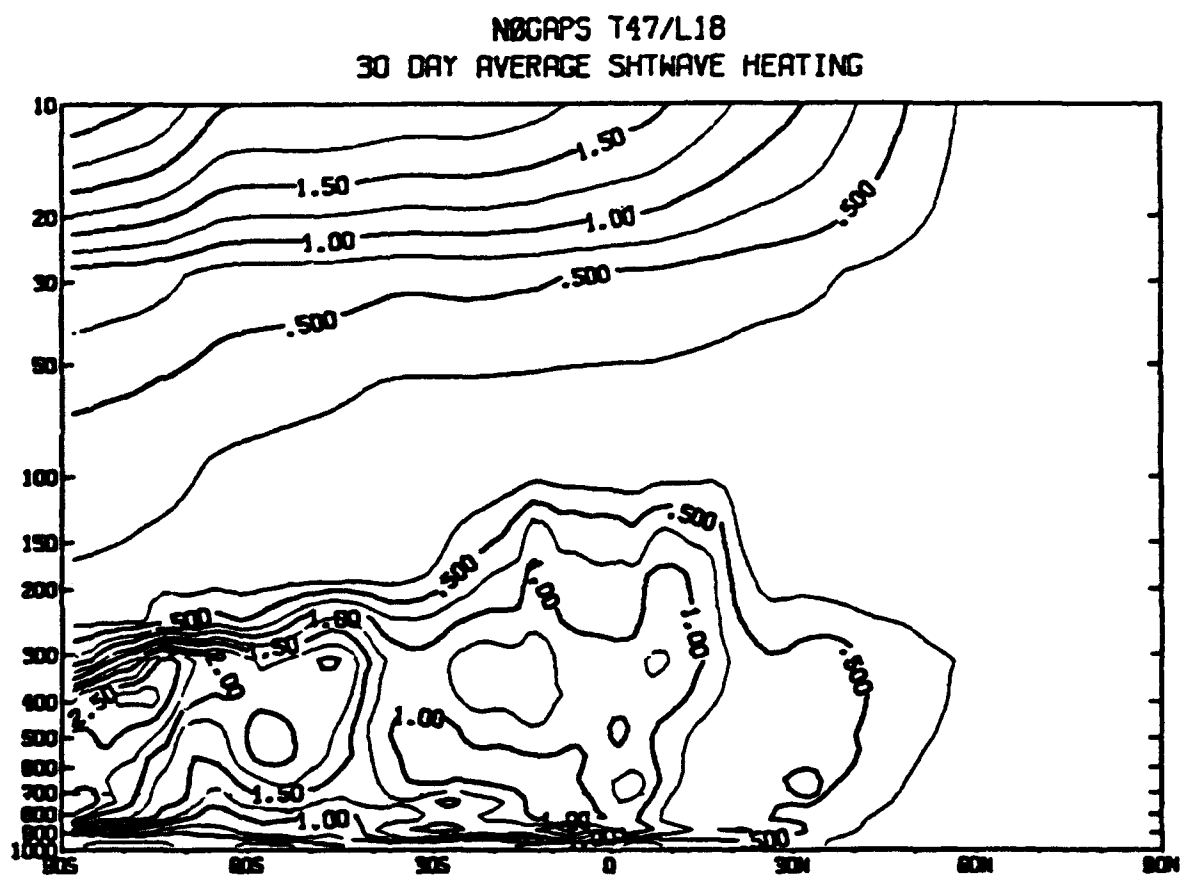


Figure 15.3: The zonal mean cross section of the 30 day cloudy shortwave heating (deg/day) for a T47 NOGAPS integration starting at 1 December 1989.

NOGAPS T47/L18
30 DAY AVERAGE CLD SW-NOCLD SW

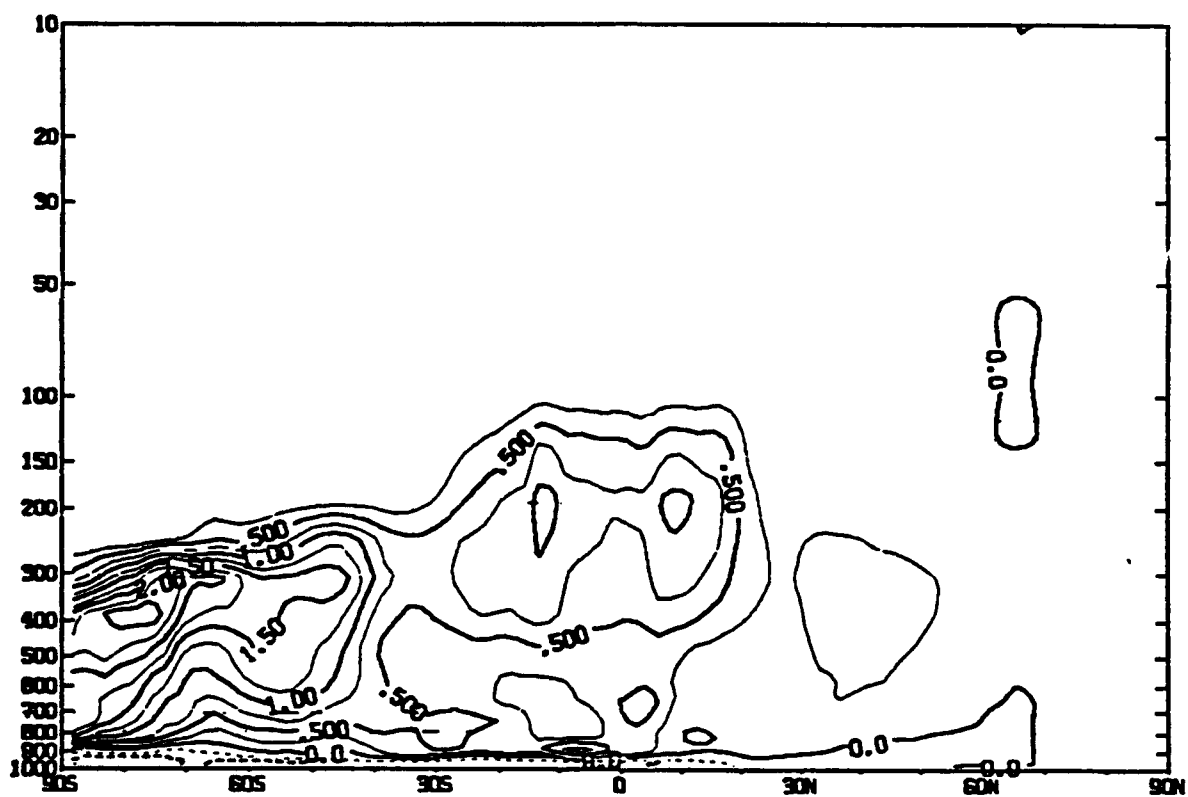


Figure 15.4: The zonal mean cross section of the 30 day difference of the cloud-free and the cloudy shortwave heating (deg/day) for a T47 NOGAPS integration starting at 1 December 1989.

Chapter 16

Summary

The purpose of this report is to present a description of the initialization and forecast components of the current Navy Operational Global Atmospheric Prediction System (NOGAPS 3.2). We hope that this report will serve three purposes: (1) provide a means of identifying those aspects of model formulation which make NOGAPS unique from other numerical weather prediction models; (2) act as a research guide for future improvements to NOGAPS numerical procedures and physical parameterizations; and (3) be a handbook for meteorological and oceanographic users of NOGAPS products, so that they can better understand the precise workings and assumptions of the model. With these purposes in mind, we have presented in detail the numerical procedures and physical parameterizations of the model.

In the introduction we give a brief history of NOGAPS. In Chapter 2 we define the vertical hybrid coordinate system and review the transformation theory for the primitive equations with this coordinate system. Chapter 3 contains the vertical hybrid finite difference formulation of the model, and Chapter 4 contains the horizontal spectral representations for the forecast fields on hybrid pressure surfaces, together with a description of the spectral transform procedures. The discussion of the nonlinear normal mode initialization (NNMI) scheme is presented

in Chapter 5. In Chapter 6, we present the time splitting numerical procedure for the adiabatic and diabatic processes. Chapter 7 contains the details of the time splitting for the calculations of the explicit adiabatic tendencies and the tendency corrections due to the implicit treatment of gravity waves and zonal advection. In Chapter 8, we describe the additional implicit adjustments, which ensure a sufficiently large time step for operational integrations.

We describe the physical parameterizations of the model in Chapters 9-15. The model contains state of the art physical parameterizations and the presentation is as detailed as any that can be found in the literature. The parameterizations include gravity wave drag due to mountains (Chapter 9), vertical turbulent diffusion (Chapter 10), shallow cumulus mixing (Chapter 11), cumulus convection (Chapter 12), large scale stable precipitation (Chapter 13), and the heating due to longwave radiation (Chapter 14) and solar radiation (Chapter 15). We have included in all the discussions not only the theory behind the parameterizations, but also our precise tunings of the NOGAPS physics, which have minimized the cold biases that plague many other numerical weather prediction models.

Chapter 17

The Bibliography

- [] Andersen, J.H., 1977: A routine for normal mode initialization with nonlinear correction for a multi-level spectral model with triangular truncation. ECMWF Internal Report No. 15, 42 pp.
- [] Arakawa, A., and V.R. Lamb, 1977: Computational design of the basic dynamical process of the UCLA general circulation model. *Methods in Computational Physics*, Vol 17, Academic Press, Inc. New York, 173-265.
- [] ———, and W.H. Schubert, 1974: Interaction of a cumulus cloud ensemble with the large-scale environment, part 1. *J. Atmos Sci.*, **34**, 674-701.
- [] Baer, F., 1977: Adjustments of initial conditions required to suppress gravity oscillations in nonlinear flows. *Contrib. Atmos. Phys.*, **50**, 350-366.
- [] ———, and J. Tribbia, 1977: On complete filtering of gravity modes through non-linear initialization. *Mon. Wea. Rev.*, **105**, 1536-1539.
- [] Baker, N.L., 1989: A PC-based system for monitoring radiosonde quality at an operational global forecast center. *Preprints, Eighth Conference on Numerical Weather Prediction*, Amer. Meteor. Soc., 392-394.

- Barker, E., J. Goerss, and N. Baker, 1989: The Navy's operational multivariate interpolation analysis method. *Preprints, Eighth Conference on Numerical Weather Prediction*, Amer. Meteor. Soc., 161-163.
- Carnahan, B., H.A. Luther, and J.O. Wilkes, 1969: *Applied Numerical Methods*, John Wiley and Sons, 604pp.
- Chandrasekhar, S., 1960: *Radiative Transfer*, Dover, 393pp.
- Charnock, H., 1955: Wind stress an the water surface. *Quart. J. Roy. Met. Soc.*, **81**, 639-640.
- Chou, M. D., 1984: Broadband water vapor transmission functions for atmospheric IR flux computations. *J. Atmos. Sci.*, **41**, 1775-1778.
- ———, M.D. and L. Peng, 1983: A parameterization of the absorption in the $15\mu\text{m}$ CO_2 spectral region with application to climate sensitivity studies. *J. Atmos. Sci.* **40**, 2183-2192.
- Coakley, J.A., and P. Chýlek, 1975: The two stream approximation in radiative transfer: including the angle of the incident radiation. *J. Atmos. Sci.*, **32**, 409-418.
- Dantzig, G. B., 1963: *Linear Programming and Extensions*, Princeton University Press, Princeton, 631 pp.
- Davies, R., 1982: Documentation of the solar radiation parameterization in the GLAS climate model. NASA Technical Memorandum 83961, 57pp.
- Dopplick, T.G., 1974: Radiational heating in the atmosphere, in the *The General Circulation of the Tropical Atmosphere and Interactions with Extratropical*

Latitudes, Vol. 2, R.E. Newell, J.W. Kindsor., D.G. Vincent, and G.J. Boer (Eds)
M.I.T. Press, Cambridge Mass. 371 pp.

- [] Eliassen, A. and E. Palm, 1961: On the transfer of energy in stationary mountain waves. *Geofys. Publ.*, **22**, No. 3, 1-23.
- [] Errico, R.M., 1987: A Description of software for determination of normal modes of the NCAR community climate model. NCAR Technical Note TN-277+STR, 86 pp.
- [] Haltiner, G.J. and R.T. Williams, 1980: *Numerical Prediction and Dynamic Meteorology, Second Edition*, John Wiley and Sons, 477pp.
- [] Harshvardhan, R. Davies, D. Randall, and T. Corsetti, 1987: A fast radiation parameterization for atmospheric circulation models. *J. Geophys. Res.*, **92**, 1009-1016.
- [] Holloway, J.L., and S. Manabe, 1971: Simulation of climate by a global general circulation model. *Mon. Wea. Rev.*, **99**, 335-370.
- [] Hoskins, B.J. and A.J. Simmons, 1975: A multi-layer spectral model and the semi-implicit method. *Quart J. Roy. Met. Soc.* **101**, 637-655.
- [] Inman, R.L., 1969: Computation of temperature at the lifted condensation level. *J. Appl. Meteor.*, **8**, 155- 158.
- [] Jenkins, G.M., and D.G. Watts, 1968: *Spectral Analysis and its Applications*, Holden-Day, 525 pages.
- [] Joseph, J.H., W.J. Wiscombe, and J.A. Weinman, 1976: The delta-Eddington approximation for radiative flux transfer. *J. Atmos. Sci.*, **33**, 2452-2459.

- [] Kasahara, A., 1978: Further studies on a spectral model of the global barotropic primitive equations with Hough harmonics expansions. *J. Atmos. Sci.*, **35**, 2043-2051.
- [] Lacis, A.A., and J.E. Hansen, 1974: A parameterization for the absorption of solar radiation in the earth's atmosphere. *J. Atmos. Sci.*, **31**, 118-133.
- [] Lanczos, C. 1956: *Applied Analysis*, Prentice Hall, 539 pp.
- [] Leary, C. A., and R.A. Houze, Jr., 1980: The contribution of mesoscale motions to the mass and heat fluxes of an intense convective system. *J. Atmos. Sci.* **37**, 784-796.
- [] Lindzen, R.S., 1981: Turbulence and stress due to gravity wave and tidal breakdown. *J. Geophys. Res.*, **86**, 9707-9714.
- [] Liou, K.N., 1980: *An Introduction to Atmospheric Radiation. Int. Geophys. Ser.* Vol. 25, Academic Press, 392pp.
- [] Lord, S.J., 1978: Development and Observational verification of a cumulus cloud parameterization. Ph.D. Thesis, UCLA, 359 pp.
- [] ———, and A.Arakawa, 1980: Interaction of a cumulus cloud ensemble with the large-scale environment. Part II. *J. Atmos. Sci.* **37**, 2677-2692.
- [] ———, W.C. Chao and A. Arakawa, 1982: Interaction of a cumulus cloud ensemble with the large scale environment. Part IV: The Discrete Model. *J. Atmos. Sci.* **39**, 104-113.
- [] Louis, J.F., 1979: A parametric model of vertical eddy fluxes in the atmosphere. *Boundary Layer Meteorol.*, **17**, 187-202.

- [] ———, M. Tiedtke, and J.F. Geleyn, 1982: A short history of the operational PBL - parameterization at ECMWF, in *ECMWF's Workshop on Planetary Boundary Parameterization, 25-27 November 1981*, 59-79.
- [] Machenhauer, B., 1977: On the dynamics of gravity oscillations in a shallow water model, with application to normal mode initializations. *Contrib. Atmos. Phys.*, **50**, 253-271.
- [] Meador, W.E., and W.R. Weaver, 1980: Two-stream approximation to radiative transfer in planetary atmospheres: A unified description of existing methods and a new improvement. *J. Atmos. Sci.*, **37**, 630-643.
- [] Monin, A.S., and A.M. Obukhov, 1954: Basic regularity in turbulent mixing in the surface layer of the atmosphere. *Akad. Nauk. S.S.S.R. Trud. Geofiz. Inst., Tr.* **24**, 163-187.
- [] Palmer, T.N., G.J. Shutts, and R. Swinbank, 1986: Alleviation of a systematic westerly bias in general circulation and numerical weather prediction models through an orographic gravity wave drag parameterization. *Quart. J. Roy. Met. Soc.*, **112**, 1001-1039.
- [] Paltridge, G.W., and C.M.R. Platt, 1976: *Radiative Processes in Meteorology and Climatology*. Elsevier, 318pp.
- [] Payne, S. W., 1981: The inclusion of moist downdraft effects in the Arakawa-Schubert cumulus parameterization. *Preprints, Fifth Conference on Numerical Weather Prediction*, Amer. Met. Soc., 277-284.
- [] Philips, N.A., 1974: Natl. Meteor Cent. Off.: Note 104. Natl. Weather Service, Washington, D.C.

- [] Randall, D.A., 1976: The interaction of the planetary boundary layer with large-scale circulations, Ph.D. Thesis, UCLA 247pp.
- [] Rasch, P.J., 1985: Developments in normal mode initialization, Part II: A new method and its comparison with currently used schemes. *Mon. Wea. Rev.*, **113**, 1753- 1770.
- [] Robert, A.J., H. Henderson, and C. Turbull, 1972: An implicit time integration scheme for baroclinic models of the atmosphere. *Mon. Wea. Rev.*, **100**, 329-335.
- [] Rogers, C.D., 1967: The use of emissivity in atmospheric radiation calculations. *Quart. J. Roy. Meteor. Soc.*, **93**, 43-54.
- [] Rosmond, T.E., 1981: NOGAPS: Navy Operational Global Atmospheric Prediction System. *Preprints Fifth Conference on Numerical Weather Prediction*, Monterey, Ca., Amer. Meteor. Soc. 74-79.
- [] Sagan, C., and J.B. Pollack, 1967: Anisotropic nonconservative scattering and the clouds of Venus. *J. Geophys. Res.*, **72**, 466-477.
- [] Sardeshmukh, P.D. and B.J. Hoskins, 1984: Spatial Smoothing on the Sphere. *Mon. Wea. Rev.*, **112**, 2524- 2529.
- [] Schubert, W. H., 1973: The interaction of a cumulus cloud ensemble with the large-scale environment. Ph.D. Thesis, UCLA, 168 pp.
- [] Silva-Dias, P.L., and W. H. Schubert, 1977: Experiments with a spectral cumulus parameterization theory. Atmos. Sci. Paper No. 275, Colorado State University, 132 pp.
- [] Simmons, A.J., D.M. Burridge, M. Jarraud, C. Girard, and W. Wergwen, 1989: The ECMWF's medium range prediction model development of the numerical

formulation and the impact of increased resolution. *Meteorol. Atmos. Phys.*, **40**, 28-60.

- [] ———, B.J. Hoskins, and D.M. Burridge, 1978: Stability of the semi-implicit method of time integration. *Mon. Wea. Rev.*, **106**, 405-412.
- [] ———, and M. Jarraud, 1983: The design and performance of the new ECMWF operational model, in *ECMWF's Workshop on Numerical Methods for Weather Prediction, Volume 2, 5-9 September 1983*, 113-164.
- [] ———, and R. Strüing, 1981: An energy and angular momentum conserving finite-difference scheme, hybrid coordinates and medium-range weather prediction. ECMWF Technical Report No. 28.
- [] Slingo J., 1987: The development and verification of a cloud prediction scheme for the ECMWF model. *Q. J. R. Meteorol. Soc.*, **113**, 899-927.
- [] ———, and B. Ritter, 1985: Cloud prediction in the ECMWF model. ECMWF Technical Report No. 46, 48pp.
- [] Stephens, G.L., 1984: The parameterization of radiation for numerical weather prediction and climate models. *Mon. Wea. Rev.*, **112**, 826-867.
- [] Tiedtke, M., 1984: The sensitivity of the time-scale flow to cumulus convection in the ECMWF model, in the ECMWF's Workshop on Convection in Large-Scale Numerical Models, 28 November- 1 December 1983. 297-316.
- [] Tokioka, T., 1978: Some considerations on vertical differencing. *J. Meteor. Soc. Japan*, **44**, 25-43.

- [] Wergen, W., 1987: Diabatic nonlinear normal mode initialization for a spectral model with a hybrid vertical coordinate. ECMWF Technical Report No. 59, 83pp.
- [] Wiscombe, W.J., and G.W. Grams, 1976: The backscattered fraction in two-stream approximation. *J. Atmos. Sci.*, **33**, 2440-2451.

Distribution List

American Meteorological Society
Meteor. & Geostroph. Abs.
P. O. Box 1736
Washington DC 20013

Applied Physics Laboratory
Johns Hopkins University
Johns Hopkins Road
Laurel MD 20707

Applied Physics Laboratory
University of Washington
1013 NE 40th St.
Seattle WA 98195
Attn: Atmospheric Sciences Dept.

Applied Research Laboratory
Pennsylvania State University
P.O. Box 30
State College PA 16801

Applied Research Laboratory
University of Texas at Austin
P.O. Box 8029
Austin TX 78713-8029

Assistant Secretary of the Navy
Research, Development & Acquisition
Navy Department
Washington DC 20350-1000

Atmospheric & Environmental
Research, Inc.
840 Memorial Drive
Cambridge MA 02139
Attn: Dr. D. Gutzler

Bureau of Meteorology
Box 1289K, GPO
Melbourne, VIC, Australia 3001

CDC
Meteorology Dept.
2800 E. Old Shakopee Rd.
Minneapolis MN 55440
Attn: T. Hansen

Centre National De Recherches
Meteorologiques
F-31057 Toulouse Cedex
France
Attn: J. F. Royer

Chief of Naval Operations
Navy Department
Washington DC 20350-2000
Attn: OP-02
OP-71
OP-987
OP-092X, Mr. R. Feden

Chief of Naval Operations
Oceanographer of the Navy
U.S. Naval Observatory
34th & Massachusetts Ave. NW
Washington DC 20392-1800
Attn: OP-096
OP-0961B

Colorado State University
Atmospheric Sciences Dept.
Ft. Collins CO 80523
Attn: Librarian
Dr. W. Gray

Cornell University
1113 Bradfield Hall
Ithaca NY 14853
Attn: Dr. S. J. Colucci

David W. Taylor Naval Research Center
Bethesda MD 20084-5000
Attn: Commander

Defense Mapping Agency
Systems Center
8613 Lee Hwy.
Mail Stop A-13
Fairfax VA 22031-2138
Attn: Code PRN

Defense Mapping Agency
Systems Center
12100 Sunset Hill Rd #200
Reston VA 22090-3207
Attn: Director
Code SGWN

Director of Navy Laboratories
Department of the Navy
Crystal Plaza #5, Rm. 1062
Washington DC 20360

European Centre for Medium
Range Weather Forecasts
Shinfield Park, Reading
Berkshire RG29AX, England
Attn: M. Molteni (2)

Fleet Antisub Warfare Tng Ctr-Atl
Naval Station
Norfolk VA 23511-6495
Attn: Commanding Officer

Fleet Numerical Oceanography Center
Monterey CA 93943-5005
Attn: Commanding Officer

Florida State University
Dept. of Meteorology
Tallahassee FL 32306-3034
Attn: Dr. T. N. Krishnamurti
G. Rohaly

Global Weather Dynamics
2460 Garden Road
Monterey CA 93940

Iowa State University
Atmospheric Science Program
3017 Agronomy Hall
Ames IA 50011
Attn: Dr. T.-C. Chen
D. McDonald

F. Selden
KNMI - Postbus 201
3730 Ae De Bilt
The Netherlands

Laboratory for Atmospheric Science
NASA Goddard Space Flight Center
Greenbelt MD 20771
Attn: Code 611, G. K. Walker

MIT
Meteorology Dept. Rm 54-1620
Cambridge MA 02139
Attn: R. Black
P. Neillay
Dr. R. Dole
M. Morgan

Meteorology Office Library
London Road
Bracknell, Berkshire
RG 12 1SZ, England

Meteorology Research Institute
1-1 Nagamine Tsukuba-Shi
Ibaraki 305 Japan
Attn: Dr. M. Sugi

NOAA/ERL/CMDL
325 Broadway
Boulder CO 80303
Attn: Dr. K. Weickmann

National Center for Atmospheric
Research
P.O. Box 3000
Boulder CO 80302
Attn: Library Acquisitions (12)

National Meteorological Center
WWB W32, Room 204
Washington DC 20233
Attn: Director

NASA Goddard Space Center
Atmos. Science Laboratory
Greenbelt MD 20771
Attn: G. K. Walker

National Ocean Data Center
1825 Connecticut Ave., NW
Universal Bldg. South, Rm. 206
Washington DC 20235
Attn: G. W. Withese

National Meteorological Center
5200 Auth Road
Washington DC 20233
Attn: Climate Analysis Center
Dr. D. Rodenhis
Dr. R. Livezey
W. Ebisuaki
Dr. Huug Van Den Dool
Dr. Wen-Yuan Chen
Dr. S. Tracton
P. Caplan
Dr. K. Mo
Development Division
Dr. E. Kalnay
Dr. M. Kanamitsu
Dr. S. Saha

National Science Foundation
Atmos. Sci. Div., Rm 644
1800 G Street NW
Washington DC 20550
Attn: P. L. Stephens

Naval Air Development Center
Warminster PA 18974-5000
Attn: Commander

Naval Air Systems Command HQ
Washington DC 20361-0001
Attn: Commander

Naval Civil Engineering Laboratory
Port Hueneme CA 93043
Attn: Commanding Officer

Naval Coastal Systems Center
Panama City FL 32407-5000
Attn: Commanding Officer

Naval Facilities Engineering
Command HQ
200 Stovall St.
Alexandria VA 22332-2300
Attn: Commander

Naval Oceanographic Office
Stennis Space Center MS 39522-5001
Attn: Commanding Officer
Library (2)
Code TD, L. Bernard

Naval Oceanography Command
Stennis Space Center MS 39529-5000
Attn: Commander

Naval Oceanographic & Atmospheric
Research Laboratory
Atmospheric Directorate
Monterey CA 93943-5006
Attn: Code 400
Code 432, Dr. R. Gelaro
Dr. T. Hogan

Naval Oceanographic & Atmospheric
Research Laboratory
Stennis Space Center MS 39529-5004
Attn: Code 100
Code 105
Code 115
Code 125L (6)
Code 125P
Code 200
Code 300

Naval Ocean Systems Center
San Diego CA 92152-5000
Attn: Commander

Naval Postgraduate School
Monterey CA 93943
Attn: Superintendent

Naval Research Laboratory
Washington DC 20375
Attn: Commanding Officer
Library (3)

Naval Sea Systems Command HQ
Washington DC 20362-5101
Attn: Commander

Naval Surface Warfare Detachment
Silver Spring
White Oak Laboratory
10901 New Hampshire Ave.
Silver Spring MD 20903-5000
Attn: Officer in Charge
Library

Naval Surface Warfare Center
Dahlgren VA 22448-5000
Attn: Commander

Naval Underwater Systems Center
Newport RI 02841-5047
Attn: Commander

Naval Underwater Systems Center Det
New London Laboratory
New London CT 06320
Attn: Officer in Charge

Office of Naval Research
800 N. Quincy St.
Arlington VA 22217-5000
Attn: Code 10D/10P, Dr. E. Silva
Code 112, Dr. E. Hartwig
Code 12
Code 10

Office of Naval Research
ONR European Office
Box 39
FPO New York 09510-0700
Attn: Commanding Officer

Office of Naval Technology
800 N. Quincy St.
Arlington VA 22217-5000
Attn: Code 20, Dr. P. Selwyn
Code 22, Dr. T. Warfield
Code 228, Dr. M. Briscoe
Code 228, CDR L. Bounds
Code 234, Dr. C. Votaw

Penn State University
Meteorology Dept.
503 Walker Bldg.
University Park PA 16802
Attn: Chairman
C. A. Reynolds
R. Tomas

Princeton University
Geophy. Fluid Dynamics Lab
Box 308
Princeton NJ 08540
Attn: Director
Dr. W. Stern
Dr. K. Miyakoda

Purdue University
Earth & Atmos. Sci. Dept.
W. Lafayette IN 47907
Attn: Dr. Wen-Yih Sun
Dr. L. Buja

SAIC
205 Montecito Ave.
Monterey CA 93940

San Jose State University
Meteorology Dept.
San Jose CA 95192
Attn: Chairman

Scripps Institution of Oceanography
University of California
291 Rosecrans St.
San Diego CA 92106-3505

Scripps Institution of Oceanography
P. O. Box 109
La Jolla CA 92037
Attn: S. Chen
Dr. A. Miller
Dr. J. O. Roads

Space & Naval Warfare Sys Com
Director of Navy Laboratories
SPAWAR 005
Washington DC 20363-5100
Attn: Commander

State University of New York
Atmos. Sci. Dept.
Albany NY 12222
Attn: H. Iskenderian
G. Bell
Dr. L. Bosart

UCLA
Atmospheric Sciences Dept.
405 Hilgard Ave.
Los Angeles CA 90024
Attn: Dr. M. Kimoto

University of Colorado (CIRES)
Campus Box 216
Boulder CO 80309
Attn: P. Sardeshmukh

University of Colorado
Campus Box 426
Boulder CO 80309-0426
Attn: P. Cehelsky

University of Colorado (CIRES)
Campus Box 449
Boulder CO 80309
Attn: Dr. Z. Toth
Dr. M. Hoerling
M. Ting
C. Penland

University of Illinois
Atmospheric Science Dept.
Urbana IL 61801
Attn: Dr. M. Ramamurthy
Dr. W. Robinson
Dr. J. Walsh
Dr. M. Mak
A. C. Yih
J. Chang

University of Maryland
Meteorology Dept.
College Park MD 20742
Attn: D. Straus
Dr. Shukla
Dr. M. Cai
Dr. F. Baer

University of Miami
4600 Rickenbacker Causeway
Miami FL 33149-1098
Attn: D. Stewart
Dr. N. Surgi

University of Michigan
Space Research Center
Ann Arbor MI 48109-3335
Attn: B. Smith
Dr. S. Mullen
S. Augustine

University of Oklahoma
Meteorology Dept.
Norman OK 73069
Attn: Chairman

University of Stockholm
S-106 91 Stockholm
Sweden
Attn: Dr. B. Reinhold
Arrhenius Lab. S. Yang
Dr. A. Johansson

University of Utah
Meteorology Dept.
Salt Lake City UT 84112
Attn: Chairman
E. H. Berbery
T. W. Barker
Dr. J. Paegle
Dr. J. Nogués-Paegle

University of Washington
Atmospheric Sciences Dept.
Seattle WA 98195

University of Wisconsin
Meteorology Dept.
Madison WI 53706
Attn: M. Alexander
S. Silberberg

Woods Hole Oceanographic Institution
P.O. Box 32
Woods Hole MA 02543
Attn: Director

Yale University
Geology & Geophysics Dept.
New Haven CT 06511
Attn: Dr. A. Sutera
L. Pandolfo

REPORT DOCUMENTATION PAGEForm Approved
OMB No. 0704-0188

Public reporting burden for this collection of information is estimated to average 1 hour per response, including the time for reviewing instructions, searching existing data sources, gathering and maintaining the data needed, and completing and reviewing the collection of information. Send comments regarding this burden estimate or any other aspect of this collection of information, including suggestions for reducing this burden, to Washington Headquarters Services, Directorate for Information Operations and Reports, 1215 Jefferson Davis Highway, Suite 1204, Arlington, VA 22202-4302, and to the Office of Management and Budget, Paperwork Reduction Project (0704-0188), Washington, DC 20503.

1. Agency Use Only (Leave blank).		2. Report Date. December 1991	3. Report Type and Dates Covered. Final
4. Title and Subtitle. The NOGAPS Forecast Model: A Technical Description			5. Funding Numbers. Program Element No 0602435N Project No RM350681 Task No 2 Accession No DN656757
6. Author(s). Drs. Timothy F. Hogan, Thomas E. Rosmond, Ronald Gelaro			8. Performing Organization Report Number. NOARL Report 13
7. Performing Organization Name(s) and Address(es). Naval Oceanographic and Atmospheric Research Laboratory Atmospheric Directorate Monterey, California 93943-5006			10. Sponsoring/Monitoring Agency Report Number.
9. Sponsoring/Monitoring Agency Name(s) and Address(es). Office of Naval Technology ONT Code 22 800 N. Quincy St Arlington, VA 22217			
11. Supplementary Notes.			
12a. Distribution/Availability Statement. Approved for public release; distribution is unlimited. Naval Oceanographic and Atmospheric Research Laboratory, Stennis Space Center, Mississippi 39529-5004.			12b. Distribution Code.
13. Abstract (Maximum 200 words). We present a description of the Navy Operational Global Atmospheric Prediction System (NOGAPS). This report details the theoretical development of the equations, the nonlinear normal mode initialization, the horizontal spectral expansions, the vertical finite differencing, and the detailed formulations of each of the diabatic parameterizations.			
14. Subject Terms. forecast model, global prediction, parameterization, normal mode initialization, numerical weather prediction			15. Number of Pages. 223
			16. Price Code.
17. Security Classification of Report. Unclassified	18. Security Classification of This Page. Unclassified	19. Security Classification of Abstract. Unclassified	20. Limitation of Abstract. Same as report